

4 Climate and climate-related conditions for the SR-Site safety assessment

4.1 Rationale and general approach

As mentioned in Section 1.2, the main scenario of the safety assessment includes a *base case* and a *global warming variant* of climate evolution. The base case is based on a *reference glacial cycle* which in turn constitutes a repetition of conditions reconstructed for the last glacial cycle, the Weichselian and the Holocene, see Figure 1-3. By modifications of the *reference glacial cycle*, this evolution is used also for constructing additional climate cases with a potentially larger impact on repository performance. For example, by defining a longer period of glacial conditions, the *reference glacial cycle* has been used to construct an *extended ice sheet duration case* (Figure 1-3), used for analysis in the additional safety assessment scenarios of SR-Site.

In order to make relevant and well-motivated definitions of the climate cases, it is essential to first have good knowledge on the climate and glacial history of the Weichselian glacial cycle, i.e. the glacial cycle on which the *reference glacial cycle* is based and the additional climate cases are constructed (Figure 1-3). To this end, Section 4.2 describes the present knowledge on Weichselian climate and glacial history to a level required to give adequate input to the definition and description of the *reference glacial cycle* and the additional climate cases. The description in Section 4.2 is based both on geological information and climate modelling.

Section 4.3 gives an overview and detailed examples of climates that occurred during the last glacial cycle, from geological information and from climate modelling.

Section 4.4 presents the reconstruction of last glacial cycle conditions that subsequently are used for the *reference glacial cycle* and the base case of the SR-Site main scenario presented in Section 4.5, see also Figure 1-3. The global warming climate case is described in Section 5.1. Since it is not possible to describe an expected evolution of climate conditions for the time perspective of the safety assessment, the base case and global warming variant should not be seen as prognoses or attempts to predict future climate evolutions. Instead, they are *examples* of future evolutions that in a realistic way cover all relevant climate-related changes that can be expected in a 100 kyr time perspective. They are complemented with additional climate cases with a potentially larger impact on long-term repository safety, described in Chapter 5.

For the reconstruction of the last glacial cycle conditions in Section 4.4, an ice sheet model reconstruction of the Weichselian glacial is used (Section 3.1.4). Despite remaining uncertainties regarding the Weichselian glacial history, especially during the earlier phases of the glacial, see Section 4.2, the Weichselian is the best-known glacial cycle. This gives possibilities to use geological information for testing and constraining the adopted models. In line with the discussion above, the purpose is not to produce a “true picture” of the Weichselian evolution, a task that obviously is not possible to achieve, but rather to construct a scientifically reasonable starting point for the analysis of potential climate impacts on repository safety.

The reconstruction of last glacial cycle conditions, Section 4.4, extend over 120 kyrs. Three numerical models are used to yield boundary conditions for the reconstruction:

1. A dynamic ice sheet model.
2. A Glacial Isostatic Adjustment (GIA) model.
3. A permafrost model.

The ice sheet model is the University of Maine Ice Sheet Model (UMISM) (see Section 3.1.4), the GIA model was developed at the University of Durham (see Section 3.3.4) and the permafrost model at Helsinki University of Technology (see Section 3.4.4), see also /SKB 2010g/. The basis for the *reference glacial cycle* of climate-related conditions is a reconstruction of the Fennoscandian ice sheet during the Weichselian employing the ice sheet model. The generated ice sheet evolution has been used as input to the global isostatic adjustment (GIA) model. The third main component in the reconstruction of Weichselian conditions is the permafrost model, yielding permafrost depths given

the evolution of ice sheet, shore-level development, and other surface conditions. The main data flows between the ice sheet, GIA and permafrost models are shown in Figure 4-1.

The *reference glacial cycle*, described in Section 4.5 and used for the base case of the SR-Site main scenario (Figure 1-3) is one example of a conceivable evolution of climate and climate-related processes and covers conditions and sequences that could be expected in a 100 kyr time perspective. The *global warming case*, described in Section 5.1 and used for the Global warming variant of the main scenario, depicts an evolution with a warming climate due to an anthropogenically increased greenhouse effect. Other possible future climate evolutions are described in additional climate cases, described in other parts of Chapter 5. A summary of the climate cases is found in Table 4-1.

In Chapter 4, the sections on Weichselian climate and glacial history (Section 4.2) and reconstruction of last glacial cycle conditions (Section 4.4) describe *past* events, and therefore the time scale in the text and figures is time before present (BP). The sections on the SR-Site *reference glacial cycle* (Section 4.5), and the section on additional climate cases (Chapter 5) all describe possible *future* climate developments and therefore the time scale in these sections reflects this.

All in all, six climate cases depicting possible future climate development at the Forsmark site are presented (Table 4-1) and used for the analysis of long-term repository safety /SKB 2011/.

Table 4-1. Climate cases in the SR-Site safety assessment.

Case number (section in present report)	Climate case	Short description
1 (Section 4.5)	<i>Reference glacial cycle</i>	Repetition of reconstructed last glacial cycle conditions
2 (Section 5.1)	<i>Global warming</i>	Longer period of initial temperate conditions than in case 1
3 (Section 5.2)	<i>Extended global warming</i>	Longer period of initial temperate conditions than in case 2
4 (Section 5.3)	<i>Extended ice sheet duration</i>	Longer duration of ice sheet coverage than in case 1
5 (Section 5.4)	<i>Maximum ice sheet configuration</i>	Largest ice configuration in past two million years
6 (Section 5.5)	<i>Severe permafrost</i>	Favourable for early and deep permafrost growth

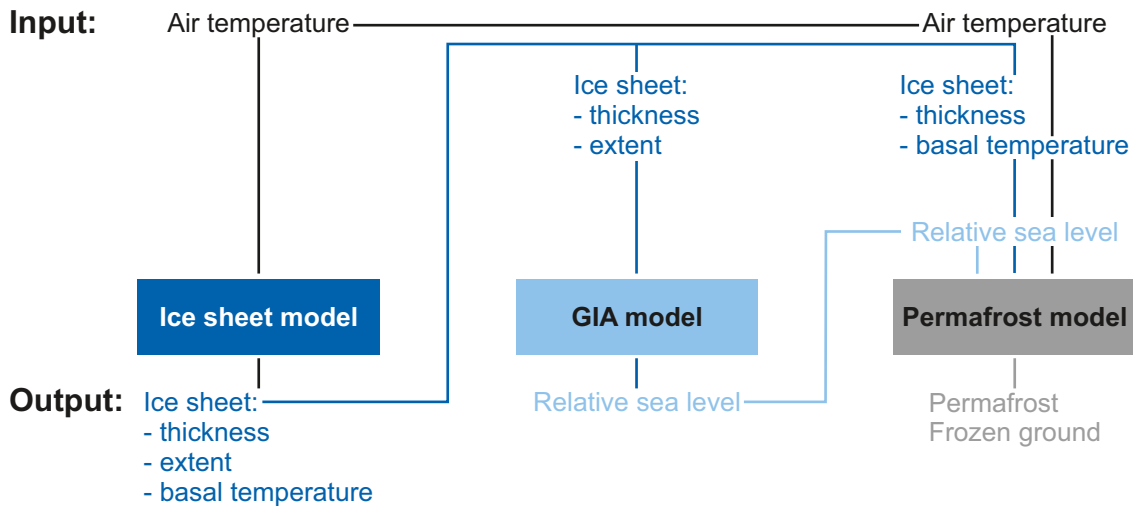


Figure 4-1. Models used to provide boundary conditions for analysis of the impact of climate-related changes on the repository. Only input and output data shared between the models used to generate the boundary conditions are shown.

4.2 Weichselian glacial history

In the previous sections, a reconstruction of Weichselian conditions of importance for the assessment of long-term repository safety has been made. Since the Weichselian constitutes the basis for the construction of the future *reference glacial cycle* in SR-Site, a brief description of the Weichselian glacial history is here presented. Special attention is given to describing ice margin stillstands documented from the Weichselian deglaciation, since such periods are of interest when assessing changes in groundwater flow around a KBS-3 repository (Vidstrand et al. 2010 and SKB 2011/).

4.2.1 Overview of Weichselian glacial history

A review of ice-marginal fluctuations during the Weichselian glaciation in Fennoscandia was presented in (Lokrantz and Sohlenius 2006/). The review is summarized below, and complemented with more recent information.

The Weichselian glaciation started 115 kyrs BP and ended at the transition to the Holocene 11.5 kyrs BP. Terrestrial and marine records show that ice volumes fluctuated drastically during the Weichselian. The marine isotope record contains information on global variations in climate and ice volume during the Weichselian and it has been used to divide the glacial into well-dated Marine Isotope Stages (MIS), MIS 5d to MIS 2 (Table 4-2, Figure 3-13). Dating of terrestrial records is often, however, problematic due to stratigraphical gaps and deposits that are difficult to date. In many areas, the timing of local and regional ice-marginal fluctuations, prior to the LGM, is therefore poorly understood. Age attribution of terrestrial deposits is often interpreted from bio- and lithostratigraphical information, which has been correlated to other records, e.g. marine stratigraphies.

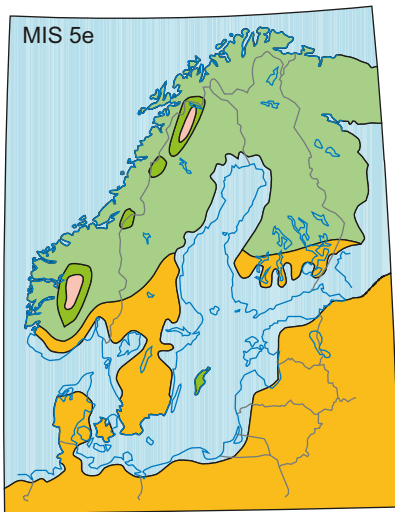
The marine record from Early Weichselian (MIS 5d–5a, Table 4-2) shows two relatively warm interstadial periods at around 105–93 kyrs BP (MIS 5c) and 85–74 kyrs BP (MIS 5a). Stratigraphical data indicate at least two periods with ice-free conditions in northern Fennoscandia, which have been correlated with the two early Weichselian interstadials Brørup and Odderade (MIS 5c and 5a). Few absolute dates have, however, been obtained from deposits formed during these interstadials. It has been suggested that two ice advances occurred during the Early Weichselian and covered a large part of northern Fennoscandia. There are, however, different opinions regarding the southernmost extension of these ice sheets. It has also been suggested that large parts of northern Fennoscandia were free of ice from the onset of MIS 5c until the end of MIS 5a. A reconstruction of the Weichselian ice sheet 90–80 kyrs BP (MIS 5b) is seen in Figure 4-2 (lower left panel) and Figure 4-3 (upper panel). According to the (Lundqvist 1992/ reconstruction (Figure 4-2) the Forsmark region was covered by the ice sheet at this time, whereas according to (Svendsen et al. 2004/ (Figure 4-3) the Forsmark region was just barely ice free.

During the cold MIS 4, global ice volume increased, and the Weichselian ice sheet reached a large configuration covering entire Sweden, Finland and Norway (Figure 4-2 (lower right panel) and Figure 4-3 (middle panel)). At this time, south-central Sweden and the Forsmark region were ice covered.

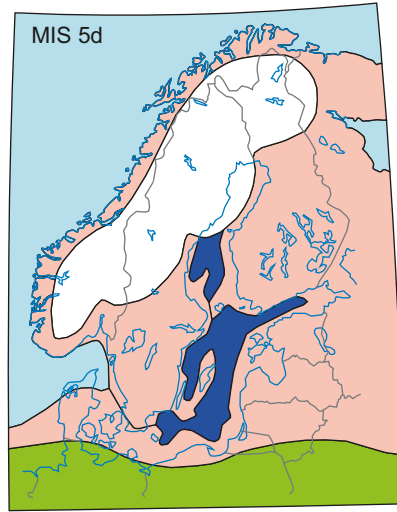
Table 4-2. Marine Isotope Stages, ages, stadials and interstadials of the Weichselian. Regional variations from the denoted warm/cold state occur see (Lokrantz and Sohlenius 2006/, and there is a wide range of names used for each of the stadials/interstadials.

Marine Isotope Stage	Age (kyrs BP)	Stadial/ Interstadial	Warm/Cold	Name (other names are also used)	Weichselian phase
MIS 5d	117–105	Stadial	Cold	Herning	Early Weichselian
MIS 5c	105–93	Interstadial	Warm	Brørup	Early Weichselian
MIS 5b	93–85	Stadial	Cold	Rederstall	Early Weichselian
MIS 5a	85–74	Interstadial	Warm	Odderade	Early Weichselian
MIS 4	74–59	Stadial	Cold	Middle Weichselian stadial	Middle Weichselian
MIS 3	59–24	Interstadials/stadials	Warm/cold	Middle Weichselian interstadials	Middle Weichselian
MIS 2	24–12	Stadial	Cold	Stadial including Last Glacial Maximum	Late Weichselian

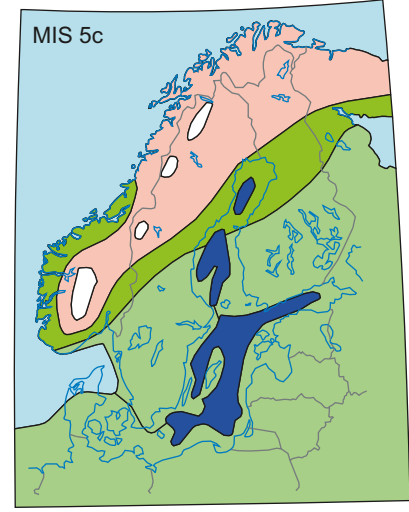
The Eemian Interglacial
c. 130 000–115 000 years BP



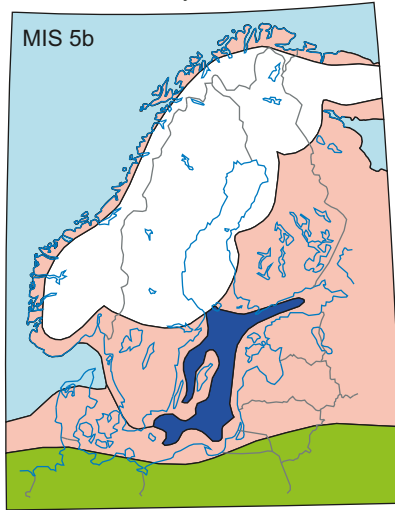
The first Weichselian Stadial
c. 115 000–100 000 years BP



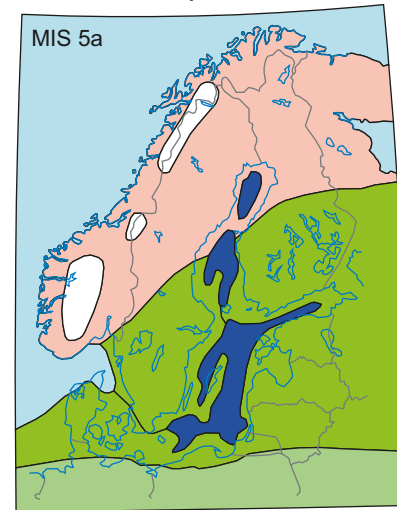
The Jämtland/Brörup Interstadial
c. 100 000–90 000 years BP



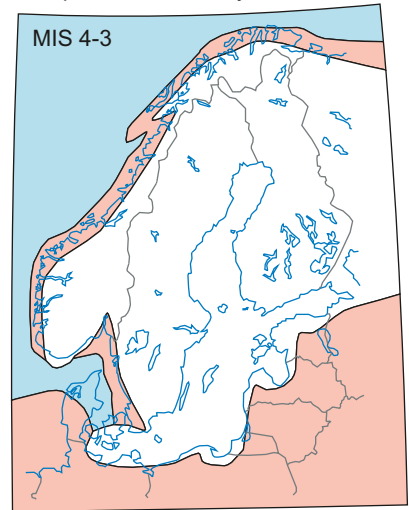
The second Weichselian Stadial
c. 90 000–80 000 years BP



The Tärenöd/Odderade Interstadial
c. 80 000–70 000 years BP



The start of the Weichselian Glaciation's
main phase, c. 50 000 years BP



Borders

-  Shore line
-  National border

Vegetation

-  Glacier
-  Lake
-  Ocean
-  Tundra
-  Birch forest
-  Coniferous forest
-  Temperate forest of broad-leaf trees

0 200 400 800 1200 km



Figure 4-2. Ice sheet and environmental development in northern Europe from the last interglacial (Eemian) to the Middle Weichselian stadial (MIS 4) according to /Lundqvist 1992/ in /Fredén 2002/. Each map shows a snapshot of the environment during each isotope stage. According to this reconstruction, there were two interstadials with ice-free conditions during Early Weichselian (Brörup and Odderade). Furthermore, in this reconstruction most of Fennoscandia was covered by ice from the Middle Weichselian until the deglaciation. More recent studies suggest that this view needs to be revised to include ice-free conditions over large parts of Fennoscandia during significant parts of MIS 3 (59–24 kyrs BP), see the text.

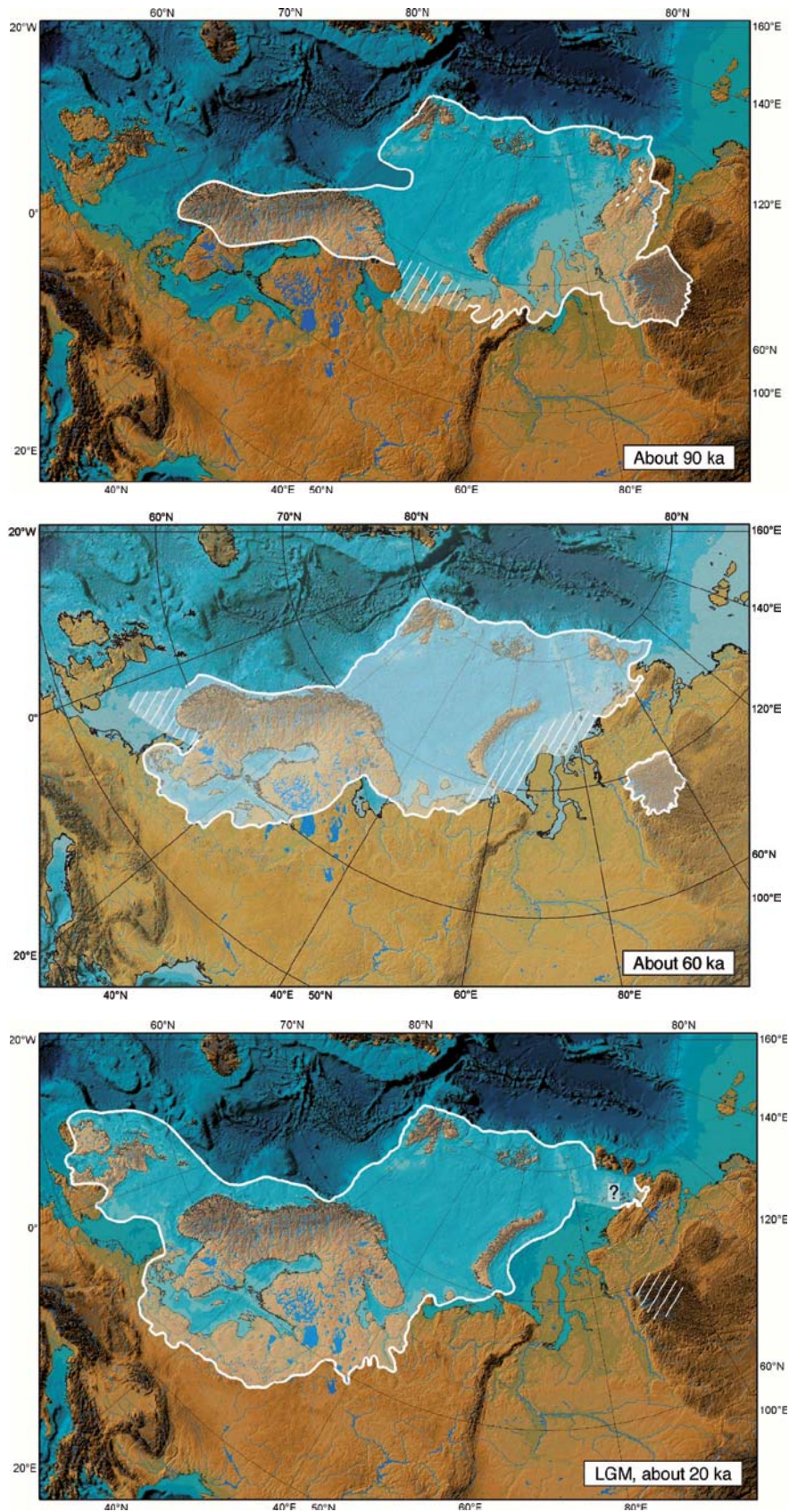


Figure 4-3. Extent of the Eurasian ice sheet during the glacial maximum stages of the Early Weichselian (90–80 kyrs BP, MIS 5b), the Middle Weichselian (60–50 kyrs BP, MIS 4) and the Late Weichselian (LGM, around 20 kyrs BP, MIS 2) as reconstructed from Quaternary geology. From /Svendsen et al. 2004/. Between these stages of maximum ice sheet extent, the ice sheet had a more restricted configuration, see the text.

According to the traditional view the ice sheet that was built up during MIS 4 remained large throughout the Middle Weichselian (74–24 kyrs BP), including MIS 3, up until the final deglaciation (Figure 4-2), e.g. /Lundqvist 1992/. However, MIS 3 was a long period characterized by distinct millennial-scale climate shifts (the so called Dansgaard-Oeschger events), which had a strong impact on the North Atlantic region. In addition, surges of Northern Hemisphere ice sheets prior to some of the longer interstadial events produced large amounts of ice-rafted debris in marine sediments, and led to a rise in global sea-level. Although surges of the Fennoscandian ice sheet could have contributed a significant amount of melt water, little is known about how and to what extent this ice sheet responded to these MIS 3 millennial-scale climate shifts. Data from Norway suggests that the youngest of the ice-free interstadials, traditionally correlated with MIS 5a, actually occurred during MIS 3. In line with this, several recent studies suggest ice-free conditions in large parts of Fennoscandia during MIS 3, e.g. /Helmens 2009a, Wohlfarth 2009, Wohlfarth and Näslund 2010, Mangerud et al. 2011/ and references therein. MIS 3 ice sheet scenarios for Fennoscandia thus range from an almost complete and persistent ice cover, to a significantly smaller ice sheet tentatively terminating in south-central Sweden. These different scenarios are discussed by /Wohlfarth 2010, Helmens and Engels 2010, Lambeck et al. 2010/.

There are still many unsolved questions related to an ice-free interstadial period during parts of MIS 3, many of them concerning the datings of various interstadial and ice advance phases, e.g. /Wohlfarth 2009, Wohlfarth and Näslund 2010/. Nevertheless, it is very likely that the Weichselian ice sheets were considerably more dynamic during the MIS 3 period of the Middle Weichselian than previously thought, in line with the variable climate (see also the description of possible MIS 3 climates in Fennoscandia below). One implication of such a revised MIS 3 glacial history is that the Forsmark site was free of ice for a considerable amount of time during the Middle Weichselian, prior to the LGM. If so, the climate at the end of MIS 3 at Forsmark probably was of a clear periglacial character, allowing for permafrost conditions, see below.

In this context it is also worth noting that the average Quaternary ice sheet configuration over Fennoscandia was considerably smaller than that of a full ice sheet configuration, and also considerably smaller than during the Younger Dryas. For average Quaternary ice sheet conditions, the ice sheet is centred over the Scandinavia mountain range, e.g. /Porter 1989, Kleman et al. 2008/, resulting in ice-free conditions in south-central Sweden including Forsmark.

After the MIS 3 period, during MIS 2, the ice sheet advanced to its maximum extent during the beginning of the Late Weichselian 24–12 kyrs BP. During the LGM the entire area of Fennoscandia was covered by the Weichselian ice sheet, including south-central Sweden and the Forsmark region (Figure 4-3 lower panel). The ice volume was at its largest during the LGM (~20–21 kyrs BP), with the ice margin located in Germany and Poland. The ice reached its maximum LGM position at different times in different regions.

After the LGM, the ice sheet started to retreat across e.g. northern Germany and Poland. The timing of the deglaciation is well dated and the ages have recently been converted into calibrated years. Several re-advances took place during the deglaciation of the Danish and Norwegian coast. There are several ice-marginal zones in south-west Sweden that indicate stillstands or re-advances of the ice front, see below. For instance, the deglaciation was interrupted during the Younger Dryas stadial (12.5–11.5 kyrs BP) and there were ice re-advances and stillstands in the middle part of Sweden and southern Finland, whereas coastal areas in the west were characterised by large re-advances. The ice-marginal deposits formed during the Younger Dryas can be followed around the entirety of Fennoscandia. After the Younger Dryas, the ice retreated towards the Fennoscandian mountain range more or less continuously.

Deep weathered bedrock of Pre-Quaternary age occurs in parts of Småland and in the inner parts of northern Sweden. These deposits indicate low or negligible erosion in these regions. In the inner part of Norrbotten there are morphological features, Veiki moraines, which, according to several authors, were formed during the first Weichselian ice advance (MIS 5d). In Småland there are till-covered eskers, which may have been formed prior to the latest glacial advance. Areas with deep weathered bedrock and those with Quaternary deposits older than the last glaciation coincide to a large extent. These areas are indicators of cold-based ice and of low glacial erosion.

For more detailed descriptions of the Weichselian glacial history, see e.g. /Lokrantz and Sohlenius 2006, Lundqvist 2007, Wohlfarth 2010, Helmens and Engels 2010, Lambeck et al. 2010/. For recent examples of reconstructions of last glacial cycle Northern Hemisphere ice sheets, see e.g. /Peltier 2004, Svendsen et al. 2004, Peyaud et al. 2007, Charbit et al. 2007, Kleman et al. 2008, Bonelli et al. 2009, Clark et al. 2009/.

4.2.2 Ice-marginal stillstands

From Quaternary geological information it is known that temporary halts in the ice sheet retreat took place several times in southern and south-central Sweden during the Weichselian deglaciation, e.g. /Lundqvist and Wohlfarth 2000, Fredén 2002/. Similar, and in cases corresponding, halts are also documented from e.g. Finland, Denmark, Norway, Russia, Poland and Germany e.g. /Lagerlund et al. 1995, Marks 2002, Houmark-Nielsen and Kjær 2003, Lunkka et al. 2004/. At these locations, dated marginal moraines, once formed along the former ice sheet margin, indicate areas and periods when the ice margin was more or less stable at a certain location. No traces of such moraines, indicative of temporary halts, have been found from the growth phases of the Weichselian ice sheet. It is possible that stillstands did occur also during growth phases, but that resulting moraines have been obliterated by the subsequent ice coverage. However, during the Early Weichselian stadials, i.e. during Marine Isotope Stages 5d (117–105 kyrs BP) and 5b (93–85 kyrs BP), maximum ice configurations, with ice margins that may have been quasi stable for some period of time, have been envisaged for central Sweden /Lundqvist 1992/, see also /Lokrantz and Sohlenius 2006/.

The longest and most prominent halt during the last deglaciation took place during the cold Younger Dryas stadial. On the basis of data from the GRIP ice core from Greenland, the Younger Dryas stadial began around 12,800 years BP and ended around 11,500 BP, resulting in a ~1,300 year long Younger Dryas period. Quaternary geological information suggests that the associated Younger Dryas ice sheet margin stillstands in Sweden occurred during a period of around 900 years /Fredén 2002/. On glaciological grounds, /Fastook and Holmlund 1994/ concluded that the climatic event responsible for the Younger Dryas stillstand could have been short, even less than 500 years.

It should be noted however that during the Younger Dryas period, as well as for several other less prominent stillstands south of the Younger Dryas moraine complex, the position of the ice margin was not completely stable. Instead, as a response to climate variability and ice sheet dynamics, the ice front typically oscillated back and forward, in cases up to several tens of km, e.g. /Lundqvist and Wohlfarth 2000, Lunkka et al. 2004/. For the Younger Dryas, the resulting zone of ice-marginal deposits is typically around 20–25 km wide in central and eastern Sweden /Fredén 2002/. During shorter halts in the deglaciation, this zone may be considerably narrower or absent. During phases of maximum ice sheet configuration, such as during the LGM, the ice margin typically also oscillates back and forward as a response to ice sheet dynamics and climate variability.

South of the Younger Dryas zone, at least six older stillstands in the Weichselian deglaciation of southern Sweden have been documented /Lundqvist and Wohlfarth 2000/. At several of these sites, ice-marginal moraines have been suggested to have formed during periods of up to 100–200 years, such as the large Göteborg Moraine which formed sometime between 15,400 and 14,500 kyrs BP /Lundqvist and Wohlfarth 2000/. The suggested, often maximum, formation times of these moraines indicate that the ice margin was relatively stable for these periods or shorter. In southern Finland, it has been estimated that the largest Younger Dryas end moraine complexes, i.e. the First and Second Salpausselkä end moraines, as well as the younger Central Finland end-moraine, also were formed during periods up to a few hundred years long /Lunkka et al. 2004/. These estimates thus give an indication of the duration of periods with stable ice margin position during the last deglaciation.

In summary, it may be concluded that during the deglaciation of the Weichselian ice sheet, the general ice sheet retreat temporarily halted several times. This is seen from dated ice-marginal moraines, including the deposits from the Younger Dryas stadial. During such halts, the ice margin either oscillated back and forth or moved slowly within a zone that could be many km wide, in the case of the Younger Dryas, several tens of km. During the formation of individual moraine ridges, the ice margin is estimated to have been at stable positions for up to a few hundred years. It has to be assumed that similar types of stillstands may occur also during phases of ice sheet advance, see Section 4.5.1.

4.3 Examples of Weichselian climates

During the Weichselian, climate shifted many times between warmer and colder periods, as reflected in the growth and decay phases of the Weichselian ice sheet, see Section 4.2.1. The variability and range within which the climate shifted during the last glacial cycle could be expected also during future glacial cycles. Therefore, quantitative descriptions of prevailing climate conditions for periods with fundamentally different climates during the Weichselian are given below for Sweden and the Forsmark region, examples of climates that are of high relevance for e.g. the SR-Site *reference glacial cycle* presented in Section 4.5.

The aim of the following descriptions of Weichselian climates is not to give a full review of all that is known on climate and climate variability during the last glaciation. Instead, the intention is to provide examples that demonstrate a range within which the climate varied during the Weichselian by selecting climate reconstructions for both stadial and interstadial phases and to cover a broad time span of the glacial cycle.

4.3.1 Early Weichselian (117–74 kyrs BP)

The Fennoscandian climate during the Early Weichselian (MIS 5d–5a, 117–74 kyrs BP) varied significantly, as reflected in the glacial history with intervening stadial and interstadial conditions described above. Detailed quantifications of Fennoscandian climate conditions for these early periods are very rare. However, in northern Fennoscandia, quantifications of interstadial climate conditions have been made within an SR-Site project from the Sokli sediment sequence in Finnish Lapland, northern Fennoscandia e.g. /Helmens 2009a/. The sediment record at Sokli is one of the few well-dated sites in northern Europe that covers the Early Weichselian in high detail. The Sokli sequence consists of tills, glacio-fluvial beds, and fluvial beds, interlayered with fossil-rich lacustrine sediments that according to multiple accelerator mass spectrometer (AMS) ^{14}C and optically stimulated luminescence (OSL) datings extend from the present into the penultimate glacial, i.e. representing the last ~130 kyrs, e.g. /Helmens 2009a/.

Past environmental and climate conditions have been reconstructed for MIS 5d (the Herning stadial 117–105 kyrs BP, Table 4-2) by analysis of insect remnants and botanical and zoological macro remains /Engels et al. 2010/. The results show that, for the ice-free stadial conditions at the investigated site, the summer July air temperature may have been ~7°C, which is ~6°C colder than the present summer mean temperature (13°C), and indicative of arctic climate conditions.

During MIS 5c (the Brørup interstadial, 105–93 kyrs BP, Table 4-2), summer temperatures inferred from plant macrofossil remnants indicate surprisingly warm conditions for northern Fennoscandia /Väliranta et al. 2009, Engels et al. 2010/. Minimum July temperatures were as high as 16°C, which is 3°C warmer than at present /Väliranta et al. 2009/. At that time, open birch woodland existed at the site within a subarctic climate. This result is in contrast to other (lower-resolution) reconstructions from northern Fennoscandia indicate MIS 5c temperatures 6–7°C lower than present, see /Engels et al. 2010/. However, several central European sites indicate that there was a phase during the MIS 5d interstadial that was characterized by high summer temperatures, and a comparison between the high-resolution reconstructions from western Europe and the results presented in /Engels et al. 2010/ suggests that the north–south July air temperature gradient between the mid- and high-latitudes was much weaker during MIS 5c than at present.

One suggested reason for the warm climate conditions during this interstadial could be that the contemporary astronomical forcing resulted in a weaker north-south temperature gradient and a longer growing period, creating more favourable climate conditions that at present /Väliranta et al. 2009/.

4.3.2 Middle Weichselian (74–24 kyrs BP)

Examples of Fennoscandian climates during the MIS 3 interstadial (59–24 kyrs BP) have been studied by use of geological information /Helmens 2009a, Wohlfarth 2009/ and by climate modelling /Kjellström et al. 2009b (including erratum Feb 2010)/. MIS 3 covers a long time period that includes both rapid millennial-scale climate shifts and longer trends in changing climate, see /Wohlfarth 2009/. A few examples of climates occurring during MIS 3 are given below.

Early MIS 3 (at ~50 kyrs BP)

A comprehensive environmental reconstruction of early MIS 3 conditions, at around 50 kyrs BP, was made based on multi-proxy analysis on a two metre thick laminated, lacustrine clay-silt sequence obtained at the Sokli site in northern Finland /Helmens 2009a/. The analyses included lithological characteristics; organic content (loss-on-ignition, LOI); plant microfossils (pollen, spores, algal and fungal remains); macrofossils of plants (e.g. seeds, moss remains) and of aquatic animals (e.g. statoblasts of Bryozoa); head-capsules of chironomids (i.e. aquatic insects); and diatoms and other siliceous microfossils (e.g. phytolits, chrysophyte stomatocysts). Additionally, geomorphic evidence and analysis of DEM data are employed in the environmental reconstruction. Mean July temperatures were reconstructed by applying transfer functions to the pollen, chironomid and diatom records.

The results have been surprising in various aspects, seriously challenging previous concepts on environmental conditions during early MIS 3 in the near-central area of the Weichselian glaciation. Traditionally, the area is thought to have been ice covered throughout MIS 4–2, i.e. from around 60 kyrs BP to the final deglaciation, see above. /Helmens 2009a/ show not only ice-free interstadial conditions but also climate warming to present-day temperatures. The laminated sediments seem to have been deposited in a sheltered embayment of a glacial lake impounded along the ice front of the Weichselian ice sheet. Throughout the deposition of the lacustrine sediments, the reconstructed terrestrial ecosystem on the deglaciated land is low-arctic shrub tundra very similar in composition to modern tundra in the continental sector of northern Fennoscandia. The distributional ranges of pine and tree birch were probably only a few hundred kilometres south or south-east of the Sokli site. This is concordant with the sparse evidence for the presence of boreal tree taxa during MIS 3 in the Baltic countries and further east in Europe but contradicts with the commonly inferred treeless tundra or grass-dominated steppe conditions in central Europe.

Mean July air temperatures in the magnitude of present-day values are reconstructed by the chironomid and diatom records as well as by fossils from aquatic plants and Bryozoa. Temperature inferences based on the terrestrial pollen are consistently lower than the temperatures reconstructed from the fossil aquatic assemblages. It is possible that the regional terrestrial and the local aquatic systems responded differently to the climatic and landscape features at around 50 kyrs BP. Warmest and moistest conditions are recorded in the lower part of the laminated lacustrine sequence. This is consistent with the pattern of the Greenland millennium-scale Dansgaard-Oeschger interstadials in which abrupt warming is followed by a gradual cooling. The chironomid-inferred mean July air temperatures amount to around 13°C (i.e. the current temperature) $\pm 1.15^\circ\text{C}$ in the lower part of the lake sequence and to around 12 $\pm 1.15^\circ\text{C}$ in the upper part. The mean July air temperatures inferred from the terrestrial pollen data lie within the range of around 12 $\pm 1.5^\circ\text{C}$ (lower part of sequence) and around 11 $\pm 1.5^\circ\text{C}$ (higher part of sequence). High summer temperatures are ascribed in part to enhanced July insolation compared with present at the high latitude site of the site.

Comparison with recently published, well-dated sediment sequences in eastern and western Finland suggests ice-free and warm conditions in major part of eastern Fennoscandia at ~50 kyrs BP. Open birch forest seems to be registered in eastern Finland during part of the warming event. Direct evidence is lacking to reconstruct the total time span with ice-free conditions at the studied sites. It is argued that the Sokli site was glaciated during the overall colder late MIS 3. The absence of well-dated geological data in northern Sweden hampers a reconstruction of the total ice-marginal retreat in the continental sector of the Fennoscandian Ice Sheet during the early MIS 3 climate warming event. For more details on this study, see /Helmens et al. 2007a, Engels et al. 2008, Bos et al. 2009, Helmens 2009a, Helmens et al. 2009b, Helmens and Engels 2010, Engels et al. 2010/.

A warm climate during early MIS 3, such as reconstructed for northern Fennoscandia by e.g. /Helmens 2009a, is in line with, and probably necessary for, a deglaciation of the large ice sheet that existed during MIS 4, see above.

Middle MIS 3 (at 44 kyrs BP)

A comprehensive climate modelling study was made to investigate climate extremes within which the climate in Fennoscandia may vary on a 100 kyr time scale /Kjellström et al. 2009b, including erratum dated Feb 2010/. Three different periods were simulated, a cold glacial climate (at LGM,

~21 kyrs BP), a periglacial climate (at MIS 3, 44 kyrs BP) and a warm future climate dominated by global warming (a few thousands of years after present). In the present section, results from the periglacial climate simulation are presented. Results from the LGM climate simulation are presented in Section 4.3.3 whereas results from the global warming simulation are described in Section 5.1.7

In order to give a detailed example of a modelled periglacial MIS 3 climate over northern Europe, climate modelling was performed using the global climate model (GCM) that produced boundary conditions that were used by a regional climate model (RCM) /Kjellström et al. 2009b/. This model study was designed to also test whether a cold and dry climate favourable for permafrost growth would exist in the ice-free regions surrounding a Fennoscandian MIS 3 ice sheet with a restricted ice configuration. Based on forcing conditions for a selected period during MIS 3 (Greenland stadial 12 at 44 kyrs BP), a simulation of middle MIS 3 climate conditions was made with the climate models. For the simulations performed and analyzed within this study, atmospheric and land components of the CCSM3 used a grid spacing of approximately 2.8° in latitude and longitude. The vertical resolution is 26 levels in the atmosphere and 40 levels extending to 5.5-km depth in the ocean. The regional climate model used a horizontal resolution of 50 km and a time resolution of 30 minutes. For details on the models, how they were employed, and a discussion on climate model uncertainties, see /Kjellström et al. 2009b/.

The choice of period to simulate for MIS 3 followed from a workshop on MIS 3 organised by SKB in September 2007 /Näslund et al. 2008/ with the specific purpose of supporting this selection. Only limited and in some cases controversial, palaeo-information is available to reconstruct the extent of the Fennoscandian ice sheet during the different warm and cold intervals of MIS 3. We here assumed, in line with several recent studies, see above, that the southern part of Fennoscandia was ice free during some of the MIS 3 stadials.

The modelling activities included the use of; i) a fully coupled Atmosphere-Ocean General Circulation Model (AOGCM), ii) a Regional Climate Model (RCM), and iii) a dynamic vegetation model (DVM). The AOGCM was used to simulate the global climate in steady-state simulation for the selected time period. Even though AOGCMs are powerful models they are relatively coarse in their resolution due to computational limitations. Therefore, the output from the AOGCM was used as input to the RCM that provides output at a relatively high horizontal resolution for Europe. Both global and regional climate models hold descriptions of the land surface, including vegetation. In the regional model, it is important to describe the vegetation cover with a high degree of regional detail. Such details are missing in available global fields and details of the vegetation cover have to be estimated, based on the global fields and consideration of among other things land/sea distribution. In order to improve the representation of the regional vegetation, a dynamic vegetation model was used to simulate the European vegetation resulting from the RCM-simulated climate. In a subsequent step, the new vegetation was used in a new RCM simulation that provides the final climate output. For the studied MIS 3 period, data on relevant climate parameters was extracted from the regional model for the Forsmark area.

The global model simulation of the periglacial MIS 3 climate used a CO₂ concentration in the atmosphere of 200 ppm /Kjellström et al. 2009b/. An ice sheet with a restricted configuration was assumed, and in line with this, a simulated MIS 3 ice sheet configuration obtained from the Weichselian ice sheet reconstruction described in Section 3.1.4 was used /Kjellström et al. 2009b/. For a detailed description of the assumptions made in the modelling process, model forcing and initial conditions (such as astronomical and solar forcing, concentration of greenhouse gases and aerosols in the atmosphere, extents of ice sheets, distribution of land and sea, topography and vegetation), also see /Kjellström et al. 2009b/.

In addition to the modelling activities, an effort was made to collect palaeoclimatic information by compiling various MIS 3 and LGM proxy data from different sources /Kjellström et al. 2009b, Wohlfarth 2009/. An attempt to use part of this palaeoclimatic information to constrain the forcing conditions used in the climate models was made. Other proxy data were used for model evaluation purposes. Results from the global climate model were compared with proxy records of sea-surface temperatures and with terrestrial climate records. The regional climate model results have been compared with existing terrestrial palaeoclimate records from Europe.

Global climate

Figure 4-4 shows the simulated global warming climate from the middle MIS 3 simulation. Seasonal mean changes in temperature as compared with a simulation of the pre-industrial climate (with forcing conditions set at levels consistent with those preceding the 18th century) climate are also shown. Figure 4-5 shows the development over time of the simulated global mean temperature for this steady-state climate simulation. The figure also shows the temperature development of a LGM climate simulation that the MIS 3 simulation was initiated from.

The annual mean surface cooling in the MIS 3 simulation as compared with pre-industrial conditions is most pronounced over the Laurentide and the Fennoscandian ice sheets and over the Greenland-Iceland-Norwegian Sea, with a maximum cooling of 25°C (Figure 4-4). A large portion of the cooling over the Fennoscandian and Laurentide ice sheets is due to the increased elevation over the ice sheet. The cooling amounts to 5–10°C north of 40°N in the Atlantic Ocean, the Arctic Ocean and over Antarctica and the Southern Ocean. The sea-ice extent is increased in the MIS 3 simulation in the North Atlantic and north Pacific as compared with the pre-industrial simulation (Figure 4-4).

Even though proxy data for the period around 44 kyrs BP are sparse, comparison with available sea surface temperature data shows that the globally modelled temperatures and proxy data are in reasonable agreement. For further results and discussion of the MIS 3 simulation from the global climate model, and for details about the comparison with MIS 3 climate proxy data, see /Kjellström et al. 2009b/.

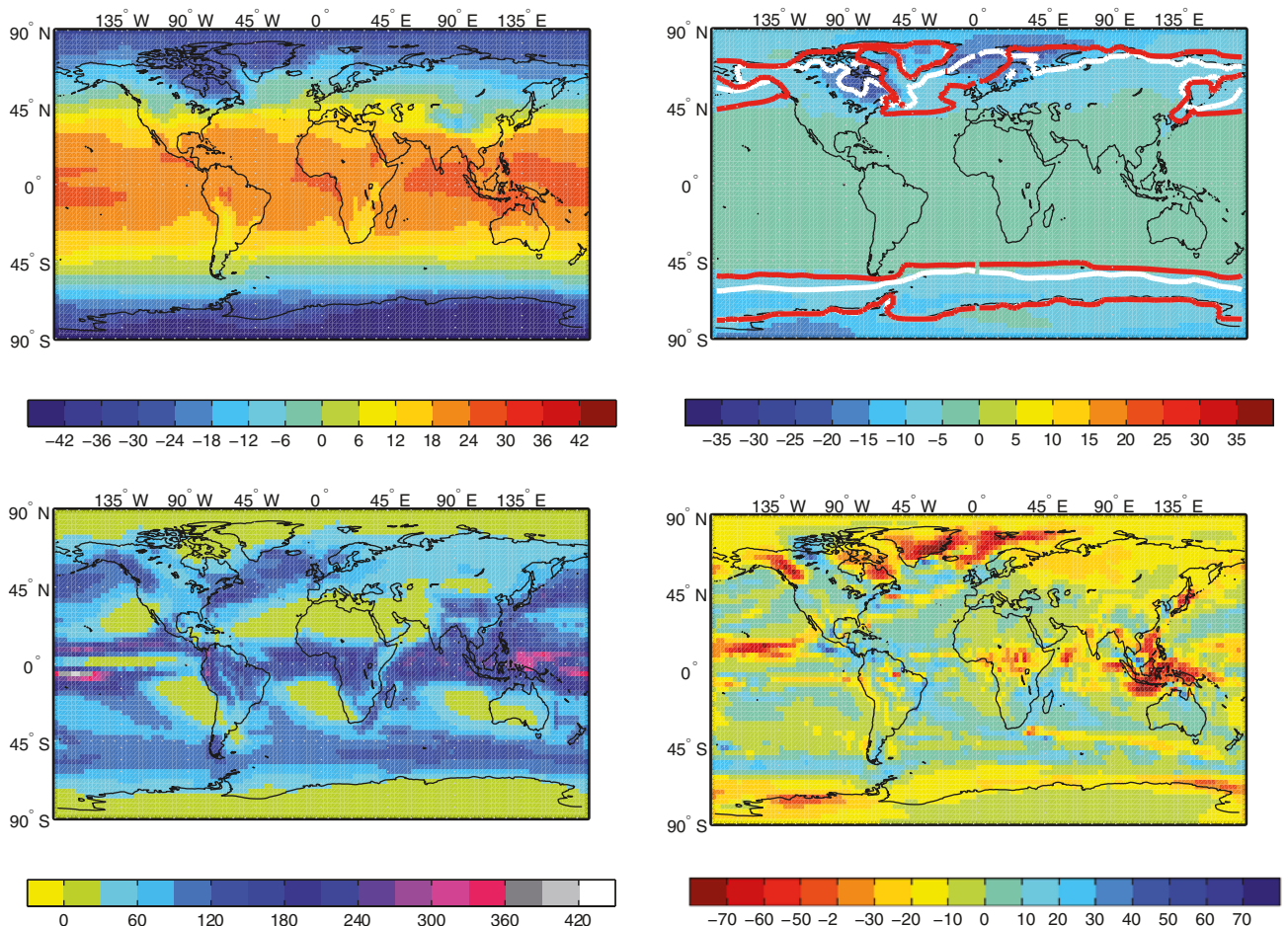


Figure 4-4. Annual mean near-surface air temperature in the MIS 3 simulation (upper left) and the difference compared with a simulated pre-industrial climate (upper right). Units are °C. Also shown is the annual mean sea ice edge (defined at 10% areal sea ice cover) for the pre-industrial simulation (white; upper right) and the MIS 3 simulation (red; upper right). The lower panels show the simulated precipitation (lower left) and the difference compared with the simulated pre-industrial climate (lower right). Units are mm/month. From /Kjellström et al. 2009b/.

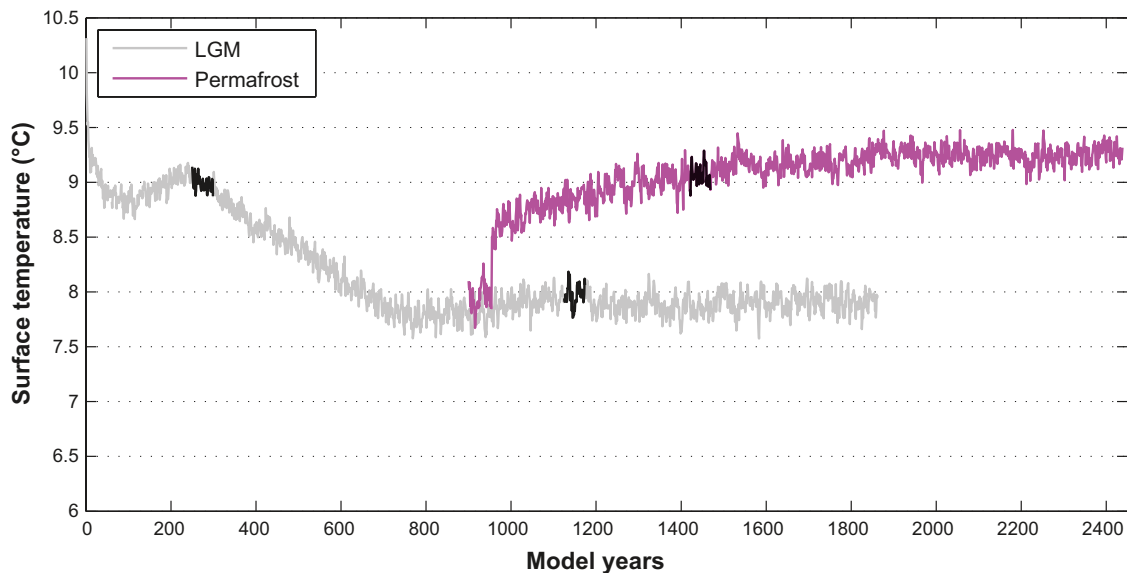


Figure 4-5. Annual global mean near-surface air temperature in the MIS 3 (pink) and LGM (grey) climate simulation. Black parts of the curves marks the 50-year periods analysed in /Kjellström et al. 2010/ and presented here. Units are °C. From /Kjellström et al. 2009b erratum Feb 2010/.

Climate in Europe and Sweden

The regional climate model was then used to downscale the model results of the global climate model in order to obtain a higher resolution data over Europe and Sweden. The resulting climate over Europe was used to produce a new vegetation distribution with the vegetation model. This vegetation was in turn, used as input to the regional climate model, to produce a climate in line with the new vegetation. An evaluation of the results from this iterative process is given in /Kjellström et al. 2009b/. Figure 4-6 and 4-7 presents selected results on temperature and precipitation from the regional modelling.

During this part of the middle Weichselian, the temperature climate is dominated by a very strong seasonal cycle (Figure 4-7) and a pronounced north-south gradient in the winter (Figure 4-6, upper row, middle panel). In the north, the effect of the Weichselian ice sheet is clearly seen in the isolines of temperature showing low temperatures in parts of Fennoscandia. The isotherm showing 0°C annual mean temperature goes south of Ireland, through England and the southern parts of Denmark, just south of Sweden and then eastwards (Figure 4-6, upper row, right panel). Compared with the present climate (1961–2000), the annual mean temperature in the MIS 3 simulation is ~5°C colder around the Mediterranean, 5–10°C colder in central Europe and more than 8°C colder in the ice-free parts of Fennoscandia (Figure 4-6, lower row, right panel). The same values as for difference in annual temperature apply for winter temperature in southern and central Europe. The winter temperature of the British Isles is 10–15°C colder and the southern tip of Fennoscandia around 15°C colder in comparison with the present climate (Figure 4-6, lower row, middle panel). Over the ice sheet in northern Fennoscandia, temperatures are at least 30°C colder than in the present climate (1961–2000) simulation. On Iceland and over the Norwegian Sea, the difference from the late 20th century is even larger. In summer, most of continental Europe is 0–5°C colder than in the late 20th century, western Europe and the British Isles are 5–10°C colder and northern Fennoscandia is 10–15°C colder than in the simulated present climate (Figure 4-6, lower row, left panel).

The annual mean precipitation in the MIS 3 simulation is characterized by considerably drier conditions than in the simulated present climate (1961–2000), by more than 360 mm/year in large parts of Fennoscandia and over the North Atlantic, and by an increase in precipitation of up to 360 mm/year in parts of the southwest (Figure 4-8, upper row right panel). In the rest of the model domain, differences are, with few exceptions, smaller.

The drier climate in northern Europe is reflected in the seasonal cycle of precipitation. For Sweden there is a reduction of more than a factor of two in winter and substantial reduction also during summer (Figure 4-9). Further south, the reduction is most evident in the winter half of the year whereas in southernmost Europe the changes relative to the present climate are small for all months.

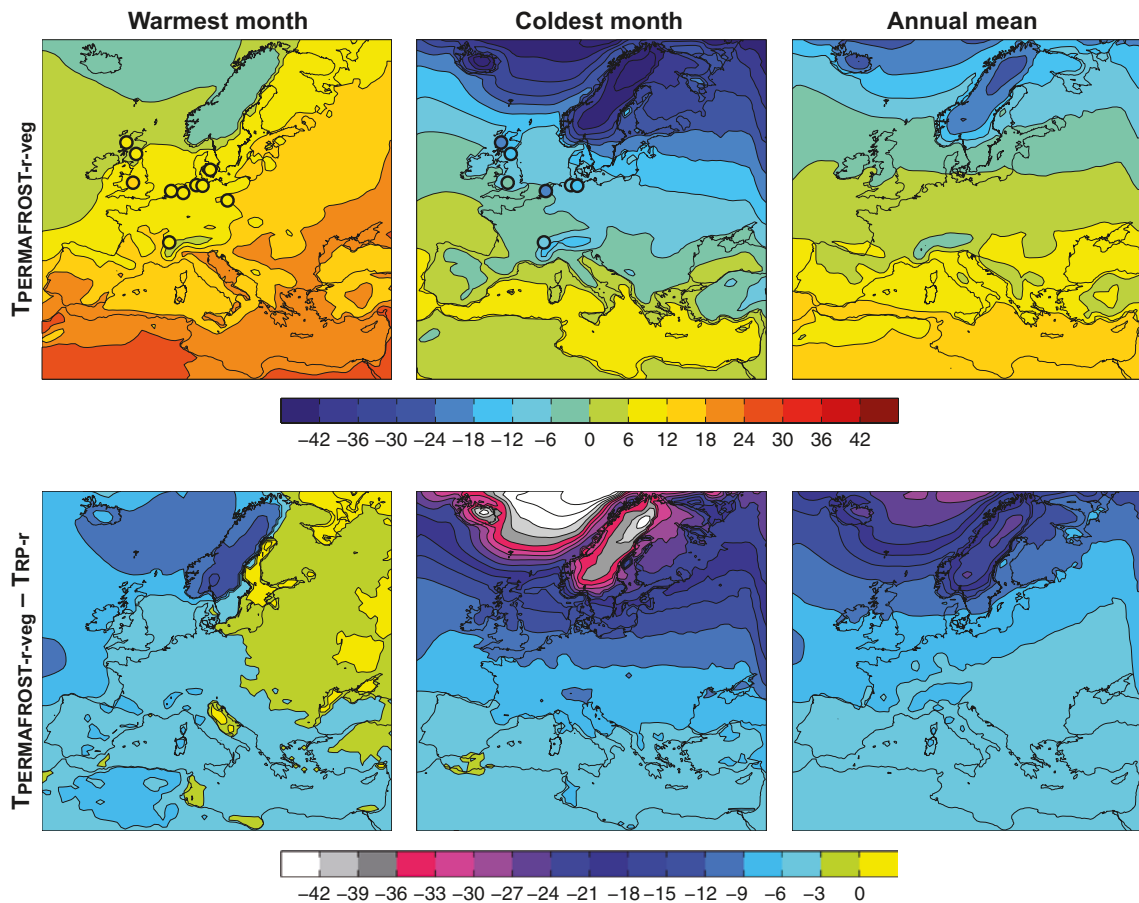


Figure 4-6. Mean air temperatures of the warmest month, coldest month and annual mean in the MIS 3 simulation (top). Shown also are temperature estimates based on proxy data as described in /Kjellström et al. 2009b, Section 2.4/ (coloured circles). The lower row shows the differences between the simulated MIS 3 climate and a recent-past climate simulated for the period 1961–2000. From /Kjellström et al. 2009b/.

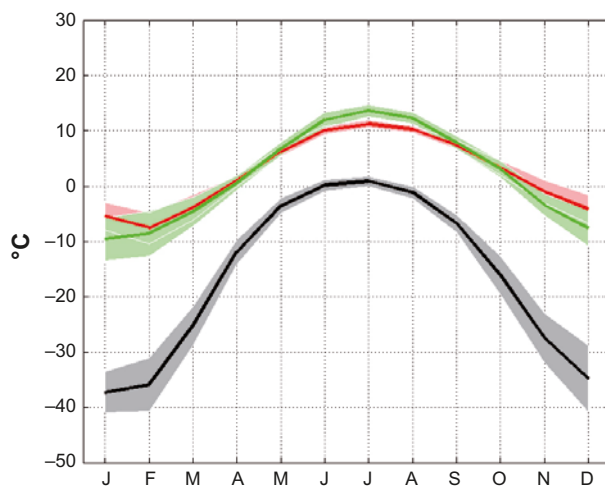


Figure 4-7. Annual temperature range in Sweden for MIS 3 (black), simulated present climate (red) and according to the CRU (Climate Research Unit, East Anglia) observational data for the time period 1961–1990 (green). Shaded areas in corresponding colours indicate the ± 1 standard deviation range of individual monthly averages in the three data sets. From /Kjellström et al. 2009b/.

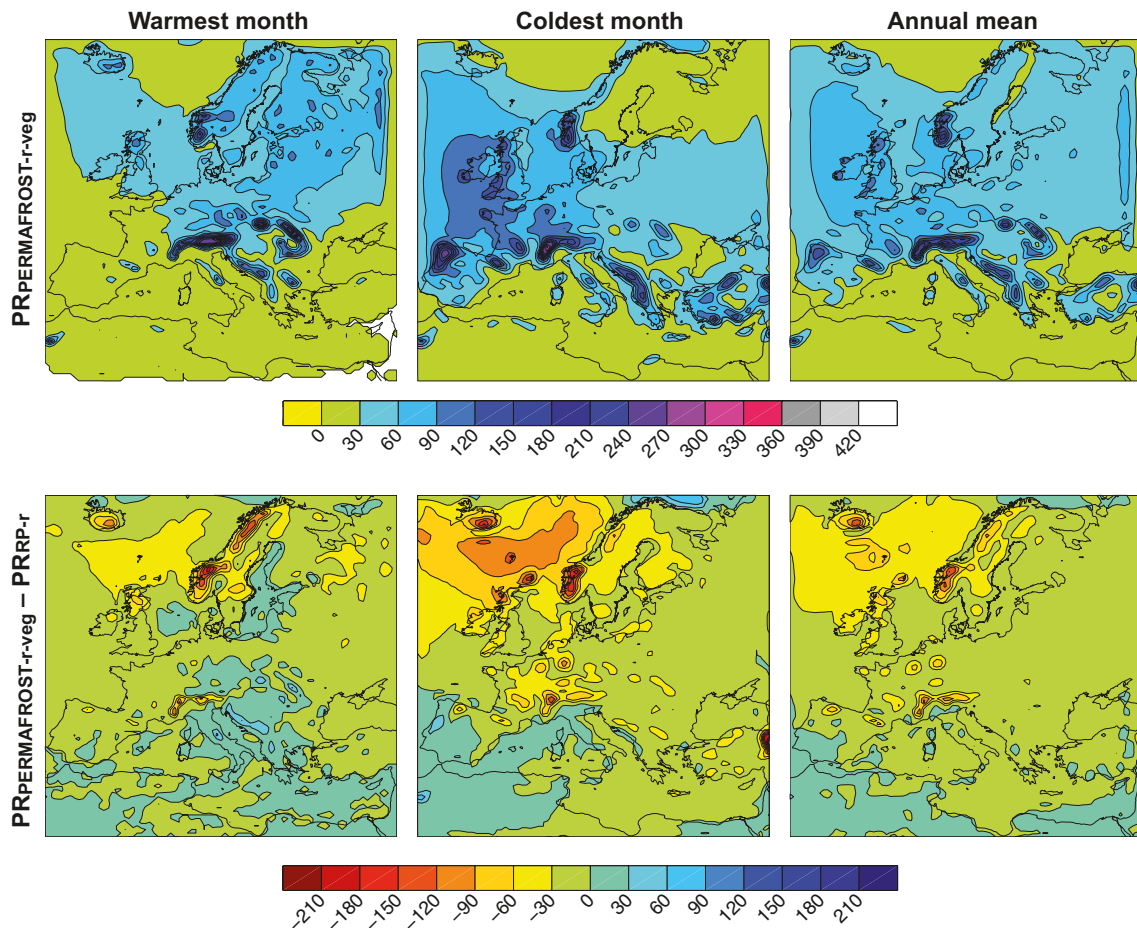


Figure 4-8. Mean precipitation of the warmest month, coldest month and annual mean in the MIS 3 climate simulation (upper row). Also shown are differences between MIS 3 simulation and the simulation of the present (1961–2000) climate. Units are mm/month. From /Kjellström et al. 2009b/.

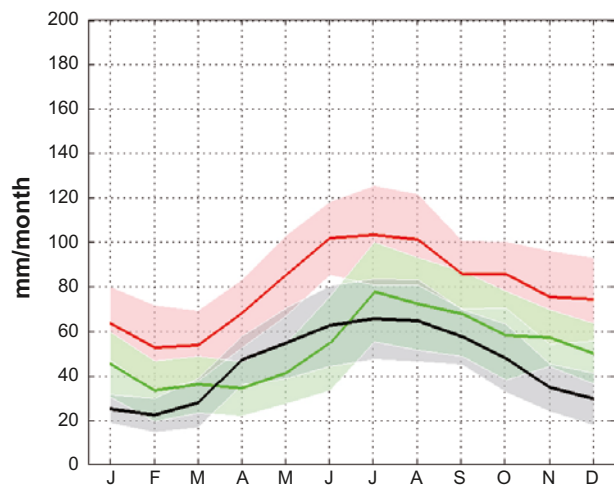


Figure 4-9. Annual precipitation range in Sweden in the MIS 3 simulation (black), present climate simulation (1961–2000) (red) and according to the CRU observational data (green). Shaded areas in corresponding colours indicate the ± 1 standard deviation range of individual monthly averages in the three data sets. From /Kjellström et al. 2009b/.

For further results, on the European scale, from the MIS 3 climate simulations, including results and discussion of the simulations of MIS 3 vegetation, comparisons with climate proxy data, and comparisons with other model simulations of MIS 3 climates, see /Kjellström et al. 2009b/.

Do the results support a cold and dry climate favourable for permafrost growth? /Heginbottom et al. 1995/ examined the relation between ground temperature and permafrost continuity. An annual ground temperature of between -5 and -2°C is defined as the boundary for discontinuous permafrost (50–90% of landscape covered by permafrost) and -5°C and colder as the boundary for continuous permafrost (90–100%). However, it is also stated that a large part of areas with continuous permafrost has a ground temperature warmer than -5°C . Since the ground temperature differs from the near-surface air temperature by a few degrees, see Section 3.4, the simulated annual mean ground temperatures over Europe for MIS 3 are presented in Figure 4-10.

In central and northern Fennoscandia, outside of the prescribed ice sheet, the modelled MIS 3 annual average ground temperature is colder than -5°C (Figure 4-10), which suggest that the climate conditions are favourable for development of continuous permafrost. South of this, the modelled annual average ground temperature increases, reaching 0°C in the southernmost parts of Fennoscandia. The higher ground temperatures in the southern areas including northernmost Denmark, southern Sweden, Estonia and part of what today is the Baltic Sea and Gulf of Finland do not fulfil the thermal requirements for extensive permafrost. However, it is cold enough for sporadic permafrost (less than 50% of landscape covered), which may exist when the annual mean ground temperature is between 0 and -2°C . Based on these results of /Kjellström et al. 2009b/ it is concluded that conditions are favourable for permafrost growth in the inferred ice-free parts of Fennoscandia.

Do the results support a restricted MIS 3 Fennoscandian ice sheet? The global and regional climate models do not include dynamical modelling of ice sheets and thus an ice sheet cannot form in the models, even if the climate conditions are favourable for ice sheet growth. The snowpack is, however, allowed to build up in the model. If the snow depth increases in time in a specific region, we can take this as an indication that an ice sheet would grow in this region if such processes were included in the model. However, the opposite situation, a lack of snow accumulation in front of, or at the margins of, a prescribed ice sheet, does not necessarily mean that the ice sheet would not grow (simply the lowermost part of the ice sheet would have a net mass loss, which is typical for ice sheets ending on land). Growth of the ice sheet could still be possible if the precipitation over the ice sheet were large enough compared with its mass loss by melting, i.e. if conditions for the common pattern of ice sheet growth were satisfied.

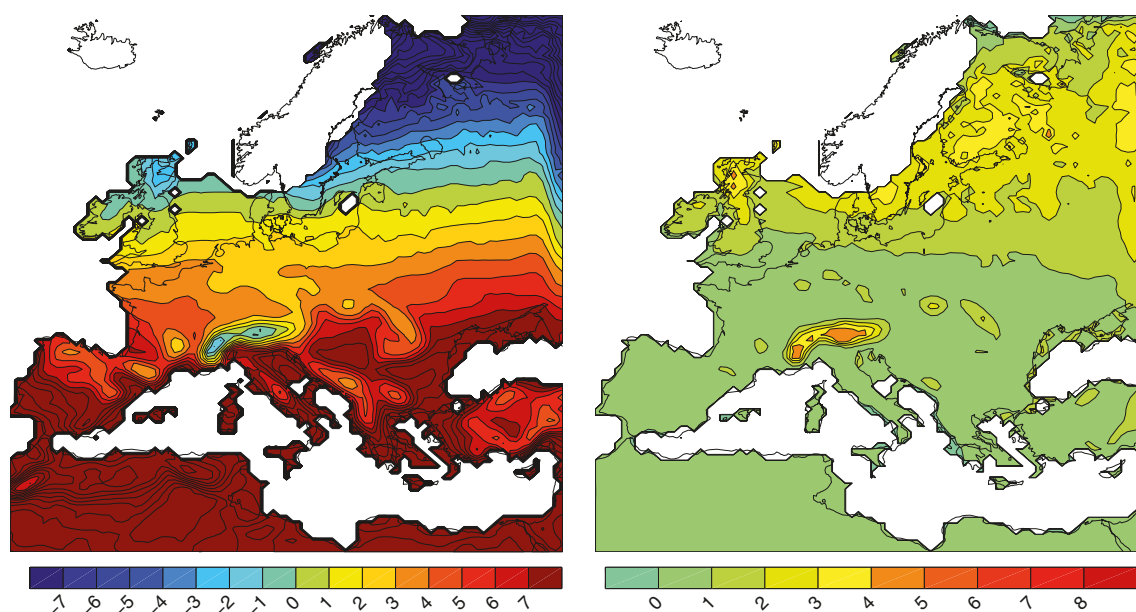


Figure 4-10. Annual mean ground temperature (left) and difference between near-surface air temperature and the ground temperature (right) in the MIS 3 simulation. Units are $^{\circ}\text{C}$. White areas in Fennoscandia are covered by the prescribed restricted MIS 3 ice sheet. From /Kjellström et al. 2009b/.

In the middle MIS 3 simulation, the snow depth in eastern Sweden, including the Forsmark region, does not increase in time. The annual minimum snow depth (occurring in September) is close to zero (varying from 0–0.02 m equivalent water depth). For the issue of whether the simulated climate is in line with the prescribed restricted middle MIS 3 ice sheet configuration, with ice-free conditions in e.g. the Forsmark region (Figure 4-10), one can therefore conclude that 1) an ice sheet would not grow locally from the local precipitation in front of the ice margin, 2) the modelled temperature and precipitation climate in front of the ice sheet is consistent with the assumed ice-free conditions and restricted ice sheet coverage, but it does not exclude the possibility of a larger ice sheet.

Climate in the Forsmark region

Figure 4-11 and 4-12 show average air temperature and precipitation for a 50 year period of the simulated MIS 3 climate, and a comparison with the climate simulated for present conditions. The results show that the climate is significantly colder and drier than at present, with arctic climate conditions prevailing in the Forsmark region.

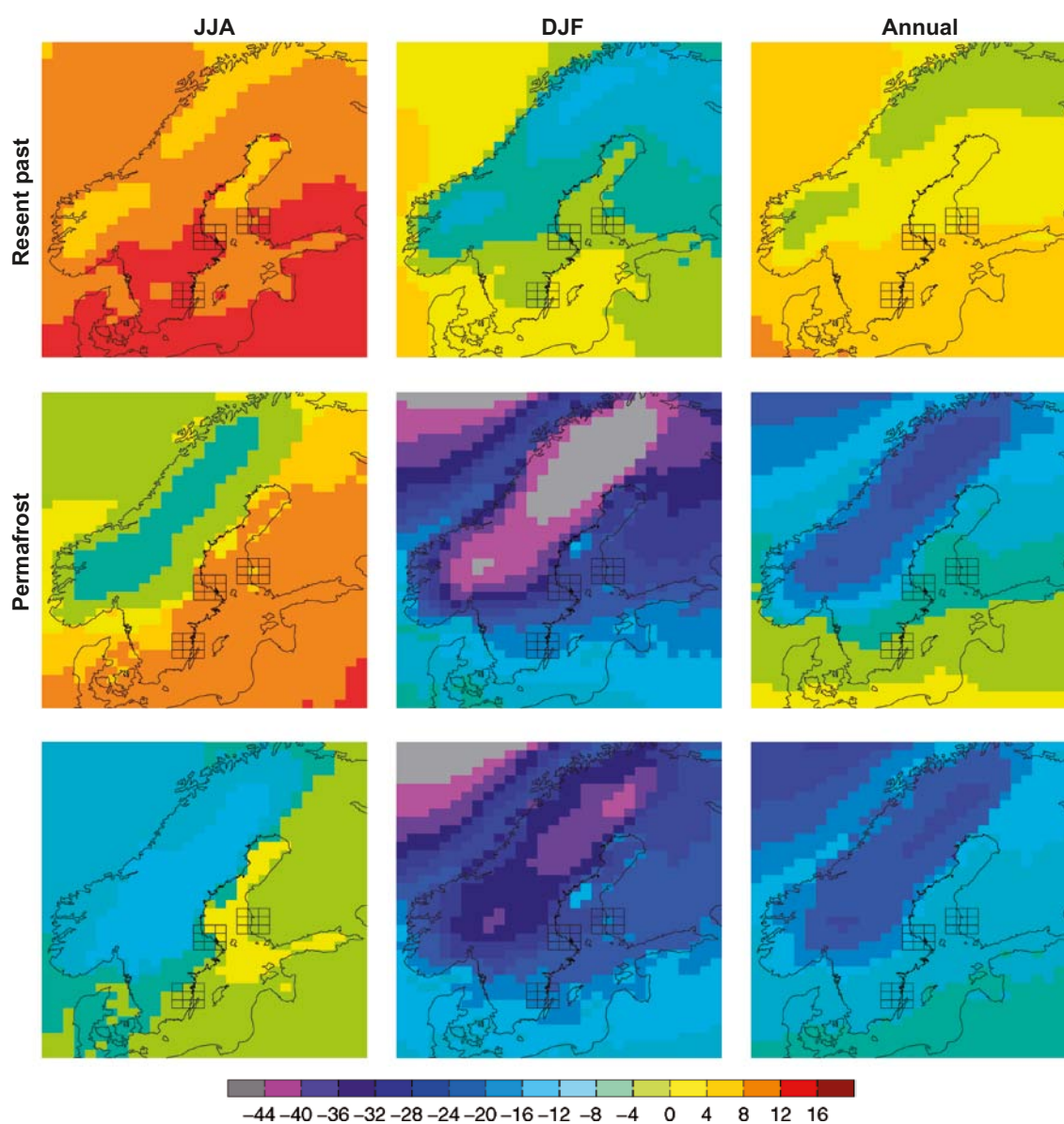


Figure 4-11. Seasonal and annual mean temperature for the present (1961–2000) (upper row) and MIS 3 (middle row) climate simulations. The lower row shows the difference between the two. Units are °C. From /Kjellström et al. 2009b/.

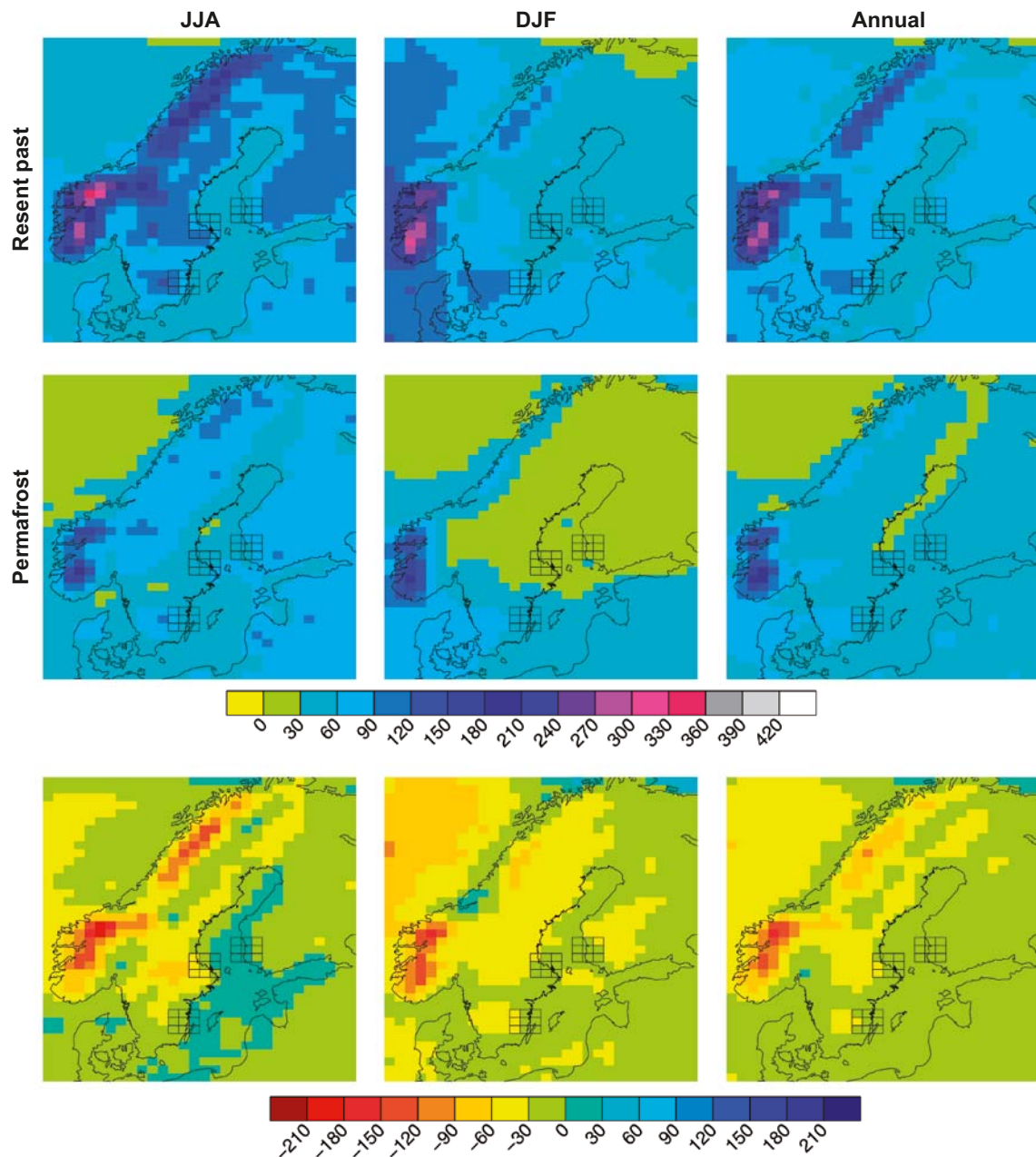


Figure 4-12. Seasonal and annual mean precipitation in the present (1961–2000) (upper row) and MIS 3 (middle row) climate simulation. The lower row shows the difference between the two. Units are mm/month. From /Kjellström et al. 2009b/.

The last step in the MIS 3 climate modelling study was to extract climatological data for the Forsmark region from these regional modelling results. Figure 4-13 shows the grid boxes used for extraction of data. Information was extracted from the model grid point located closest to the Forsmark site.

50-year averages values from the regional MIS 3 climate simulation show that the annual mean air temperature in the Forsmark region is -7.6°C during the inferred ice free stadial 44 kyrs ago. This is 12 degrees lower than in the simulated present climate (1961–2000). The largest difference compared with the simulated present climate in the seasonal cycle of temperature is seen in winter (Figure 4-14, upper row, second column).

The mean annual precipitation in the Forsmark region is 441 mm, which is 225 mm (or 30%) less compared with the simulated present climate. In this periglacial climate, the precipitation is lower than in the present climate for most parts of the year, and there is a very strong seasonal cycle in snow cover as the temperatures during summer get well above 0°C allowing complete snow melting

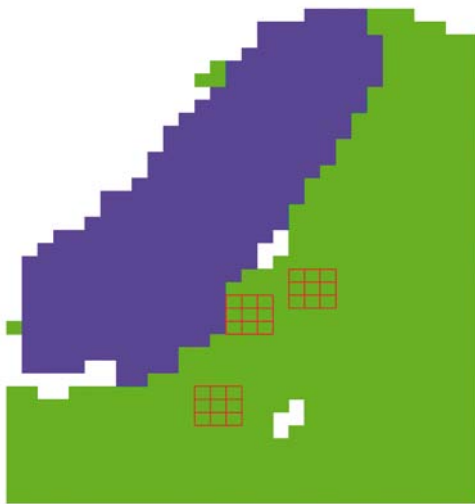


Figure 4-13. Land (green), ice sheet (blue) and sea extent (white) in the Fennoscandian region used for the MIS 3 climate simulation. The 3-3-grids represent grid boxes covering the Forsmark, Oskarshamn and Olkiluoto sites (centre box) and the eight surrounding boxes. Grid boxes with a land fraction lower than 20% are not filled. Results from Oskarshamn and Olkiluoto are presented in /Kjellström et al. 2009b/. From /Kjellström et al. 2009b/.

(Figure 4-14, upper and lower row, second column). The length of the completely snow-free season is three months and there is a more or less constant snow cover during at least 3 months.

The annual surface runoff is 139 mm in this exemplified periglacial climate, which is somewhat less (36 mm/year) than in the simulated present climate. In the MIS 3 climate, there is a clear spring peak in runoff connected with the snow melt which is more extensive than in the simulated present climate, since more snow is accumulated on the ground during the winter. During the remaining part of the year, the runoff is fairly small, due to the cold conditions during winter and the relatively small amounts of precipitation during summer. Given the uncertainties and assumptions used in the climate modelling, the model results thus show that the MIS 3 climate in the Forsmark region may be characterized by a significantly colder and drier climate than at present and also that the surface runoff is reduced.

The annual mean ground temperature is about -4°C in the Forsmark region (Figure 4-10). According to /Heginbottom et al. 1995/ these temperatures indicate that climate conditions are favourable for discontinuous permafrost (covering 50–90% of the landscape). The cold and dry climate with partially snow-free conditions implies that the climate is very favourable for permafrost growth.

In summary, the results from /Kjellström et al. 2009b, including erratum dated Feb 2010/ show that i) the climate models produce a cold and dry arctic climate in the Forsmark region for a stadial during MIS 3, ii) the resulting climate is in agreement with ice-free conditions in south-central Fennoscandia and iii) that this climate is suitable for permafrost growth in the Forsmark region.

The major uncertainties in the climate simulation are related to uncertainties in forcing, model formulation and natural variability. These uncertainty aspects are discussed in detail in /Kjellström et al. 2009b/. For further details on the setup, results, and discussion of the MIS 3 climate modelling results, see /Kjellström et al. 2009b (including erratum Feb 2010), Kjellström et al. 2010a, Brandefelt et al. 2011/. For other climate modelling studies focussing on MIS 3, see /Barron and Pollard 2002, van Huissteden and Pollard 2003, van Huisseden et al. 2003/ and references in /Kjellström et al. 2009b/ and /Wohlfarth 2009/.

Following the very warm temperatures reconstructed for *early* MIS 3, described above, which are suggested to have resulted in ice-free conditions over large parts of Fennoscandia during MIS 3, e.g. /Helmens et al. 2009b, Wohlfarth 2009, Wohlfarth and Näslund 2010/, the low air temperatures simulated for Fennoscandia for the middle MIS 3 stadial (44 kyrs BP) are in line with the view that the Weichselian ice sheet needs to re-grow to attain the known large MIS 2 (LGM) ice configuration in a relatively short time.

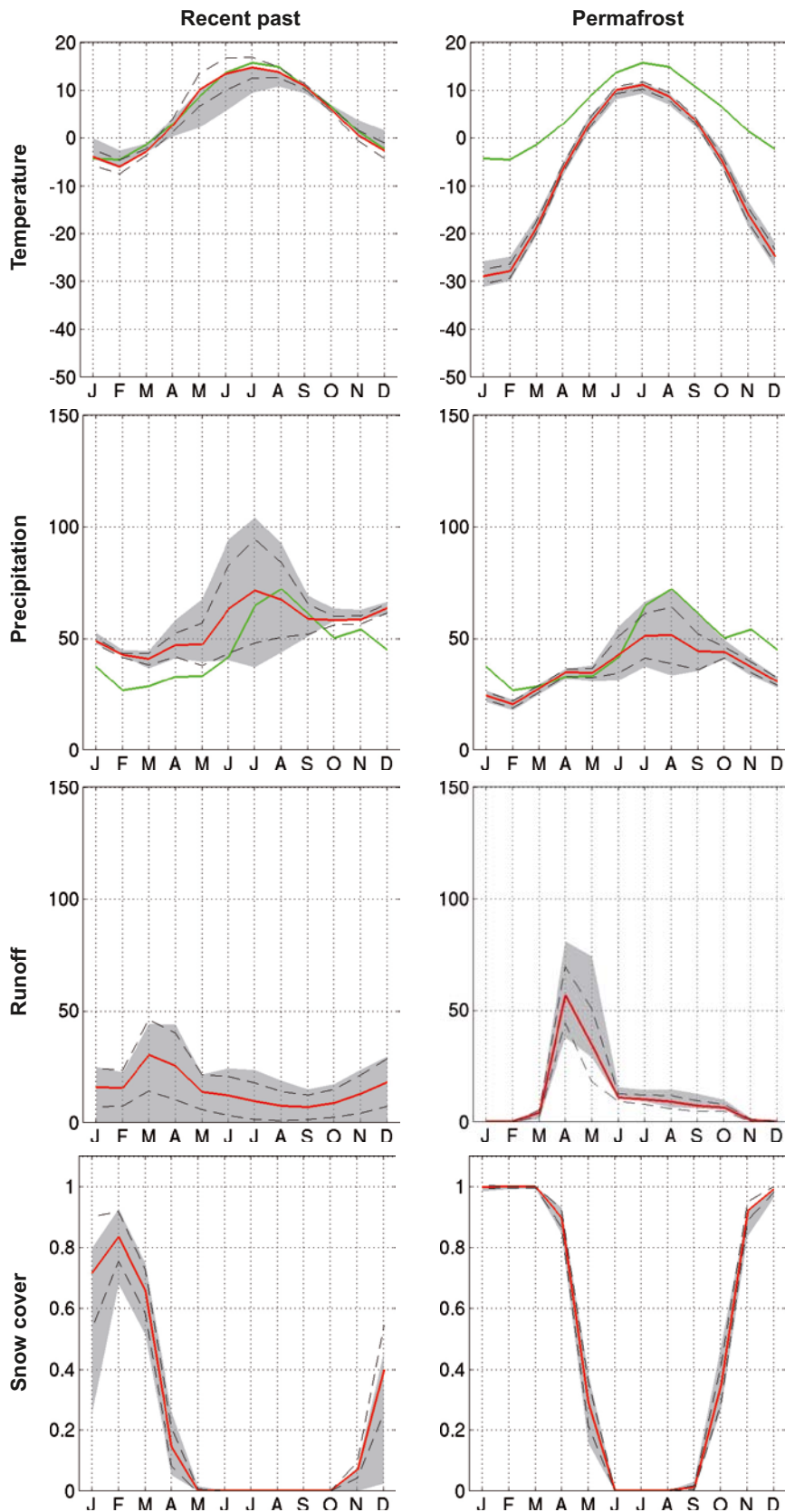


Figure 4-14. Simulated seasonal cycles of temperature ($^{\circ}\text{C}$), precipitation (mm/month), runoff (mm/month) and snow fraction (dimensionless ranging from 0 to 1) at the grid box closest to the Forsmark site (red line). The spatial variability in the 3-3-grids (Figure 4-13) is displayed with the dashed lines representing ± 1 standard deviation calculated from the 9 grid boxes, and the grey area representing the absolute maximum and minimum, of the 9 grid boxes. The green line for temperature and precipitation is the observed seasonal cycle from the CRU data set in the period 1961–1990, see /Kjellström et al. 2009b/. From /Kjellström et al. 2009b/.

4.3.3 Late Weichselian including LGM (24–12 kyrs BP)

All of Fennoscandia was covered by the Weichselian ice sheet during the Last Glacial Maximum (LGM), which occurred during the Late Weichselian (Figure 4-3, lower panel). At that time, air temperatures were among the lowest of the last glacial cycle /Jouzel et al. 2007/ and Figure 3-13. In order to study the climate during the LGM in a consistent way with the simulation of a periglacial climate, the same models and modelling approach as for the periglacial climate modelling described in Section 4.3.2 was used for LGM simulations. The LGM climate model simulations were set up to resemble conditions at the time of LGM in a way as similar as possible to what was done in the Palaeoclimate Modelling Intercomparison Project /Joussaume and Taylor 2000, Harrison et al. 2002/. This choice facilitates comparisons with other GCM results. It also allows the use of pre-existing long simulations with the general circulation model CCSM3 performed at the National Centre for Atmospheric Research (NCAR) in the USA /Otto-Bliesner et al. 2006/, reducing the model spin-up time needed for this study. Further, as the LGM is part of the most recent Weichselian glacial period, there is a better possibility of finding climate proxy data than for earlier cold stadials during the Weichselian. The orbital year 21 kyrs BP and a CO₂ level of 185 ppm were used in the LGM simulation. Ice sheet configurations were the same as in the PMIP-2 project /Harrison et al. 2002/, which were based on the ICE-5G data /Peltier 2004/. For a description of the set up of all other forcing conditions, see /Kjellström et al. 2009b/.

Global climate

The global LGM simulation is a continuation of a LGM simulation performed at NCAR /Otto-Bliesner et al. 2006/. The simulation was originally initiated from a simulation of pre-industrial climate, except for the ocean which was initiated by adding three-dimensional anomalies of ocean temperature and salinity derived from a LGM simulation with the Climate System Model version 1.4 (CSM1.4) /Shin et al. 2003/ to the CCSM3 pre-industrial simulation. The simulation was first run for 400 years at NCAR, and was then continued for another 856 years within the present study. The annual global mean surface temperature reaches quasi-equilibrium after 100–150 years, then it continues to cool and reaches a new quasi-equilibrium after a total of 750–800 years. This second quasi-equilibrium extends until the simulation is ended at model year 1,538 /Kjellström et al. 2009b erratum Feb 2010/. The annual global mean surface temperature is 9.0°C in the first quasi-equilibrium and 7.9°C in the second LGM equilibrium, i.e. 4.5°C and 5.6°C colder than the corresponding simulated pre-industrial temperature /Kjellström et al. 2009b, Brandefelt and Otto-Bliesner 2009/. The second equilibrium also results in a 30% reduction in the strength of the Atlantic Meridional Overturning Circulation (AMOC) compared with the first quasi steady-state /Brandefelt and Otto-Bliesner 2009/.

The global climate model LGM simulation thus shows that the global mean air temperature during the LGM could have been more than one degree colder than previously thought, and also that the variability in global mean temperature was larger. The variability is attributed to coupled ocean-atmosphere-sea ice variations in the North Atlantic region. The difference between globally warm and cold years is focussed over oceans in the Northern Hemisphere outside the tropics. The largest difference between cold and warm years is found over Greenland and Northern Europe, with a maximum of 6.8°C. The total amount of precipitation is up to 32% higher over the North Atlantic and North Pacific region in warm years than in cold years at the LGM. Furthermore, the sinking branch of the AMOC is shifted further north in globally warm years as compared with cold years. Further results, and discussions of their significance, are found in /Kjellström et al. 2009b, including erratum dated Feb 2010/.

Significant effort was made to compile LGM climate proxy data for model validation. For the comparison between global LGM model results and marine and terrestrial LGM climate proxy data, see /Kjellström et al. 2009b, Section 3.2.1/.

Climate over Europe and Sweden

A very cold LGM climate, with annual mean temperatures below 0°C in all of Europe north of about 50°N and also in high-altitude regions in southern Europe is clearly seen in the regional climate model results (Figure 4-15, upper row right). In winter the situation is even more striking with the 0°C line encompassing basically all of continental Europe and monthly mean temperatures below –40°C over the northern parts of the ice sheet (Figure 4-15, upper row middle). During summer,

the area with the lowest temperatures is more confined to the ice sheet, the extent of which is readily visible in Figure 4-15 (upper left). In winter when most parts of Europe are snow covered, the gradient is less pronounced as there is no abrupt shift from snow-covered to snow-free conditions. The annual mean temperature in the LGM simulation is 25–30°C lower than the simulated present climate. Over the southern parts of the ice sheet (British Isles, southern Fennoscandia) the annual mean temperature is around 15°C lower than today. At the edge of the ice sheet, there is a strong gradient towards smaller temperature differences. Central Europe is around 8°C colder than today and southern Europe around 6°C colder. In winter the temperature over the Fennoscandian ice sheet is around 40°C colder than present Fennoscandian temperatures.

Annual mean precipitation has its maximum over the North Atlantic and over parts of western Europe (Figure 4-16, upper right). Relatively small amounts of precipitation are simulated in the northern parts of Fennoscandia and over the Mediterranean Sea and North Africa. Compared with the simulated present climate (1961–2000), Fennoscandia, the British Isles and Iceland are drier (Figure 4-16, lower right). More precipitation than at present is seen in southernmost Europe (the Iberian Peninsula, Italy) and northwest Africa. Fennoscandia and western Europe receive less precipitation than in the present climate. The steep coastlines of western Fennoscandia and Scotland which today are facing the ocean and therefore get a lot of precipitation were, during the LGM, parts of the ice sheet that extended further westward. Without the strong orographic effect, precipitation is considerably smaller in this region during the LGM. In summer, as in winter, precipitation is less than in the present climate in most parts of northern Europe. However, more precipitation in the LGM simulation is seen on the edge of the Weichselian ice sheet northwest of Fennoscandia and the British Isles (Figure 4-16, upper and lower left panels). Another area with more precipitation than in the present climate is the area of what is today the Baltic Sea. During the LGM this area partly coincided with the most elevated parts of the ice sheet in which the regional climate model produces large amounts of precipitation during summer.

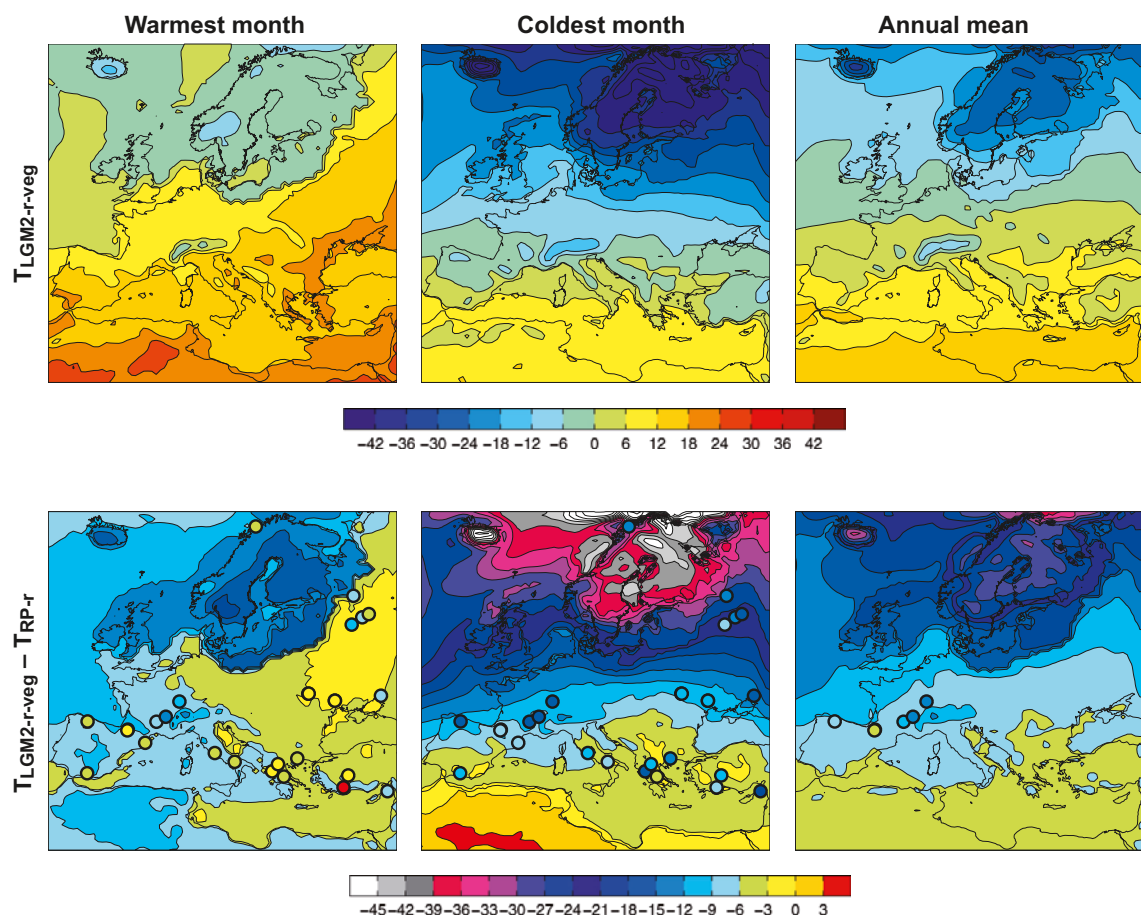


Figure 4-15. Mean temperatures of the warmest and coldest month and annual mean for the LGM simulation (denoted LGM2-r-veg) (upper row). Also shown are differences between LGM simulation and the simulations of the present climate (years 1961–2000) (denoted RP-r) (lower row). Climate proxy based temperature reconstructions are denoted in the filled circles. Units are °C. From /Kjellström et al. 2009b/.

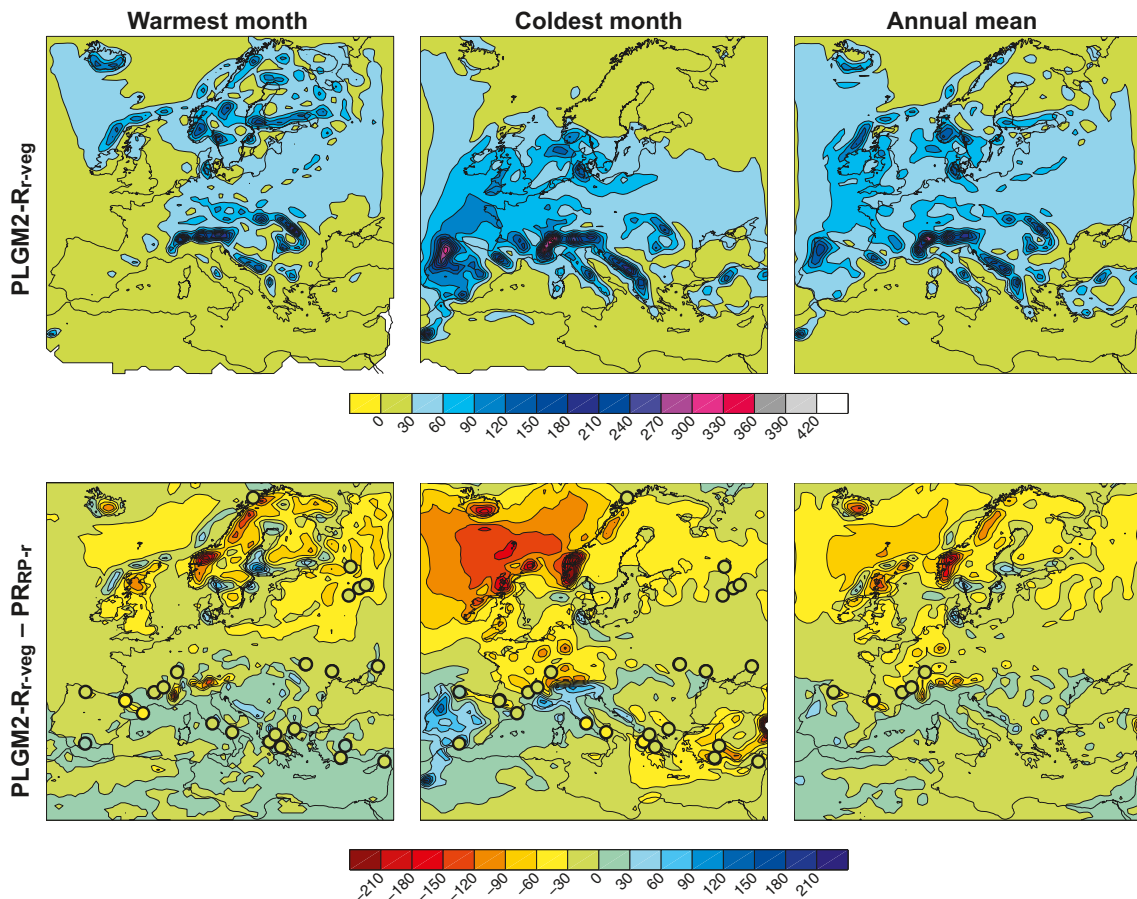


Figure 4-16. Mean precipitation of the warmest month, coldest month and annual mean in the LGM simulation (denoted PLGM2-r-veg) (upper row). Also shown are differences between the LGM simulation and the simulation of the present (year 1961–2000) (denoted RP-r) (lower row). Units are mm/month. From /Kjellström et al. 2009b/.

Comparison to other model simulations

The simulated annual global mean temperature in the LGM simulation (i.e. the second quasi-equilibrium described in the beginning of this section) is 6.9°C lower than in the present climate. This is a stronger response than in most of the PMIP1 (full range is 1.85–9.17°C colder than in the present climate) and PMIP2 simulations (3.4–5.46°C colder than the pre-industrial climate) presented by /Kageyama et al. 2006/. The results indicate that much of the strong cooling is associated with low Sea Surface temperatures (SSTs) (up to 6°C colder than some proxy data indicates) and extensive sea-ice cover in the North Atlantic and North Pacific.

These changes in sea-ice extent are a result of the changes in the temperature climate, but they also act to amplify the changes, as increased sea-ice extent leads to a colder climate through the feedback mechanisms involving increased surface albedo and reduced heat fluxes from the ocean to the atmosphere. This connection between low SSTs at high northern latitudes and the global mean temperature for the LGM simulation is in contrast with the PMIP simulations discussed by /Kageyama et al. 2006/. They find that winter and summer temperature changes over the North Atlantic, Europe and western Siberia do not relate closely to global temperature changes. Another uncertainty relates to the response of the Atlantic Meridional Overturning Circulation (AMOC). This has previously been shown to differ among different PMIP2 models for the LGM; one model gives an unchanged AMOC, whereas two models give an increased AMOC strength /Otto-Bliesner et al. 2007/. The simulations presented in /Kjellström et al. 2009b/ indicate a relatively severe weakening of the AMOC; the strength is reduced by more than 50% in the LGM simulation compared with the pre-industrial climate.

Regardless of possible biases in SSTs, the simulated changes in annual mean temperatures over Europe in the global model are similar to those obtained in the high-resolution atmosphere-only CCM3-simulations by /Kim et al. 2008/. In both our global and regional models, the coldest month of the year is warmer than proxy data indicate. This is a result also shown for the PMIP1 and PMIP2 simulations /Ramstein et al. 2007, Kageyama et al. 2006/. However, even though the models are warmer than the proxy data indicates, /Ramstein et al. 2007/ conclude that they are within the confidence interval of the proxy based reconstructions. /Wu et al. 2007/ suggest that LGM winter temperatures were $\sim 10\text{--}17^\circ\text{C}$ lower than today outside the ice sheet margin in Eurasia, with a more significant decrease in northern regions. This is in line with the results by /Kjellström et al. 2009b/.

For a description of the results concerning using an improved European vegetation for the regional LGM climate simulations, as well as for a detailed description of the comparison with climate proxy data, see /Kjellström et al. 2009b/.

Just as for the simulation of a periglacial climate (Section 4.3.2), results from the regional climate modelling were extracted for the Forsmark region also for the LGM simulation. However, for this situation, the results naturally show the climate conditions prevailing at the ice sheet surface, high above that overridden Forsmark landscape. They are thus of less importance for the present report and are therefore not included here. The interested reader is referred to /Kjellström et al. 2009b/.

4.3.4 Climate variability during the last glacial cycle

The difference between the present warm interglacial temperatures and the *coldest* temperatures during the last glacial cycle as recorded in the GRIP ice core is on the order of 12°C (Figure 3-13). Using an alternative way of interpreting $\delta^{18}\text{O}$ values from the ice core in terms of air temperature, /Lang et al. 1999/ suggested that this cold event reflects a temperature change of 16°C , which is several degrees more than proposed in /Dansgaard et al. 1993/. From the LGM climate modelling study described in Section 4.3.3, annual air temperatures in front of the southern sector of the ice sheet are around $9\text{--}12^\circ\text{C}$ colder than at present (Figure 4-15, lower right) while further towards northeast, annual air temperatures are around $12\text{--}15^\circ\text{C}$ lower than at present. The largest difference compared to present occurs during the winter season (Figure 4-15, middle).

In a similar way, the air temperature simulated for the Forsmark region for an prescribed ice-free MIS 3 stadial at 44 kyrs BP (see Section 4.3.2) are low, 12.5 degrees lower than at present (Figure 4-11, lower right). Also for this situation, the largest change compared to present occurs during the winter season.

As exemplified by the climate development around the modelled cold stadial at 44 kyrs BP, such cold events were relatively short lived, around a few thousands of years long, and alternated with warmer interstadials. A striking climate variability was found also in the simulated LGM climate (Section 4.3.3). These results, from geological archives and from climate modelling, illustrate a typical feature of the last glacial cycle, namely that the climate was highly variable on both long and short time scales. This is also described in for instance the section on abrupt climate change in the description on palaeoclimate characteristics in /IPCC 2007/. The last glacial cycle climate variability is also seen for example if looking at the full GRIP temperature proxy record (Figure 3-13).

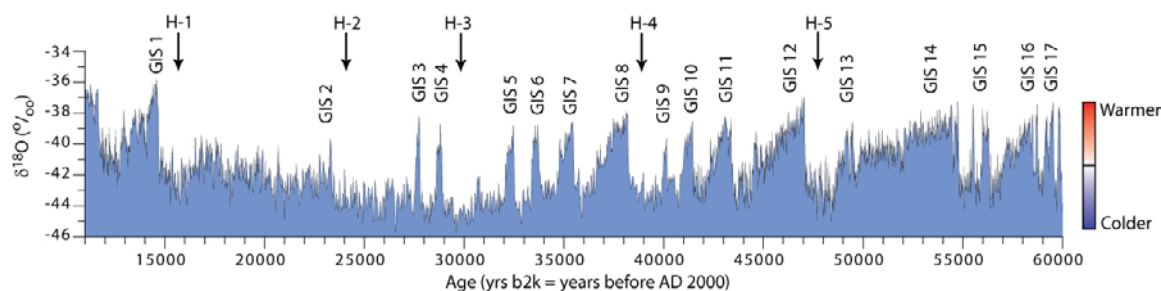


Figure 4-17. The NorthGRIP oxygen isotope ($\delta^{18}\text{O}$) stratigraphy for MIS 2 and 3. Warmer Greenland interstadials were succeeded by colder stadial intervals. Heinrich (H) events 1–5, which have been described from North Atlantic marine sequences, occurred after a series of progressively colder interstadials and in the coldest phase of a stadial. From /Wohlfarth 2009/, modified after /Krogh Andersen et al. 2006/.

When severe cold conditions occur, these conditions do not persist for long periods of time. Such climate variability is observed also in frequency analysis of climate records /Moberg et al. 2005, Witt and Schumann 2005/.

How low could temperatures have been in the Forsmark region during the last glacial cycle? The simulated temperatures for the MIS 3 stadial suggest that the annual mean air temperature in the Forsmark region was -7.6°C , which is 12.5°C lower than at present. If looking at the air temperature curve produced for the region (Figure 3-13), transferred from Greenland conditions to regional conditions in Sweden in a rather simplistic way (Appendix 1), the curve suggests that annual mean air temperatures during the ice-free stadials of the last glacial cycle may have been around -10 to -11°C in the Forsmark region (Figure 3-13), that is c. 2–3 degrees colder than the temperature modelled for MIS 3 (Greenland Stadial 12) at 44 kyrs BP. However, considering the uncertainties in e.g. the transfer functions between $\delta^{18}\text{O}$ and temperature when constructing the temperature proxy curve (Appendix 1), temperatures could even have been lower.

The climate variability seen during the last glacial cycle, e.g. (Figure 3-13 and 4-17) was caused by the combined effect of variations in external orbital forcing (Section 2.2.2) and internal feedback mechanisms within and between the atmosphere, ocean, cryosphere and vegetation systems (Section 2.3). These mechanisms will continue to operate also in the future. Therefore, it is reasonable to assume that a similar climate variability that was characteristic for the last glacial cycle would be characteristic also for future glacial cycles.

For further descriptions of last glacial cycle temperatures, see Appendix 1. Descriptions of geological climate archives from various parts of the last glacial cycle found in Fennoscandia and Europe are presented in e.g. /Hohl 2005, Kjellström et al. 2009b, Wohlfarth 2009, Helmens 2009a/.

4.4 Reconstructed last glacial cycle conditions at Forsmark

In this section, results from Sections 3.1.4, 3.3.4 and 3.4.4 are summarized to present key parameters (development of ice sheet, shore-level, and permafrost) for the reconstruction of last glacial cycle conditions at Forsmark. Additional results from these simulations are presented in Section 4.5, where the results have been used for the construction of the future *reference glacial cycle*. Section 4.5 also presents the resulting evolution of climate domains, as defined in Section 1.2.3.

4.4.1 Ice sheet evolution

In Section 3.1.4, an ice sheet model simulation of the Weichselian ice sheet was made, based on e.g. the temperature reconstruction of the last glacial cycle (Appendix 1). The modelled ice sheet configurations during Weichselian stadials were calibrated against the known maximum ice margin positions for these periods. In the Weichselian ice sheet reconstruction, the overall behaviour of the ice sheet can be characterised as being distinctly dynamic throughout the glacial cycle (Figure 3-14). For instance, during the MIS 3 period (which was *not* used for model calibration), large parts of Fennoscandia were modelled to be ice free (Figure 3-14), in line with several recent independent Quaternary geological studies (Section 4.2.1).

From the ice sheet simulation, data on ice sheet thickness was extracted for the Forsmark region (Figure 4-18). The Forsmark region was subject to two phases of ice sheet coverage, during the cold stadials of MIS 4 and 2. During the last glacial maximum, the ice sheet thickness reached $\sim 2,900$ m. Further description and discussion of this ice sheet evolution is given when these data are used to construct the future SR-Site *reference glacial cycle* (Section 4.5).

In this ice sheet reconstruction, the two very short phases of ice sheet coverage at Forsmark at around 70 kyrs BP (with 40 and 750 m of ice thickness occurring over 500 and 1900 yrs) are considered very uncertain. They are the result of two short and severe cold phases existing in the palaeotemperature curve used to run the ice sheet model. However, the ice sheet model response to these very rapid and strong temperature events is considered uncertain. Therefore these short phases of ice coverage are not included here, nor in the construction of the SR-Site *reference glacial cycle* (Section 4.5). However, a case with longer periods of ice sheet coverage than in the *reference glacial cycle* is described in the *extended ice sheet duration case* (Section 5.3). Further uncertainties related to the ice sheet model simulation are discussed in Section 3.1.4, 3.1.7 and Appendix 1.

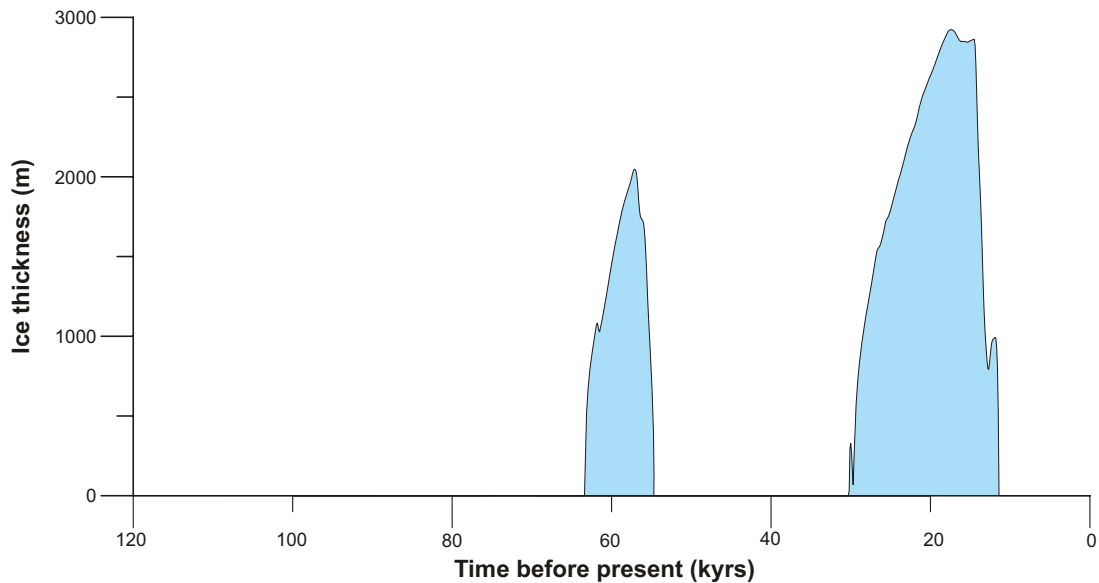


Figure 4-18. Reconstructed ice sheet thickness over Forsmark for the last glacial cycle using ice sheet modelling (Section 3.1.4).

4.4.2 Shore-level evolution

In Section 3.3.4, a GIA model was used to reconstruct changes in shore-level during the last glacial cycle, given input from various Earth models as well as ice load history from Section 3.1.4. Shore-level data were extracted for the Forsmark region (Figure 4-19) showing that the area was submerged after both reconstructed phases of ice sheet coverage (Figure 4-18). At times of maximum isostatic depression, the Forsmark region was covered by the Weichselian ice sheet. The uncertainties in reconstructed levels are rather large (Section 3.3.4). This has resulted in that, at the time of deglaciation (10,800 BP), the inferred water depth at Forsmark in Figure 4-19 probably is too large /Söderbäck 2008/. The results from the GIA modelling have for the following part of the Holocene been combined with results from other shore-level estimates /Påsse 2001/ in order to decrease the uncertainty (Section 4.5.2).

Further description and discussion of this shore-level displacement, and the associated development of the Baltic Sea, is given when these data are used to construct the future SR-Site *reference glacial cycle* (Section 4.5). Uncertainties related to the GIA model simulation are discussed in Section 3.3.4.

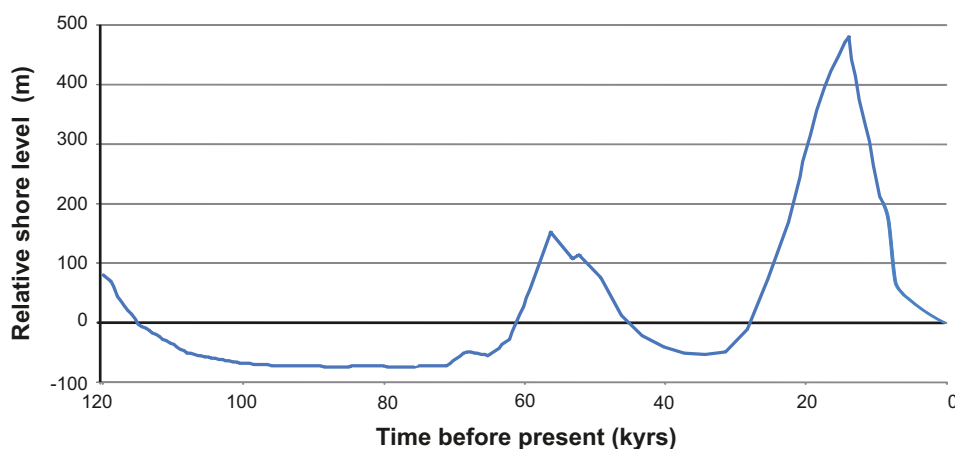


Figure 4-19. Reconstructed shore-level displacement at Forsmark for the last glacial cycle using GIA modelling (Section 3.3.4) and Holocene data /Påsse 2001/. Positive values mean that the area is submerged under the contemporary level of the Baltic Sea. Note that during periods of maximum isostatic depression, the area is situated under the ice sheet.

4.4.3 Permafrost evolution

In Section 3.4.4, reconstructions of permafrost and freezing depths for the last glacial cycle at Forsmark were made using two permafrost models (Figure 4-20 and 4-21). The simulations were made by employing the air temperature curve reconstruction for the last glacial cycle (Appendix 1 and Section, 3.1.4) together with site-specific data on e.g. bedrock, soil, groundwater, lakes and shore-level development, see Section 3.4.4 and /Hartikainen et al. 2010/.

The maximum Weichselian permafrost depth at the Forsmark repository location is ~250 m and it occurs around 70 kyrs BP, prior to the MIS 4 ice sheet advance over the region (Figure 4-20 and 3-69). The maximum permafrost in the surrounding region, here represented by a 15 km long profile, is ~300 m and it occurs at the same time (Figure 4-21 lower part). At this time the area is subject to continuous permafrost coverage (more than 90% spatial coverage), see Figure 4-21, upper part. During periods of ice sheet coverage, permafrost declines, especially during periods when the ice sheet is warm-based (Figure 4-22). At the time of the deglaciations, there is no permafrost or frozen ground present.

The values estimated for last glacial cycle air temperatures at ground level (Section 3.4.4 and Appendix 1) are typically 2–4°C lower than mean annual temperature in the uppermost part of the ground for the same climate, see Section 3.4.4 and Figure 4-10. As discussed above, really low air temperatures during the last glacial cycle only prevailed during stadials which had a restricted duration. During cold ice-free periods, permafrost developed at the Forsmark site, but climate variability with alternating cold and warm periods, e.g. Figures 3-54 and 3-65, as well as the presence of the ice sheet (e.g. Figure 4-18), prevented permafrost from developing to great depths (Figure 4-20 and 4-21) and Section 3.4.4. Further description and discussion of this permafrost evolution is given when these data are used to construct the future SR-Site *reference glacial cycle* (Section 4.5).

It should be noted that in the reconstruction of last glacial cycle permafrost development, heat from the repository has been included in order to make the results useful for the subsequent construction of a future *reference glacial cycle* with a repository present. The difference between including and excluding heat from the repository has also been evaluated, see Figures 3-51, 3-87, as well as /SKB 2006a, Figure 3-59/. All uncertainties related to the permafrost simulations are examined in detail in Section 3.4.4 and in /Hartikainen et al. 2010/.

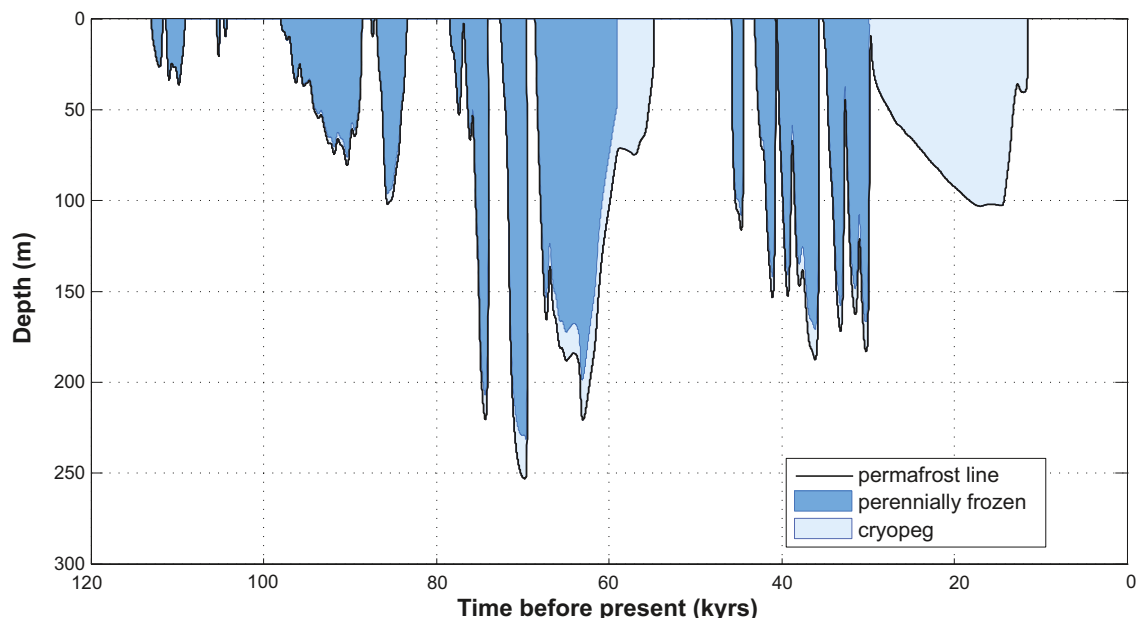


Figure 4-20. Evolution of permafrost and perennially frozen ground depth for the reconstruction of last glacial cycle conditions for the repository location in Forsmark. The results were obtained using a 1D permafrost model (Section 3.4.4). Due to the high sub-glacial pressure, a thick unfrozen cryopeg exists within the permafrost (defined by the 0°C isotherm) after 60 kyrs and after 30 kyrs before present (including the LGM). For the corresponding 2D modelling results see Figure 3-69.

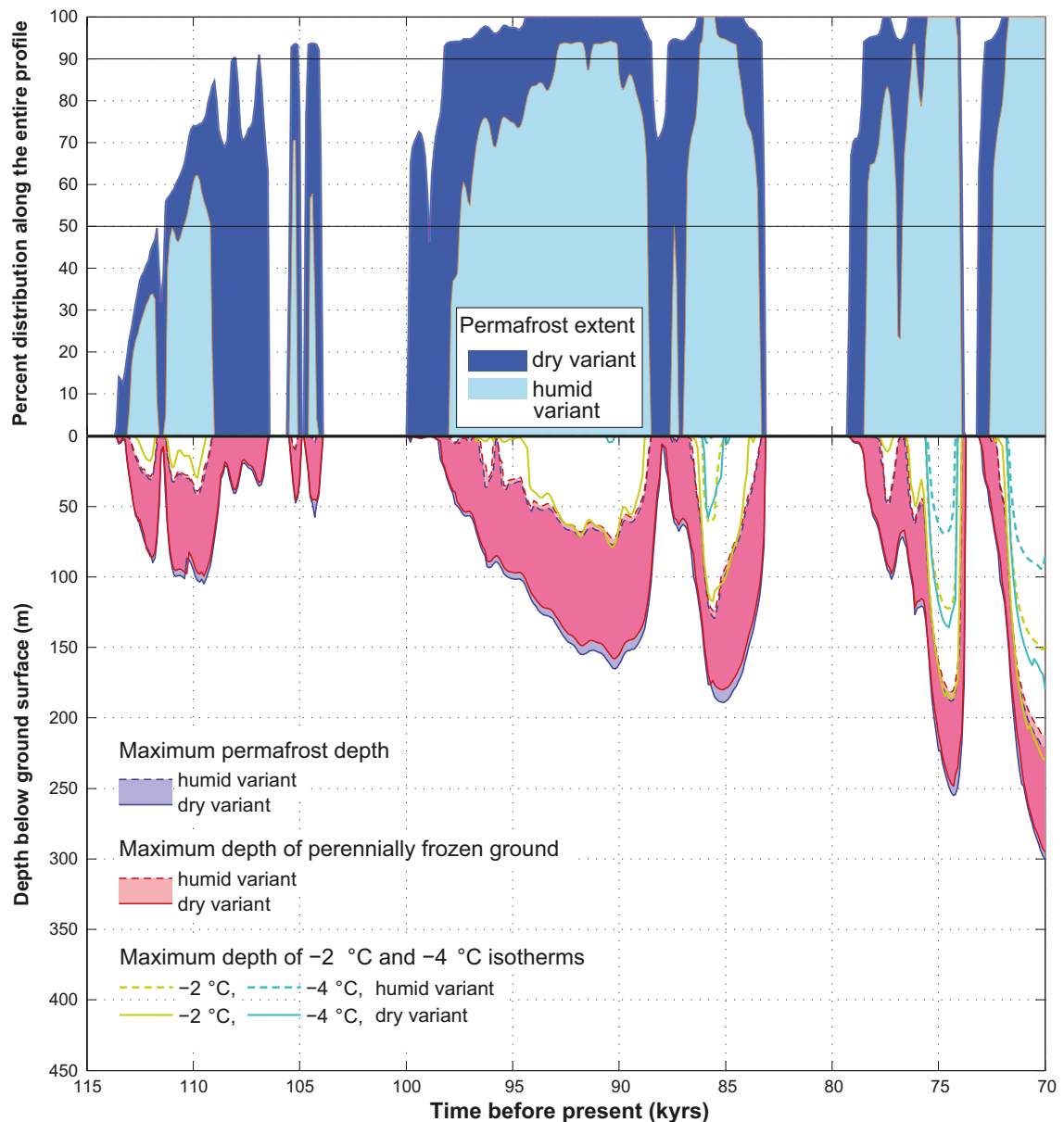


Figure 4-21. Reconstructed evolution of maximum permafrost depth, maximum freezing depth and percent permafrost distribution over a 15 km long transect over the Forsmark area for the first 50 kyrs of the last glacial cycle, see Section 3.4.4 . Upper panel: the transition from sporadic to discontinuous permafrost occurs at 50% spatial coverage and from discontinuous to continuous permafrost at 90% coverage. Lower panel: the shaded area in blue and red represents the range obtained when considering one dry and one humid climate variant. The lilac colour indicates that the results for permafrost and perennially frozen ground overlap.

4.4.4 Combined reconstructed last glacial cycle parameters

Figure 4-22 shows the combined evolution of ice sheet thickness, shore-level changes, permafrost- and frozen ground depth at Forsmark as reconstructed in Sections 3.1.4, 3.3.4, 3.4.4 and above. This reconstruction was used to construct the SR-Site *reference glacial cycle* for the coming 120 kyrs (Section 4.5).

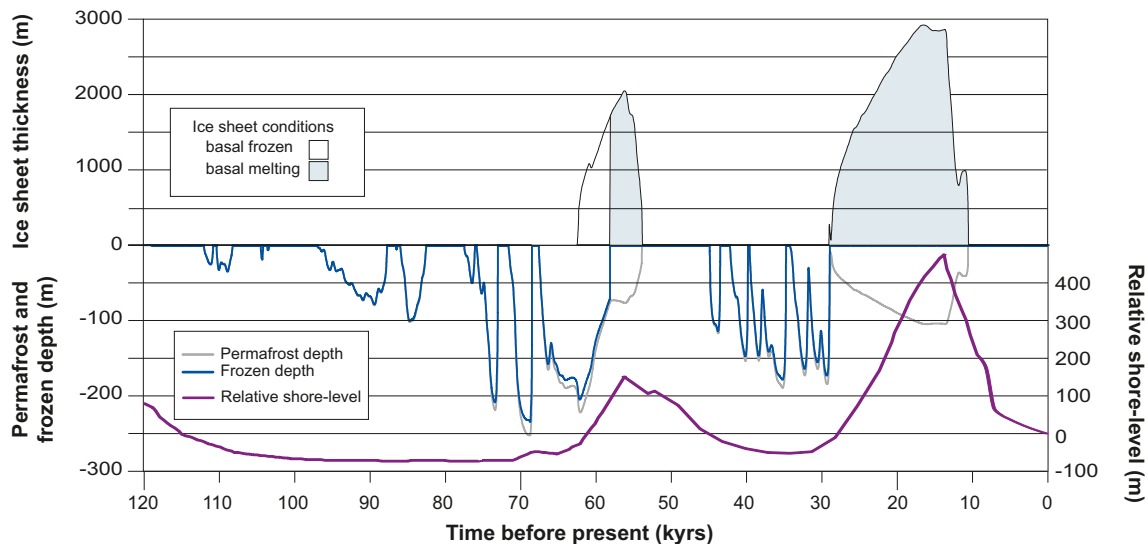


Figure 4-22. Reconstructed Weichselian evolution of ice sheet, shore-level, permafrost and frozen ground at Forsmark. This evolution was used to construct the SR-Site reference glacial cycle.

4.5 Reference glacial cycle

The SR-Site *reference glacial cycle* describes a conceivable future evolution of climate and climate-related conditions and sequences that could be expected in a 100 kyr time perspective. It is constructed by repeating the reconstructed conditions for the last glacial cycle described in Section 4.4. The *reference glacial cycle* constitutes a climate evolution fully dominated by natural climate change, i.e. without anthropogenic influence on climate. Therefore, the length of the present temperate interglacial period is assumed to be within the range of interglacial durations as observed within the past 800 kyr /Tzedakis et al. 2009/, see further Section 4.5.4. The case of having a climate evolution e.g. affected by increased amounts of greenhouse gases in the atmosphere due to human activity, resulting in a longer duration of the present interglacial period, is dealt with in Section 5.1 and 5.2.

In the SR-Site safety assessment the *reference glacial cycle* is used for constructing the base case of the Main scenario, see Figure 1-3.

The climate evolution of the *reference glacial cycle* starts in the present warm interglacial climate, characterized as a temperate, humid cold climate with year-round precipitation. For a description of the present climate at Forsmark, see Section 2.4.2.

4.5.1 Ice sheet evolution

In the *reference glacial cycle*, the lowering of air temperature during the onset of the glacial results in ice sheet inception. Following the ice sheet evolution in the model reconstruction of the Weichselian glacial, see Section 3.1 and 4.4, the evolution of ice covered area and ice volume for the *reference glacial cycle* are shown in Figure 4-23. The corresponding ice configurations for selected time slices, depicting future stadial and interstadial configurations in the *reference glacial cycle*, are shown in Figure 4-24. During the glacial cycle, the ice sheet grows progressively larger in a number of distinct growth phases, with intervening phases of more restricted ice coverage. The Glacial Maximum (corresponding to the LGM of the Weichselian glaciation), is reached at around 100 kyrs into the future. As described in the previous section, the overall behaviour of the ice sheet can be characterised as being distinctly dynamic throughout the glacial cycle.

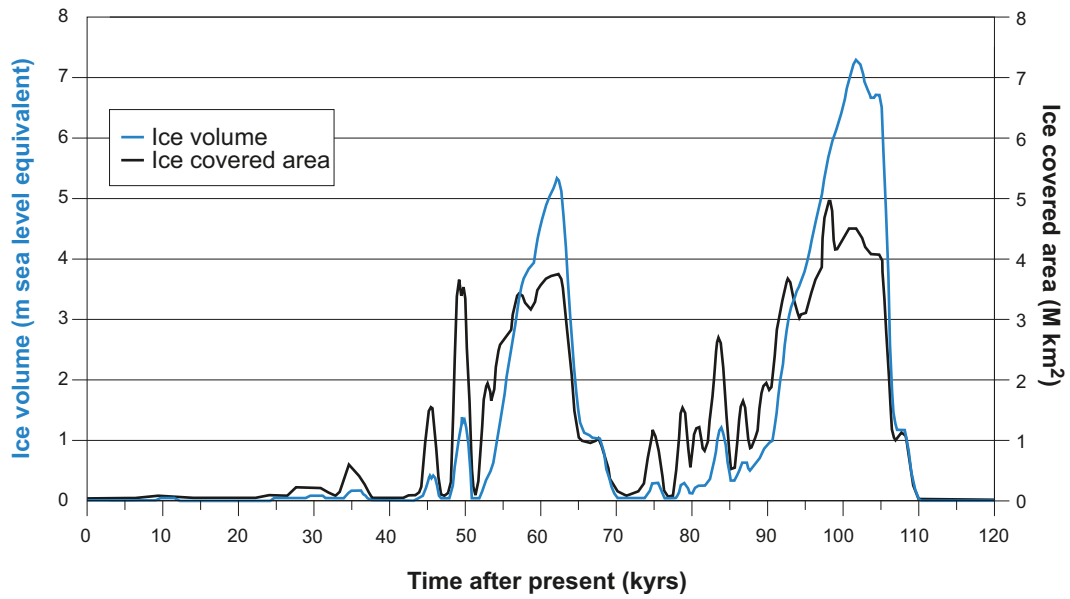


Figure 4-23. Ice sheet volume and ice covered area for the reference glacial cycle.

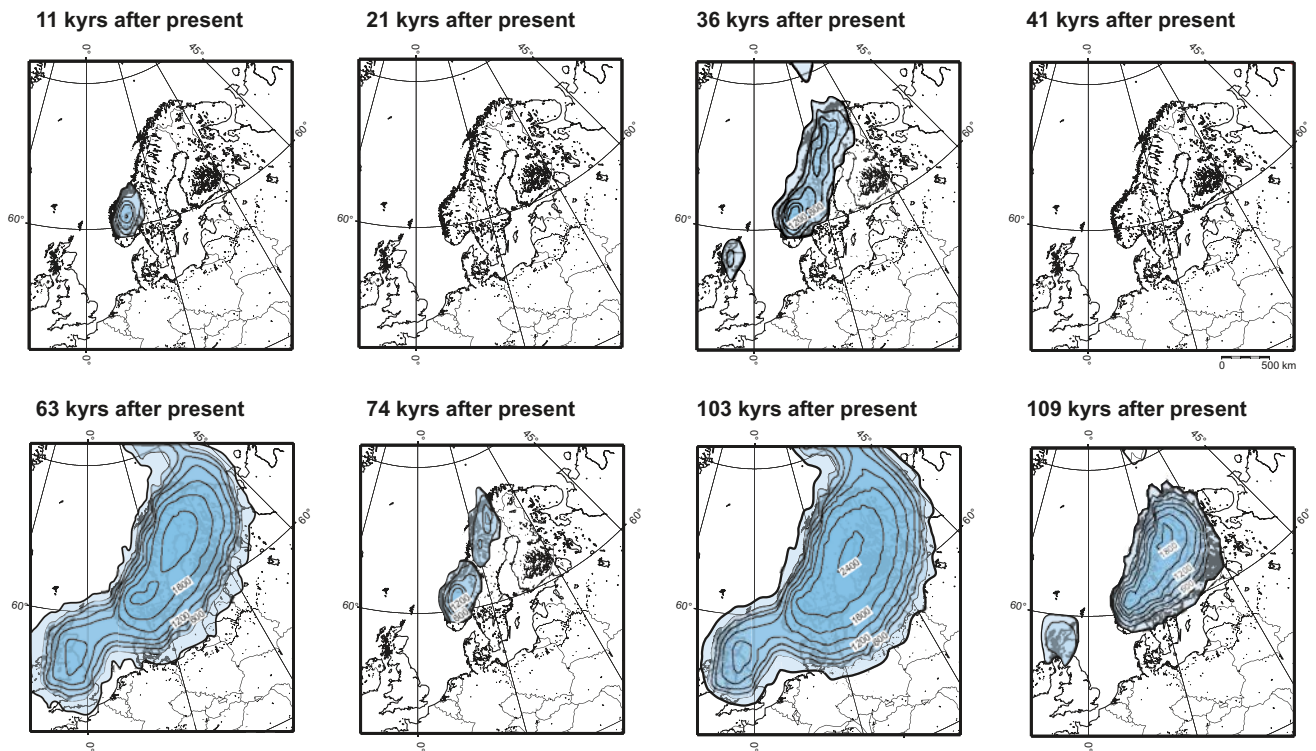


Figure 4-24. Ice sheet configurations at stadials and interstadials for the reference glacial cycle. Contour lines show ice surface elevation with a 300 m interval. All maps show present day shoreline position.

The dynamic behaviour of the ice sheet during the glacial cycle is seen also at the Forsmark site. The site is covered by ice during the cold stadials at around 60 and 100 kyrs after present (Figure 4-25). Between these stadials, the site experiences ice-free warmer interstadial conditions (corresponding to Marine Isotope Stage 3 in the reconstructed Weichselian glacial cycle). Advances of the Fennoscandian ice sheet during stadials around 14 and 38 kyrs after present do not reach the Forsmark site (Figure 4-24), although the ice sheet margin is close to Forsmark during latter stage. Note that even though an ice sheet is present in Fennoscandia during most of the glacial cycle (Figure 4-23), the Forsmark site, located in south-central Sweden, is not covered by the ice sheet for the majority of the time (Figure 4-25).

In the *reference glacial cycle*, the Forsmark region is covered by the ice sheet for a total time of ~30 kyrs. For most of the ice-covered time, the numerical ice sheet modelling suggests that the site is covered by warm-based ice with free water present at the ice-bed interface. Forsmark is covered by wet-based ice for ~23 kyrs, corresponding to about 75% of the ice-covered time. This means that during most of the time when the ice sheet covers the site in the *reference glacial cycle*, meltwater is present at the ice sheet bed, typically produced at rates of a few mm/year, up to ~10 mm/year, and hence groundwater recharge by glacial meltwater takes place.

The short periods of cold-based conditions, with no basal water production, always follow immediately after each time the sites become ice covered. During these periods, as well as during deglaciation periods when the site is close to becoming ice free, water from *surface* melting may still reach the bed. However, in cases when the ice sheet margin is located over permafrost ground, this melt water would not contribute significantly to groundwater recharge. The prerequisites for groundwater flow under glacial- and permafrost conditions are further discussed below. A study of groundwater flow under glacial- and permafrost conditions is found in /Vidstrand et al. 2010/.

During the glacial maximum of the *reference glacial cycle*, at around 100 kyrs after present, the maximum ice sheet thickness over Forsmark is ~2,900 m (Figure 4-25). It is worth noting that the modelled ice sheet reaches significant thickness over the site not only during the glacial maximum, but also during the cold stadal at around 60 kyrs after present. At that time, the modelled maximum ice thickness is ~2,000 m.

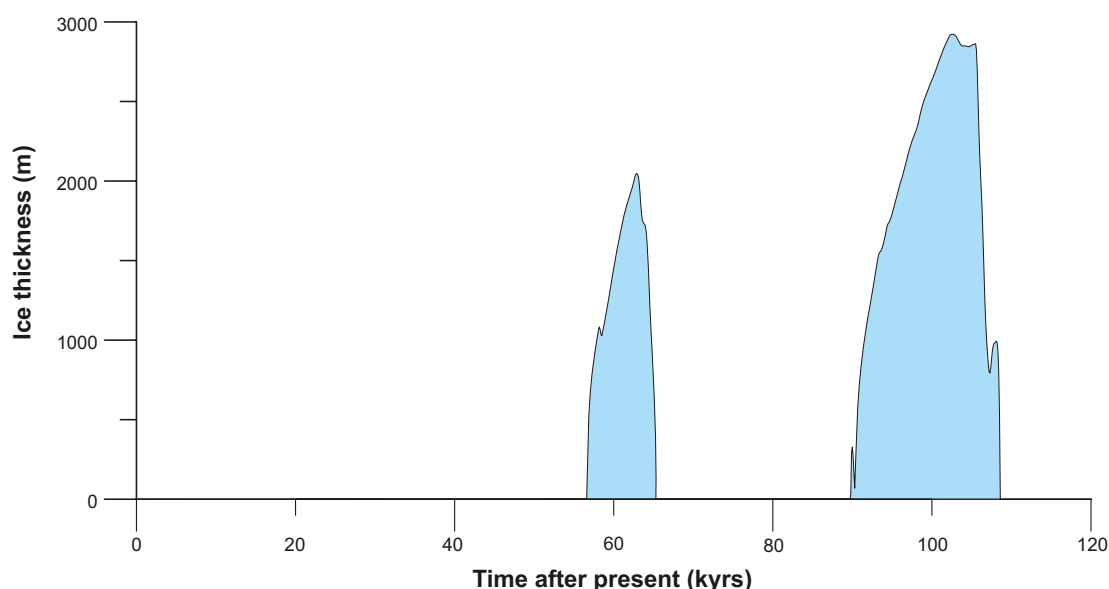


Figure 4-25. Development of ice sheet thickness at the Forsmark site in the SR-Site reference glacial cycle. Note that even though an ice sheet is present in Fennoscandia during most of the glacial cycle (Figure 4-23) the Forsmark site, located in south-central Sweden, is not covered by the ice sheet for the majority of the time.

The groundwater pressure at repository depth is, for non-glacial conditions, determined by the depth of the repository, and for glacial conditions by the repository depth as well as an additional pressure induced by the ice load. The ice sheet thickness sets a limit to the maximum hydrostatic pressure that may occur at the ice sheet/bed interface. The additional hydrostatic pressure related to the maximum thickness in the *reference glacial cycle* (Figure 4-25) is 26 MPa for Forsmark. This value is listed in Table 5-6 together with other estimates of *maximum* possible ice loads and associated *maximum* hydrostatic pressures.

Ice-marginal stillstands

Although not the case during the deglaciation of the Weichselian ice sheet, or in the SR-Site *reference glacial cycle*, future periods of ice sheet-frontal stillstands cannot be excluded for the Forsmark site during ice advance, maximum or retreat phases, given suitable climate conditions. An extreme case in terms of hydraulic gradients and associated increased groundwater flow would occur if the ice front came to a temporary halt with the frontal part of the ice sheet situated above the repository. According to /Vidstrand et al. 2010/ there is an approximately one km wide zone of high groundwater fluxes in front of the ice sheet margin and a similarly wide zone of increased flux behind the ice sheet margin, i.e. two km wide influence area with significantly increased groundwater flux. This situation is valid when there is no permafrost at the Forsmark site. If continuous permafrost is present, which is the case in the SR-Site *reference glacial cycle*, and also very likely during a future glaciation of the Forsmark site, a zone of increased groundwater flow is significantly less pronounced /Vidstrand et al. 2010/. Using a two km wide near-frontal zone with significantly increased groundwater flux is therefore a pessimistic choice for an analysis of the probability for a future situation with an ice margin stillstand over the repository.

Assuming that future periods of ice margin stillstands would have the same characteristics as the stillstands associated with the last deglaciation described above, one could make an estimate of the probability of having such a situation occurring at the Forsmark site. By generalizing the development of the last deglaciation, one could postulate ten temporary halts of shorter duration and one major halt of longer duration, corresponding to the Younger Dryas event, for a deglaciation of a full-sized ice sheet equivalent to the one of the LGM. For halts of short duration, completely stable ice margin conditions are set to persist for 200 years, while during the major stillstand a completely stable position of the ice margin is pessimistically set to a full 1,000 years. This is somewhat longer than the time period that the ice margin was located somewhere within the 20–25 km wide Younger Dryas zone in Sweden, which lasted around 900 years. In reality, it is likely that, during such long phases, the ice margin would move slowly and/or oscillate within an ice-marginal zone. Nevertheless, in order to cover uncertainties in future ice sheet behaviour, a completely stable margin position for 1,000 years is assumed for the major stillstand. In this way, the major stillstand constitutes a pessimistically chosen case in terms of the duration of a high hydraulic gradient and associated high groundwater fluxes.

The deglaciation of the Weichselian ice sheet, from its LGM position in Poland and Germany to the Scandinavian mountain range, occurred over a distance of ~2,500 km /Fredén 2002/. For each of the postulated stillstands, there is a ~2 km wide frontal zone with significantly increased groundwater fluxes /Vidstrand et al. 2010/. For each advance- or deglaciation phase, the probability of having a 200 year long stillstand at Forsmark is therefore 0.008 (10·2 km/2,500 km), while the probability of having the postulated 1,000 year long stillstand at Forsmark is 0.0008 (2 km/2,500 km). For a complete glacial cycle with two phases of ice advance and two phases of deglaciation over Forsmark, i.e. a glacial cycle similar to the SR-Site *reference glacial cycle*, the probabilities for the 200 year and 1,000 year ice margin stillstands at Forsmark are 0.03 (0.008·4) and 0.003 (0.0008·4), respectively. For the full assessment period of 1 million years, comprising eight repeated identical glacial cycles, the probabilities grow correspondingly larger. There is thus a relatively low probability that the ice margin zone with high groundwater flux would come to a temporary halt above the repository, especially when considering the rarer stillstands of long duration. In this context, it should again be pointed out that the assumption of a completely stable ice margin over the repository for 1,000 years is a highly pessimistic case compared to what is known from the last deglaciation.

4.5.2 Evolution of the Baltic Sea and the Forsmark shore-level

At the start of a GIA model run, the Earth is assumed to be in isostatic equilibrium. In reality, the Earth is unlikely to reach such a state if glaciations occur with similar periodicity as in the past. To correct for this, the GIA-modelling, Section 3.3.4, has been initiated by a glacial loading history yielding shore-levels comparable to those reported by /Funder et al. 2002/ at the peak of marine inundation in the Early Eemian about 130 kyrs before present. This gives shore-levels similar to the present at the early phase of the *reference glacial cycle*. However, during the first 1,000 years after present, and for the analysis of biosphere and hydrological evolution during the initial period of temperate climate domain, the shore-level evolution is extrapolated from shore-level data /Påsse 2001/. From about 8 kyrs after present to the end of the *reference glacial cycle*, the shore-level evolution is based on the GIA modelling described in Section 3.3.4.

The evolution of the Baltic Sea

During the initial phase of the *reference glacial cycle*, when climate is getting colder and ice sheets expand globally, global sea-levels fall. At the same time, the rate of isostatic rebound from the last glacial cycle decreases. However, even if the rate is low, the amount of remaining uplift for parts of Fennoscandia is significant. For the central parts of the Fennoscandian ice sheet it has been estimated to ~100 m, and in the distal parts to ~25 m. As long as the Baltic Sea is connected to the Atlantic, the relative shore-level along the Baltic Sea coast is determined by isostatic rebound and global sea-level change. If and when the relative sea-level at Darss sill, in the southern Baltic Sea south of Denmark, falls below the sill depth (at present 18 m below mean sea-level), the Baltic Sea is transformed into a lake. The surface level of this lake is determined by the altitude of the contemporary Darss sill.

In the *reference glacial cycle*, results from the GIA simulations (Section 3.3.4) indicate that the Baltic Sea is isolated from the Atlantic around 9 kyrs after present. However, due to the uncertainties in the GIA modelling, discussed in Section 3.3.4, it is likely that the suggested timing for this isolation is too early. Given these uncertainties, the salinity of the Baltic Sea could thus remain high for a considerably longer period than 9 kyrs after present. If extrapolation of present observed relative sea-level trends /Påsse 2001/ is made, it seems unlikely that isolation of the Baltic Sea from the Atlantic would occur at all, even if excluding the possibility of a considerable future global sea-level rise due to global warming.

In addition, the northern part of the Baltic Sea, i.e. the Gulf of Bothnia at which the Forsmark site is located, will be isolated from the rest of the Baltic Sea due to the remaining isostatic uplift. This occurs around 25 kyrs after present /SKB 2010d/, i.e. well before the onset of the first phase of glacial conditions in the Forsmark region in the *reference glacial cycle* (after 60 kyrs after present), see Figure 4-25. The salinity in the Gulf of Bothnia is reduced as a consequence of this isolation, since the Gulf at this stage constitutes a large lake fed by freshwater from surrounding terrestrial regions. This freshwater stage is formed regardless of the isostatic and eustatic conditions in the southern Baltic Sea (Darss sill). Note that at this stage, the Forsmark site is situated far from the shoreline of the Gulf of Bothnia due to land uplift /SKB 2010d/.

In the *reference glacial cycle*, the isostatic load from the first major ice sheet advance, at ~60 kyrs after present (Figure 4-25), most likely depresses the Gulf of Bothnia lake threshold so that the Gulf of Bothnia regains contact with the southern part of the Baltic Sea. However, it is uncertain if the Baltic Sea has contact with the Atlantic or not at this stage. The uncertainties in the GIA simulations for the southern Baltic Sea region are too large to give useful information for that region at this time. However, according to modelling studies by /Lambeck et al. 2010/, the Baltic may have constituted a freshwater lake during MIS 3 of the Weichselian, which corresponds to the period following the deglaciation of the first glacial period of the *reference glacial cycle*.

Following the deglaciation of the second and larger ice sheet coverage, at around 110 kyrs after present (Figure 4-25) the Baltic regains contact with the Atlantic. Given that the *reference glacial cycle* is based on the repetition of conditions reconstructed for the last glacial cycle (including the Holocene), the development of the Baltic Sea for this future post-glacial period is envisaged to follow the Holocene development, which includes both saline and freshwater stages. After this deglaciation, large parts of southern Sweden are submerged by a predominantly saline Baltic Sea. At the end of the *reference glacial cycle*, and as isostatic rebound proceeds, the Baltic Sea is transformed to an inland brackish sea, similar to today's situation.

Shore-level displacement in Forsmark

For the first 30–40 kyrs of the *reference glacial cycle*, the Forsmark site continues to rise due to post-glacial isostatic uplift. When the isostatic uplift is completed, the site is, according to the GIA simulations (Section 3.3.4), elevated ~70 m above the contemporary sea-level (Figure 4-26).

During the first glaciated period of the *reference glacial cycle*, at 60–70 kyrs after present, the Forsmark site is isostatically depressed by the weight of the ice sheet (Figure 4-26). The glacial phase is followed by interstadial ice-free conditions around 65–90 kyrs after present. In connection with the deglaciation that follows the first glaciated period, the isostatic depression results in the Forsmark site being situated below the Baltic Sea water level, at around 70 kyrs after present (Figure 4-26). In line with the description of the development of the Baltic Sea above, it is uncertain if the site during this stage is submerged by a freshwater lake only, or if the water is more saline as a result of a contact with the Atlantic.

Subsequently during this future interstadial, isostatic recovery results in the Forsmark site rising above the Baltic water level, after 75 kyrs after present. At this time in the *reference glacial cycle*, the Forsmark site is situated above sea-level, and is free of ice, for approximately 15 kyrs.

During the second and main phase of glaciated conditions around 100–110 kyrs after present (Figure 4-25) the Forsmark site is again isostatically depressed (Figure 4-26). After the deglaciation that follows this glaciated period, at around 110 kyrs after present, the Baltic Sea is in contact with the Atlantic and the Forsmark site is submerged by a saline sea. In line with the development of the Baltic Sea presented above, the development of salinity over the Forsmark site during this submerged period follows that of the Holocene. The site finally rises above the Baltic Sea-level again during a brackish phase at around 120 kyrs after present (corresponding to present-day conditions).

During periods of maximum salinity in the Baltic Sea, generally following sometime after periods of maximum glaciation, the Forsmark site is submerged (Figure 4-26). A more detailed description of the development of salinity in the Baltic Sea for this submerged period of the *reference glacial cycle* is found in /SKB 2010d/.

The most important factor affecting modelled shore-level displacement is the Earth structure and ice loading history, primarily the near-field history. The uncertainty in modelled shore-level mainly manifests itself in that reported relative sea-level values are too high, resulting from an overestimation of isostatic depression during glaciated periods, see Section 3.3.4. The size of the uncertainty varies over the modelled glacial cycle. Postulating that the ice sheet evolution is correct, the mean overestimation of relative sea-level over the whole glacial cycle may be up to 45 m for Forsmark.

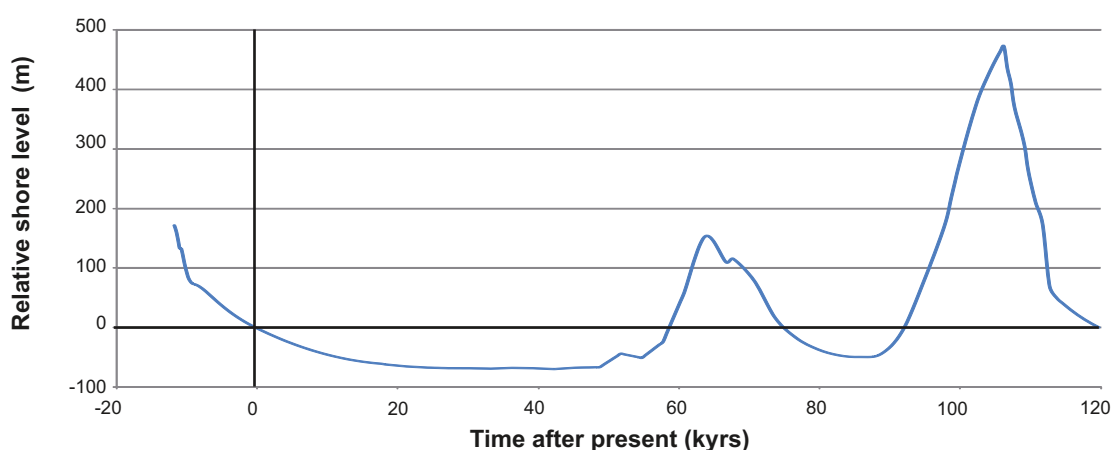


Figure 4-26. Shore-level displacement at Forsmark during the *reference glacial cycle*. The first c. 8,000 years of the future period are based on observed relative sea-level data /Pässe 2001/ whereas the following part of the curve is constructed from Glacial Isostatic Adjustment modelling (Section 3.3.4). The shore-level is expressed relative to the contemporary Baltic sea-level. Positive numbers indicate that the site is submerged and vice versa. Note that for most of the time when the figure show submerged conditions, the site is covered by an ice sheet (Figure 4-25). The figure also includes the relative shore-level from the time of deglaciation up to present, used in e.g. the SR-Site biosphere programme.

4.5.3 Permafrost evolution

The permafrost modelling is described in Section 3.4.4. The input data of geological, hydrogeological, geothermal, geochemical and geomechanical properties are based on site-specific descriptions and are summarised in /SKB 2006a/ and /Hartikainen et al. 2010/. In the reconstruction of last glacial cycle conditions, permafrost develops during the progressively colder phases of the glacial cycle. When the ice sheet subsequently comes to cover an area of permafrost, the permafrost typically stops developing and starts to slowly diminish. When the ground is re-exposed to a cold climate permafrost starts to grow again.

In the SR-Site *reference glacial cycle*, the development of permafrost at Forsmark starts about 8 kyrs after present (Figure 4-27 and 4-28). The 1D modelling approach used for the results in Figure 4-27 could, in certain situations, result in somewhat higher temperatures than would be calculated using a multi-dimensional model. However, a comparison between the 1D modelling results /SKB 2006a/ and the results from the 2D model /Hartikainen et al. 2010/, using the same air temperature curve as input, shows that the results for this site and settings are in line with each other (Figure 4-28). Since lateral groundwater flow only has a minor role in permafrost development compared to heat conduction, e.g. /Hartikainen 2010/, it is likely that modelling including a 3D groundwater flow (instead of the used 2D groundwater flow, and the 1D approach without groundwater flow) would only contribute with minor changes of the permafrost and perennially frozen depths.

When permafrost starts to grow over the site, it starts as sporadic permafrost (i.e. with a spatial coverage less than 50%). As climate gets colder, discontinuous permafrost (with a spatial coverage between 50 and 90%) and continuous permafrost (more than 90% spatial coverage) form over the site (Figure 4-29). Examples of permafrost development along the investigated profile (for profile location, see Figure 3-58) for the dry climate variant of the *reference glacial cycle* are seen in Figure 4-30. The upper panel in Figure 4-30 shows the situation at 8.5 kyrs after present when a Subarctic climate prevails at the site. The profile is partially submerged by the Baltic and sporadic permafrost has started to grow at the site (too shallow to be seen in the figure). At this time the temperature is at its maximum within the repository, which has a large influence on the temperature of surrounding bedrock. Figure 4-30 middle panel shows the situation at 25 kyrs after present in the *reference glacial cycle*, with discontinuous permafrost coverage over the site. In Figure 4-30 lower panel, the situation 50 kyrs after present is shown. At this time an Arctic climate prevails at the site which has resulted in a continuous permafrost cover. At this time the permafrost reaches its maximum depth in the *reference glacial cycle*. As seen from the temperature contours, the heat from the repository has decreased considerably at this time.

During periods of permafrost an unfrozen active layer develops above the permafrost during summer conditions. The thickness of the active layer could typically be c. 40–70 cm deep, depending on the vegetation and soil. For a bare surface the active layer thickness is greater, up to ~1 m.

During the permafrost development prior to the first ice sheet advance, unfrozen taliks are formed under the two future lakes that are located along the profile (Figure 3-58). This is exemplified by the dry climate variant of the *reference glacial cycle* (Figure 4-31). The upper panel shows the situation at 25 kyrs after present when the taliks have formed 9 and 15 km from the south-western starting point of the profile. Groundwater recharge and/or discharge is likely to occur in such taliks. The lower panel of Figure 4-31 shows the situation at 46 kyrs after present. At this time permafrost growth has developed further and none of the taliks reach through the permafrost anymore. In this situation groundwater flow is heavily reduced or stopped.

The permafrost and frozen ground depth reach a maximum prior to the first major glacial advance, at about 50 kyrs after present. At this time the maximum modelled permafrost depth reaches ~260 m at Forsmark (Figure 4-27 and 4-28). The perennially frozen depth is, at the same time, a few tens of metres shallower. When the ice sheet advances over the site, the permafrost stops developing and instead starts to diminish, for example around 60 kyrs after present. Subsequently, permafrost develops again at the site during the ice-free interglacial period between the two major ice advances, but at this time to a somewhat shallower depth, about 180 m (Figure 4-27). During the major phase of ice coverage, including the ice sheet maximum at more than 100 kyrs after present, the maximum permafrost depth (defined by the 0°C isotherm) is around 100 m at Forsmark. Note that, at this time, the permafrost consists only of a completely unfrozen cryopeg due to the insulation effect of the ice sheet and due to the high pressure induced by ice load. Hence all bedrock is at this time at the pressure melting point temperature (Figure 4-27).

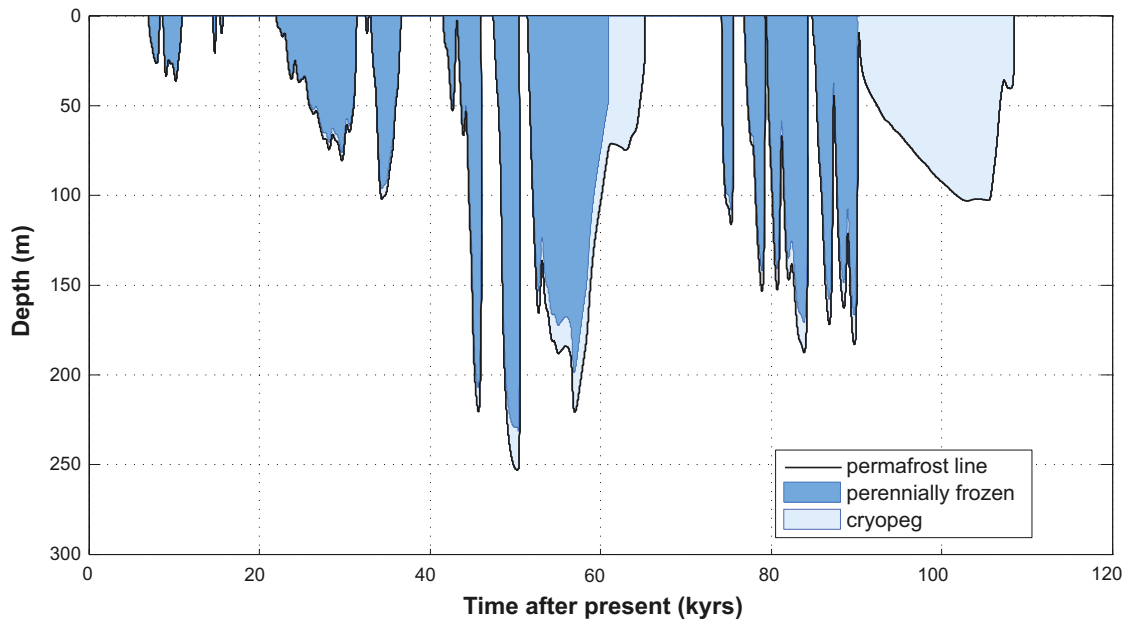


Figure 4-27. Evolution of permafrost and perennially frozen ground depth for the reference glacial cycle for the repository location in Forsmark. The results were obtained using a 1D permafrost model (Section 3.4.4). Due to the high pressure, a thick unfrozen cryopeg exists within the permafrost (defined by the 0°C isotherm) after 60 kyrs and 90 kyrs after present.

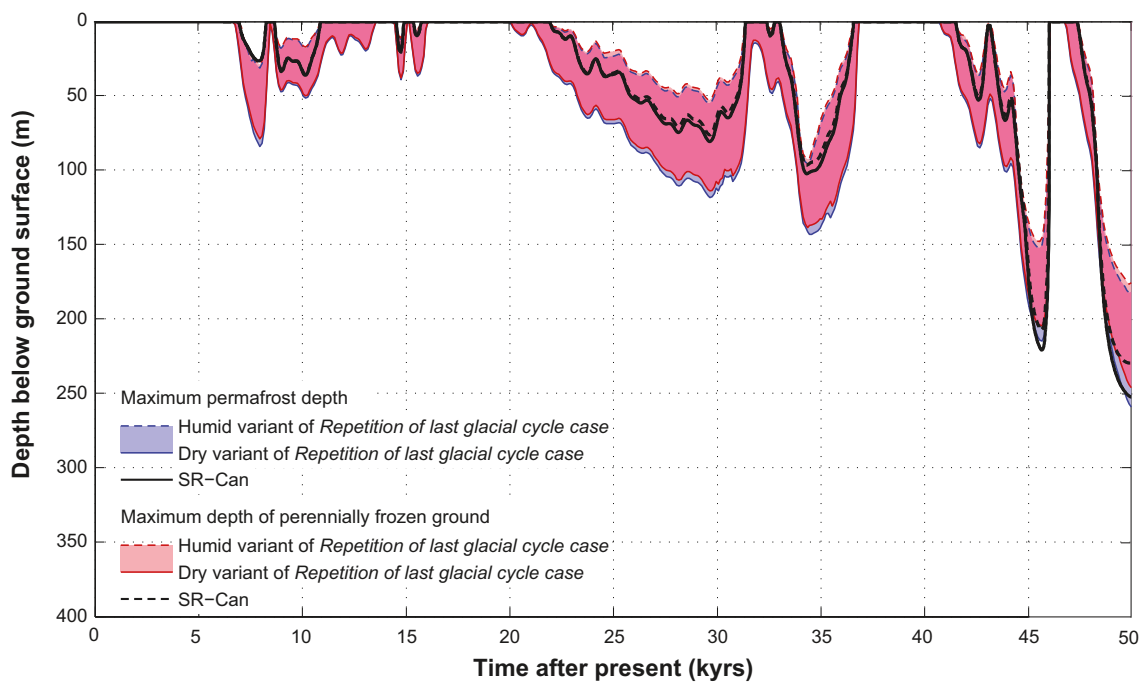


Figure 4-28. Evolution of permafrost and perennially frozen ground depth at the repository location for the first 50 kyrs of the reference glacial cycle as simulated by the 2D and 1D permafrost models (Section 3.4.4). The shaded area in blue and red represents the range obtained from the 2D modelling when considering one wet and one humid climate variant. Further uncertainties in the permafrost modelling are discussed in Section 3.4.4. Both model simulations show that permafrost starts to grow around 8 kyrs after present and that the maximum permafrost depth is ~250 m around 50 kyrs after present.

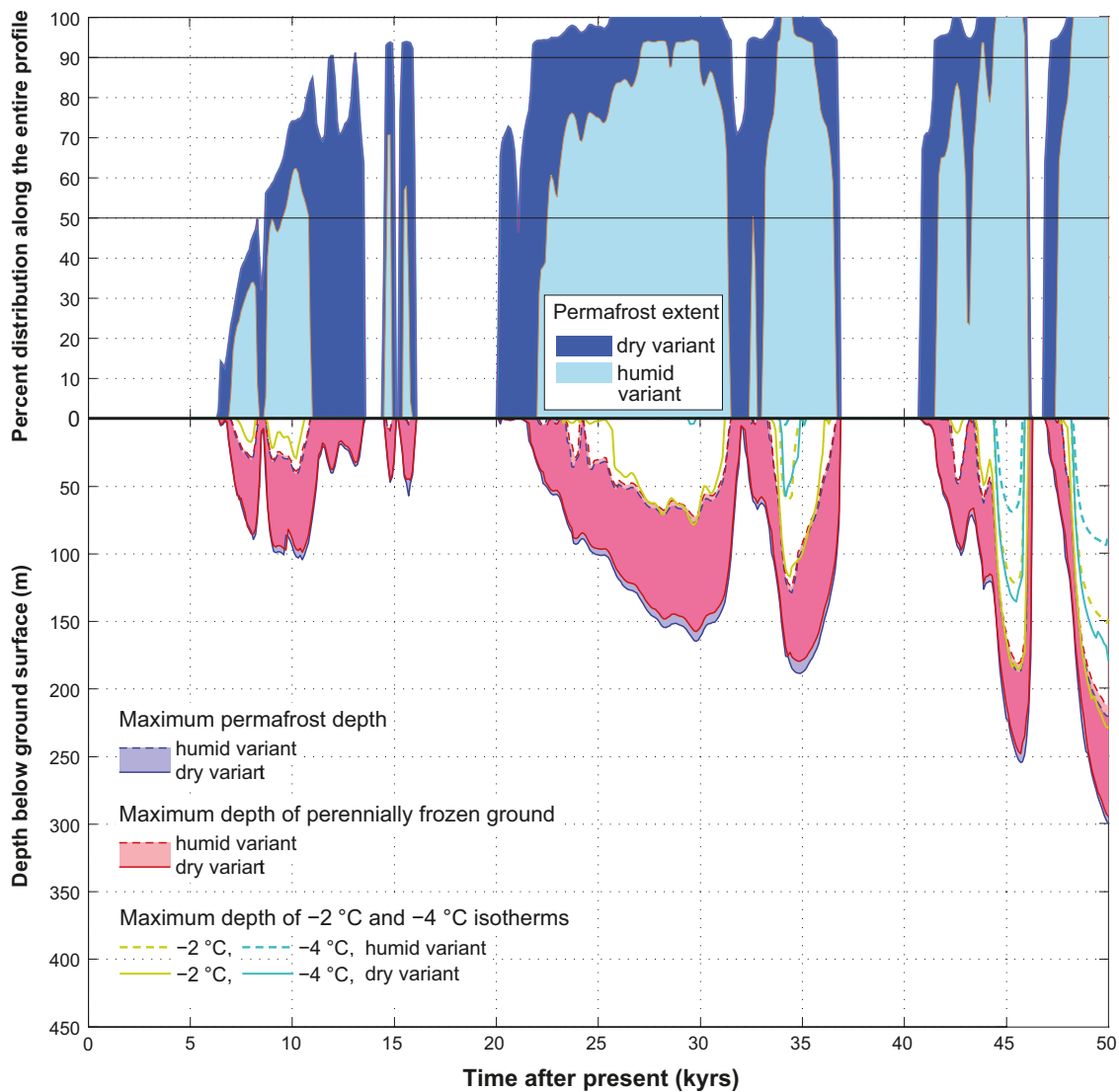


Figure 4-29. Evolution of maximum permafrost depth, maximum freezing depth and percent permafrost distribution over the entire investigated profile (Figure 3-58) for the first 50 kyrs of the reference glacial cycle. Upper panel: the transition from sporadic to discontinuous permafrost occurs at 50% spatial coverage and from discontinuous to continuous permafrost at 90% coverage. Lower panel: the shaded area in blue and red represents the range obtained when considering one dry and one humid climate variant of the reference glacial cycle. The lilac colour indicates that the results for permafrost and perennially frozen ground overlap.

Some of the input data for the permafrost simulations are associated with significant uncertainty. The largest uncertainty relates to the air temperature curve reconstructed for the Forsmark site for last glacial cycle, which is estimated up to $\pm 6^{\circ}\text{C}$ (Appendix 1). If this uncertainty in air temperature is combined with the uncertainty in climate humidity, the permafrost (e.g. 0°C isotherm) uncertainty range in the *reference glacial cycle* reach a maximum depth of ~ 410 m, while the uncertainty range for the perennially frozen ground reaches ~ 380 m (Figure 3-79).

Uncertainties related to other surface conditions (vegetation type, surface wetness, snow cover) and subsurface conditions (thermal conductivity and diffusivity, and geothermal heat flow) have a smaller impact on the simulated permafrost results. If they all are combined with the uncertainty in climate humidity, they result in a permafrost uncertainty interval down to between ~ 170 to ~ 290 m depth (Figure 3-85).

Setting *all* known uncertainties (in air temperature curve, climate humidity, surface wetness, vegetation, snow cover, bedrock thermal conductivity and diffusivity, and geothermal heat flux) at their most extreme values favourable for permafrost growth, the permafrost uncertainty range reaches a

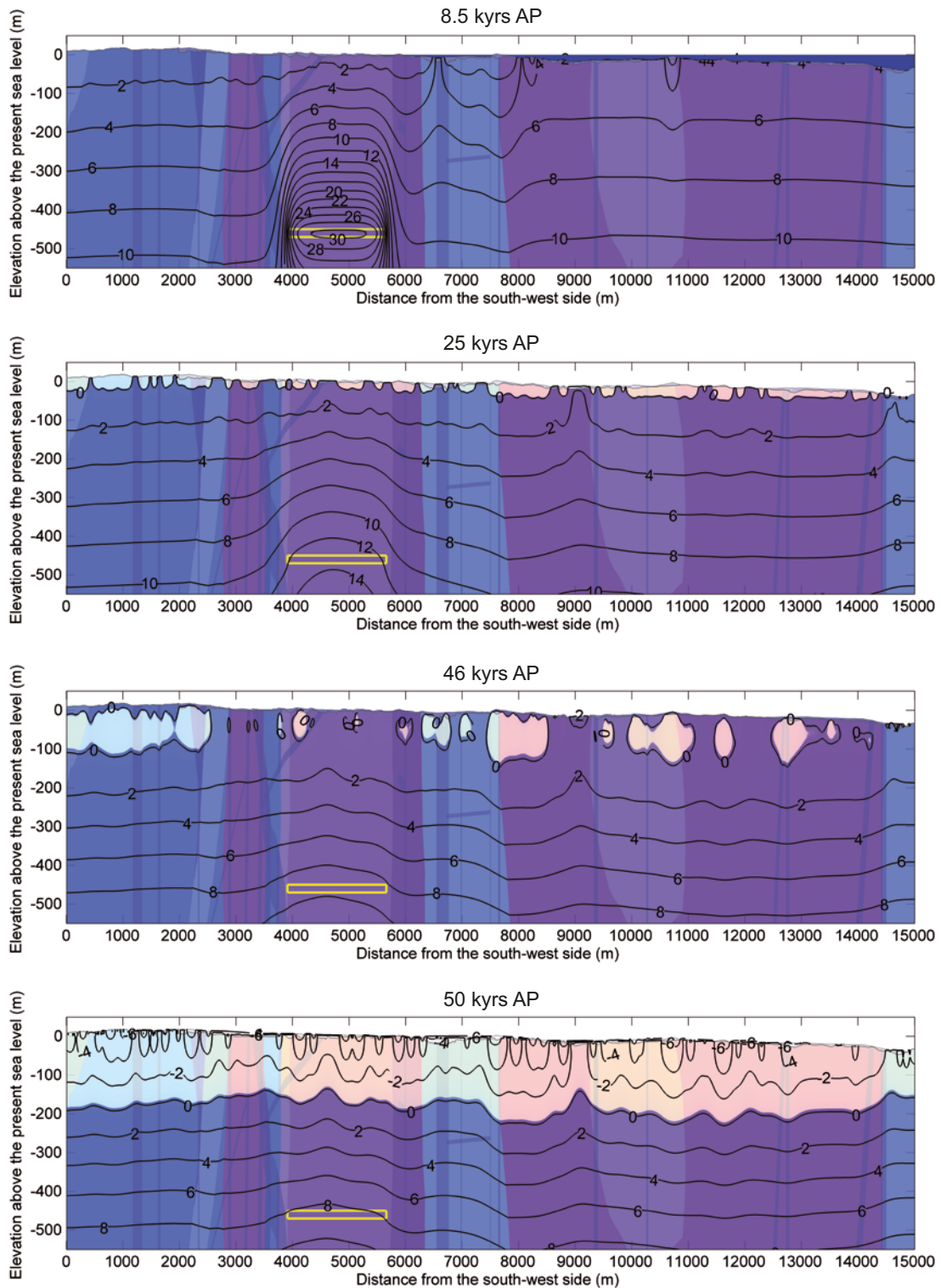


Figure 4-30. Temperature contours in ($^{\circ}\text{C}$) and the extent of perennially frozen ground (light colour) and permafrost (0°C isotherm) at times 8.5, 25, 46 and 50 kyr after present for the reconstruction of last glacial cycle conditions (humid climate variant, see Section 3.4.4). Blue colour on the top of the profile at 8.5 kyr after present shows the Baltic Sea. The yellow rectangle indicates the location of the repository. Vertical areas with various light colours denote different rock domains. At 8.5 kyr after present (upper panel) a subarctic climate prevails. At this time the profile is partially submerged and the exposed ground surface is partially underlain by permafrost (too thin to be seen in the figure). At this time the ground temperature is at its maximum within the repository. At 25 kyr after present (middle panel) a subarctic climate prevails and discontinuous permafrost is developing. At 50 kyr after present (lower panel) an arctic climate prevails and continuous permafrost reaches its maximum depth in this humid climate variant of the reference glacial cycle. In the dry climate variant, the permafrost grows deeper (Figure 4-29 and 4-31).

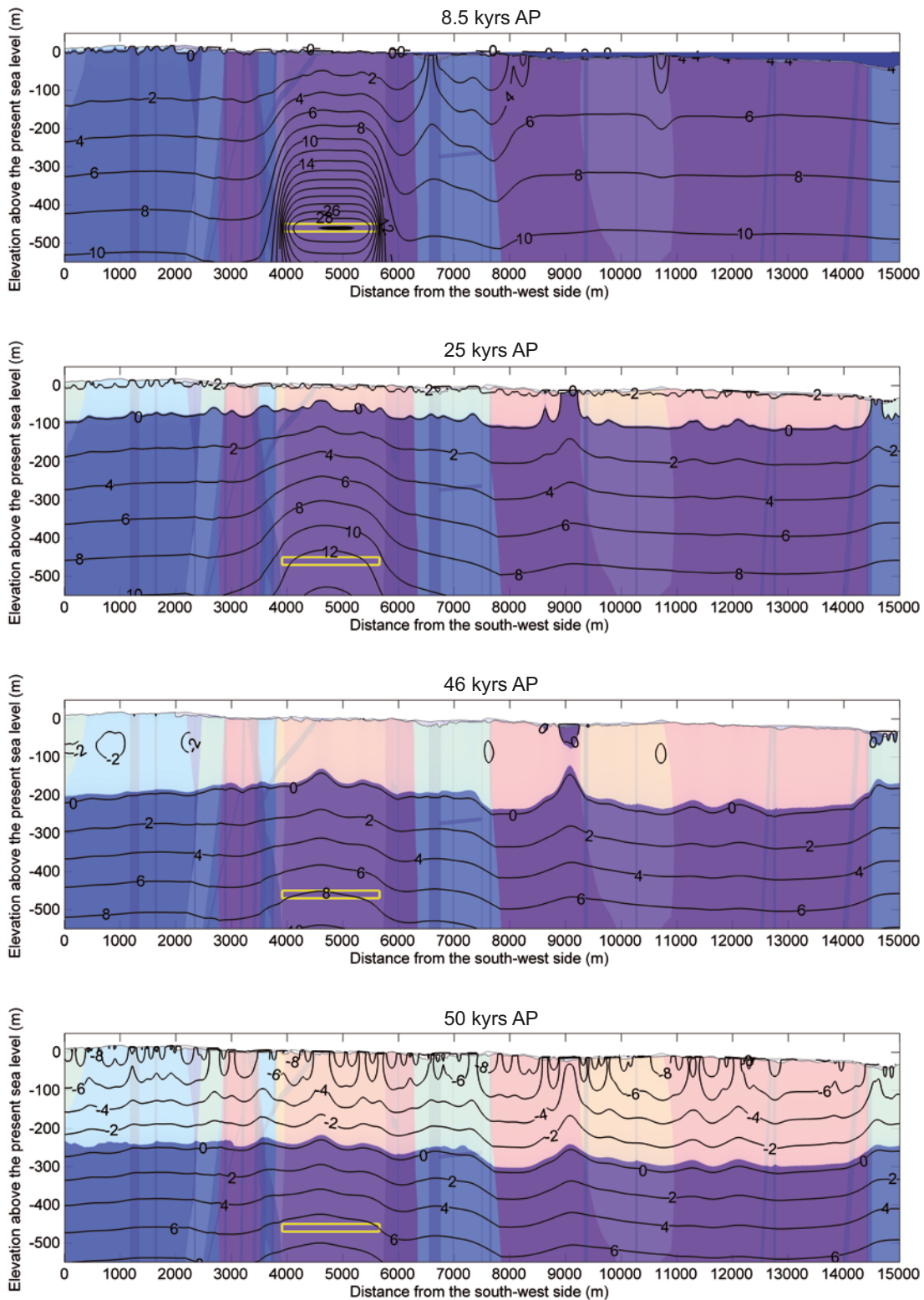


Figure 4-31. Temperature contours in ($^{\circ}\text{C}$) and the extent of perennially frozen ground (light colour) and permafrost (0°C isotherm) at times 8.5, 25, 46 and 50 kyr after present for the reference glacial cycle (dry climate variant, see Section 3.4.4). The yellow rectangle indicates the location of the repository. Vertical areas with various light colours denote different rock domains. At 25 kyr after present (Upper panel) a subarctic climate prevails and continuous permafrost has developed. Two major taliks have formed under the future lakes located at c. 9,000 and 14,600 m along the profile. At 46 kyr after present (middle panel), the taliks are shallow, and not in contact with the deep groundwater. At 50 kyr after present (lower panel) an arctic climate prevails and continuous permafrost reaches its maximum depth in the reference glacial cycle. The maximum permafrost depth is shallower in the humid climate variant (Figure 4-29 and 4-30).

maximum depth of ~460 m, whereas the uncertainty range for the perennially frozen ground reaches a maximum depth of ~420 m (Figure 3-86). It must be noted, however, that this most extreme combination of uncertainties is quite unrealistic. Given that the uncertainty in the maximum depth of perennially frozen ground does not reach 450 m depth even in the most extreme combination of all uncertainties, freezing of groundwater at repository depth is excluded in the *reference glacial cycle*. For a more detailed description of e.g. individual contributions of uncertainty from various parameters affecting permafrost growth, see Section 3.4.4 and /Hartikainen et al. 2010/.

The presence of permafrost and perennially frozen ground may impact the buffer and backfill material. The temperature criterion used in SR-Site for buffer freezing is -4°C /SKB 2011/. However, in reality it is likely that buffer clay material freezes at even lower temperatures /Birgersson et al. 2010/. The criterion used for freezing of the material to be used for filling of e.g. deposition tunnels is -2°C /SKB 2011/. The reference glacial cycle evolution of the 0°C isotherm (e.g. permafrost depth) and the -4°C isotherm for the repository location are shown in Figure 4-32. The figures show results from the dry climate variant, i.e. the climate variant with deeper permafrost. The 0°C and -4°C isotherms reach a maximum depth at prior to the first major ice advance, around 50 kyrs after present. As previously mentioned the 0°C isotherm (permafrost) reaches a maximum depth of 250 m, whereas the -4°C isotherm reaches a maximum depth of 150 m (Figure 4-32) in the *reference glacial cycle*.

Table 4-3 summarizes the maximum permafrost depths, frozen depths, and depths of the -2°C isotherm and -4°C isotherm for the *reference glacial cycle*, and also presents the maximum depth of the associated uncertainty intervals.

In this context it should be noted that the depths presented above and in Table 4-3, which were calculated including the (declining) contribution of heat from the repository, are relevant for the first future glacial cycle. In SR-Site, the full safety assessment period is 1 Myrs. This means that for the second and following glacial cycles, the permafrost and frozen depths will be somewhat deeper (~37 m), see Figure 3-87, since the heat contribution from the repository has become insignificant. This issue is included in the analysis in the SR-Site buffer freezing scenario /SKB 2011, Section 12.3/.

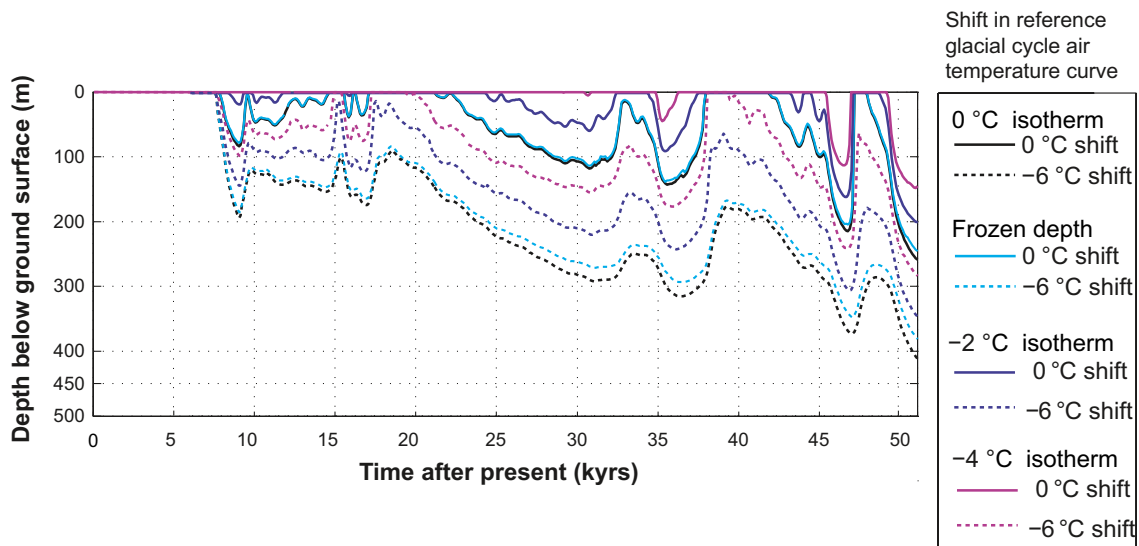


Figure 4-32. Evolution of 0°C isotherm (permafrost depth), perennially frozen ground and -2 and -4°C isotherms at the Forsmark repository location for the first ~50,000 years of the reference glacial cycle (solid lines, i.e. 0°C shift of reference glacial cycle air temperature curve). Dashed lines show the lower boundaries of the corresponding uncertainty intervals when considering the maximum uncertainty in air temperature ($\pm 6^{\circ}\text{C}$) (Appendix 1). The results are from the dry climate variant, i.e. the variant with deeper permafrost, see Section 3.4.4. For corresponding results for other shifts of the temperature curve, see /Hartikainen et al. 2010/.

Table 4-3. Maximum depths of permafrost (0°C isotherm), perennially frozen ground, –2°C isotherm and –4°C isotherm for the reference glacial cycle calculated using the 2D permafrost model /Hartikainen et al. 2010/. The uncertainty interval includes the unlikely combination of having all uncertainties, including air temperature, set at the most pessimistic values favouring permafrost growth.

	Maximum permafrost depth (0°C isotherm) [max uncertainty interval]	Maximum depth perennially frozen ground [max uncertainty interval]	Maximum depth –2°C isotherm [max uncertainty interval]	Maximum depth –4°C isotherm [max uncertainty interval]
Reference glacial cycle	259 m [down to 463 m]	246 m [down to 422 m]	200 m [down to 388 m]	148 m [down to 316 m]

The climate that may prevail in the Forsmark region during periods of periglacial climate domain was as previously described, studied by climate modelling /Kjellström et al. 2009b/, including erratum Feb 2010/, see Section 4.3.2.

The results show that, given a prescribed restricted ice sheet coverage during the interstadial between the two phases of ice sheet coverage (Figure 4-25), the climate at Forsmark is subject to dry and cold periglacial conditions at the end of the interstadial. For the selected modelled time period (44 kyrs BP), the climate in the Forsmark region is considerably colder and drier than at present. The modelled mean annual air temperature is 12°C colder than at present whereas the precipitation is reduced by more than 30% (Section 4.3.2). The results of the study thus show that climate conditions are clearly favourable for permafrost growth during this cold stadial of the *reference glacial cycle*. These climatological description, and several other climatic parameters reported in /Kjellström et al. 2009b/, together give one detailed example of the climatic characteristics that may prevail at the Forsmark site during periods of periglacial climate domain. In addition to the climate modelling performed by /Kjellström et al. 2009b/, the same study also simulated vegetation types associated with the different climate cases studied. The results of the vegetation simulations for e.g. the periglacial climate case are reported in /Kjellström et al. 2009b/ and /SKB 2010d/.

Some general conclusions about the site-specific evolution of permafrost and perennially frozen ground for the *reference glacial cycle* can be drawn.

- Permafrost (i.e. the 0°C isotherm) reaches a depth of ~250 m in the *reference glacial cycle*.
- If considering the combined uncertainties related to surface conditions (vegetation types, snow cover and climate humidity) and subsurface conditions (e.g. bedrock thermal conditions and geothermal heat flow), the uncertainty range for the perennially frozen ground reaches a maximum depth of ~290 m (Figure 3-85).
- If considering the uncertainties in climate (in air temperature curve and humidity), the uncertainty range for the perennially frozen ground reaches a maximum depth of 380 m (Figure 3-79).
- If considering the extreme and unrealistic combination of setting *all* known uncertainties (in air temperature curve, climate humidity, surface wetness, vegetation, snow cover, bedrock thermal conductivity and diffusivity, and geothermal heat flux) at their values most favourable for permafrost growth, the uncertainty range for the permafrost depth reaches a maximum depth of ~460 m and for the perennially frozen ground ~420 m (Figure 3-86).
- The maximum depth of the –4°C isotherm reaches a depth of ~150 m over the repository in the *reference glacial cycle* (Figure 3-69).
- If including the extreme and unrealistic combination of setting *all* uncertainties (in air temperature curve, climate humidity, surface wetness, vegetation, snow cover, bedrock thermal conductivity and diffusivity, and geothermal heat flux) in their most favourable setting for permafrost growth, the uncertainty range for the –4°C isotherm reach a maximum depth of ~320 m (see Figure 3-86).

Given these results, freezing of groundwater at repository depth is excluded in the *reference glacial cycle*.

The maximum depths of permafrost, frozen ground, –2°C isotherm, –4°C isotherm, and uncertainties for both the *reference glacial cycle* are summarised in Table 4-3. For a detailed description of the uncertainties associated with the permafrost modelling, see Section 3.4.4.

4.5.4 Evolution of climate domains

Based on the above evolutions of ice sheet, shore-level and permafrost, the climate development at the Forsmark site for the *reference glacial cycle* can be described as successions of climate domains and submerged periods (Figure 4-33). The temporal evolution of all climate domains relevant for Forsmark in the SR-Site *reference glacial cycle* is presented in Figure 4-34. Considering that the development of permafrost in Figure 4-34 has been simulated specifically for the repository location (Section 3.4.4 and 4.5.3), the development of climate domains in Figure 4-33 and 4-34 also refers specifically to the repository location and not to the entire Forsmark site (Figure 3-58). For a description of the spatial representativity and development of the climate domains, see the description on *Transitions between climate domains* below in this section.

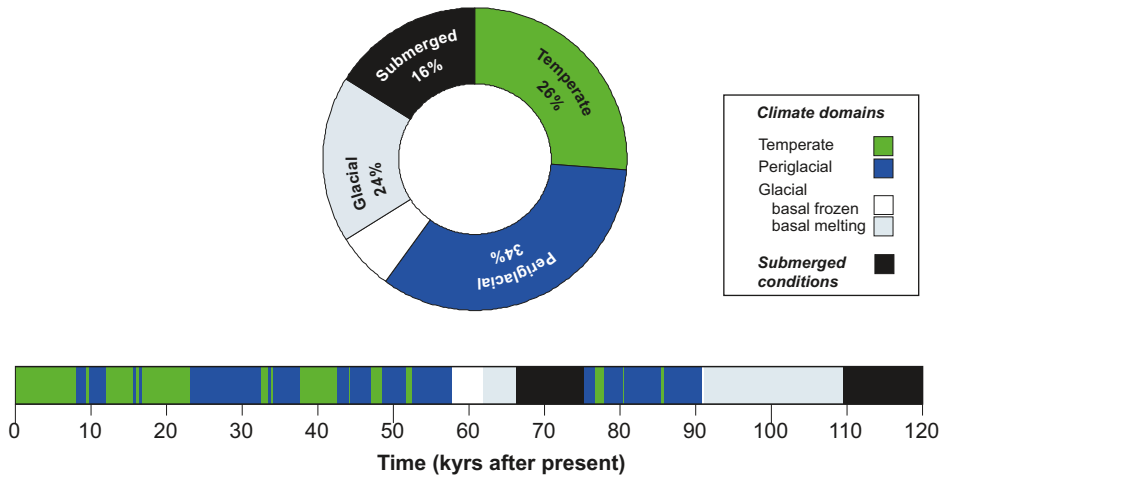


Figure 4-33. Duration of climate domains and submerged conditions at Forsmark in the SR-Site reference glacial cycle, expressed as percentage of the total time of the reference glacial cycle. The bar below the pie chart shows the development of climate-related conditions for the reference glacial cycle as a time series of climate domains and submerged periods. Other possible future climate developments are described in Chapter 5.

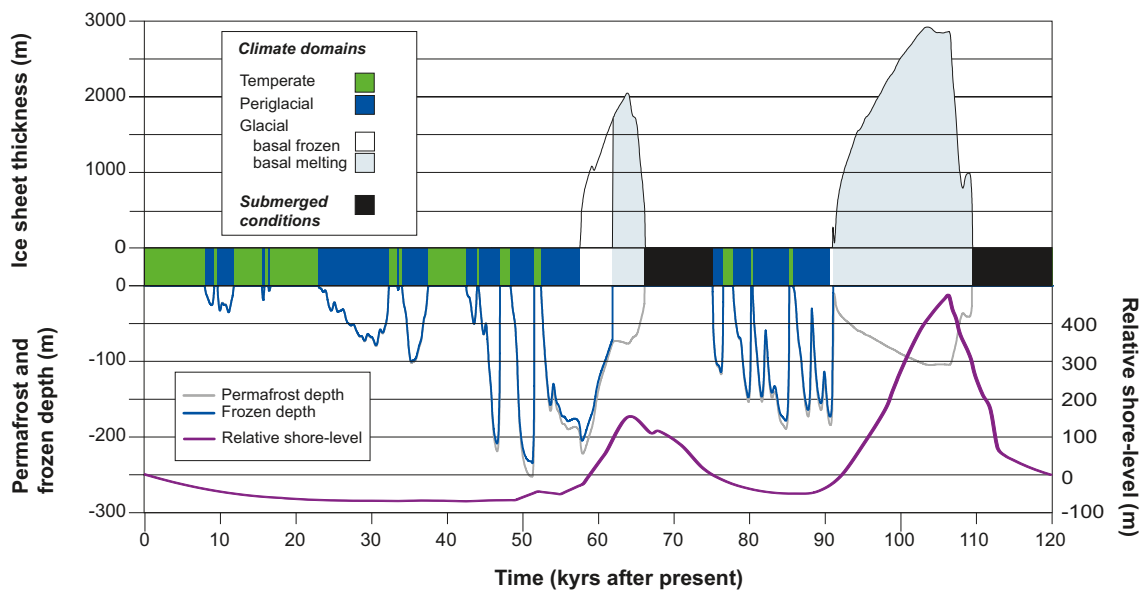


Figure 4-34. Evolution of important climate-related variables at Forsmark for the coming 120 kyr in the SR-Site reference glacial cycle. Other possible future climate developments are described in Chapter 5.

At Forsmark, periods with periglacial climate domain correspond to 34% of the total time of the *reference glacial cycle* (Figure 4-33), whereas periods with temperate climate domain occupies 26%, the glacial climate domain 24% and periods with submerged conditions 16% of the *reference glacial cycle*, see also Table 4-4.

Table 4-4. Duration of climate domains in the SR-Site reference glacial cycle.

Climate domain	Duration (% of reference glacial cycle)	Duration (years)
Temperate climate domain	26%	31,200
Periglacial climate domain	34%	40,800
Glacial climate domain	24%	28,200
Submerged conditions	16%	19,200

The climate succession bar in Figure 4-33 shows that the Forsmark site is dominated by temperate climate conditions for the first ~25 kyrs, although shorter periods of periglacial climate domain occur around 10 kyrs after present. Subsequently, up to the first period of glacial climate domain, temperate conditions are gradually replaced by periglacial conditions. The ice-free interstadial period around 80–90 kyrs after present in the *reference glacial cycle* is dominated by permafrost conditions. The trend with gradually more dominating permafrost conditions is a natural result of the progressively colder climate during the glacial cycle. An exception to this trend is the short period after the submerged phase that follows the final deglaciation, at the very end of the scenario. At that time, ice-free conditions are again dominated by temperate conditions in a warm interglacial climate. Yet another effect of the progressively colder climate during the glacial cycle is the increasing length of the periods with glacial climate domain.

Periods of temperate climate domain occurs in Forsmark in the early phase of the glacial cycle, during short periods of the interstadial between the two major ice advances, and during the interglacial period following the glacial maximum. The periods of temperate climate domain in the early phases of the *reference glacial cycle* are generally warmer and longer than those occurring during interstadials in the later part of the glacial.

During the first 50 kyrs of the *reference glacial cycle*, and in the period between the two ice advances, the increasingly colder climate results in progressively longer periods of periglacial conditions. The total duration of the periglacial climate domain at Forsmark is about 41 kyrs (Table 4-4). During the most severe permafrost periods in the *reference glacial cycle*, at around 70 kyrs BP (Figure 4-34), the permafrost at the repository location develops to between ~180 and ~250 m depth depending on assumed ground cover. The corresponding depths of perennially frozen conditions are between ~180 and ~250 m. The maximum permafrost depth along the entire profile investigated for permafrost development (Figure 4-21) is between 220 and 300 m for the same simulation. The maximum depth of perennially frozen ground along the profile is from 210 to 300 m. The uncertainties related to the simulated permafrost depths are described in Section 3.4.4 and 4.4.3.

Forsmark is exposed to two major ice advances and retreats during the *reference glacial cycle*, the first advance occurs around 60 kyrs after present and the second after about 90 kyrs after present (Figure 4-34). Prior to both of these glaciated periods, the Forsmark site is situated above sea-level with prevailing permafrost conditions when the ice sheet advances towards and over the site. A period of basal frozen conditions initiates the first major period of glacial climate domain. The period of basal frozen conditions is ~4 kyrs long.

After the first glacial period, the site is submerged under the Baltic Sea (Figure 4-34). Following from the warm climate conditions reconstructed for the first part of MIS 3 during the Weichselian (Section 4.3.2), with present-day air temperatures during summer in northern Fennoscandia, temperate climate conditions are envisaged to prevail at Forsmark during the first several thousands of years of the submerged period (not seen in Figure 4-34). That is, if the site were not submerged after the first glacial period, due to a thinner ice sheet and less isostatic depression, subaerial temperate climate conditions would prevail at the site for considerable amount of time after ~66 kyrs after present.

The landscape is in a state of continuous permafrost coverage during the time of the first ice advance over the site, at around 70 kyrs after present (Figures 4-29 and 4-34). At this time, all present and future lakes at the Forsmark site are infilled /SKB 2010d/, and hence there are no taliks present under lakes. Nevertheless, a hypothetical situation with an ice sheet co-existing with taliks under lakes at the Forsmark site is investigated by groundwater modelling in /Vidstrand et al. 2010/.

When the ice sheet expands over the site, it insulates the ice sheet bed from the cold air temperatures and in time induces ice sheet basal melting conditions. During periods of ice sheet coverage, the development of subglacial permafrost is more restricted than permafrost development during ice-free conditions (Figure 4-34). The total length of periods of glacial climate domain in the *reference glacial cycle* is 28 kyrs at Forsmark (Table 4-4). During this time, basal melting conditions dominate.

For detailed examples of how the climate may be characterized in Sweden and in the Forsmark region under periglacial and glacial conditions, see the exemplified climates of the Weichselian glacial cycle in Section 4.3.

The climate simulations /Kjellström et al. 2009b/, show that there is a large range in possible climates for the Fennoscandian region in a 100 kyr time perspective. Excluding the situation when the region is covered by an ice sheet, annual mean air temperatures for the Forsmark region differ from the simulated cold MIS 3 stadial climate (Section 4.3.2) to the future warm climate (Section 5.1.7) by 12–15°C. Correspondingly, annual mean precipitation is almost a factor two higher in the future warm climate compared with MIS 3 at these sites.

Figure 4-35 shows both the first and second repetition of conditions reconstructed for the last glacial cycle (i.e. the *reference glacial cycle*), illustrating how glacial cycles are envisaged to follow each other in the 1 million year time perspective of the safety assessment reference evolution see /SKB 2011/.

The first full interglacial period, following the present one, is shown at around 110 to 130 kyrs after present (Figure 4-35). The onset and ending of this future interglacial period, as well as the corresponding onset and ending of the Holocene, is here defined from the development in the Forsmark region; the onsets of the interglacials are defined by the timing of the deglaciation of the area, whereas the ending is defined by the first occurrence of permafrost in the *reference glacial cycle* (Figure 4-35). The timing and duration of the Holocene and future interglacial period in Figure 4-35 is thus determined from the development in the *reference glacial cycle*, which for this part of the glacial cycle is based on site-specific observations and modelling. The resulting, *locally defined*, Holocene interglacial and future interglacial periods have a length of ~18 kyrs. This duration is in line with the longer of the two types of interglacials, with durations roughly of either ~20 kyrs or ~10 kyrs, that have occurred during the past eight glacial cycles /Tzedakis et al. 2009/.

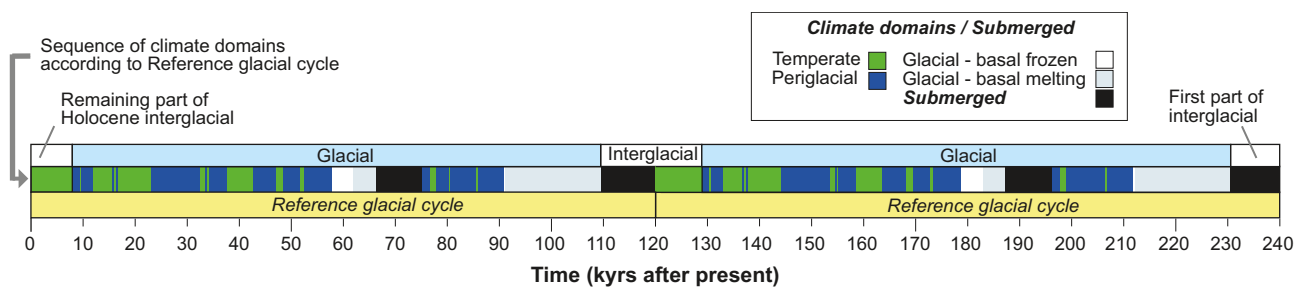


Figure 4-35. Evolution of climate at Forsmark for the coming 240 kyrs using repetitions of the reference glacial cycle. The figure illustrates how the reference glacial cycle is repeated in order to finally cover the 1 million year time perspective of the SR-Site reference evolution see /SKB 2011/. The resulting duration of the locally defined interglacial periods, see the text, is in this case approximately 19 kyrs. For approximately half of that interglacial time, the Forsmark site is submerged under the Baltic water level. Other possible future climate developments are described in Chapter 5.

The uncertainties in the *actual* length of the present and future interglacial periods are naturally very large. Given these uncertainties, it is again emphasized that the evolution of climate domains as described in the *reference glacial cycle* (Figures 4-33, 4-34, 4-35), and corresponding base case of the SR-Site main scenario (Figure 1-3), is not an *expected* future climate evolution. It is one relevant example of an evolution covering the climate-related conditions that can be met in a 100 kyr time perspective. Other possibilities for the length of the present interglacial period are handled in the additional climate cases, including the *global warming case* and *extended global warming case* (Chapter 5).

The sequence of main climate-related events for the *reference glacial cycle*, including times of transitions between events and corresponding climate domains, is summarized in Table 4-5.

For the set up of the groundwater modelling, a simplified climate development for the reference glacial cycle has been produced (Figure 4-36, Table 4-6). In the simplified reference glacial cycle, climate periods of short duration have been removed and longer periods are used to describe the general climate development in Figure 4-33 and 4-34. In the simplified reference glacial cycle, the total duration of each climate domain is however the same as in the detailed reference glacial cycle presented in Table 4-4.

Table 4-5. Sequence of climate-related events for the reference glacial cycle, including the full Holocene. The same sequence of events is seen in Figure 4-33 and 4-34.

Event	Time for transition between events	Climate domain
Deglaciation/ Start Holocene interglacial (locally defined as time of deglaciation of Forsmark)	10,800 before present (BP) (8800 BC)	–
Holocene interglacial	–	Temperate climate domain (incl. submerged conditions)
Present	0 BP	
End of Holocene interglacial (locally defined as first occurrence of permafrost in reference glacial cycle)	7400 after present (AP) (9400 AD)	–
Periglacial and temperate conditions (progressively longer periods of permafrost conditions)	–	Periglacial- and temperate climate domains (progressively shorter phases of temperate climate conditions)
End of periglacial and temperate conditions. Start of glacial conditions	57,600 AP (59,600 AD)	–
First phase with glacial conditions	–	Glacial climate domain
Deglaciation at site. Start interstadial conditions	66,200 AP (68,200 AD)	–
Interstadial conditions	–	Mainly periglacial climate domain (incl. submerged conditions and short temperate periods)
End of interstadial conditions. Start of glacial conditions	90,800 AP (92,800 AD)	–
Second and main phase with glacial conditions	–	Glacial climate domain
Deglaciation/start of interglacial (locally defined as time of deglaciation of Forsmark)	109,500 AP (111,500 AD)	–

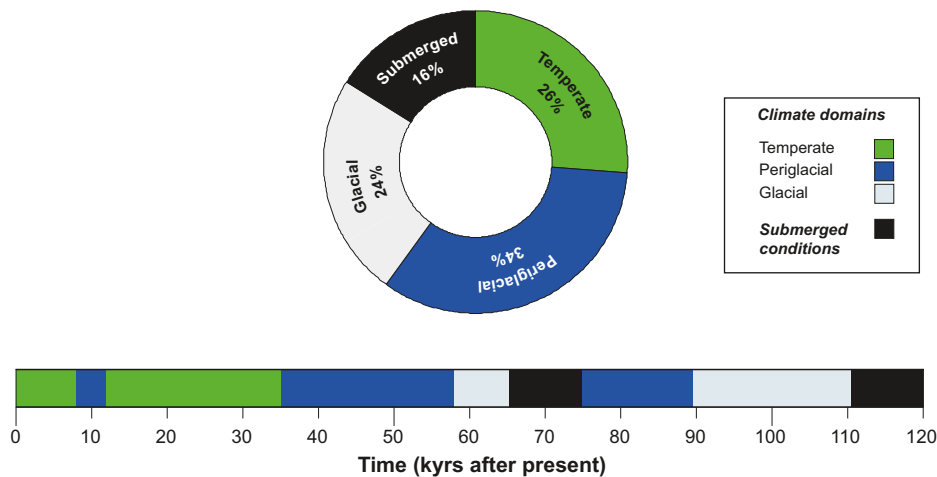


Figure 4-36. Simplified reference glacial cycle. The total durations of the climate domains are the same as in the detailed reference glacial cycle seen in Figure 4-33.

Table 4-6. Simplified climate development for the reference glacial cycle.

Climate domain/ Submerged conditions	Time (kyrs after present)	Duration (kyrs)
Temperate	0–8	8
Periglacial	8–12	4
Temperate	12–35	23
Periglacial	35–58	23
Glacial	58–65	7
Submerged	65–75	10
Periglacial	75–89	14
Glacial	89–111	22
Submerged	111–120	9

Transitions between climate domains

Depending on what spatial scale is considered, the transitions between climate domains need to be described differently. If considering the repository site only, or even the central part of the repository, the transitions between climate domains (temperate-, periglacial-, glacial domain and submerged conditions) may be described as more or less instantaneous in time, as perceived from the way the succession of climate domains are depicted in Figure 4-34. This is in line with the fact that the permafrost modelling used for Figure 4-8 was conducted specifically for the repository site, see Section 3.4.4 and 4.5.3. (The ice sheet and GIA modelling used for Figure 4-34 were done on a much coarser spatial scale, but the results from the larger model grid cells are here taken to represent the ice sheet- and shore-level development at the repository location).

However, if looking at Forsmark on a site-scale, i.e. several hundreds of square km (see Figure 4-37), the transition between climate domains is of a gradual nature, both spatially and temporally. The main transitions within the *reference glacial cycle* occur when the site goes from i) temperate climate domain to periglacial climate domain, ii) periglacial climate domain to glacial climate domain, iii) glacial domain to submerged conditions and finally iv) from submerged conditions back to temperate climate domain.

The transient nature of the change from temperate climate domain to periglacial climate domain is illustrated in Figure 4-29. Sporadic permafrost starts to grow more or less simultaneously over the site. Subsequently, if climate allows, the permafrost may develop to a discontinuous- and continuous spatial coverage. The duration of such a full transition in the *reference glacial cycle*, i.e. the development from a landscape without permafrost to a landscape with a permafrost coverage of 90% or more at the Forsmark site, is approximately between 2 and 5 kyrs (Figure 4-29).

The transition from periglacial- to glacial climate domain manifests itself as an ice sheet margin that advances over the site. A spatially transient change takes place in one specific direction over the Forsmark site, by which the periglacial climate domain is replaced with glacial climate domain following the advance of the ice sheet front. In the *reference glacial cycle*, the ice sheet margin advances over the site at a speed of ~50 m/year. The duration of this transition in the *reference glacial cycle*, i.e. the time it takes for the ice sheet to advance over the Forsmark site, is around 250 years. Note that permafrost may still exist under the ice sheet for some of the time that the site is assigned to the glacial climate domain (Figure 4-34).

The transition from glacial to submerged conditions constitutes the deglaciation phases of the site, when ice sheet conditions are replaced by submerged conditions. The retreat rate of the ice sheet margin during deglaciation of the Forsmark site is, in the *reference glacial cycle*, ~300 m/year. The duration of this transition, i.e. the time during which one deglaciation occurs over the Forsmark site in the reference glacial cycle, is around 50 years.

According to the model reconstruction of the last phase of ice sheet coverage in the Forsmark area (Section 3.1.4), the ice flow direction during the MIS 2 ice sheet advance was approximately from north, while the ice flow direction during the deglaciation was from north-west. This is in line with the interpretation of glacial striae, with a northerly direction recorded both in the oldest glacial striae and the oldest documented directional transport of the till material as recorded in clast fabric analysis /Sundh et al. 2004/, and with an overall dominating younger striae system showing transport and deposition from the north-west /Sohlenius et al. 2004/. This demonstrates that the transition to and from the glacial climate domain may be spatially different during phases of ice sheet growth and decay.

The transition from submerged conditions to temperate climate domain is manifested by the shore-level displacement caused by the isostatic rebound that follows deglaciation. The duration of this transition in the *reference glacial cycle*, i.e. the time it takes from the very first appearance of land at the site (Figure 4-37) until the last remnants of sea have disappeared from the site is around 12 kyrs /SKB 2010d/. This is the transition that is occurring at the Forsmark site at present, manifested by the slow movement of the shore line across the site. The transient nature of shore-level displacement over the site is further described in /SKB 2010d/.

The durations of the four transitions above are summarised in Table 4-7.

Given the climate evolution of the *reference glacial cycle*, the assumptions made in all modelling exercises (Chapter 3), and the physiographical characteristics of the site, the glacial processes result in the fastest transition between climate domains (Table 4-7). The transition from glacial climate domain to submerged conditions for the Forsmark site is around 50 years. The transition from periglacial to glacial climate domain is about five times slower. These two fastest transitions relate to the glacial climate domain, i.e. to the relatively fast processes of ice sheet advance and decay. The transition from temperate- to periglacial climate domain with continuous permafrost is 40 to 100 times slower than the transition from glacial climate domain to submerged conditions (Table 4-7). The slowest transition is the one from submerged conditions back to temperate climate domain, which, in the *reference glacial cycle*, is around 240 times slower than the transition from glacial climate domain to submerged conditions. This is due to very slow glacial isostatic adjustment of the Earth's crust to the unloading associated with the ice sheet deglaciation (Section 3.3).

Table 4-7. Approximate durations of full transitions between climate domains over the Forsmark site (as shown in Figure 4-37) for the SR-Site reference glacial cycle. In order to compare the duration of the transitions from and to various climate domains, the relative duration time of the transitions are in the last column expressed as numbers compared to the duration that takes place during the deglaciation of the site.

Transition	Approximate duration in reference glacial cycle	Relative duration of transition
Temperate- to periglacial climate domain with continuous permafrost coverage	~2,000 to ~5,000 years	40 to 100
Periglacial- to glacial climate domain	~250 years	5
Glacial climate domain to submerged conditions (deglaciation)	~50 years	1
Submerged conditions to temperate climate domain	~12,000 years	240

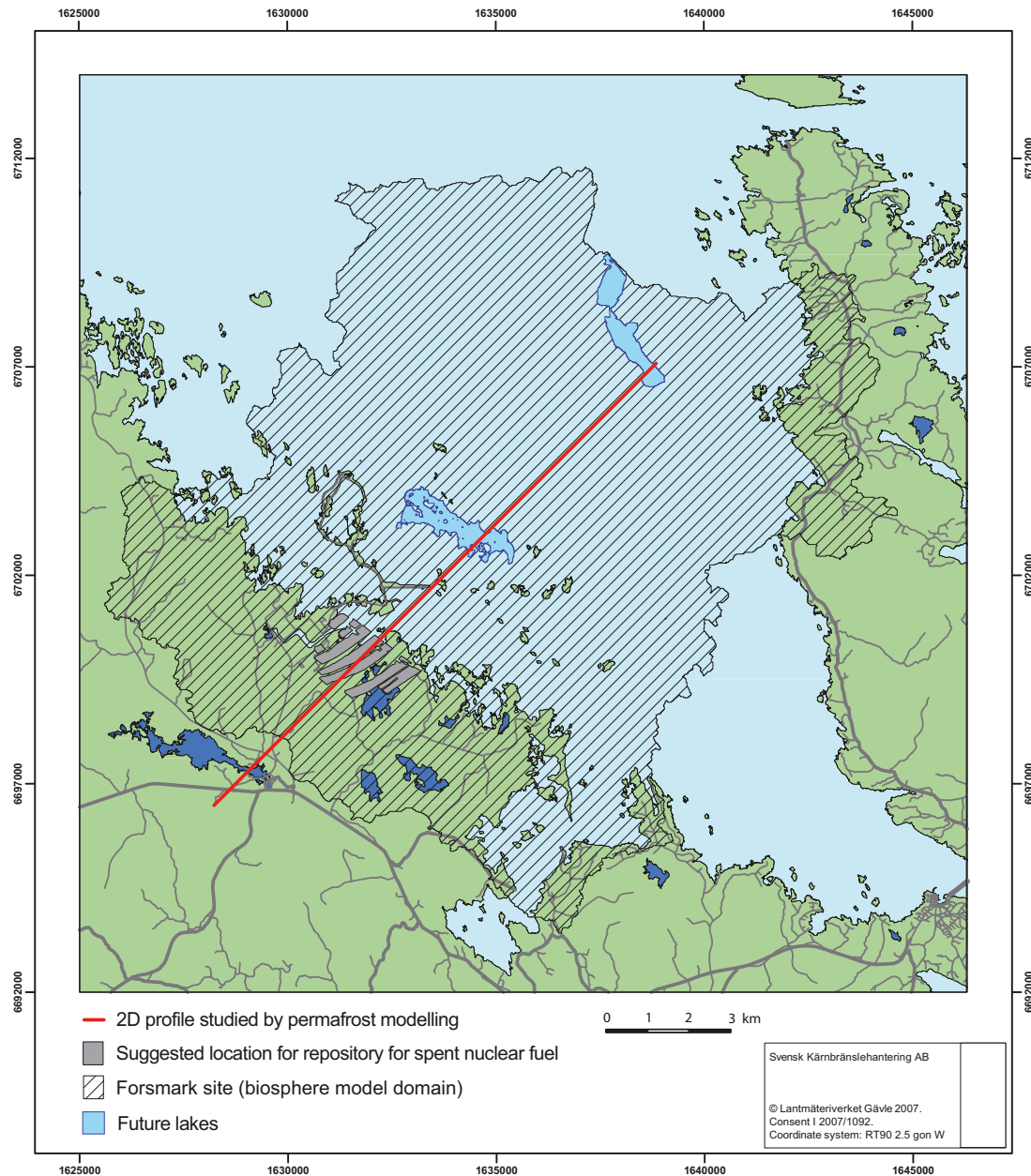


Figure 4-37. The Forsmark site as defined and analysed in the SR-Site biosphere programme (stippled) /SKB 2010d, e/ and the location of the profile studied by 2D permafrost modelling (red line) (Section 3.4.4 and 5.5). The figure is the same as Figure 3-58.

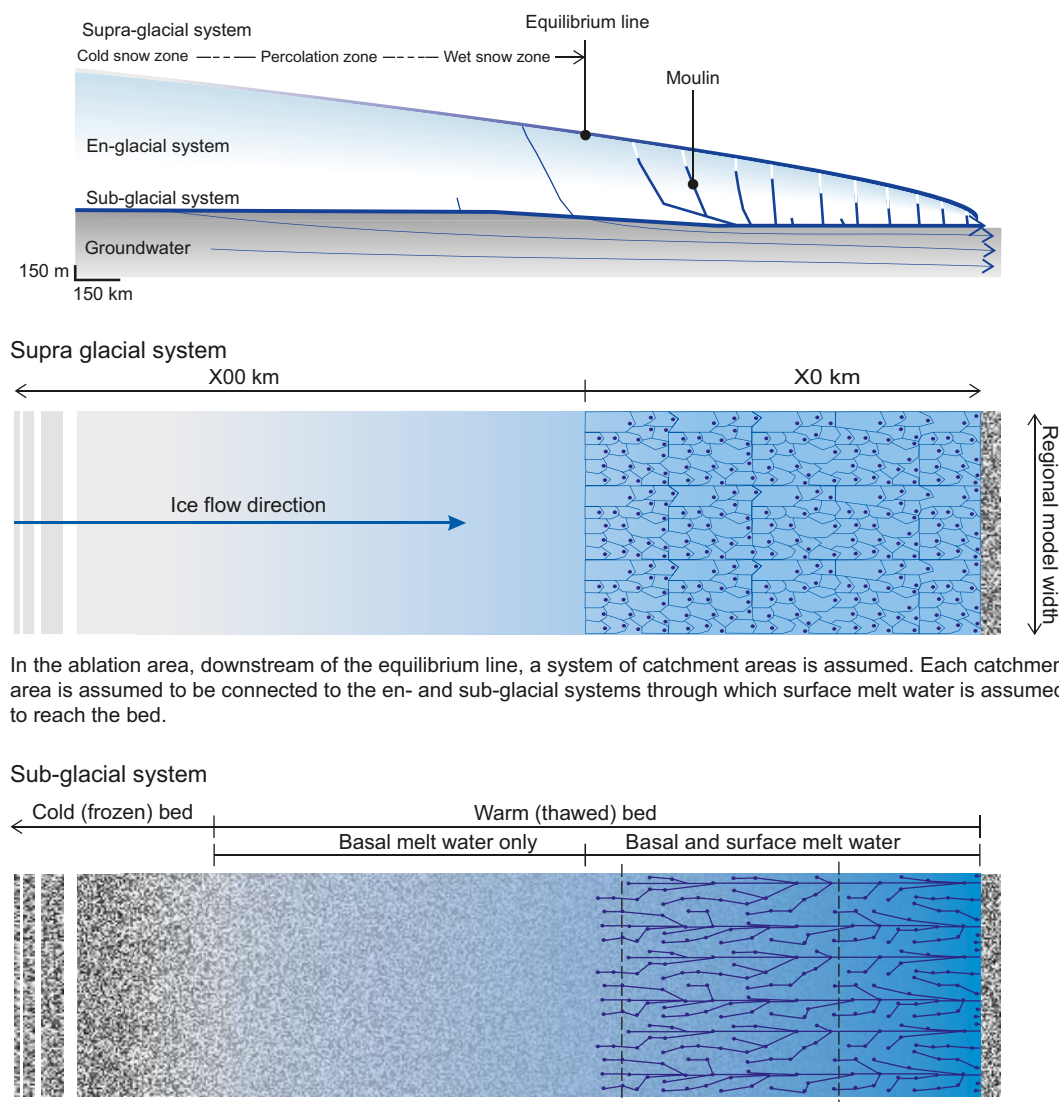
Note that for any given time during these transitions, the Forsmark site (Figure 4-37) contains more than one type of climate domain. For instance, parts of the site may be subject to the periglacial climate domain, having permafrost conditions without an ice sheet, at the same time as another part of the site may be overridden by an ice sheet and thus being subject to the glacial climate domain. Also note that the transition from one climate domain to another over the site does not need to be a full transition (as in the above examples). For instance, discontinuous permafrost may start to form within the site due to lower air temperatures, transforming the affected areas to periglacial climate domain. Thereafter, climate may become warmer and permafrost (and the periglacial climate domain) diminishes and disappears.

The hydrogeological consequences of the ongoing transition from submerged conditions to temperate climate domain at Forsmark is analysed in /Salas et al. 2010/. The hydrogeological consequences of transitions between temperate-, periglacial- and glacial climate domains are analysed in /Vidstrand et al. 2010/.

4.5.5 Evolution of hydrological conditions and groundwater

In SR-Site, dedicated groundwater flow modelling has been performed for all types of climate domains that occur in the *reference glacial cycle*. Groundwater flow modelling of periods with temperate climate conditions are found in /Joyce et al. 2010/, while groundwater modelling of periods with periglacial and glacial conditions are found in /Vidstrand et al. 2010/. The geochemical development during the different climate conditions are presented in /Salas et al. 2010/. An overview of the hydrological and groundwater conditions of the *reference glacial cycle* is given below.

A schematic section through an arbitrary south-western sector of a Fennoscandian ice sheet large enough to cover the Forsmark site is shown in the upper panel of Figure 4-38. A zone of basal melting reaches some hundreds of kilometres from the ice margin in the southeast. The production of basal melt water here varies between 1 and 10 mm/year and can be regarded as constant over the year. In the ablation area below the equilibrium line, melt water from the ice surface and rain is brought to the ice sheet bed through crevasses and moulin. In the *reference glacial cycle* (Figures 4-23 and 4-24) surface melt water production in the ablation area typically varies up to 4–8 m of water per year.



In the ablation area, downstream of the equilibrium line, a system of catchment areas is assumed. Each catchment area is assumed to be connected to the en- and sub-glacial systems through which surface melt water is assumed to reach the bed.

In the area of basal melting, where the water supply is from basal melting only, a slow system is assumed. In the ablation area, downstream the equilibrium line, where both basal and surface melt water are assumed to reach the bed, a fast system with channels or tunnels is assumed.

Figure 4-38. Conceptual model of the ice sheet hydrological system. Upper panel: arbitrary south-western section through a Fennoscandian ice sheet. Middle and lower panels: possible configurations of the supra- and sub-glacial hydrological systems. At present it is not known if water generated at the surface could reach the bed also upstream of the equilibrium line.

More ice melts in lower parts of the ice sheet, and less ice closer to the equilibrium line. During the final deglaciation of the ice sheet in this *reference glacial cycle*, a maximum modelled surface melt rate of 14 m/year occurs. The modelled typical surface melt rate values of 4–8 m/year can be compared with observed present average surface ablation rates of the Greenland ice sheet of a few metres/year /Krabill et al. 2000/ up to ~10 m/year /Bøggild et al. 2004/. During the deglaciation of the Weichselian ice sheet, melt rates of more than 10 m/year may have occurred /Humlum and Houmark-Nielsen 1994/.

During periods of temperate climate domain, the groundwater flow pattern is similar to the present ice free situation, with a mixture of local areas of groundwater recharge, typically at topographically high positions, and discharge, typically in low positions. The groundwater flow is at this time to a large degree driven by topographic gradients in the landscape.

During the initial periods of periglacial climate domain, the permafrost distribution in the Forsmark region is first sporadic followed by discontinuous spatial permafrost coverage, see section on permafrost development above. This results in a modified pattern of groundwater flow, but still with significant groundwater recharge and discharge taking place. When climate gradually gets colder, permafrost grows progressively thicker and more widespread (see section on permafrost development above and Section 4.5.3). When the climate is cold enough, continuous permafrost forms. When continuous permafrost occurs, the precipitation recharge of groundwater is strongly reduced or even stopped, since permafrost influences subsurface hydrology by drastically reducing the hydraulic conductivity of the frozen unit /Burt and Williams 1976, Vidstrand et al. 2010, Hartikainen et al. 2010/. At locations of future deep lakes, unfrozen taliks may exist where groundwater recharge and discharge takes place, see section on permafrost development above and Section 4.5.3. Details on the permafrost and hydrological conditions during such situations are found in /Hartikainen et al. 2010, Vidstrand et al. 2010/.

In this context it is worth noting that even in cases when continuous permafrost is present in the landscape, it is unlikely that the permafrost layer has zero permeability for groundwater flow. A zero permeability would probably require a uniform and very deep permafrost distribution. In many cases, the permeability of the frozen ground could instead be large enough to allow for some groundwater flow through the permafrost. In addition, the increased groundwater flow associated with an advancing ice sheet margin over permafrost terrain is likely to enhance the creation of taliks.

During the first period of glacial climate domain, the ice sheet overrides ground with permafrost (Figure 4-34). In line with the situation with ordinary permafrost, subglacial permafrost under the ice sheet margin acts as a hydrological barrier for groundwater flow /King-Clayton et al. 1997/. Therefore, this phase is characterised by a period with no groundwater recharge under the frontal near part of the ice sheet. Groundwater recharge may still take place further in under the ice sheet, where permafrost may have melted. Even though the ice sheet is cold-based in its frontal-near parts at this time, water from surface melting may still reach the glacier bed or forefield. However, since permafrost is present, this water does not contribute significantly to groundwater recharge.

Even if the 2D permafrost modelling (Section 3.4.4) did not indicate any taliks at the time of ice sheet overriding (at 50 kyrs after present in the *reference glacial cycle*) it is probably not correct to assume an effective large-scale permeability of zero for the pro-glacial landscape at this time. The permeability of the frozen ground can in places be large enough to allow some groundwater flow through the permafrost, and furthermore, the increased groundwater flow due to the large pressure gradient associated with an advancing ice sheet /Vidstrand et al. 2010/ could enhance a creation of taliks.

After the initial cold-based period, subglacial groundwater recharge again takes place at the Forsmark site, this time under the ice sheet due to melting of basal ice (Figure 4-34). In local areas of former groundwater discharge, groundwater recharge typically occurs under glacial conditions e.g. /Breemer et al. 2002/. This results in a dominant subglacial groundwater flow directed downwards under the major part of the warm-based ice sheet, recharging the groundwater aquifer. Subglacial groundwater discharge may possibly occur close to the ice margin /Breemer et al. 2002, Vidstrand et al. 2010/. Even if the permeability of the bedrock were to decrease under the load of an ice sheet, the increased physical and hydraulic gradient, especially associated with passages of the ice sheet margin, would likely increase groundwater flow in bedrock compared to temperate climate domain conditions /Hökmark et al. 2010, Vidstrand et al. 2010/.

As known from present glaciers and ice sheets e.g. /Jansson and Näslund 2009, Jansson et al. 2007/, as well as from the esker and geomorphological record in e.g. Sweden, subglacial ice tunnels may be present at the ice sheet bed. The reason why an ice tunnel may form, and is kept open, is the presence of a high enough basal water pressure and water flux. From observations from glaciers, it is known that atmospheric pressure may exist in parts of the tunnels during parts of the year, typically at the end of the melting season when the input of surface melt water is reduced or stopped, and the ice deformation has not yet reduced the size of the tunnel. However, the tunnel width and length are reduced during the winter season due to the ice deformation and since no meltwater from the surface system is entering the glacial en- and subglacial hydrological system. There are very few observations of these processes from ice sheets. However, it is likely that this closing process is more efficient some distance away from an ice sheet margin, where the ice thickness is greater and associated ice deformation faster. Over one full year, it is likely that the major stretch of subglacial tunnels under ice sheets is dominated by water pressures higher than atmospheric pressure.

The first direct observation of these processes from an ice sheet was made by Wadham et al., see /GAP team members 2009/. For summer conditions at the Russel Glacier, located in the marginal zone of the Greenland ice sheet (Figure 4-39), they concluded that meltwater generated in the lower ablation zone was routed by an efficient, channelized basal drainage system during the height of the melt season. At this time, the conduits were water filled, except for a few km near the ice sheet margin where the tunnels were at atmospheric pressure. The water-filled conduits fluctuated between open and closed channel flow over timescales of days to weeks, as a response to the varying melt water fluxes. Given the information from theory and from observations at smaller glaciers and the Greenland ice sheet, it is unrealistic to envisage large open subglacial ice channels at atmospheric pressure stretching many tens of km in under the ice sheet at Forsmark, and that such channels would stay constantly open for many years.

After the first period of glacial climate domain, the Forsmark site is submerged for up to 9 kyrs (Figure 4-34). When the site subsequently is situated above sea-level during this interstadial at around 80–90 kyrs after present (Figure 4-34), climate is generally cold, which induces new long



Figure 4-39. Part of the Greenland ice sheet in the Kangerlussuaq region, west Greenland. During summer conditions, subglacial channels are here water filled except for a few km near the ice sheet margin where the tunnels were at atmospheric pressure, see Wadham et al. in /GAP team members 2009/. The proglacial area is characterized by continuous permafrost with sub-lake taliks that penetrate the permafrost down to the deep groundwater system. Within this region, SKB, Posiva and NWMO carry out the Greenland Analogue project (GAP) in order to study questions on glacial hydrology and hydrogeology. Photo: Jens-Ove Näslund.

periods of deep permafrost, and associated reduced conductivity in the upper part of the bedrock. During the short temperate conditions during this interstadial, groundwater flow may again be characterized by local areas of recharge and discharge.

During the second and most severe glacial phase, starting around 90 kyrs after present, the ice sheet is cold-based for a considerably shorter initial time than during the first major glacial phase (Figure 4-34). This makes water from surface and basal melting available for groundwater recharge during most of this period of ice sheet coverage. As in the case of the first ice-covered period, steeper physical and hydraulic gradients, especially associated with the passage of the ice sheet front, may, for a limited period, induce more rapid and substantial groundwater flow than under present ice-free conditions, see /Vidstrand et al. 2010/.

Thereafter, at the very end of the *reference glacial cycle*, an evolution corresponding to the Holocene occurs, with Forsmark first being submerged after deglaciation for around 10 kyrs. When the site emerges above sea-level, the climate is much warmer than during the non-submerged period between the two major glacial advances. The Forsmark site is again dominated by temperate climate conditions, with groundwater flow similar to present-day conditions. For a description of the geochemical evolution in this scenario, see /SKB 2011/.

4.5.6 Evolution of mechanical conditions

During the *reference glacial cycle* (Figure 4-23 and 4-24) the temporal evolution of the ice sheet will cause time-varying stresses and deformations in the Earth /Lund et al. 2009/. Due to the long time spans both elastic and viscous deformation occurs. Properties of the ice sheet controlling the deformation and stress change are duration, areal extent, thickness and slope of the ice margin. The evolution of stresses in the crust during a glacial cycle has been studied by /Lund et al. 2009/, who used numerical finite-element modelling of the glacially induced stresses based on the ice sheet development in the *reference glacial cycle*. As the ice sheet advances and the load from the ice increases, the vertical and horizontal stresses will both increase in direct and immediate response to the increasing load. The elastic lithosphere will bend and the viscoelastic mantle will flow laterally. This will, on a large scale, result in a depression beneath the load, where crustal flexure will give an additional slow increase in horizontal stresses in the upper crust. Outside the ice sheet margin, crustal flexure will result in an up-warping peripheral bulge (see also Section 3.3.4), in which the horizontal stresses are reduced. The thicker the ice sheet and the longer duration an area is covered by ice, the larger the induced bending stresses will become. When the growth rate of the ice sheet decreases, the induced horizontal stresses under the load grow larger than the vertical stress and remain so during times of steady-state ice conditions and all through the deglaciation phase. As the ice sheet retreats during deglaciation, the depressed lithosphere will experience isostatic rebound, which is a much slower process than the ice load removal process. Consequently, high horizontal stresses remain in the lithosphere for a significant amount of time after the ice sheet induced vertical stress has disappeared.

The pore pressures in the crust are increased during glaciation as a result of the consolidation of the bedrock, the recharge of meltwater available at the base of the ice sheet and the additional hydrostatic pressure induced by the ice sheet itself. Furthermore, increased pore pressure-levels may also potentially develop beneath an impermeable permafrost layer in front of an approaching ice sheet, cf. /Lönnqvist and Hökmark 2010/. Estimates of the magnitude of the glacially induced pore pressure at different depths and during different phases of a glacial cycle have been made by /Hökmark et al. 2010/.

The discussion on glacially induced stresses and pore pressures implies that the effective rock stress (i.e. the normal stress reduced by the water pressure) varies both with changes in the mechanical load and changes in the pore pressure produced by the ice sheet. The evolution and magnitude of the effective stress during the different parts of the glacial cycle will dictate the mechanical behaviour of rock fractures, and hence, also their water-conducting ability, see /Hökmark et al. 2010/. In general, the increase in total stress during ice sheet advance will act to reduce the transmissivity of fractures and fracture zones. But since the vertical stress increases more rapidly than the horizontal stresses, upper crustal stress axes may rotate so that the vertical stress is the intermediate or largest principal stress. These stress changes, together with the increase in pore pressure as compared with non-glacial hydrostatic conditions, may result in changed transmissivity anisotropy.

Outside the edge of the ice sheet, the reduction in horizontal stresses may give rise to a decreased normal stress acting across steeply dipping fractures, leading to an increase in transmissivity. In the absence of reduced temperatures or increased pore pressure levels due to proglacial permafrost, calculations by /Hökmark et al. 2010/ indicate that the increase will be modest. /Hökmark et al. 2010/ also consider two cases associated with the scenario of proglacial permafrost coinciding with the forebulge stress regime. Firstly, they consider the possibility of increased pore pressure-levels beneath the permafrost layer. Secondly, a further reduction of the horizontal stresses due to reduced temperatures /Hartikainen et al. 2010/ is considered in combination with high pore pressures. /Hökmark et al. 2010/ found that, for the former case, the transmissivity will increase by a factor 2–3 at most. For the latter case, significant transmissivity increases of some vertical fracture orientations (factor around 7) were found at shallow depths. For repository depth more moderate increases by a factor 2–3 were found for identically oriented fractures.

Increased deviatoric stresses may also give rise to shearing of critically oriented fractures, which in turn can yield larger fracture apertures and increased transmissivities. The same effect may also result from elevated pore pressures that will act to reduce the shear strength. However, /Hökmark et al. 2010/ argue that transmissivity increases resulting from shear displacements taking place at high normal stress (>6–7 MPa) are negligible. As described by /Lönqvist and Hökmark 2010/, hydraulic jacking of fractures is also possible, but most likely not deeper than at most 200 metres.

In general, the emplacement of a large ice sheet stabilises faults in the crust and suppresses earthquake activity. During deglaciation, however, the rapid decrease in vertical stress tends to destabilise the crust. Crustal pore pressures are of great significance in the faulting process, since an increased pore pressure decreases the effective normal stress on faults, and hence, reduces their shear strength. If the pore pressure is still enhanced at the end of glaciation, when the vertical load from the ice disappears, fault stability will be further reduced. Observations of large end- or postglacial faults in northern Scandinavia show that such a process was indeed active at the end of the last glaciation.

4.5.7 Surface denudation

For the *reference glacial cycle*, the total amount of surface denudation, i.e. the combined effect of surface erosion and weathering, is expected to be 1–2.6 m for the repository location in Forsmark (Section 3.5.4, Table 3-17).

The major part of this denudation is a result of glacial erosion, occurring during phases of warm-based ice sheet coverage. These warm-based periods of glacial erosion occur after 60 kyrs, and between 90 and 110 kyrs into the *reference glacial cycle* (Figure 4-34). The amount of glacial erosion at the repository location is estimated to 1–2 m for this glacial cycle (Table 3-17). This relatively low amount of expected glacial erosion is a result of the very flat topography in the area, and that the erosional capacity of the ice sheet is relatively small (compared with considerably more active erosion by more active ice sheets or smaller glaciers in other climatological and topographic settings, such as along the Norwegian coast or alpine environments. For examples of various glacial erosion rates from different climatological and topographic environments, see /Olvmo 2010/, and references therein).

The non-glacial component of surface denudation, resulting from all other active erosion and weathering processes, such as weathering and fluvial erosion during temperate- and periglacial climate conditions, is estimated to amount up to 0.6 m for the *reference glacial cycle* (Table 3-17).

All in all, the total denudation for the *reference glacial cycle* is estimated to be limited at Forsmark (less than 3 m), since the area is dominated by the well-preserved sub-Cambrian peneplain (Section 3.5.4). The dissected area with sometimes considerable relief in the coastal areas, some 25 km south-east of Forsmark, may experience more efficient glacial erosion during a glaciation with a similar erosional characteristics as during the Weichselian. In this area, glacial erosion of more than 10 m is expected locally in low topographic positions. However, this is not the case for Forsmark and the repository location.

The removal of bedrock by surface denudation results in a reduction of the repository depth. A reduced repository depth could in turn lead to permafrost and frozen ground reaching closer to the repository. However, a total denudation of less than 3 m for the *reference glacial cycle* (Table 3-17) has a negligible effect, in terms of repository safety, on the estimated permafrost- and freezing depths presented in Section 4.5.3 and 5.5.3. In this context, also the estimated total denudation of around 20 m over the repository in a 1 Myr time perspective (Table 3-17) is insignificant in terms of repository safety.

5 Additional climate cases for the safety assessment SR-Site

In order to cover the uncertainty in future climate development, the *reference glacial cycle* (Section 4.5) has been used to construct additional climate cases with a potentially larger impact on repository safety than the reference cycle, see Figure 1-3. Consequently, they form the basis for the global warming variant of the main SR-Site safety assessment scenario, and also for other additional safety assessment scenarios, see Figure 1-3 and /SKB 2011/. The climate-related issues having the greatest impact on repository safety functions are:

- Maximum permafrost and ground freezing depth;
- Maximum hydrostatic pressure;
- Penetration of oxygen to deep groundwater;
- Occurrence of dilute or extremely saline groundwater;
- Reduction of retardation in the geosphere due to high groundwater fluxes and/or mechanical influences on permeability.

These issues are mainly related to extremes within the temperate-, periglacial-, and glacial climate domains. For a description of the strategy for using and selecting the additional climate cases, see the section on *Strategy for managing long-term evolution of climate-related processes* (Section 1.2.3), and the section on *Rationale and general approach* (Section 4.1). For the SR-Site safety assessment, the climate cases presented in Table 5-1 are considered.

Chapter 5 describes climate cases 2–6 in Table 5-1 and Figure 1-3. In addition to the description of the parameters that the climate cases were designed to take care of, for instance maximum thick ice sheets, a description of expected changes in surface denudation are also described for each case. The removal of bedrock by surface denudation affects the repository depth, which in turn may affect e.g. the possibility for permafrost- and frozen ground to reach the repository. Climate cases with an expected larger total denudation than in the *reference glacial cycle* are therefore considered more important, and are thus described in more detail, compared with cases with an expected denudation smaller than in the *reference glacial cycle*, which are described only briefly.

5.1 Global warming case

5.1.1 Background

There is a large range of potential future climate developments when considering the combined effect of natural and anthropogenic climate change. One such case is described in the present *global warming case*. This case describes a future climate development influenced by both natural climate variability and climate change induced by anthropogenic emissions of greenhouse gases, with the latter resulting in weak to moderate global warming. In order to cover a reasonably broad array of future climate developments based on present knowledge, a case of *extended global warming* is also included in the SR-Site safety assessment (Section 5.2), describing a situation with stronger and longer-lasting global warming.

Table 5-1. Climate cases considered in the SR-Site safety assessment. Cases 2 to 6 are described in the present chapter of the report. The table contains the same information as Table 4-1.

Case number (section in present report)	Climate case	Description
1 (Section 4.5)	<i>Reference glacial cycle</i>	Repetition of reconstructed last glacial cycle conditions
2 (Section 5.1)	<i>Global warming</i>	Longer period of initial temperate conditions than in case 1
3 (Section 5.2)	<i>Extended global warming</i>	Longer period of initial temperate conditions than in case 2
4 (Section 5.3)	<i>Extended ice sheet duration</i>	Longer duration of ice sheet coverage than in case 1
5 (Section 5.4)	<i>Maximum ice sheet configuration</i>	Largest ice configuration in past two million years
6 (Section 5.5)	<i>Severe permafrost</i>	Favourable for early and deep permafrost growth

The purpose of the *global warming case* and the *extended global warming case* is to give a picture of the possible impact of global warming on the repository and also to cover extremes of warm conditions with respect to repository safety. In general, temperate climate conditions are not negative for the repository safety, as the conceivable conditions occurring within the temperate domain have limited impact on repository safety functions. However, if for some reason, a release from the repository does occur, previous safety analyses have shown that peak doses occur during periods when the area above the repository is situated above sea-level, and areas of discharge are located within that area. In addition, prolonged periods of temperate climate conditions above sea-level may result in lower groundwater salinity. The effects of this also needs to be assessed in terms of e.g. buffer stability /SKB 2011/.

There is a large amount of published information on various aspects of global warming in recent literature. The intention with this section and the section on the *extended global warming case* is not to give a comprehensive description of the present status on knowledge in the global warming issue (with its causes, effects, uncertainties etc). Instead, the aim is to include information and data that support the treatment of this complex topic at a level required for the safety assessment. To this end, both general scientific literature is used as well as dedicated studies performed for SR-Site. For further descriptions of the topic of global warming, the reader is referred to the compilations by /IPCC 2007, Bates et al. 2008, Jol et al. 2008, Allison et al. 2009, Richardson et al. 2009, Rummukainen and Källén 2009, Arndt et al. 2010/, and references therein. Detailed descriptions of global warming and its effects specifically on Sweden and the Baltic region is found in /SOU 2007, Miljöförhållanden 2007, BACC author team 2008/.

In SR-Site, there are two main reasons for analysing cases of climates warmer than the *reference glacial cycle*; i) modelling studies of the climate response to increased greenhouse gas emissions, mainly CO₂, indicate that global temperatures will increase in the future under such conditions, e.g. /IPCC 2007, Kjellström et al. 2009b/, and ii) natural long-term climate cycles are believed to be driven mainly by changes in solar insolation (Section 2.2). The coming 100 kyr period is initially characterised by exceptionally small amplitudes of insolation variations /Berger 1978/, suggesting that the present interglacial may be exceptionally long. If considering the known future changes in insolation, /Loutre and Berger 2000/ and /Berger and Loutre 2002/ suggest that the interglacial may end ~50 kyrs after present. This is illustrated in Figure 5-1, showing modelled Northern Hemisphere ice sheet volumes for the coming 130 kyrs, based on a model forcing only by future variations in insolation and natural as well as anthropogenically increased CO₂ levels. Given this insolation forcing, the model results suggest that a growth of the Greenland-, Eurasian- and North American ice sheets would not start until after 50 kyrs after present even without increased CO₂ levels.

However, /Müller and Pross 2007/ suggest that under natural climate forcing conditions, the present insolation minimum holds the potential to terminate the Holocene interglacial. This supports a hypothesis by /Ruddiman 2003/ which proposes that early anthropogenic greenhouse gas emissions prevented the inception of a glacial that otherwise already would have started.

In addition to handling future variations in insolation, the *global warming case* also includes the effect of low to moderate global warming from an anthropogenic increase of atmospheric CO₂ levels, e.g. /IPCC 2007/. (Higher levels of greenhouse gas concentrations, also described by e.g. /IPCC 2007/, with an associated longer period of temperate climate conditions, are treated in the *extended global warming case*, see Section 5.2). In the *global warming case*, peak air temperatures are envisaged to be reached within the first hundreds to thousands of years. Mean annual air temperatures several degrees warmer than at present then occur in central Sweden and Forsmark. Subsequently, following a decline in atmospheric CO₂ concentrations, air temperatures are envisaged to show a general slow decline for the rest of the long initial period with temperate climate conditions.

The reduction of atmospheric CO₂ concentrations, following peak values, is a very slow process, e.g. /Archer 2005, Lenton and Britton 2006, Tyrell et al. 2007, Archer and Brovkin 2008, Schaffer et al. 2009/. This suggests that the onset of colder climate conditions, after the initial temperate period, also would be a gradual and slow process. Therefore, it is appropriate to use the mild onset of colder climate conditions reconstructed for the last glacial cycle (Section 4.5.4) for the climate development following the initial temperate period. In order to describe the combined effect of known variations in insolation and a low- to moderate global warming, the *global warming case* therefore assumes

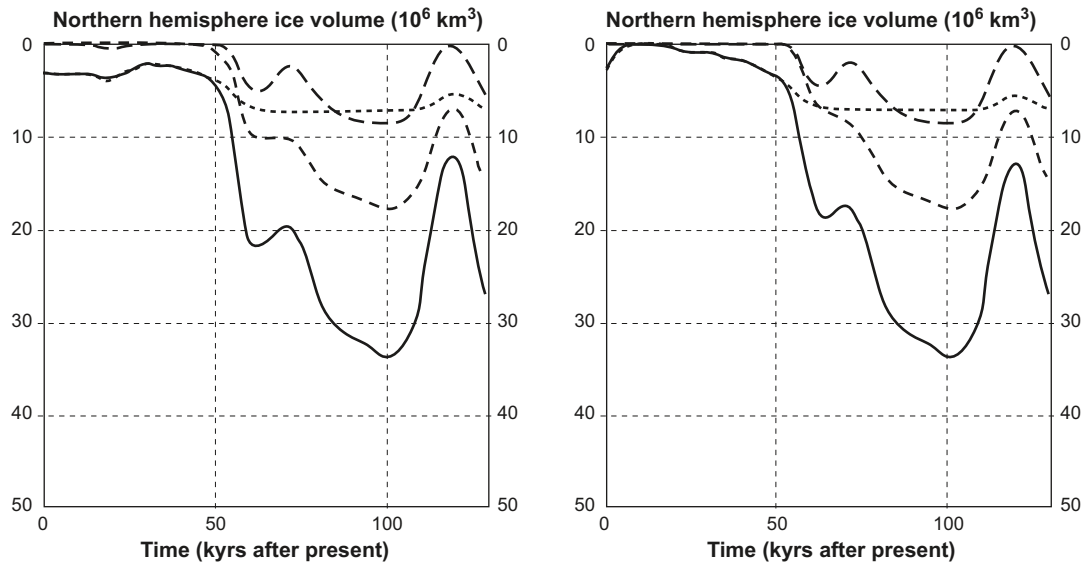


Figure 5-1. Simulated ice volume of the Northern Hemisphere over next 130 kyr using model forcing only by variations in insolation and natural CO₂ levels (left). The right figure shows a corresponding simulation but with a global warming scenario with an atmospheric CO₂ concentration peak of 750 ppmv within 200 yrs. Ice volume of the Northern Hemisphere (full line), Greenland ice sheet (dotted line), North American ice sheet (dashed line) and Eurasian ice sheet (long-dashed line). The initial Greenland ice sheet corresponds to the present one. Modified from /Loutre and Berger 2000/.

that the present temperate climate domain, albeit with higher initial air temperatures, will prevail for 50,000 years longer than in the *reference glacial cycle*. Following the first 50 kyr of additional temperate climate conditions, the first 70 kyr of the *reference glacial cycle* is assumed to follow. This results in c. 60 kyr of temperate climate conditions at Forsmark before the ending of the present interglacial (the ending locally defined as the time of first occurrence of periglacial conditions with permafrost, see Section 4.5.4). This development is in broad agreement with results simulated for two global warming cases within the BIOCLIM project /BIOCLIM 2003/.

5.1.2 Ice sheet evolution

In this case of low to moderate global warming, colder climates again arise in the latter half of the coming 120 kyr. The climate cooling associated with a slow reduction in atmospheric greenhouse gas concentrations results in a Fennoscandian ice sheet forming in the same way as in the *reference glacial cycle*, but in this case 50,000 years later. In the *reference glacial cycle*, two main phases of ice sheet coverage took place at Forsmark. In the *global warming case*, only the first of these two phases occurs, around 110 kyr after present. The characteristics of this glacial period are identical to the first major glacial period of the *reference glacial cycle*. The maximum ice sheet thickness during this event is just above 2,000 m. The glacial climate domain persists for around 10 kyr, of which the first half consists of cold-based ice sheet conditions, without local formation of groundwater, whereas the second half consists of warm-based ice sheet conditions with active sub-glacial groundwater formation at Forsmark. Prior to the ice sheet overriding, periglacial conditions with permafrost exist at the site.

5.1.3 Shore-level evolution

The main process of importance for repository safety in the temperate climate domain is changes in shore-level. Due to the near-coastal location of Forsmark, one question related to future global warming is the response of the present glaciers and ice sheets, and associated changes in sea-level and shore-level.

Ice sheets and sea-level

At present, there are major uncertainties in the estimates of future sea-level rise due to global warming. A major part of this uncertainty relates to the response of the cryosphere to increased temperatures. Given the location in a warmer climate at present, the Greenland ice sheet may be more sensitive to increases in air temperature than are the Antarctic ice sheets, especially the East Antarctic ice sheet. After the publication of the fourth assessment report from the Intergovernmental Panel on Climate Change (IPCC) /IPCC 2007/, a wealth of scientific literature has highlighted aspects of the Greenland ice sheet response to climate change, e.g. /Hall et al. 2008, Hanna et al. 2008, Howat et al. 2008, Mernild et al. 2009, van den Broeke et al. 2009, Vinther et al. 2009, Wake et al. 2009, Robinson et al. 2010, Stone et al. 2010b/, including the role of oceanographic warming e.g. /Holland et al. 2008, Hanna et al. 2009, Rignot et al. 2010, Straneo et al. 2010/ and the coupling between climate, ice sheet dynamics and glacial hydrology, e.g. /van de Wal et al. 2008, Joughin et al. 2008, Price et al. 2008/. A summary of various aspects of the Greenland ice sheet in a warming climate is found in /AMAP 2009/. The sea-level contribution from glacial sources are specifically dealt with in e.g. /Gregory and Huybrechts 2006, Meier et al. 2007, Shepherd and Wingham 2007, Pfeffer et al. 2008, Velicogna 2009, Bamber and Riva 2010/.

The present volume of the Greenland ice sheet corresponds to a global sea-level rise of 7.3 m /Bamber et al. 2001/, whereas the maximum contribution to future global sea-level change from melting glaciers and ice caps (i.e. excluding the Greenland and Antarctic ice sheets) is considerably smaller, no more than 0.5 metres (corresponding to the total volume of water stored in glaciers and ice caps at present) /IPCC 2007/.

In some studies, the decay of the Greenland ice sheet under global warming is a relatively smooth function of the temperature increase /Huybrechts and de Wolde 1999/. However, many recent studies have highlighted that the response of the Greenland ice sheet is a complex process, involving internal ice sheet processes as well as the interaction between the cryosphere, atmosphere and ocean, e.g. /Huybrechts et al. 2004, Howat et al. 2008, Thomas et al. 2009, Wake et al. 2009, Vinther et al. 2009, Rignot et al. 2010/. According to /Gregory and Huybrechts 2006/ an increase in annual temperature of $4.5 \pm 0.9^\circ$ or more over Greenland, corresponding to a global temperature increase of $3.1 \pm 0.8^\circ$, could result in an irreversibly collapsing Greenland ice sheet. In the most pessimistic CO₂ scenario of /IPCC 2007/, with a 4° global climate warming by the year 2100 (compared to the period 1980–1999), with a likely range of 2.4° – 6.4° , the warming would in the long run be sufficient to lead to a complete Greenland ice sheet collapse /Huybrechts and de Wolde 1999, Gregory et al. 2004, Alley et al. 2005a, Gregory and Huybrechts 2006, Lunt et al. 2008, 2009, Stone et al. 2010a, b/, and eventually a global mean sea-level rise by 7 m. According to these model simulations, which are acknowledged to not properly represent the dynamics of fast-flowing ice streams, this could happen within a few millennia. If proper ice stream dynamics could have been considered, the ice sheet response to a warmer climate could perhaps be faster than this.

One crucial aspect of sea-level rise due to ice sheet collapse is that the effect of the rising sea-level is not distributed evenly over the seas and along continental coasts. This is due to changes in the gravity field associated with the melting of ice sheets and water entering the ocean basins /Milne et al. 2009, Whitehouse 2009, Bamber and Riva 2010/. For instance, a complete collapse of the Greenland ice sheet would result in gravitational changes that counteracts the sea-level rise in the near field of the collapsed ice sheet, resulting in a *lower* sea-level, in the near field, than when the ice sheet was present /Milne et al. 2009/. This aspect is one key aspect of the GIA model used for SR-Site, see below. /Milne et al. 2009/ studied this spatially-variable change in sea-level assuming a complete melting of the Greenland ice sheet, and they predicted a ~ 0 mm/yr sea-level change in the region of Fennoscandia.

Even if considered less sensitive to global warming, several studies have been published, since the publication of /IPCC 2007/, on the possible contribution to sea-level rise by the West Antarctic ice sheet e.g. /Mitrovica et al. 2009, Bamber et al. 2009, Ivins 2009, Rignot et al. 2008/. According to the literature reviewed in /IPCC 2007/, a collapse of the West Antarctic ice sheet could contribute with a maximum of ~ 5 m of global sea-level rise. A more recent study suggests that the potential maximum rise in global mean sea-level from the West Antarctic Ice Sheet is 3.3 m /Bamber et al. 2009/. The effects of a collapse of the West Antarctic ice sheet was studied by /Mitrovica et al. 2009/ and /Bamber et al. 2009/. By using the traditional ice volume value for West Antarctica,

corresponding to 5 m of global mean sea-level rise, /Mitrovica et al. 2009/ estimated that a collapse of the West Antarctic ice sheet would result in a sea-level rise around Fennoscandia of 5 ± 1 m, when including the gravitational effects associated with the ice sheet collapse. However, using the revised West Antarctic ice volume value, corresponding to 3.3 m of global mean sea-level rise, /Bamber et al. 2009/ suggested that a full collapse of the West Antarctic ice sheet would give a sea-level rise around Fennoscandia of around 3 m, gravitational effects taken into account.

Sea-level rise up to year 2100

The fourth assessment report from IPCC did a summary of expected future global mean sea-level rise given various greenhouse gas emission scenarios. The maximum global mean sea-level rise for year 2100 was estimated to +59 cm /IPCC 2007/. The maximum corresponding value reported by IPCC in 2001 amounted to +88 /Church et al. 2001/. The difference between these two estimates is dependent on how the risks of global sea-level changes are evaluated. Primarily, in /IPCC 2007/, the contribution response to global warming from internal ice sheet dynamics was excluded from the estimate of sea-level rise because of its large uncertainty.

In addition to the studies mentioned under the ice sheets and sea-level heading, many studies have attempted to improve the numbers and approach to address the question on future sea-level rise since /IPCC 2007/, e.g. /Rahmstorf 2007, Grinsted et al. 2009, Sidall et al. 2009, Cazenave et al. 2009/. /Rahmstorf 2007/ predicted a maximum global sea-level rise by year 2100 of +138 cm (relative to the level year 1990). This is considerably higher than the value reported by /IPCC 2007/, a difference that is mainly due to the different methodological approach taken by /Rahmstorf 2007/. In /Rahmstorf 2007/, a semi-empirical relationship is used to connect global sea-level rise to global mean surface temperature, proposing that the rate of sea-level rise is roughly proportional to the magnitude of warming above the temperature of the pre-Industrial Age. In a study by /Pfeffer et al. 2008/, the Greenland and Antarctic ice sheet dynamic response to global warming is estimated and included. Also in this study the large uncertainty in sea-level rise is emphasised. /Pfeffer et al. 2008/ points to two probable cases of global sea-level rises by year 2100 (relative to the level year 2000) amounting to +79 and +83 cm, respectively. /Pfeffer et al. 2008/ also describe a less probable, but still possible, worst case where a calculated *maximum* ice discharge from the Greenland and West Antarctic ice sheets result in a global sea-level rise of +200 cm by year 2100, i.e. +141 cm above the /IPCC 2007/ estimate (that excluded this process).

The short term effect (by year 2100) of these worst case estimates of global sea-level rise for the Forsmark site is described in the *extended global warming case*, Section 5.2.3, and in /Brydsten et al. 2009/.

Sea-level rise beyond year 2100

The long-term sea-level response to global warming is naturally also associated with major uncertainties, and is for instance not discussed in /IPCC 2007/ which does not describe events more than 3,000 years into the future. It is clear however, that global sea-level would continue to rise far beyond year 2100 as a response to global warming. The effects on sea-level related to the response of the Greenland and West Antarctic ice sheets to global warming are discussed above, where a full collapse of the Greenland and West Antarctic ice sheets are suggested to contribute with a sea-level rise around Fennoscandia of ~ 0 and ~ 3 m respectively. There are major uncertainties related to the amount of global warming and the associated amount of ice sheet disintegration, as well as on the timing of such events.

/Rohling et al. 2009/ showed the (non-linear) relationship between Antarctic temperatures and sea-level elevation for the past five glacial cycles, indicating that the equilibrium sea-level for the present day CO₂ concentration in the atmosphere lie within the broad range of 0 and +25 (± 5) m, and that such levels might be reached within the next two to five millennia. The higher CO₂ levels that result from future emissions, results in even higher equilibrium sea-levels.

Another uncertainty relates to the long-term response from thermal expansion of ocean (thermosteric sea-level rise) due to a global warming climate. The rate of global sea-level rise from thermal expansion of ocean water would initially be low and then increase. /IPCC 2007/ estimated the total

sea-level increase due to thermal expansion in year 2300 to be 0.3–0.8 m (A1B emission scenario), and to be 0.5–2 m in year 3000 AD compared with year 2000 AD. Because of the large heat capacity of the ocean, thermal expansion would continue for many centuries after a warmer climate has stabilised. The final maximum contribution to sea-level change from thermal expansion would thus be considerably larger than at the time of peak climate warming.

There is thus a large uncertainty in the future long-term response of global sea-level on global warming. Despite these uncertainties, it is clear that the final sea-level rise resulting from global warming is reached several thousands of years into the future, and that the global mean sea-level rise could amount to several tens of metres.

GIA modelling

Despite the large uncertainty in future sea-level rise, reflected in the references above, many researchers believe that substantial long term sea-level rise will continue for centuries as a result of global warming, e.g. /IPCC 2007, Overpeck and Weiss 2009/. For the *global warming case* it is not meaningful or possible to assign probabilities to the various predictions of future global sea-level change above. Instead, for the GIA model simulations, it is adequate to assume a complete collapse of the Greenland ice sheet as a response to global warming. It is assumed that this ice sheet completely melts away at a linear rate during the coming 1,000 years, resulting in 7 m of global sea-level rise. If the rate would be different, or if the ice sheet response would be non-linear and more complex, which is very likely, this does not influence the modelled long-term (glacial cycle time scale) shore-level signal at the Forsmark site.

Just as for the reconstruction of last glacial cycle conditions (Section 3.3.4) and the resulting *reference glacial cycle* (Section 4.5.2), the effect of sea-level rise on the development of the Baltic shore-level was for the *global warming case* investigated by GIA modelling. In the GIA simulations made for the reconstruction of last glacial cycle conditions there was a discrepancy between the GIA results on modelled present-day uplift rates and present uplift rates as observed by GPS measurements. In Section 3.3.4 and in /Whitehouse 2009/ it was shown that the discrepancy was partly due to the fact that a laterally homogeneous Earth model (2D Earth model) was used in the GIA simulations. A 3D modelling approach significantly reduces this discrepancy (Section 3.3.4 and Whitehouse 2009). Another contributing factor to the discrepancy can be a too large an ice load provided to the GIA model from the ice sheet model (Section 3.1.4). By sensitivity tests made in SR-Can using the GIA model, it was found that a reduction in ice thickness to 80% of the value in the *reference glacial cycle* yielded GIA results on present uplift rates that were in accordance with the observed present-day uplift. Even if a large part of the discrepancy now can be attributed to the 2D GIA modelling approach (Section 3.3.4), the *global warming case* for SR-Site uses the 2D GIA model simulation together with an 80% reduction in ice sheet thickness. However, this is judged as not having a large impact on the usefulness of the results on relative sea-level, given the large uncertainty interval presented for the results.

In line with the approach used in the GIA modelling of the *reference glacial cycle*, the GIA model was initiated by running one full glacial cycle in order to obtain realistic initial uplift rates for the greenhouse scenario. This was followed by linear melting of the Greenland ice sheet over 1,000 years, inducing corresponding changes in global sea-levels. This was followed by a 50 kyr long period of no change to the loading model, simulating a warm global warming climate without a Fennoscandian ice sheet forming. Finally a second full glacial cycle was added in the simulation. No contribution from thermal expansion of oceans was included, which adds an uncertainty to the results, see below.

After the GIA simulation, the relative shore-level curve from the GIA model was combined with observed shore-level data for the present day /Pässe 2001/ in order to produce the final shore-level curve for the global warming variant (Figure 5-2). In the GIA simulation, the rise in global sea-level due to the melting of the Greenland ice sheet does not result in a sea transgression at Forsmark. This is due to the counterbalancing gravitational effect associated with the removal of the mass of the Greenland ice sheet mentioned above, in Section 3.3 and in /Milne et al. 2009, Whitehouse 2009/.

As mentioned above, /Milne et al. 2009/ studied the spatially-variable change in sea-level assuming a melting of the Greenland ice sheet, and predicted a ~0 mm/yr sea-level change in the region

of Fennoscandia. This is in line with the results of the GIA modelling performed for the *global warming case*, where the isostatic rebound is larger than the sea-level rise even when including a 1,000 year long complete melting of the Greenland ice sheet. The results show that the Forsmark site is situated above sea-level basically for the entire coming 120 kyrs in the *global warming case*.

However, here it is important to note that there are large uncertainties in the shore-level curve presented in Figure 5-2. They relate to uncertainties and assumptions made in the GIA modelling and also to the uncertainties in present knowledge on future global sea-level rise discussed above. The main uncertainty in future global sea-level rise is, as described above, related to the uncertain response of the Greenland and West Antarctic ice sheets to global warming and to the contribution from thermal expansion. The assumed complete collapse of the Greenland ice sheet covers the uncertainty of the most sensitive ice sheet. The uncertainty in the shore-level curve may thus be up to several tens of metres, see also Section 3.3.4.

Given the uncertainties described above, it is possible that, in contrast to what is shown in Figure 5-2, there might be an initial period of sea transgressions at the Forsmark site in the *global warming case*, lasting some thousands of years, before the isostatic uplift component starts to dominate. After an early phase with these large uncertainties in the *global warming case*, the results of the GIA modelling suggest that in the long run the Forsmark site is situated above sea-level until the end of the 120 kyr period (Figure 5-2).

Situations with worst case scenarios for global sea-level rise up until year 2100, and the resulting effect on shoreline migration at the Forsmark site, are described in Section 5.2.3 and /Brydsten et al. 2009/.

Another expected effect of a global warming climate is that the increased precipitation in the Baltic drainage basin leads to increased surface runoff to the Baltic Sea, with less saline conditions in the Baltic as result, e.g. /BACC author team 2008/.

5.1.4 Permafrost evolution

In the *global warming case*, the evolution of permafrost is postponed 50 kyrs compared to the development in the *reference glacial cycle*. After the first 50 kyrs, the development of the temporal pattern and depths of permafrost is identical to the development in the *reference glacial cycle*. The permafrost starts to develop at around 60 kyrs after present. After that, progressively longer periods of permafrost conditions and shorter periods of temperate climate conditions occur, up until the glacial period at around 110 kyrs after present. The maximum permafrost depth is, in this climate case, the same as in the *reference glacial cycle*, ~260 m (with a maximum uncertainty interval down to ~460 m), but it occurs later, c. 100 kyrs after present. At the same time, the depth of the frozen ground is somewhat shallower than the permafrost depth, due to the pressure and salinity; ~245 m (with a maximum uncertainty interval down to ~420 m).

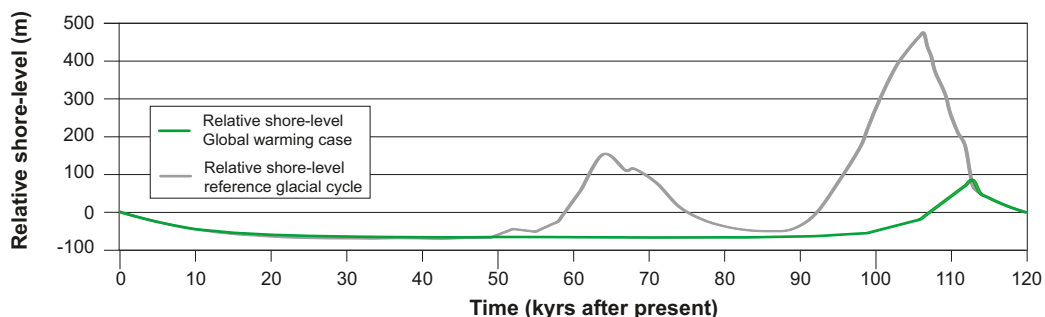


Figure 5-2. Shore-level evolution at Forsmark for the global warming case. For comparison, the shore-level evolution for the reference glacial cycle (Section 4.5.2) is also shown. Negative numbers indicate that the area is situated above the contemporary sea-level. The curve was constructed by GIA modelling combined with results from observations of present-day uplift rates /Pässe 2001/. There are significant uncertainties in the future shore-level development, which, in contrast to what is shown in the figure, may result in a sea transgression at Forsmark during the first thousands of years of the evolution.

5.1.5 Evolution of climate domains

The development of climate domains for the *global warming case* is shown in Figure 5-3 and 5-4. Given the assumption of a long initial period of temperate climate conditions, the temperate climate domain is dominating. Temperate conditions prevail for ~78,000 years (65% of the time), permafrost conditions for ~28,000 years (23% of the time), glacial conditions for ~11,000 years (9% of the time) and submerged conditions prevail for ~3,000 years (~3% of the time).

In this climate case, the climate at Forsmark is dominated by the initial ~60 kyr long period with temperate climate conditions. The variation in air temperature and precipitation is considerable within this temperate period, with air temperatures and precipitation rates considerably higher than at present in the early phase of the 120 kyr period. A detailed example of the characteristics of a climate dominated by global warming in Forsmark is given below, derived from the climate modelling study by /Kjellström et al. 2009b/. In time the high temperatures are slowly reduced, as a response to the slow decrease in atmospheric CO₂ concentrations. During the initial long temperate period, climate

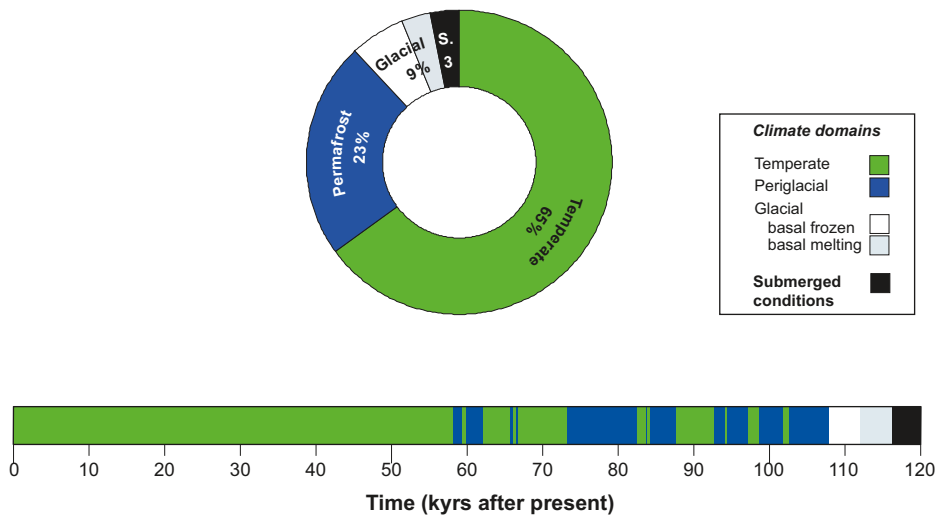


Figure 5-3. Duration of climate domains at Forsmark, expressed as percentage of the total time for the *global warming case*. The bar below the pie chart shows the development of climate as a future time series of climate domains and submerged periods.

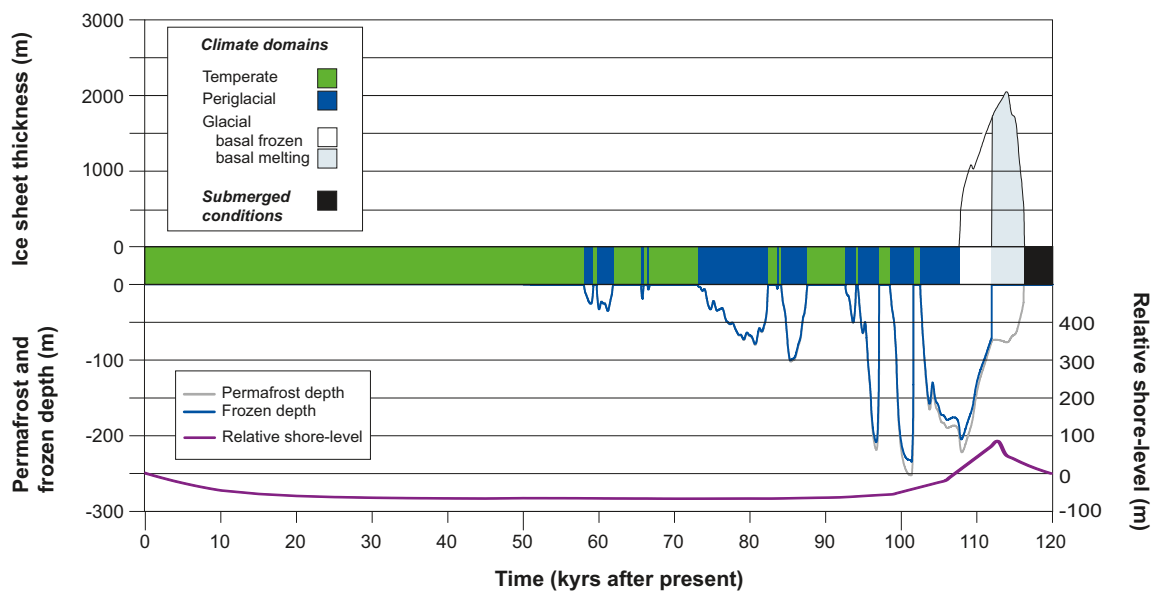


Figure 5-4. Evolution of climate-related conditions at Forsmark as a time series of climate domains and submerged periods for the *global warming case*.

varies within a range that is larger than that during the preceding parts of the Holocene. The length of the initial period of temperate climate domain should not be taken as a prediction or statement on how a future global warming climate will manifest itself. Under a future warming climate, this period could be shorter or longer than that described here. One such alternative case, with an even longer duration of temperate climate conditions, is described in the *extended global warming case*, see Section 5.2.

Between ~60 kyrs after present and more than 100 kyrs after present, periods of periglacial conditions with permafrost occur and get progressively more severe (Figure 5-4). The first major ice sheet advance in the *global warming case* occurs at around 110 kyrs after present. The maximum ice sheet thickness, around 2,000 m, occurs at around 115 kyrs after present. Table 5-2 summarizes the sequence of events for the *global warming case*.

During the second half of the *global warming case* (Figure 5-3 and 5-4), climate varies within the same range as during the first part of the *reference glacial cycle* (Section 4.5), and consequently the climate-related processes act in the same way as in the *reference glacial cycle*. The global warming variant reduces the effects of climate-related processes of importance for repository safety that are related to cold climate conditions, i.e. in the periglacial- and glacial climate domains.

Another possible course of events within a generally warming global climate, is that the annual mean Atlantic Meridional Overturning Circulation (AMOC) in the North Atlantic is reduced, e.g. /Wu et al. 2004, IPCC 2007, Zickfeld et al. 2007, Drijfhout et al. 2008/. This would result in less heat being transported towards Fennoscandia by the North Atlantic Drift sea current, which in theory could lead to a regional cooling over Fennoscandia. However, in the global warming climate simulations by /Kjellström et al. 2009b (including erratum Feb 2010)/, the AMOC is reduced by up to 22% compared with the control period (1961–2000). These changes are not large enough to cause regional cooling over Fennoscandia. This results in general agreement with the Atmosphere Ocean General Circulation Model (AOGCM) simulations of the 21st century as presented by /Meehl et al. 2007/. They show that the AOGCMs suggest a decreased intensity of the AMOC in the 21st century in the range from 0 to 50%. As in the simulations by /Kjellström et al. 2009b/, none of these AOGCM simulations indicates a cooling over Fennoscandia.

However, it is believed that the general warming would be considerably larger than such a cooling effect, resulting in net warming in Fennoscandia /IPCC 2007, Kjellström et al. 2009b/. Nevertheless, a case with a more severe permafrost development than in the *reference glacial cycle* is investigated in the *severe permafrost case* (Section 5.5).

Table 5-2. Sequence of climate-related events for the global warming case.

Event	Transition date	Climate domain
Deglaciation/ Start Holocene interglacial (locally defined)	–9,500 after present	–
Holocene interglacial	–	Temperate climate domain (incl. submerged conditions)
End of Holocene interglacial (locally defined)	c. 59,400 after present	–
Periglacial conditions (progressively longer periods of permafrost conditions)	–	Periglacial climate domain (incl. progressively shorter phases of temperate climate conditions)
End of periglacial conditions Start of glacial conditions	109,600 after present	–
First phase with glacial conditions	–	Glacial climate domain
Deglaciation at site, Start interstadial conditions	118,200 after present	–
Interstadial conditions (corresponding to MIS 3)	–	Periglacial climate domain (incl. submerged conditions and short temperate periods)

In the global warming climate variant, the warmer annual mean air temperatures do not affect repository safety functions. Furthermore, the increase in precipitation would not affect groundwater formation significantly, since, on a regional scale, the major part of the groundwater aquifer is filled already by present-day precipitation rates. Instead surface-runoff is increased, discussed further under the section on surface denudation. However, low groundwater salinity due to persistent infiltration of meteoric water during the prolonged temperate periods in the greenhouse variant may have a potential effect on the function of the clay buffer /SKB 2011/.

5.1.6 Surface denudation

The relative importance of different denudation processes, as well as the resulting amount of surface denudation, is expected to change in the *global warming case* as compared with the *reference glacial cycle*. The major difference between the *global warming case* and the *reference glacial cycle* is that glacial conditions with warm-based erosive ice only exist for a few thousands of years in the former case compared with around 24,000 years in the latter case. Glacial erosion is identified as the most important denudation process in the *reference glacial cycle*, with the largest contribution to the total denudation rate (Section 4.5.7). Since the duration of periods with glacial erosion is significantly shorter in the *global warming case*, the expected amount of glacial erosion is also significantly smaller in this case compared with the *reference glacial cycle*.

In the *global warming case*, the annual air temperature and precipitation are expected to increase in Forsmark during the initial part of the temperate climate domain, see above. For the first tens of thousands of years of this climate case, increased precipitation results in increased surface runoff, see above and /Kjellström et al. 2009b/, which probably leads to increased fluvial erosion. In this global warming variant, with 50,000 initial extra years of temperate climate conditions, the effect of this increased fluvial erosion is most probably significantly smaller than the effect of the anticipated decrease in glacial erosion. The increased fluvial erosion most probably has a minor impact on total denudation rates for this climate case. Even if the fluvial erosion process were to have been large, the resulting amount of fluvial erosion is limited by the fact that fluvial erosion cannot erode deeper than the level of the Baltic Sea and that the site is located at sea-level today. The period of increased precipitation is accompanied by a slowly regressing, stationary or even transgressing sea-level (Section 5.1.3), which further precludes deep fluvial erosion during the period influenced by increased precipitation.

Increased temperatures in a global warming climate could lead to somewhat higher weathering rates. Some studies suggest that such climate change feedbacks may be weaker than previously thought and in fact could even accelerate the recovery from fossil fuel CO₂ perturbations /Lenton and Britton 2006/. However, given the large expected reduction in glacial erosion, and a considerably smaller expected effect of increased weathering rates, the feedback mechanisms between climate, weathering and vegetation, are not further treated in the present report.

Other, minor, differences compared with the *reference glacial cycle* relate to periglacial conditions, which have a shorter duration in this climate case than in the *reference glacial cycle*. Aeolian erosion is therefore expected to contribute even less to the total denudation in the global warming variant.

All in all, the relative importance of various erosion and denudation processes are changed in the *global warming case*, with the overall result that total denudation is more restricted in this climate case than in the *reference glacial cycle*. The one process that could give a relevant contribution to increased denudation, fluvial erosion, is limited by the near-sea-level location of the site. The *reference glacial cycle* is judged as resulting in a larger surface denudation than the *global warming case*, mainly because of the reduction in duration of periods with the most efficient denudation process (glacial erosion), as identified in Section 3.5.4.

A climate case with an estimated larger amount of surface denudation than in the *reference glacial cycle* is described in the *extended ice sheet duration case* (Section 5.3).

5.1.7 Exemplified climate conditions for the global warming case

In order to give a detailed example of how a climate influenced by global warming could appear in Forsmark, climate modelling was used to describe a situation with a temperate climate with increased greenhouse gas concentrations in the atmosphere (750 ppm), a few thousands of years from now /Kjellström et al. 2009b, including erratum Feb 2010/. According to /Lenton et al. 2006/, a 750 ppm CO₂ level still means that all “conventional” fossil fuel resources (including coal, oil, and gas) need not have been used.

In the climate modelling simulations, a complete loss of the Greenland ice sheet was assumed. Since this deglaciation is a process that may take up to a couple of thousand years, it is very uncertain what other climate-related conditions may be prevailing at that time. According to climate-change scenarios from simulations with GCMs, irreversible melting of the Greenland ice sheet may start at a time when the global mean temperature has increased by about 1.9–5.1°C above today’s conditions and the temperature over Greenland has increased by about 3–6.5°C /Gregory et al. 2004, Gregory and Huybrechts 2006/. Recent studies indicate that the ice sheet might be more sensitive to increased concentrations of atmospheric greenhouse gases than previously thought /Stone et al. 2010a, b/.

Increases in temperature large enough for making the Greenland ice sheet collapse are projected by GCMs within the 21st century for some emission scenarios /Meehl et al. 2007/. If such high temperatures persist for a long enough time (several hundreds to a couple of thousand years depending on the degree of warming) the Greenland ice sheet will eventually collapse and disappear. In this time perspective, CO₂ levels will start to decrease again (when emissions cease). Nevertheless, at one thousand years from now, the atmospheric CO₂ concentrations will remain considerably higher than today /Lenton et al. 2006/. Here, the time period for the global warming simulation was chosen as a compromise between a high level of CO₂ (needed to simulate a warm climate that melts the Greenland ice sheet), and a not too high level (that remains in the atmosphere a long time after the emissions have ceased). Thus, the simulations can be considered as representative of the climate a few thousand years into the future after a complete melting of the Greenland ice sheet and a partial recovery towards lower background CO₂ concentrations.

For these simulations, a global GCM model (Community Climate System Model version 3, CCSM3), a regional climate model (Rossby Centre Regional Climate Model RCA 3) and a vegetation model (LPJ-GUESS) were used. For the simulations performed and analyzed within this study, atmospheric and land components of the CCSM3 used a grid spacing of approximately 2.8° in latitude and longitude. The vertical resolution is 26 levels in the atmosphere and 40 levels extending to 5.5-km depth in the ocean. The regional climate model used a horizontal resolution of 50 km and a time resolution of 30 minutes. For details on the models, how they were employed, and a discussion on model uncertainties, see /Kjellström et al. 2009b/. The simulation of the global warming climate used a CO₂ concentration in the atmosphere of 750 ppm. In order to include the effect of also other greenhouse gases in the RCA 3 model, a CO₂ equivalent value of 841 ppm was used /Kjellström et al. 2009b/. For a detailed description of the assumptions made in the modelling process, model forcing and initial conditions (such as astronomical and solar forcing, concentration of greenhouse gases and aerosols in the atmosphere, extents of ice sheets, distribution of land and sea, topography and vegetation), also see /Kjellström et al. 2009b/.

The simulated global warming climate should not be taken as a prediction or prognosis on how a future global warming climate will manifest itself. Instead, it is a *detailed example* of how such a climate may be manifested. Given another model forcing, for instance using a lower or higher CO₂ concentration, the resulting climate would have been different. However, the model results are useful for exemplifying a climate affected by global warming, also for Forsmark. In this context it is worth noting that the results of /Kjellström et al. 2009b/ resemble those for many of the scenarios for the 21st century from the climate model intercomparison project (CMIP3) /Meehl et al. 2007/. For a detailed discussion and comparison with other climate model results, see /Kjellström et al. 2009b, Section 3.1.4/.

Global climate

Figure 5-5 shows the simulated global warming climate from the GCM simulations. Seasonal mean changes in temperature in the global warming simulation as compared with a simulation of the present (1961–2000) climate are also shown in Figure 5-5. The removal of the Greenland ice sheet

produces a strong heating of up to 17°C over Greenland in both summer and winter. This heating is primarily due to a combination of i) the lowering of the surface by up to 3,000 m and ii) the decrease in surface albedo and changes in heat fluxes between the atmosphere and the ground produced by the replacement of the glacier ice surface by tundra /Kjellström et al. 2009b/. Similar to all greenhouse warming scenarios presented in the IPCC AR4 report /Meehl et al. 2007/, the Arctic region exhibits strong heating by up to 15°C in winter (due to a substantial decrease in the Arctic sea-ice cover and a decrease in the snow cover). The seasonal mean temperature is up to 5°C warmer in summer and up to 7.5°C warmer in winter over Fennoscandia in the global warming simulation as compared with the simulation of the present climate. Seasonal mean summer temperatures in Sweden vary in the range 12–18°C and winter temperatures vary in the range 0–6°C. Sensitivity to changes in vegetation in these GCM simulations is discussed in /Kjellström et al. 2009b/.

The change in precipitation in the global warming simulation as compared with the simulation of the present climate is also shown in Figure 5-5. The removal of the Greenland ice sheet leads to a 25% decrease in precipitation in particular over south-eastern Greenland in both summer and winter, indicating that much of the precipitation in that area in today's climate is triggered by the steep ice sheet topography. Similar to all greenhouse-warming scenarios presented in the IPCC AR4 report /Meehl et al. 2007/, precipitation is increased over mid-latitude Northern Hemisphere continents and the Arctic. For Fennoscandia there is an increase in precipitation, most notably in the north.

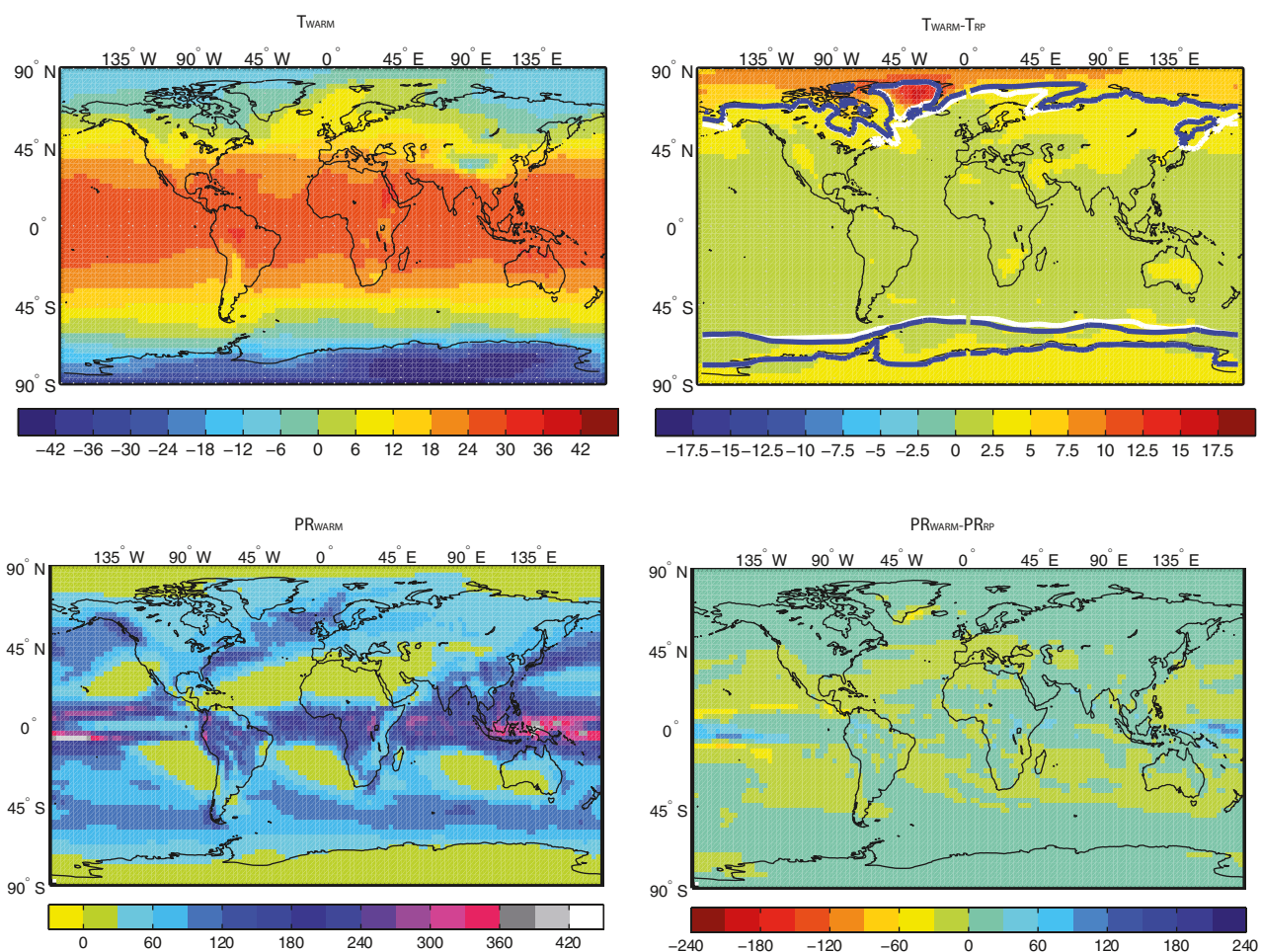


Figure 5-5. Upper panels: Simulated near-surface air temperature in the global warming simulation (T_{WARM}) and the difference compared with the simulated present climate (T_{RP}) (1961–2000). Units are °C. Also shown by isolines in the rightmost panels is the extent of sea-ice in the simulation of the present climate (white) and in the global warming simulation (blue). Lower panels: Precipitation in the global warming simulation ($P_{R_{WARM}}$) and the difference compared with the simulated present climate (P_{RP}). Units are mm/month. From /Kjellström et al. 2009b/.

Climate in Europe and Sweden

The regional climate model was then used to downscale the model results of the global climate model in order to obtain higher resolution data over Europe and Sweden. The resulting climate over Europe was used to produce a new vegetation distribution with the vegetation model. This vegetation was in turn, used as input to the regional climate model, to produce a climate in line with the new vegetation. An evaluation of the results from this iterative process is given in /Kjellström et al. 2009b/. Figures 5-6, 5-7 and 5-8 present selected results on temperature and precipitation from the regional modelling.

In the regional global warming simulation, the warming compared with the simulated present climate (1961–2000) is strongest over northern Europe in winter. The simulated temperature increase for the coldest month is more than 5°C in northern Fennoscandia (Figure 5-6, second row, middle panel). In southern Europe the warming is stronger in summer, where the temperature of the warmest month increases with more than 4°C in large areas (Figure 5-6, second row, left panel). The stronger warming in the areas of the Bothnian Bay, Bothnian Sea and in the Gulf of Finland in summer in this experiment is due to the land uplift converting sea to land in those areas. The same phenomenon is also responsible for the weaker warming in these areas in winter. Differences between the results of the global and regional model simulations are discussed in /Kjellström et al. 2009b/.

As expected, the simulated climate of the *global warming case* clearly resembles many of the scenarios for the 21st century from the climate model intercomparison project (CMIP3) as presented by IPCC /Meehl et al. 2007/. Seasonal mean changes in precipitation and temperature from a large number of the CMIP3 scenarios have been analysed for Sweden by /Lind and Kjellström 2008/.

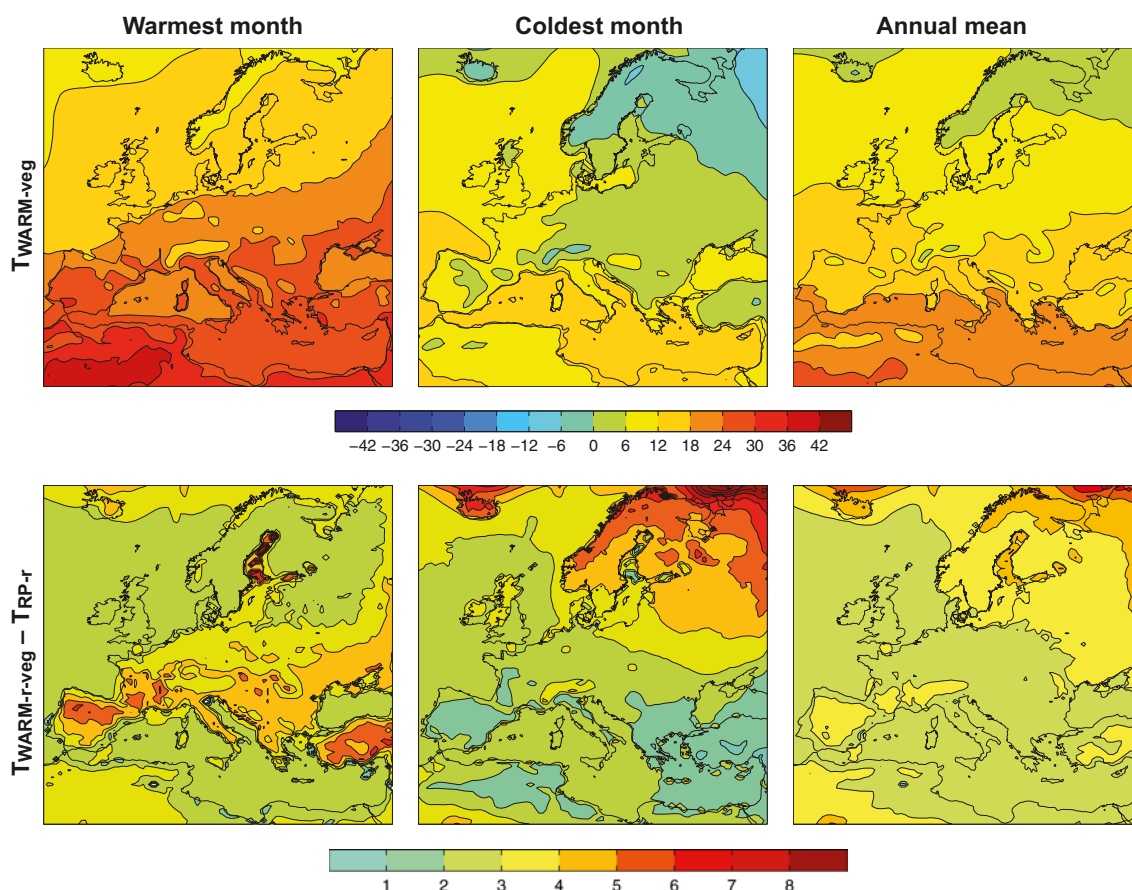


Figure 5-6. Mean near-surface air temperatures of the warmest month, coldest month and annual mean in the global warming simulation with improved vegetation (upper row). Also shown are differences between the global warming simulation and the simulations of the present climate (RP-r) (1961–2000) (lower row). Units are °C. From /Kjellström et al. 2009b/.

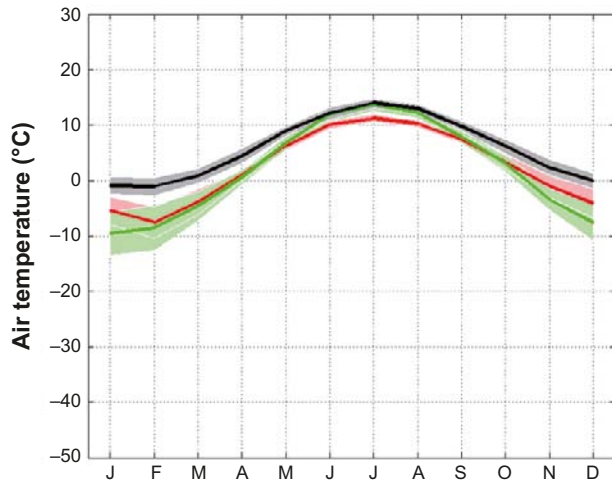


Figure 5-7. Annual cycle of temperature for Sweden in the global warming (black line) and simulated present climate (1961–2000) (red line). Also shown is the CRU observational data from 1961–1990 (green line). Shaded areas in corresponding colours indicate the ± 1 standard deviation calculated for the range of individual monthly averages in the three data sets. From /Kjellström et al. 2009b/.

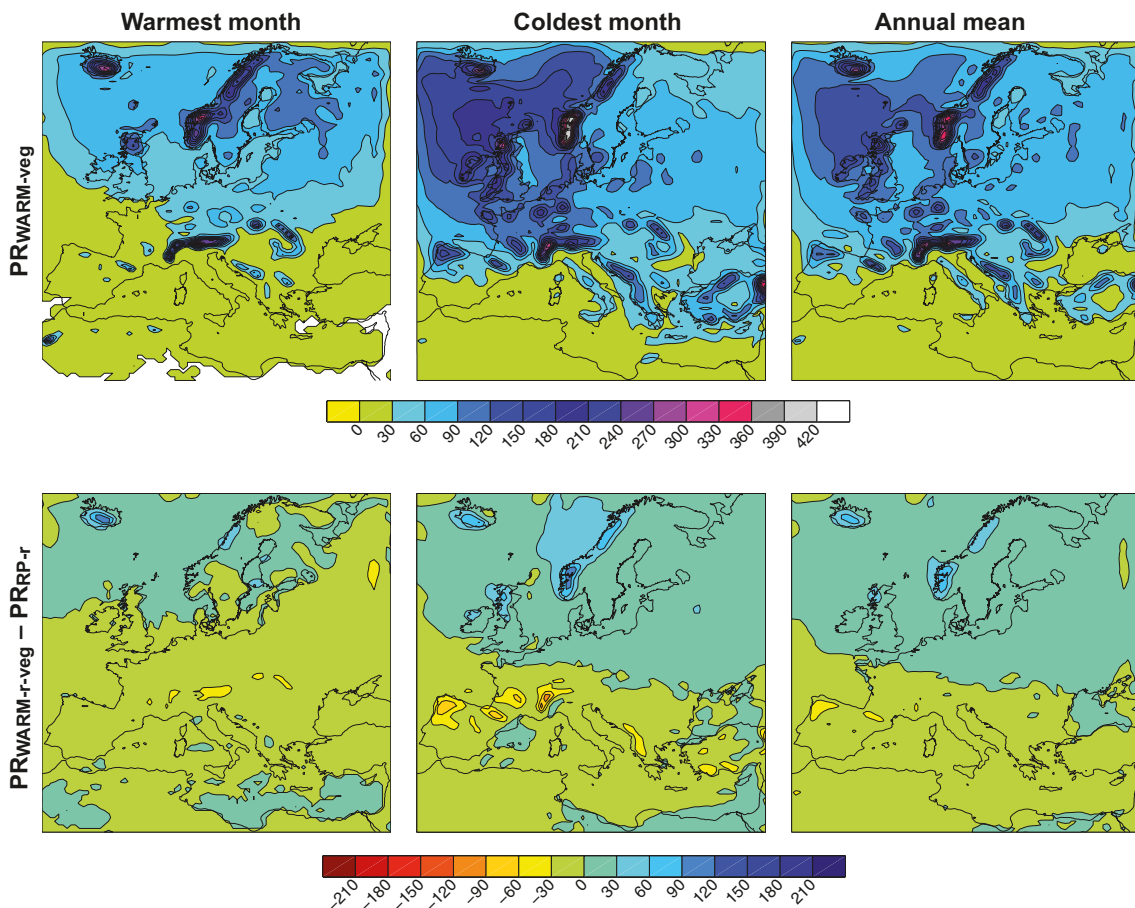


Figure 5-8. Mean precipitation of the warmest month, coldest month and annual mean in the global warming simulation. Also shown are differences between the global warming simulation and the simulated present climate (RP-r) (1961–2000). Units are mm/month. From /Kjellström et al. 2009b/.

/Lind and Kjellström 2008/ report increased temperatures of 4–6°C by the end of the 21st century in northern Sweden and about 3°C in southern Sweden relative to the 1961–1990 period. The corresponding increases in precipitation are about 25% in the north and only a small average increase in the south albeit with a large spread between the models. These changes are annual averages over a range of different emission scenarios. As noted in /Kjellström et al. 2009b/, the uncertainties related to the future forcing in the global warming simulation are large and substantially lower or higher greenhouse-gas concentrations than the one used cannot be ruled out. Considering the large spread between the emission scenarios and the uncertainty related to the climate models one cannot rule out that a future warmer climate can be warmer than the one simulated in /Kjellström et al. 2009b/. However, the high-end emission scenarios (A1FI and A2) /Nakićenović and Swart 2000/ may have CO₂ concentrations that are too high to be sustained over the long period that it takes to melt the Greenland ice sheet, which was part of the set-up here. But, even so, the CO₂ concentrations may very well reach levels high enough to sustain long-term (i.e. multi-century) temperature anomalies exceeding those simulated here.

Clearly, the results from the regional model gives a climate change signal that is within the range defined by the global model results for southern Sweden compiled in /Lind and Kjellström 2008/, see Figure 3-15 in /Kjellström et al. 2009b/. The climate change signal for entire Sweden is +4°C in winter and +3.5°C in summer and the corresponding numbers for precipitation are +37% in winter and no change (±0%) in summer. Further model results and discussion for all of Sweden from the global- and regional climate modelling and from the vegetation modelling are presented in /Kjellström et al. 2009b/.

The vegetation simulated by LPJ-GUESS for the global warming climate is reported in the context of the biosphere studies /SKB 2010d/.

Here it is also worth noting that the Greenland summer temperatures are well above 0°C, clearly indicating that there is no chance of ice sheet regeneration under these circumstances once the ice has been removed. A similar result was obtained previously for the pre-industrial climate when the Greenland ice sheet was removed in the Hadley Centre HadCM3 coupled model /Toniazzo et al. 2004/.

Climate in the Forsmark region

In the last step in the climate modelling study of the global warming climate, climatological data for the Forsmark region were extracted from the regional modelling. Figure 5-9 shows the grid boxes used for extraction of data. Information was extracted from the grid point located closest to the Forsmark site. As there is a high degree of spatial heterogeneity in land-sea distribution and topography, information from the surrounding eight grid boxes were also used to discuss uncertainties related to these inhomogeneities.

In addition to the results from the modelled case, data from the simulation of the present climate (1961–2000) (RP-r) and from the CRU observations representing conditions in the late 20th century are also shown for the Forsmark region (Figure 5-10). In addition to this, results from three other climate-change simulations with RCA3 for the 21st century as described in /Persson et al. 2007/ are also shown. These simulations follow the A2, A1B and B2 emission scenarios /Nakićenović and Swart 2000/. The A1B emission scenario leads to greenhouse gas concentrations close to the one in the *global warming case* by the end of the 21st century. The two other scenarios have more (A2) or less (B2) emissions than the A1B scenario.

The fairly small annual temperature range in the present climate is even smaller in the future global warming climate for the Forsmark region (Figure 5-10, upper row, first column). This reduction in the seasonal cycle of temperature is a consequence of the future warming being stronger in winter than in summer. The snow season is much shorter, or even totally absent, in the warm climate. The seasonality of the runoff is closely connected to the presence or absence of snow. In the warmer future climate, the spring peak in runoff is absent and there is now a more widespread wintertime maximum related to the large amounts of precipitation for that season.

In the global warming simulation, the spread in the presented variables due to differences in geographical location is reduced compared with that in the simulation of the present climate. This is partly a result of the land uplift turning two of the Baltic Sea grid boxes east of Forsmark into land

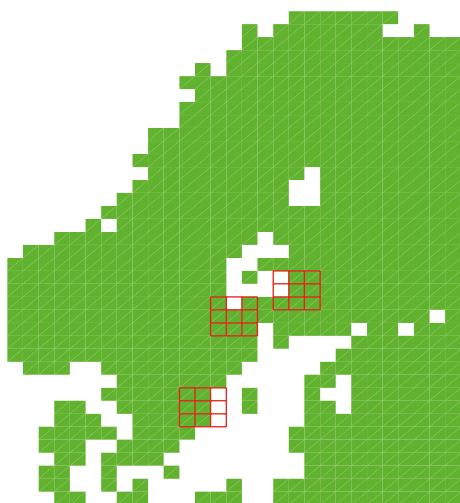


Figure 5-9. Land (green) sea extent (white) in the regional climate model in the Fennoscandian region used for the global warming climate simulation. The 3-3-grids represent grid boxes covering the Forsmark, Oskarshamn and Olkiluoto sites (centre box) and the eight surrounding boxes. Grid boxes with a land fraction lower than 20% are not filled. Results from Oskarshamn and Olkiluoto are presented in /Kjellström et al. 2009b/.

in the *global warming case*. Thereby, the surrounding area becomes more homogeneous than in the present-day situation. When including also the uncertainty ranges based on results from the three other climate simulations for the 21st century, also simulated with RCA3 /Persson et al. 2007/, it is seen that the weakening of the annual cycle is a robust trend when going to a warmer climate.

50-year averages values from the regional global warming climate simulation show that the annual mean air temperature in the Forsmark region is $+8.3^{\circ}\text{C}$. This is a temperature increase of 3.6°C compared with the simulated present climate (1961–2000). The future warming is stronger in winter than in summer and there is an associated reduction in the seasonal cycle amplitude in temperature. The mean annual precipitation in the region is 804 mm, which is an increase of 138 mm (or 20%) compared with the simulated present climate. Most of the precipitation increase occurs during the winter season (DJF). The snow season is much shorter than at present or even totally absent (Figure 5-10). Finally, the annual surface runoff is 337 mm in this exemplified global warming climate, which is an increase of 162 mm compared with the present climate. Given the uncertainties and assumptions used in the climate modelling, and the CO_2 level chosen, the model results thus show that the global warming climate in the Forsmark region, may be characterized by a clearly warmer and wetter climate than at present, and also that the surface runoff is significantly increased.

The major uncertainties in the climate simulation are related to uncertainties in forcing, model formulation and natural variability. These uncertainty aspects are discussed in detail in /Kjellström et al. 2009b/.

Another recent study that focussed on regional climate modelling is /Kjellström et al. 2010b/ where changes in seasonal mean temperature, precipitation and wind over Europe were studied in an ensemble of 16 regional climate model simulations for 1961–2100. The study used the A1B emission scenario /Nakićenović and Swart 2000/ in which the CO_2 equivalents in RCA 3 were set to 902 ppm, somewhat higher than the 841 ppm used in /Kjellström et al. 2009b/. Six-member ensemble means of winter season (DJF) conditions suggest an increase in temperature by c. 4°C and precipitation by 20–30% in south central Sweden, including the Forsmark region, by year 2100. Corresponding model ensemble means for the summer season (JJA) indicate an air temperature increase of $2\text{--}3^{\circ}\text{C}$ and a precipitation increase of c. 10%. The study also shows that the climate-change signal gets stronger the larger the forcing becomes, i.e. more greenhouse-gas emissions leads to a stronger warming and larger changes in precipitation. The results of the A1B-scenario-simulations are thus in line with the detailed results described above from /Kjellström et al. 2009b/. Similar results were obtained also in the SWECLIM project /Rummukainen 2003, Tjernström et al. 2003/. Other modelling results that give similar pictures of future global warming climates are reported in /BIOCLIM 2003, Meehl et al. 2007 and Lind and Kjellström 2008/.

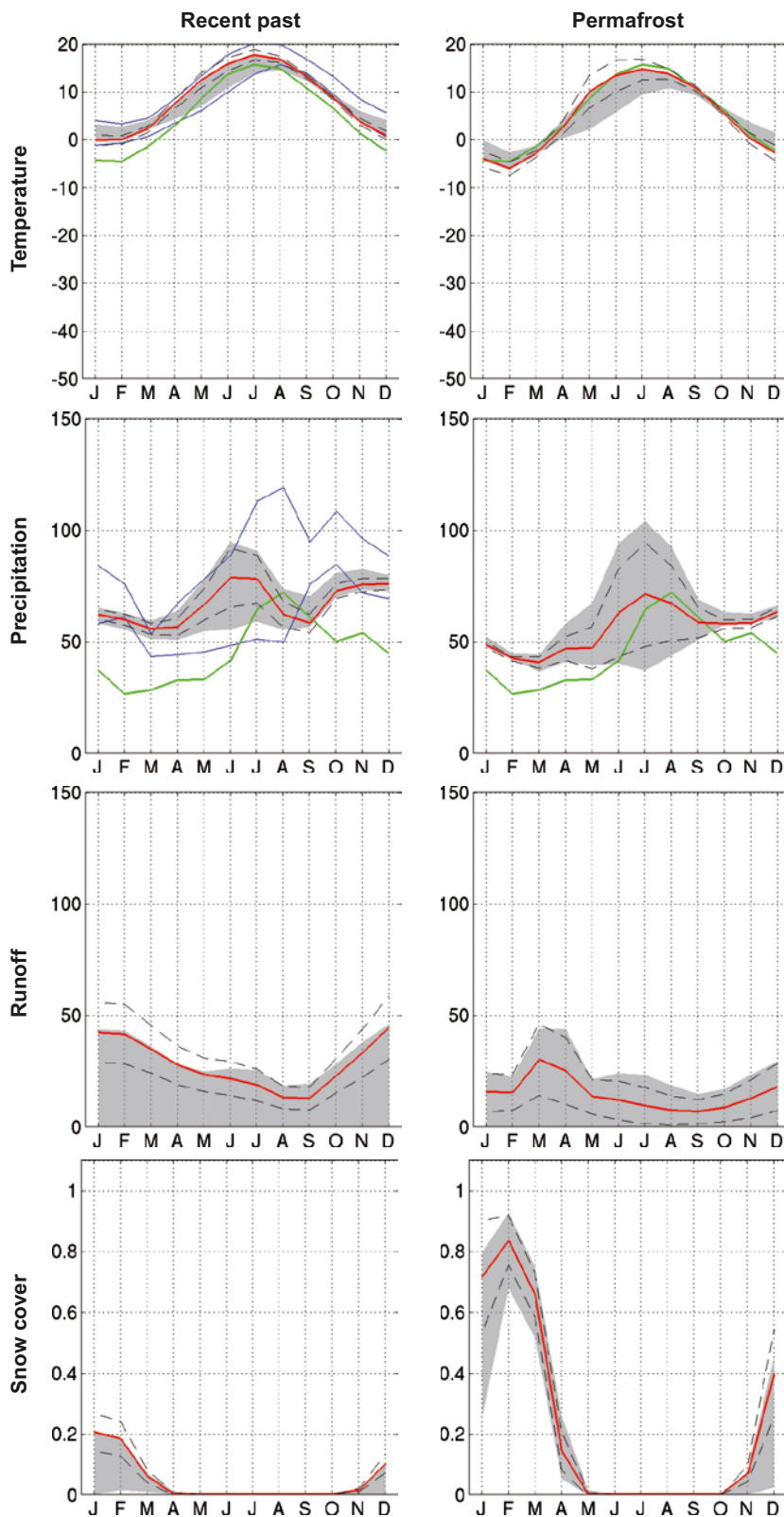


Figure 5-10. Simulated seasonal cycles of temperature ($^{\circ}\text{C}$), precipitation (mm/month), runoff (mm/month) and snow fraction (dimensionless ranging from 0 to 1) at the grid box closest to the Forsmark site (red line). The spatial variability in the 3-3-grid (Figure 5-9) is displayed with the dashed lines representing ± 1 standard deviation calculated from the 9 grid boxes, and the grey area representing the absolute maximum and minimum, of the 9 grid boxes. The green line for temperature and precipitation is the observed seasonal cycle from the CRU data set in the period 1961–1990. In the global warming case (left column), an additional uncertainty range defined by ± 1 standard deviation of the data calculated from the 9 surrounding grid boxes from three additional simulations for the 21st century with RCA3 is shown with blue full lines. From /Kjellström et al. 2009b/.

5.2 Extended global warming case

5.2.1 Background

There is a large range of potential future climate developments when considering the combined effect of natural climate variability and anthropogenic climate change, e.g. /IPCC 2007, Archer and Brovkin 2008, Kjellström et al. 2010b/ and references therein. One such case is the *global warming case* described in Section 5.1. In order to cover a reasonably broad array of future climate developments based on present knowledge, an *extended global warming case* is also included in the SR-Site safety assessment. This case describes a future climate heavily influenced by anthropogenic emissions of greenhouse gases, resulting in strong global warming. In this case, all fossil fuel sources are envisaged to have been used, resulting in that peak CO₂ levels might reach above 1,000 ppm, cf. /Rahmstorf and Ganopolski 1999, IPCC 2007/, before the CO₂ concentration again start to decline. One consequence of this, together with the known future insolation changes from the orbital cycles, is the possibility of a very long duration of the present interglacial period, prior to the onset of ice sheet growth.

One case of long-lasting global warming is described in /Archer and Ganopolski 2005/, suggesting that a release of 1,000 Gton of greenhouse gases together with orbital variations would result in the present interglacial persisting for another 130 kyrs, before ice sheet growth commences on the Northern Hemisphere. A larger release is suggested to result in an even longer interglacial. Naturally, such estimates of the length of the present interglacial are associated with very large uncertainties. They relate both to the uncertain amount of future greenhouse gases in the atmosphere, and to poorly known feed-back mechanisms in the ice sheet-, climate-, vegetation- and carbon cycle system, and how, or if, these mechanisms are implemented in the models.

In order to cover a reasonable wide range of possibilities, an additional 100 kyrs of temperate climate conditions is added prior to the slow onset of a *reference glacial cycle* for the *extended global warming case*. This results in a temporal development of climate and ice sheet growth very similar to the case with 130 kyrs until the next glaciation as described by /Archer and Ganopolski 2005/, see below, and it is also in broad agreement with results in /BIOCLIM 2003/.

For a more detailed motivation for addressing climate cases of global warming and a long interglacial, see Section 5.1.1.

5.2.2 Ice sheet evolution

This climate case results in there being no ice sheets present at the Forsmark site during the coming 120 kyrs. The first glacial conditions at Forsmark occur at ~160 kyrs (158 kyrs) after present.

5.2.3 Shore-level evolution

Given the envisaged strong global warming for the *extended global warming case*, also the sea-level response to the warming is envisaged to be strong. And just as in the *global warming case*, there are significant uncertainties in the estimated sea-level changes and associated shore-level displacement.

Sea-level rise up to year 2100

In order to investigate worst-case scenarios for sea-level and shore-level displacement at Forsmark for year 2100, /Brydsten et al. 2009/ conducted a study that included estimates of global sea-level rise, local isostasy (e.g. ongoing isostatic rebound) and their trends, as well as regional (North Sea) and local (Baltic Sea) annual extremes of today's sea-levels and those in year 2100. The aim of the study was to illustrate the location of the shoreline at Forsmark if applying worst-case assumptions on global- and local sea-level from the literature, together with short-term effects that increase the shore-level during severe storms. The most uncertain factor of the various input parameters is the future global sea-level change, and specifically the contribution by ice sheets (see Section 5.1.3). Possible future developments on global sea-level rise were included from /IPCC 2007, Rahmstorf 2007, Pfeffer et al. 2008/.

/Rahmstorf 2007/ estimated the maximum global sea-level rise by year 2100 to be +138 cm relative to the year 1990. In the study by /Pfeffer et al. 2008/, the Greenland and Antarctic ice sheet response to global warming is estimated and included. Also in this study the large uncertainty in sea-level rise is emphasised. /Pfeffer et al. 2008/ points to two probable cases of global sea-level rises by year 2100 (relative to the level year 2000) amounting to +79 and +83 cm, respectively. /Pfeffer et al. 2008/ also describe a less probable, but still possible, worst case where a calculated *maximum* ice discharge from the Greenland and West Antarctic ice sheets result in a global sea-level rise of +200 cm by year 2100, i.e. +141 cm above the /IPCC 2007/ estimate (that excluded this process).

According to model simulations reported by /IPCC 2007/, the North Sea is expected to have a +20 cm higher level than the global mean on a permanent basis, which is termed *interregional* distribution. The *intraregional* distribution within the North Sea area has been modelled by /Woth et al. 2006/ and amounts at most to +7 cm in the Skagerrak. In order to estimate the worst case, this episodic contribution was also included, even if it is unlikely that it would occur with sufficient duration and at times that could accentuate extreme sea-levels in the Baltic Sea.

The global sea-level rise is locally compensated for by the glacial isostatic rebound that occurs at Forsmark. With the shore-level displacement equation for the site /Söderbäck 2008/, the future course of the isostasy can be calculated by subtracting the eustasy from the shore-level displacement. In this way Rahmstorf's prediction of future global sea-level rise was adjusted for local isostasy (Figure 5-11).

Besides the changing global eustasy and local isostasy, sea-level variations of short duration occur due to temporary weather systems (atmospheric pressure, winds etc). The highest sea-level measured in Forsmark occurred in 2004 and amounted to +144 cm above mean sea-level, equivalent to +141 in the height system RH70. This value was included in the assessment of extreme shore line values for Forsmark.

Future climate change may also lead to increasing wind speeds. This means that the local sea-level rises generated by weather systems in the future may be higher than the values measured so far, a process also accounted for in the study by /Brydsten et al. 2009/. For a more detailed description of the methodology and handling of global sea-level, isostasy, and for a discussion on return periods and storm surges at Forsmark, see /Brydsten et al. 2009/.

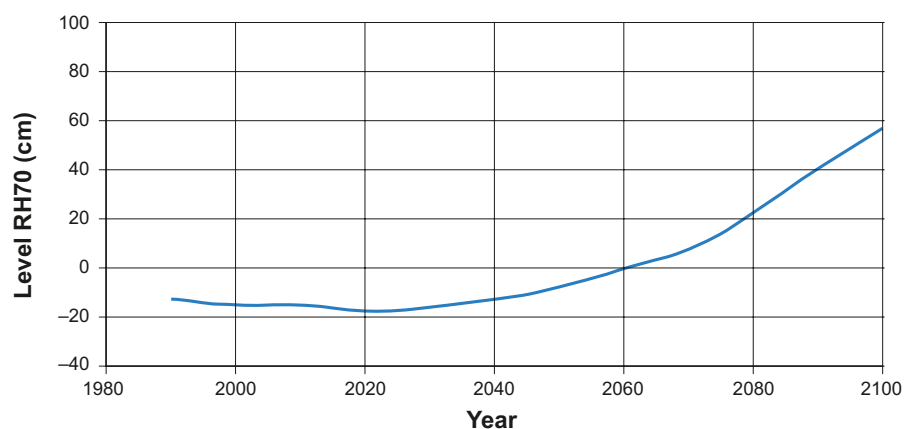


Figure 5-11. Prediction of sea-level according to /Rahmstorf 2007/ adjusted for local isostasy at Forsmark and corrected to the height system RH70. Modified from /Brydsten et al. 2009/.

The calculated extreme values on possible future sea-level elevations for Forsmark in the year 2100 are summarized in Table 5-3. For a description of the contribution from local variation in North Sea and Baltic Sea, see /Brydsten et al. 2009/. The maximum sea-level during storm events in year 2100, based on the maximum sea-level rise estimate by /Rahmstorf 2007/, is +254 cm. The uncertainty in this value is large. In addition to the estimate of maximum global sea-level change by /Rahmstorf 2007/, the /IPCC 2007/ and /Pfeffer et al. 2008/ global sea-level estimates may be used to illustrate the uncertainties in future sea-level rise.

/IPCC 2007/ predicted a 79 cm lower sea-level compared with /Rahmstorf 2007/ by year 2100, whereas /Pfeffer et al. 2008/ estimated a maximum theoretical global sea-level value 62 cm higher than /Rahmstorf 2007/. Using the /IPCC 2007/ and /Pfeffer et al. 2008/ values, the resultant total sea-level in 2100 at Forsmark, with unchanged values for the other constituent processes, is seen in Table 5-4. Figure 5-12 summarizes the various contributions to extreme sea-levels at Forsmark for year 2100. In relation to /Rahmstorf's 2007/ maximum value for year 2100 (+138 cm), the difference relative to the /IPCC's 2007/ estimate (–79 cm) is similar to the difference relative to the maximum value given by /Pfeffer et al. 2008/ (+62 cm). These differences can therefore serve as a measure of the present-day uncertainty of future global sea-level rise (see Figure 5-12).

Figures 5-13 to 5-15 show which areas will be flooded at Forsmark if the sea-level, during short events, reaches +175, 254 and 316 cm above the reference level in the height system RH70 (Table 5-4). The consequences are relatively small at a level of +175 cm, whereas more serious consequences result from levels of +254 cm and +316 cm.

The estimates on maximum sea-levels presented in Table 5-4 and Figure 5-12 to 5-15 describe what might happen due to the cumulative worst-case effects of possible future processes spanning over the global, regional and local scales. The numbers apply for occasions of short duration during heavy storms. The selected processes are characterized by the fact that they are unfavourable as regards a possible raised water level, but they can at present not be dismissed as unrealistic. However, it should again be emphasised that research on e.g. possible future global sea-level rise is in a very intensive phase, and that major uncertainties still exist in this field. Nevertheless, these uncertainties should be considered when planning to build near the present day coast-line.

Table 5-3. Maximum sea-level at Forsmark in year 2100 during storm events, based on e.g. the maximum global sea-level rise as estimated by /Rahmstorf 2007/.

Process	Forsmark	Source
Global eustasy	138	/Rahmstorf 2007/
Local isostasy	–82	/Söderbäck ed. 2008/
Global variation in North Sea	20	/IPCC 2007)
Local variation in North Sea	7	/Woth et al. 2006/
Local variation in Baltic Sea	171	/Meier 2006 and Nerheim 2008/
Total 2100	254	

Table 5-4. Resultant maximum sea-levels (cm in RH70) at Forsmark in the year 2100 based on three different estimates of future global sea-level rise.

Source	Forsmark
/IPCC 2007/	175
/Rahmstorf 2007/	254
/Pfeffer et al. 2008/	316

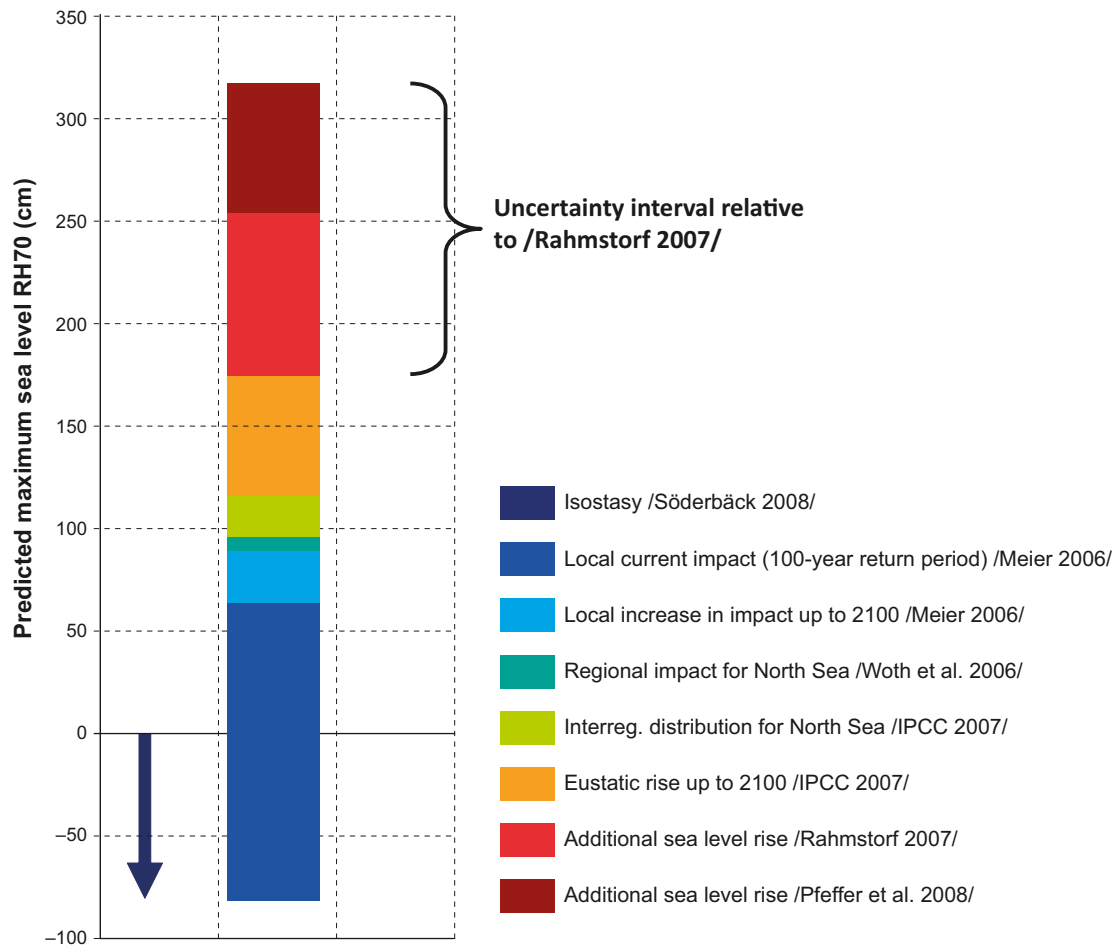


Figure 5-12. Graphic presentation of the compilation of estimated contributions to possible extreme sea-level at Forsmark in year 2100. The isostasy is indicated by downward arrows according to the colour scale. Elevations are expressed in the height system RH70. A first-order expression of uncertainty in global sea-level rise is indicated by a bracket centred on the maximum estimate of /Rahmstorf 2007/, which corresponds to the top edge of the red bar. The numbers apply for the worst possible case in regard to future sea-level rise, and for occasions of short duration during heavy storms. In this context it is important to note that the data on which these estimates are based are the subject of intense research, and that revisions are therefore to be expected.

Sea-level rise beyond year 2100

In the present climate case, air temperatures are raised more than in the *global warming case*. The Greenland ice sheet is envisaged to experience a total collapse, contributing 7.3 m to global mean sea level rise /Bamber et al. 2001/. Also a West Antarctic ice sheet collapse is envisaged included in this case, contributing with 3.3 m of global mean sea level rise /Bamber et al. 2009/. The net results of the collapse of the Greenland ice sheet may be a ± 0 mm/yr sea level change around Fennoscandia /Milne et al. 2009/, whereas the collapse of the West Antarctic ice sheet could result in a sea level rise around Fennoscandia of ~ 3 m /Bamber et al. 2009/. A 0.5 m sea level contribution from melting of all glaciers and ice caps are also envisaged for this case. The thermosteric sea level rise is larger in this case than in the *global warming case*, due to the larger temperature increase, amounting to several metres.

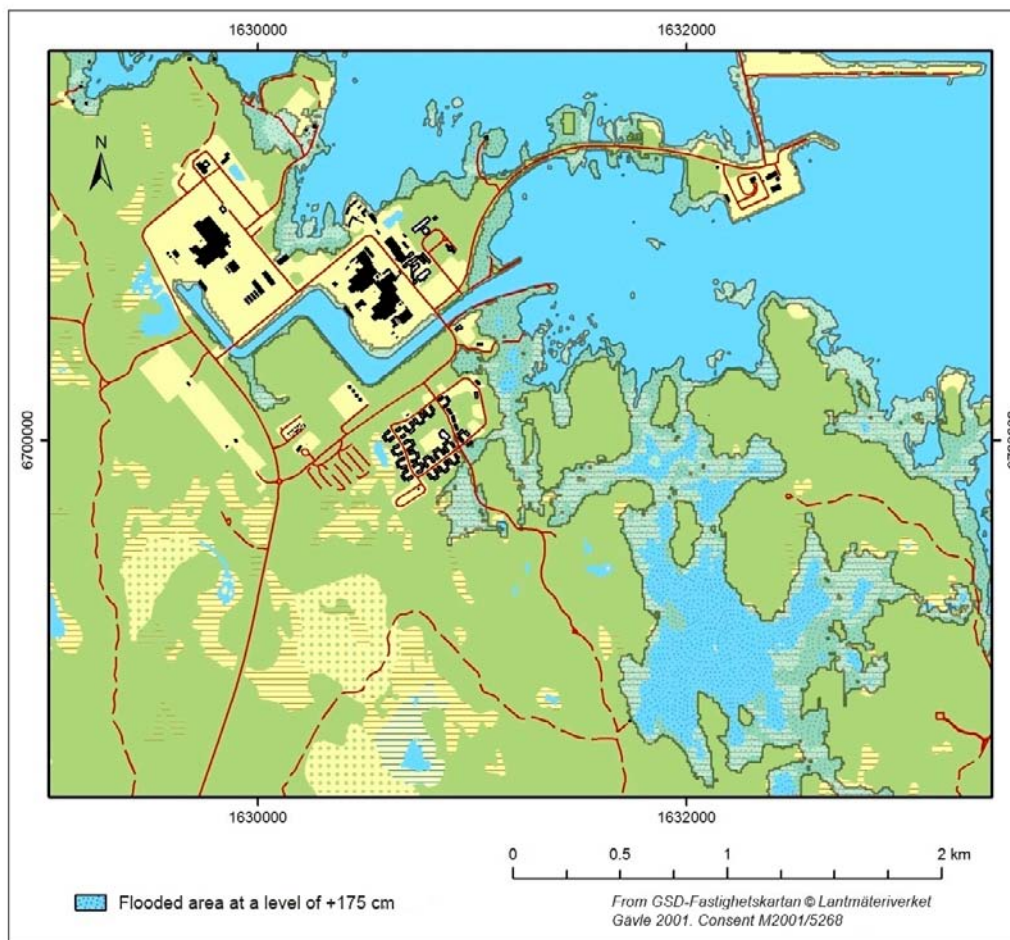


Figure 5-13. Area at risk of flooding at an extreme level of +175 cm in Forsmark in year 2100 AD. Note that these results show extreme situations when assumed worst cases from the present scientific literature are combined with local effects also set to pessimistic values. From /Brydsten et al. 2009/.

Given these contributions and the assumed extreme global warming, equilibrium sea-levels at Forsmark of up to around 10 metres may be possible. This results in an initial period with a sea-level rising faster than the isostatic uplift at the Forsmark site, resulting in submerged conditions for several thousands of years. Following the results of /Rohling et al. 2009/, that equilibrium sea-levels for the present day CO₂ concentration could be reached within the next two to five millennia, submerged conditions are somewhat arbitrarily set to prevail for 10 kyrs in this *extended global warming case*. The duration of this initial submerged period is uncertain; it could be shorter or longer than this.

After this transgression, isostatic rebound, and in time a slow lowering of global sea-level, mainly due to cooling and associated thermal contraction of sea water, results in the site again emerging from the sea. Subsequently, the site is situated above sea-level for the rest of the 120 kyr climate case, in line with the GIA modelling results on shore-level changes in the *global warming case* (Figure 5-4).

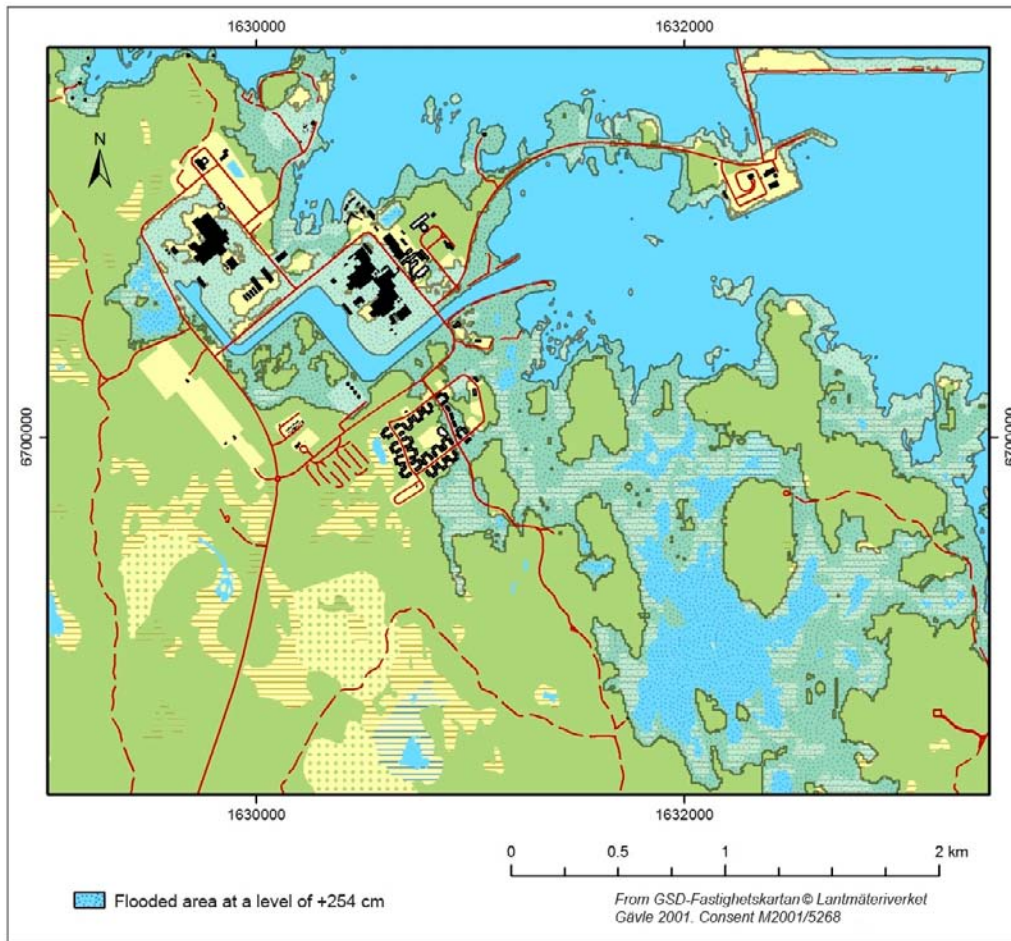


Figure 5-14. Area at risk of flooding at an extreme level of +254 cm in Forsmark in year 2100 AD. Note that these results show extreme situations when assumed worst cases from the present scientific literature are combined with local effects also set to pessimistic values. From /Brydsten et al. 2009/.

In the long run, around 130–140 kyrs after present, the growth of ice sheets results in a general lowering of global sea-level.

5.2.4 Permafrost evolution

In the *extended global warming case*, the very long period of temperate climate conditions is followed by permafrost develop at the Forsmark repository location at ~110 kyrs (107 kyrs) after present. Subsequently, temperate climate conditions develop again before the ending of the first 120 kyrs. Given the local definition of the ending of the present interglacial (by the development of permafrost at the repository location, see Section 4.5.4), the Holocene ends per definition at ~110 kyrs after present in this climate case. Periglacial conditions with permafrost prevail for c. 4 kyrs (3%) of the coming 120 kyrs.

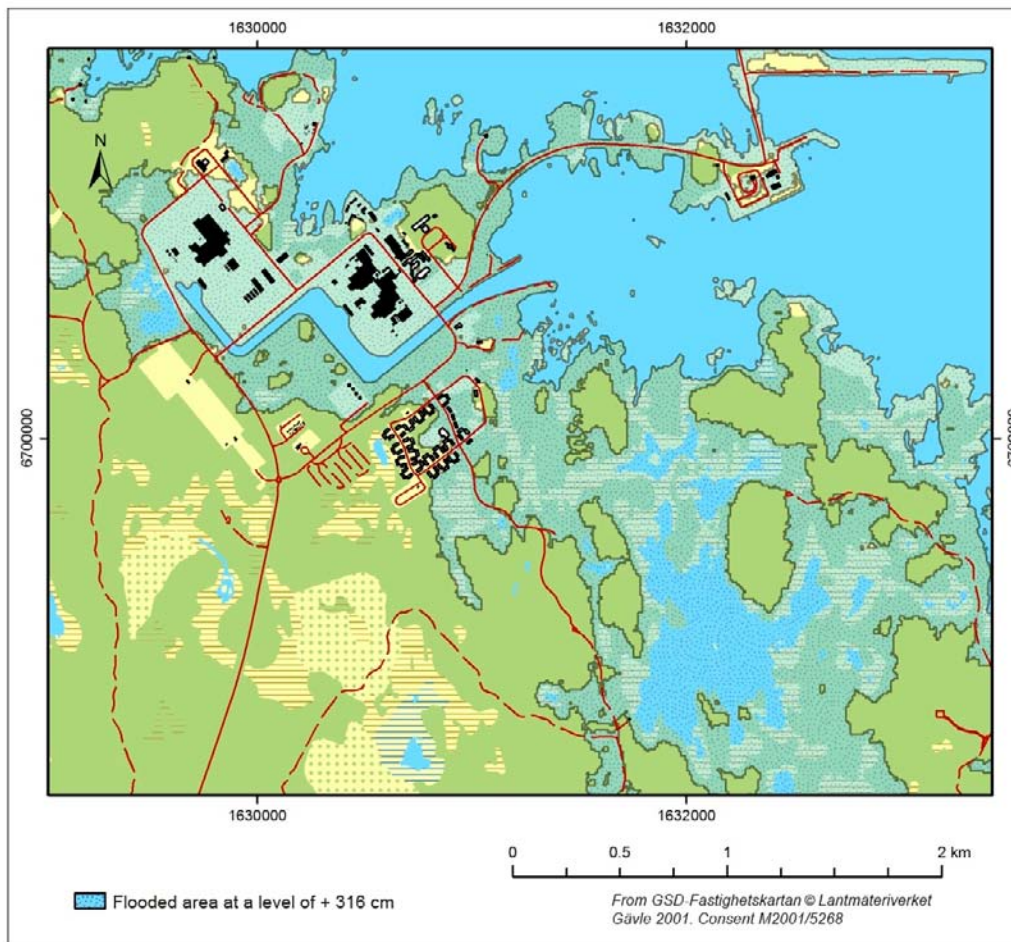


Figure 5-15. Area at risk of flooding at an extreme level of +316 cm in Forsmark in year 2100 AD. Note that these results show extreme situations when assumed worst cases from the present scientific literature are combined with local effects also set to pessimistic values. From /Brydsten et al. 2009/.

5.2.5 Evolution of climate domains

As mentioned above, a 100 kyr long period of temperate climate conditions is added before a slow onset of the first *reference glacial cycle* for the *extended global warming case*. After these additional 100 kyrs of temperate conditions, regular Late Pleistocene glacial cycles, represented by the *reference glacial cycle* described in Section 4.5, are envisaged to follow (Figure 5-16). This results in there being ~160 kyrs before the first glacial conditions occur at the Forsmark site, while the first permafrost occurs at ~110 kyrs after present. The climate development in the *extended global warming case* thus describes a situation without periglacial- or glacial climate conditions in central Sweden, including Forsmark, for a very long period of time.

Peak air temperatures are envisaged to be reached within the first hundreds to thousands of years as a result of anthropogenic greenhouse-gas emissions. Mean annual air temperatures several degrees warmer than at present then occur at Forsmark. In line with the results of /Kjellström et al. 2010b/, higher atmospheric greenhouse gas concentrations than in the *global warming case* are envisaged to give, at peak global warming conditions, air temperatures in excess of the global warming temperatures modelled for the Forsmark region (annual mean air temperature of +3.6°C a few thousands of years into the future) by /Kjellström et al. 2009b/. The changes in climate also result in a larger initial increase in precipitation than the +20% modelled for the Forsmark region /Kjellström et al. 2009b/.

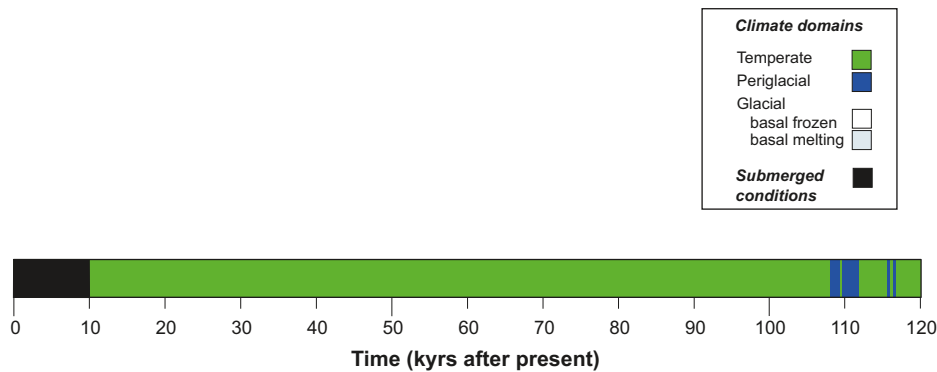


Figure 5-16. Evolution of climate conditions at Forsmark for the extended global warming case. Following from the assumption of this case, temperate climate conditions prevail at the site for the coming 120 kyrs, except for an initial period of submerged conditions and for a few thousands of years at the end of the period. The duration of the initial period of submerged conditions is uncertain; it could be shorter or longer than indicated in the figure. Note that there is a very large range in e.g. temperature, precipitation and other climate parameters within these temperate conditions, ranging from strong global warming conditions to conditions with temperatures significantly cooler than at present (prior to the development of periglacial conditions). For a detailed example of more moderate global warming conditions at Forsmark than envisaged for this case, see Section 5.1.7.

Following the reduction in e.g. CO₂ emissions, air temperature and precipitation are envisaged to slowly decline for the rest of the long interglacial period, in response to the slow decline in atmospheric CO₂ concentration e.g. /Archer 2005, Lenton and Britton 2006, Tyrell et al. 2007, Archer and Brovkin 2008, Schaffer et al. 2009/.

The cryosphere response to the extreme global warming results in raised global sea-levels and submerged conditions at the Forsmark site at the start of the period (Figure 5-16). The length of the initial submerged period is uncertain; it could be shorter or longer than illustrated in Figure 5-16.

5.2.6 Surface denudation

Since the *extended global warming case* envisages an even larger fossil fuel CO₂ climate perturbation than in the *global warming case*, fluvial erosion and chemical weathering in the wetter and warmer climate are anticipated to be more efficient than in the *global warming case* (Section 5.1). For a description of denudation processes that are anticipated to change compared with the *reference glacial cycle*, see the description of denudation under the *global warming case*.

Even if fluvial erosion and chemical weathering increase in this climate case compared with the *reference glacial cycle*, the *extended global warming case* mainly comprises temperate climate conditions for the entire 120,000 years, and consequently completely excludes the most efficient denudation process (glacial erosion) as defined in Section 3.5.4. Given this, and that feedback-mechanisms between climate, weathering and vegetation, e.g. /Lenton and Britton 2006/ could partly counteract the climate perturbation, the expected total amount of denudation for the present climate case is considered smaller, or at least not larger, than in the *reference glacial cycle*. Surface denudation is therefore not described and treated further in the *extended global warming case*. A climate case with an anticipated *larger* amount of surface denudation than in the *reference glacial cycle* is described in the *extended ice sheet duration case* (Section 5.3).

5.3 Extended ice sheet duration case

5.3.1 Background

In order to cover the uncertainty in duration of ice sheet coverage for the coming 120 kyrs, a climate case with extended ice sheet duration is constructed, describing a situation with a longer time of ice sheet coverage than in the *reference glacial cycle*. To this end, a climate evolution similar to that of the *reference glacial cycle* is used, with the important exception that the long interstadial with ice-free conditions between the two ice advances does not occur at Forsmark. In the *reference glacial cycle*, interstadial conditions, dominated by periglacial climate conditions with permafrost, occur between 66 and 91 kyrs (Table 4-5, Figure 4-34). In the present case, no ice-free conditions occur during this period. Accordingly, the scenario with extended ice sheet coverage describes one long single phase of ice sheet coverage at Forsmark, with a timing of glaciation and deglaciation according to Table 5-5.

This ice sheet evolution is similar to the Weichselian glacial history presented by /Lundqvist 1992/. In /Lundqvist 1992/, the main phase of the Weichselian glaciations starts ~50 kyrs BP with the ice sheet envisaged to cover Sweden continuously up to the final Weichselian deglaciation, see the literature review on ice-marginal fluctuations during the Weichselian glaciation by /Lokrantz and Sohlenius 2006/. Several recent studies suggest that there was a long period of ice free-interstadial conditions over large parts of Fennoscandia during MIS 3 (59–24 kyrs BP), i.e. in the middle of the main phase of glaciation as traditionally suggested, see Section 4.2.

The duration of ice sheet coverage over the Forsmark region in the *extended ice sheet duration case* is comparable with the total time of ice sheet coverage as coarsely deduced from the Weichselian reconstruction by /Lundqvist 1992/. In the Lundqvist reconstruction, most of Scandinavia is covered by ice from the mid-Weichselian (around 50 kyrs BP) until the deglaciation (around 10 kyrs BP), and during a phase of the early Weichselian (90–80 kyrs BP), which gives a total time of ice sheet coverage for the major part of Scandinavia of roughly 50 kyrs. Acknowledging that the Lundqvist reconstruction was not intended to give a detailed picture of ice sheet durations, the *approximate* duration in the Lundqvist reconstruction is similar to the duration of ice sheet coverage at Forsmark (60 kyrs) in the present climate case. In line with the ice sheet reconstruction by /Lundqvist 1992/, the Fennoscandian ice sheet is assumed to have started to grow considerably earlier than the time of ice sheet overridding at Forsmark. For a compilation of information on Weichselian glacial history, see Section 4.2 and references therein.

5.3.2 Ice sheet evolution

As an illustration of a situation with a persistent ice sheet coverage over the site for a long time (also during the ice-free phase corresponding to MIS 3 during the Weichselian glaciation, 70–90 kyrs ago), ice thickness data from an uncalibrated ice sheet model reconstruction of the Fennoscandian ice sheet are used (Figure 5-17). The data were produced by the same ice sheet model that was used for the simulation of the calibrated ice sheet development used for the *reference glacial cycle* (Section 3.1.4). In this climate case, the precise evolution of the ice thickness is not important. Therefore, the uncalibrated ice sheet simulation may be used to illustrate the ice sheet development for the case when it covers the Forsmark site without interstadial conditions between the two glacial phases in the *reference glacial cycle*.

As during the initial 4 kyrs of the first glacial phase of the *reference glacial cycle* (Figure 4-34), cold-based conditions with subglacial permafrost are envisaged to exist under the first 4 kyrs of glacial conditions in this case. Subsequently, the subglacial permafrost melts, and the ice sheet becomes warm-based at around 56 kyrs and remains so for the rest of the glacial period.

Table 5-5. Duration of climate domains at the Forsmark site in the extended ice sheet duration case.

Temperate climate domain [kyrs] (percent of time of glacial cycle)	Periglacial climate domain [kyrs] (percent of time of glacial cycle)	Glacial climate domain [kyrs] (percent of time of glacial cycle)	Submerged conditions [kyrs] (percent of time of glacial cycle)
28 kyrs (23%)	22 kyrs (18%)	60 kyrs (50%)	10 kyrs (8%)

The ice sheet evolution for this case starts with glacial conditions at c. 50 kyrs after present (Figure 5-17), i.e. around 7 kyrs earlier than in the *reference glacial cycle*. Glacial conditions persist until c. 110 kyrs after present when the site is deglaciated (Figures 5-17 and 5-18). The duration of all climate domains is summarized in Table 5-5. The ice thicknesses in this uncalibrated model run are somewhat smaller than in the *reference glacial cycle*. In this context, it should be noted that the maximum possible ice thickness over Forsmark, used for the safety assessment scenario for canister failure due to isostatic load /SKB 2011/, is not derived from this climate case or the *reference glacial cycle*, but from the case describing a maximum ice sheet configuration (Section 5.4).

In light of recent results indicating that the Weichselian ice sheet exhibited a more dynamic behaviour during the middle Weichselian than traditionally assumed (see above and Section 4.2), the ice sheet development in Figure 5-17 is considered a pessimistic estimate of the duration of ice sheet coverage for the coming 120 kyrs. The degree of pessimism in this case may also be seen in the light of the inferred present global warming, which may result in a longer than usual interglacial, and consequently shorter time of glacial conditions than in the *reference glacial cycle* (Section 4.5 and 5.2).

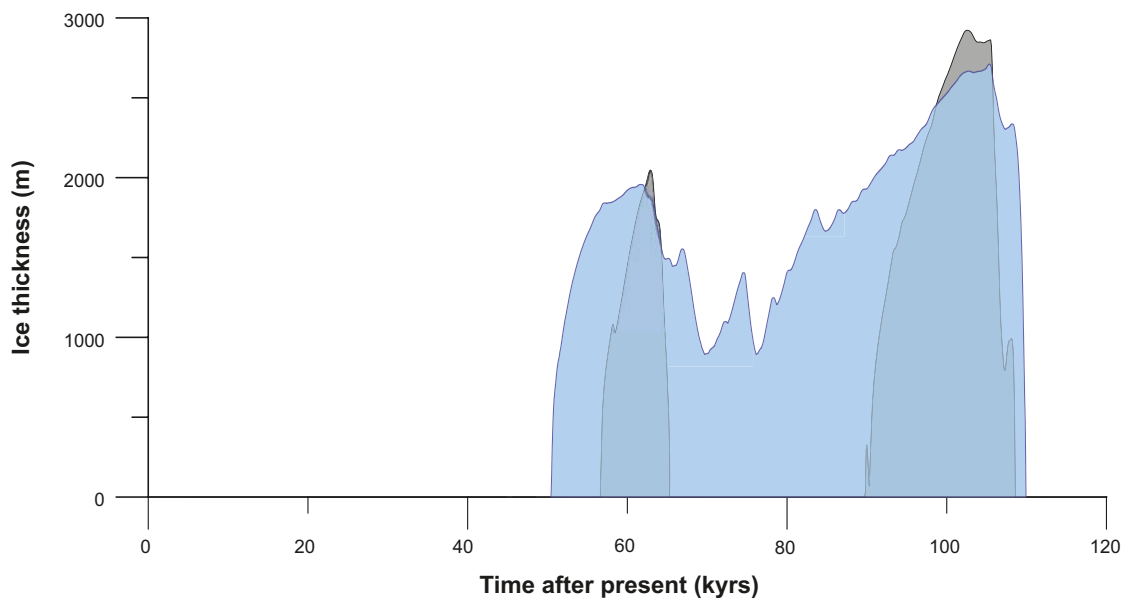


Figure 5-17. Ice sheet coverage over Forsmark in the extended ice sheet duration case (blue). For comparison, the ice sheet development of the reference glacial cycle, based on a reconstruction of Weichselian conditions, is also shown (grey).

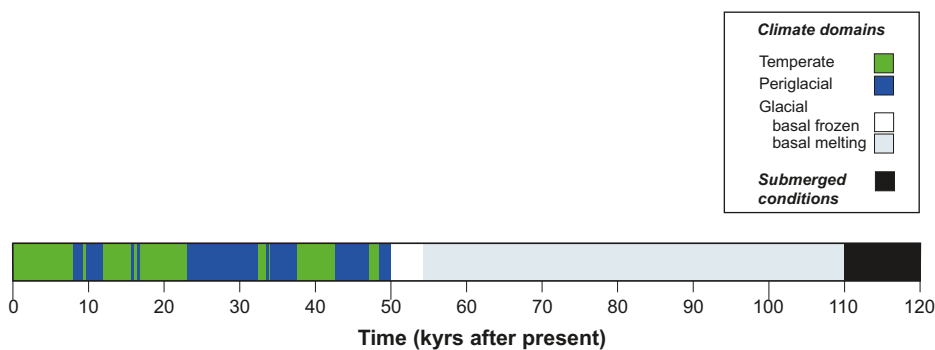


Figure 5-18. Evolution of climate conditions at Forsmark as a time series of climate domains and submerged conditions for the extended ice sheet duration case. Glacial conditions start earlier and lasts considerably longer than in the reference glacial cycle (Section 4.5.4).

5.3.3 Surface denudation

The *extended ice sheet duration case* results in the period with warm-based ice sheet conditions, and associated glacial erosion over the repository, being longer than in the *reference glacial cycle* (Section 4.5.4. and 4.5.7). Given that the ice sheet duration is about twice as long in this case (Figure 5-17) compared with the *reference glacial cycle* (Section 4.5.4), the amount of glacial erosion is estimated to be around doubled compared with the *reference glacial cycle*. The maximum amount of glacial erosion in fresh bedrock could thus be up to 2–4 m at the repository location for this case. However, if periods of cold-based, non-erosive, conditions would be longer in this climate case, which could be the case if climate conditions are colder, the duration of periods with glacial erosion would be shorter and the amount of erosion smaller.

The amount of non-glacial denudation is somewhat less than in the *reference glacial cycle*, since the time of temperate- and periglacial (mainly periglacial) climate conditions are shorter than in the *reference glacial cycle*. However, if the estimated amount of non-glacial surface denudation pessimistically is kept at the same value as for the *reference glacial cycle*, the resulting total denudation for the glacial cycle with extended ice sheet duration is still less than 5 m (4 m of glacial erosion and up to 0.6 m of non-glacial denudation, Table 3-17).

Surface denudation results in a reduction of the repository depth. A reduced repository depth could in turn lead to that permafrost and frozen ground reach closer to the repository. However, a 5 m reduction in repository depth for a glacial cycle with prolonged ice sheet duration has a negligible effect, in terms of repository safety, on the estimated permafrost- and freezing depths presented in Section 4.5.3 and 5.5.3. Also in the 1 Myr time perspective, a pessimistic use of the case of prolonged glacial conditions and the associated amount estimated glacial erosion (4 m of erosion in fresh bedrock) for each of the 8 glacial cycles, combined with the estimated 5 m of non-glacial denudation in 1 million years (Table 3-17), results in a limited amount of total denudation, less than 40 m, over the repository.

5.4 Maximum ice sheet configuration case

5.4.1 Background

For glacial conditions an additional hydrostatic pressure related to the ice sheet thickness is added to the hydrostatic pressure for ice-free conditions. The extremes regarding hydrostatic pressure in the glacial climate domain depend on the ice sheet configuration and on its hydraulic systems. Under the Antarctic ice sheet, sub-glacial lakes have been observed. The hydrostatic pressure in these lakes is assumed to correspond to the ice overburden pressure. A hydro-thermo-mechanical balance is assumed, where supply of basal melt water, re-freezing and ice deformation result in a hydrostatic equilibrium where the ice sheet rests, or floats, on the water surface, e.g. /Pattyn et al. 2004/. As further justified below, it is reasonable to assume that also for the Fennoscandian ice sheet, the maximum ice sheet thickness sets a limit to the maximum hydrostatic pressure that may occur at the ice sheet-substrate interface. To find and analyze the effects of the extremes regarding ice sheet thickness additional simulations were performed with the ice sheet model used to construct the ice sheet development of the *reference glacial cycle*.

5.4.2 Ice sheet evolution

To investigate the maximum ice sheet thickness that may occur in Fennoscandia, the UMISM ice sheet model (Section 3.1.4) was used for a sensitivity test to see what ice configurations were possible with different degrees of climate cooling. The sensitivity experiment used the same model setup as used for the reconstruction of last glacial cycle conditions (Section 3.1.4). However, the model was not run using the palaeo-temperature curve for the last glacial cycle, but instead by using a set of temperature evolutions in which annual air temperatures decreased linearly by 1° per 2 kyrs, from present-day temperatures down to various constant levels. In these sensitivity tests, temperatures were lowered between 4 and 16° (Figure 5-19). Model uncertainties and simplifications are described in Section 3.1.7.

Ice sheet growth started at a temperature lowering of 6 to 7°. If temperature is lowered by 9° or more, the ice sheet covers the Forsmark site. Warmer cases did not produce an ice sheet. In all cases

of ice sheet growth, the model simulated a total period of 100 kyrs, after which approximately steady-state conditions were obtained with little further change in ice volume and area. The results indicate that cold climate conditions with annual mean temperatures lowered by 10°C are required for the ice sheet to advance to and over the Forsmark site. The resulting maximum ice sheet thicknesses from the sensitivity simulations are shown in Figure 5-20.

As expected, the maximum ice sheet thickness increases with colder climates (Figure 5-20, black line). However, the degree of increase in thickness with temperature lowering declines as colder cases are considered. For a temperature lowering of more than approximately 13°C, colder climates do not generate thicker ice sheets. This result is in general agreement with what is known of Antarctic ice sheet variations, see below.

These simulated temperature cases (Figure 5-19) are extreme as regards their prolonged duration. Variations in temperature of this magnitude have occurred in the past, e.g., but never of this long duration without interruptions, see Appendix 1 and references therein. The extreme nature of these sensitivity cases is reflected also in the resulting ice sheet configurations. For the colder cases, the ice sheet covers all of northern and central Europe, and extends southward all the way to the Alps. Geological observations of traces from Fennoscandian ice sheets show that such large ice configurations have never occurred during the last 2 million years e.g. /Ehlers and Gibbard 2004/, and can thus be considered unrealistic for the time scale of interest for the safety assessment.

The maximum ice thickness at Forsmark in the *reference glacial cycle* was 2,920 m (Section 4.5). In the sensitivity tests, the maximum ice sheet thickness developed over Forsmark was 3,670 m. The uniform and high values reflect that the Forsmark site has an interior location within these unrealistically large ice sheets.

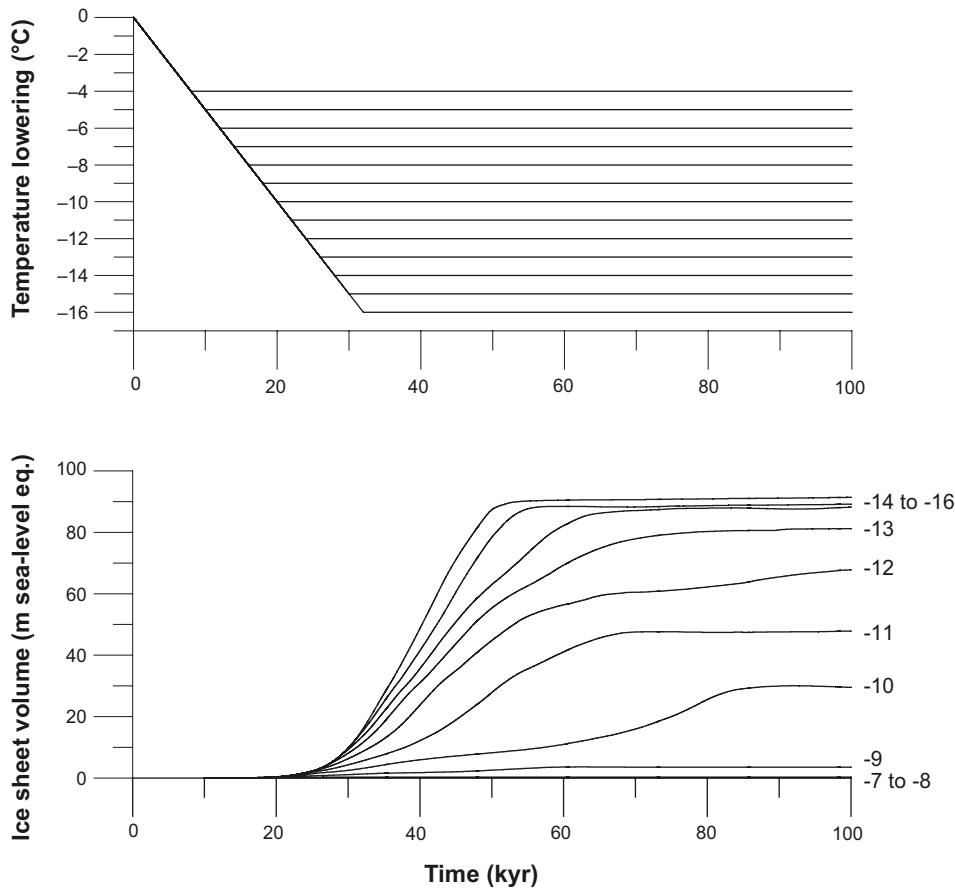


Figure 5-19. Temperature lowering schemes (upper graph) and resulting development of Fennoscandian/Eurasian ice sheet volumes (lower graph) in the sensitivity test on air temperatures and ice sheet configurations. The volume of the ice sheets is expressed as metres sea-level contribution.

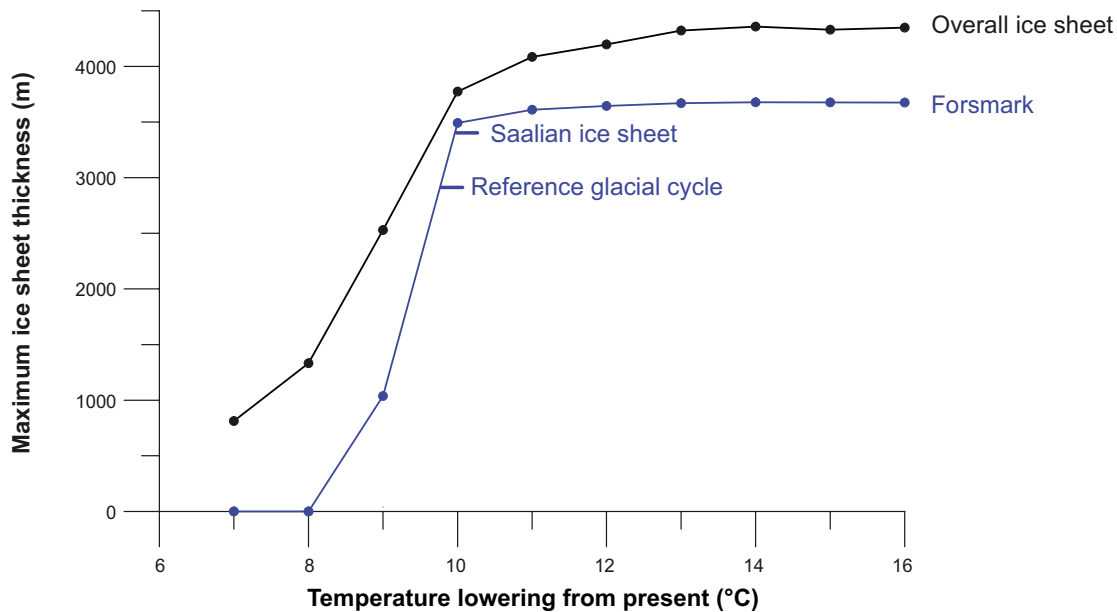


Figure 5-20. Maximum modelled ice sheet thicknesses for the ice sheets modelled using the schematic climate evolutions in Figure 5-19. The blue curve represents maximum ice thicknesses extracted specifically over the Forsmark region. The overall largest ice thicknesses for these ice sheets are shown in black. The short line marked Reference glacial cycle show the maximum ice thickness of the ice sheet in the reference glacial cycle (Section 4.5.1), whereas the line marked Saalian ice sheet shows the maximum ice thickness for the largest Fennoscandian ice sheet configuration supported by geological observation for the past 2 million years.

Estimate of maximum ice thickness during the past 2 million years

From geological information, it is known that the maximum ice extents of Pleistocene Fennoscandian ice sheets (i.e. those occurring during the past ~2 million years) were larger than that of the Weichselian ice sheet, and occurred during the Saalian glaciation, e.g. /Svendsen et al. 1999, 2004, Lambeck et al. 2006, Colleoni et al. 2009/. At the peak of the Saalian glaciation, around 140 kyrs BP, the ice sheet reached up to c. 200 km further south and more than 1,000 km further east than the Weichselian ice sheet. Modelling of the maximum Saalian ice sheet configuration (Section 5.4.2) indicated that the maximum ice thickness of this ice sheet was c. 3,100 m over the Forsmark region. According to /Lambeck et al. 2006/ the maximum Saalian ice thickness over the Forsmark region at 140 kyrs BP was around 3,400 m. Similar values may be inferred from /Colleoni et al. 2009/. Based on this information, the maximum expected ice sheet thickness for Forsmark is set to 3,400 m.

From the results of the extreme cases in the sensitivity test (Figure 5-20), it is unlikely that the ice thickness at Forsmark could under any circumstance exceed 3,700 metres. The results of the sensitivity tests can be considered as high values since it is unlikely that the Fennoscandian ice sheet would, in reality, ever reach its maximum equilibrium size, i.e. the size simulated in these experiments.

In the climate cooling sensitivity tests, the maximum simulated *overall* thickness of the ice sheets is 4,360 metres. This is 1,000 m more than the maximum overall ice thickness for the *reference glacial cycle* which is 3,300 m. Estimating the maximum thickness of the largest geologically feasible Pleistocene ice sheet yields a maximum *overall* Saalian ice thickness of 3,600 m. Other simulations of the Saalian ice sheet result in a maximum ice thickness of 4,500 m, over the Kara Sea in the Arctic /Lambeck et al. 2006/.

For comparison, the maximum ice sheet thickness occurring on Earth today is ~4,500 m for parts of the East Antarctic ice sheet /Lythe et al. 2001/. The Greenland ice sheet has a maximum thickness of ~3,400 m /Bamber et al. 2001/. In a colder glacial climate, the maximum ice thickness of the Antarctic ice sheet will probably not change significantly. In a colder climate, the marginal parts of the Antarctic ice sheet grow significantly, whereas, at the same time, more interior parts of the ice sheet keep the same thickness or even gets thinner due to moisture starvation /Huybrechts 1990, Näslund et al. 2000/. Therefore, it is likely that the maximum thickness of the Antarctic ice sheet seen also over an entire glacial cycle is around 4,500 m. This value is close to the largest overall ice thickness obtained in the sensitivity test, 4,360 metres (Figure 5-20). These results are also in line with a largest inferred thickness of the Laurentide ice sheet of 4,300 metres (Tarasov and Peltier 2004). These observations and results suggest that Pleistocene ice sheets up to date have not grown thicker than approximately 4,500 m, which gives an upper limit for ice sheet thickness.

Hydrostatic pressures exceeding ice overburden pressure

Hydrostatic pressures exceeding ice overburden can occur in some situations, for example in relation to jökulhlaups, i.e. large sudden outburst floods of glacial melt water from subglacial or supraglacial ice-dammed water reservoirs /Roberts et al. 2000/. In a few cases, higher pressures of non-jökulhlaup origin have been registered also in the ablation area of smaller glaciers. These high pressures are of artesian character, with the amount of pressure being ultimately determined by upglacier ice thickness and the presence of meltwater. This may also occur in near-frontal parts of ice sheets /Roberts 2005/. However, during times of maximum ice sheet thickness over Forsmark, e.g. during the Last Glacial Maximum, this site is located within the ice sheet interior, far from the ablation area and the margin. For this ice sheet configuration, surface melting is thus absent or negligible above and upstream of the Forsmark site, due to the high ice surface elevation and associated low air temperatures. In addition, climate is at its coldest at this time during the glacial cycle, also precluding surface melt in these high-polar regions of the ice sheet. Therefore, it is reasonable to assume that maximum hydrostatic pressures at Forsmark are dependent only on the local ice thickness during periods of maximum ice thickness, and not on ice thickness and surface melting upstream of the site.

Conclusions

For the *reference glacial cycle*, the additional hydrostatic pressure related to ice thickness over Forsmark is 26 MPa (Table 5-6). The *maximum* expected additional hydrostatic pressure, pessimistically derived from the largest ice sheet configuration during the past 2 million years, as supported by geological observations, is 30 MPa. Maximum ice thicknesses of the more extreme and unrealistic ice sheet configurations discussed above, with associated additional hydrostatic pressures, are also presented in Table 5-6.

Table 5-6. Maximum ice sheet thickness and associated additional hydrostatic pressure at Forsmark for various Fennoscandian ice sheet configurations.

	Maximum ice thickness (m)	Hydrostatic pressure contribution (MPa)
Reference glacial cycle	2,920	26
Largest Fennoscandian ice sheet during past 2 Myrs (Saalian ice sheet)	3,400	30
Extreme ice sheets from climate sensitivity test	3,670	32

5.4.3 Surface denudation

The large size of this ice sheet would take a longer time to build than the maximum ice sheet of the *reference glacial cycle* (Section 4.5.1), but not a longer time than the 60 kyrs of ice sheet presence in the *extended ice sheet duration case* (Section 5.3). Therefore, the present climate case does not contribute to a longer time of glacial erosion, or resulting larger total amount of denudation, than the *extended ice sheet duration case*. For that reason, surface denudation is not described and treated further in the *extended global warming case*.

5.5 Severe permafrost case

5.5.1 Background

The main factors of importance for repository safety in the permafrost climate domain are the permafrost- and frozen depths, the depth of the isotherm at which the buffer and backfill freezes, and the possible freezing out of salt that may result in a zone with high salinity beneath the freeze front. The prevailing climate conditions are the main factor determining the evolution of permafrost, see Section 3.4.4 and /Hartikainen et al. 2010/. A mean annual air temperature well below 0°C for long periods is a prerequisite for the development of permafrost to greater depth, Section 3.4.4.

In order to investigate remaining uncertainties within the periglacial climate domain that were not studied in the permafrost simulations reported in Section 3.4.4 and 4.5, a *severe permafrost case* was investigated /Hartikainen et al. 2010/. These remaining uncertainties mainly consist of the possibility of having a cold dry climate at Forsmark, but without the presence of an ice sheet. An assumption of a cold periglacial climate is here combined with an assumption of a very dry climate in order to favour permafrost growth. In this climate case, the dry climate also limits ice sheet growth so that an ice sheet does not reach the Forsmark site during the first glacial cycle. If an ice sheet covers the site, any pre-existing permafrost decays due to the insulating effect of the ice sheet, especially if the ice sheet is warm-based (Section 4.5.4). In line with the dry and cold assumption, and that no ice sheet forms over the site, it is further assumed that no post-glacial periods of submerged conditions occur, and that no insulating winter snow and vegetation cover exist.

In addition to the simulation using the above assumptions, a number of sensitivity studies have also been done in order to investigate the climate conditions required to develop permafrost and perennially frozen ground to repository depth.

5.5.2 Ice sheet evolution

One of the main assumptions in the *severe permafrost case* is that there is no ice sheet coverage over the Forsmark site for the coming 120 kyrs, and consequently there is no ice sheet development in this climate case.

5.5.3 Permafrost evolution

The *severe permafrost case* is analysed with the same 2D permafrost model that was used for the *reference glacial cycle* and for the sensitivity experiments on surface, subsurface and air temperature parameters (Section 3.4.4). The *severe permafrost case* was simulated for a full glacial cycle, from 115 kyrs BP to present. However, for the present section the results have been projected for a future glacial cycle, in the same way as the reconstruction of last glacial cycle conditions (Section 3.4.4) were used to construct a future *reference glacial cycle* (Section 4.5).

In this context it should be noted that the exact way in which the start of the previous reconstructed glacial cycle is taken to form the start of the present climate case will affect the detailed timing of permafrost events, such as the detailed timing of the first permafrost development. However, for the safety assessment of a KBS-3 repository, the precise timing of permafrost and freezing events is not central. Instead it is the maximum simulated permafrost and freezing *depths* that are of importance. Therefore, the temporal uncertainties arising from the onset of the future glacial cycle in the *severe permafrost case* do not affect the analysis of e.g. the SR-Site freezing scenario /SKB 2011/.

The following assumptions were made for the *severe permafrost case*:

- The climate is so dry that no ice sheet forms that is large enough to reach the Forsmark site at any time during the glacial cycle, i.e. ice free conditions prevail during the entire glacial cycle.
- In line with the above assumption, it is assumed that the repository location is not isostatically depressed below sea-level.
- The climate is so dry that there is no insulating snow cover during winter.
- There is no vegetation to insulate the ground from low air temperatures.
- The temperature curve reconstructed for the last glacial cycle, but without a presence of ice sheets and submerged conditions (Figure 3-54, red line) was employed for calculating ground surface temperatures.

Initial conditions are assumed to correspond to the present-day conditions (temperature, salinity and groundwater pressure). Heat generated by the radioactive decay of the spent fuel in the repository is included in the simulation. The modelled 2D profile is seen in Figure 3-58.

Regarding the choice of using the temperature curve reconstructed for the last glacial cycle also for the analysis of a *severe permafrost case*, the following needs to be considered. Northern Hemisphere mid-latitude ice sheets form essentially as a response to low air temperatures, see Section 2.1 and 3.1. In line with this, there is a correlation between cold interstadial periods during glacial cycles and large ice sheet configurations. In the *severe permafrost case*, the main assumption is that the climate is cold but without an ice sheet reaching the Forsmark site, see above. This means that the maximum ice sheet configuration for this hypothetical case does not reach middle central Sweden anytime during the glacial cycle. This ice sheet thus has very much smaller ice sheet configurations, at all times, than the Weichselian ice sheet had. This, in turn, strongly implies that that air temperatures during the fictive glacial cycle of the *severe permafrost case* would be higher than in the reconstruction of the last glacial cycle that hosted the Weichselian ice sheet (but still significantly colder than temperate climate conditions). If temperatures were to be the same during the *severe permafrost case* as during the Weichselian, a larger ice sheet would form and cover the Forsmark site for parts of the glacial cycle. It is difficult to estimate what temperatures would correspond to a glacial cycle as envisaged for the *severe permafrost case*. The temperature curve used for permafrost simulations for the *severe permafrost case* should, in line with the above reasoning, be considerably warmer than the one used for the reconstruction of the last glacial cycle.

On the other hand, the temperature curve reconstructed for the last glacial cycle also has a significant uncertainty interval, see Appendix 1. The comparison of the reconstructed last glacial cycle temperature curve with (the few) existing quantitative proxy data on Weichselian temperatures from the Fennoscandian region seems, however, to indicate that the reconstructed temperature curve is in broad agreement with proxy data, see Appendix 1. Furthermore, the comparison suggests that the temperature curve does not overestimate temperatures for the compared last glacial cycle stadials and interstadials. Instead, the general picture from the comparison with Fennoscandian proxy data is that the reconstructed temperature curve gives roughly correct or slightly too low temperatures by a few degrees.

In order to make a reasonable choice of temperature curve for the *severe permafrost case*, with the above issues in consideration, air temperatures were pessimistically assumed to fall according to the reconstructed temperature curve for the *reference glacial cycle*, but without a presence of ice sheets and submerged conditions (Figure 3-54).

Surface and subsurface properties and conditions

Just as for the 2D permafrost modelling for the *reference glacial cycle* (Section 3.4.4), the significant uncertainties associated with descriptions of the surface conditions motivate the analysis of two climate variants of the *severe permafrost case*, one humid and one dry. This is to yield a lower and upper limit for the permafrost and perennially frozen ground development, see further below.

Based on the Köppen climate classification /Lohmann et al. 1993/ and long-term observations /Eugster et al. 2000/ the climate of the *severe permafrost case* may be divided into three climate zones: *Boreal*, *Subarctic* and *Arctic*, which may be characterized by the annual mean air temperature, the monthly mean maximum summer air temperature and the monthly mean minimum winter air temperature, together with the monthly mean maximum summer and winter precipitations (Table 5-7), see /Hartikainen et al. 2010/. The large ranges in the monthly mean air temperatures and precipitations are explained by the fact that the description and modelling of surface conditions involve significant data-, conceptual- and model uncertainties, see /Hartikainen et al. 2010/.

Other surface properties and conditions are the same as in the 2D permafrost modelling of the *reference glacial cycle* (Section 3.4.4). All subsurface properties for the *severe permafrost case* are the same as for the 2D permafrost modelling of the *reference glacial cycle* (Section 3.4.4).

In order to construct an air temperature curve for a full glacial cycle without the presence of an ice sheet at the Forsmark site, the site-specific air temperature curve reconstructed for the last glacial cycle (Figure 3-54 blue line) was used together with the ice sheet surface elevations of the *reference glacial cycle* to making a correction for the difference in elevation between the height of the ice sheet and that of the ice-free ground surface (see also Appendix 1). Subsequently, by using the same n-factor approach as in the modelling of the *reference glacial cycle*, calculations of ground-surface temperatures were made from air temperature (Section 3.4.4). The resulting air temperature curve for the *severe permafrost case* is seen in /Hartikainen et al. 2010, Figure 2-15/.

Figure 5-21 exemplifies modelled ground surface temperatures along the profile at four different times for the *severe permafrost case* considering different climate conditions: 8.5 kyrs after present – Subarctic and partially submerged, 16.5 kyrs after present – Boreal, 25 kyrs after present – Subarctic, 50 kyrs after present – Arctic. The partially submerged conditions at 8.5 kyrs after present refer to locations away from the repository location, the repository location is never submerged in this climate case. For details on the setup of the *severe permafrost case*, see /Hartikainen et al. 2010/.

The extent of perennially frozen ground over the Forsmark site for the *severe permafrost case* is exemplified by time slices at 8.5, 25, 46, 50 kyrs after present in Figures 5-22 and 5-23. The evolution of maximum permafrost depth and depth of perennially frozen ground at the repository location is shown in Figure 5-24. Figure 5-25 shows the same results over the whole profile, as well as the extent of permafrost summarised along the investigated profile.

Table 5-7. Climate information for the severe permafrost case. Summer precipitation is close to 5 mm/month for dry case while it is close to 50 mm/month for the humid case. The winter precipitation is the same (< 1) for both cases.

Climate zone	Annual mean air temperature (°C)	Monthly mean max. summer air temperature (°C)	Monthly mean min. winter air temperature (°C)	Monthly mean max. summer precipitation (mm/month)	Monthly mean max. winter precipitation (mm/month)
Boreal	> 0	+10 – +20	–15 – +5	5 – 50	< 1
Subarctic	0 – –6	+5 – +15	–25 – –10	5 – 50	< 1
Arctic	< –6	< +5 – +10	–35 – –20	5 – 50	< 1

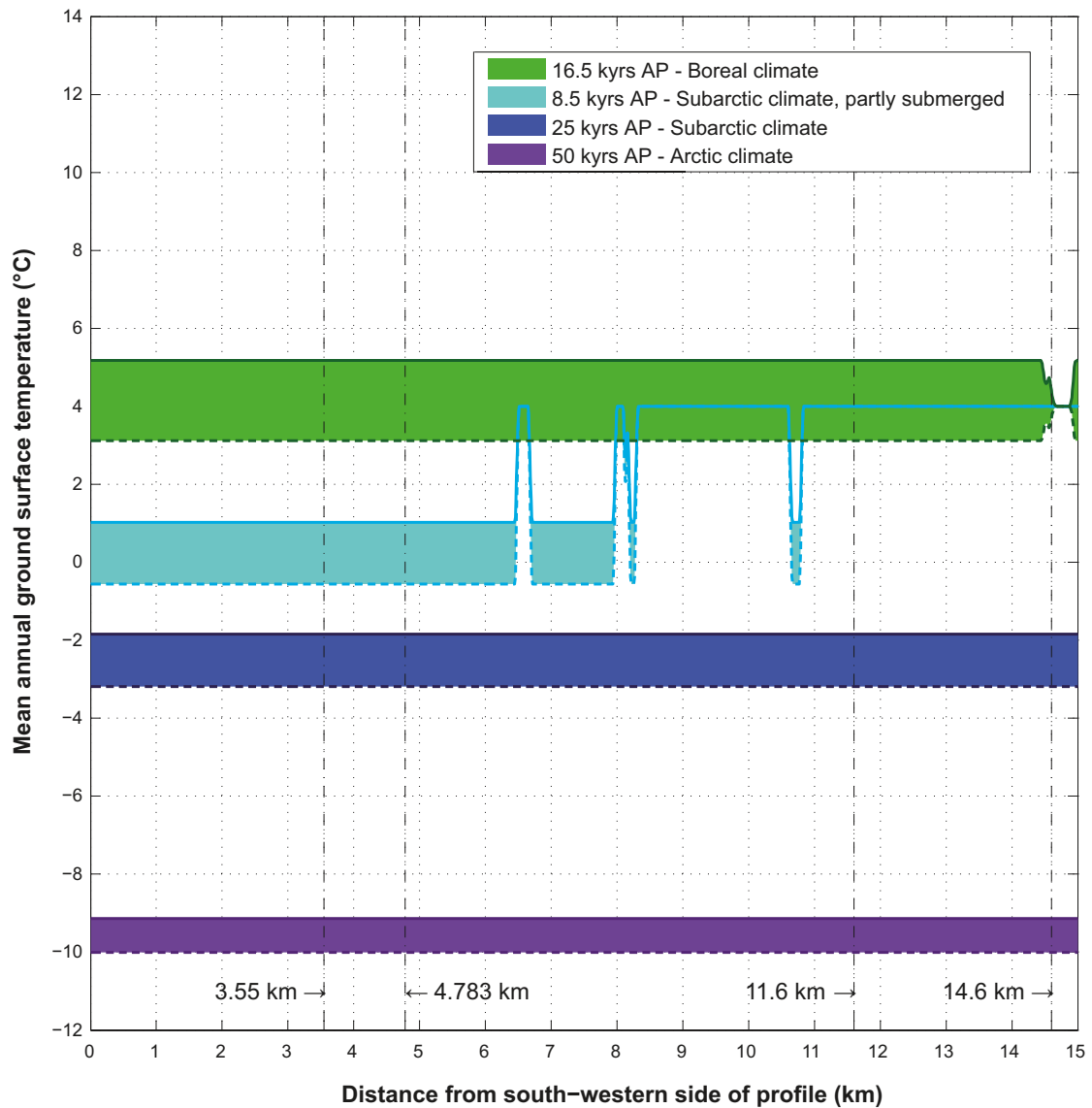


Figure 5-21. Modelled ground surface temperatures along the profile at four different times for the severe permafrost case considering different climate conditions: 8.5 kyrs after present – Subarctic and partially submerged, 16.5 kyrs after present – Boreal, 25 kyrs after present – Subarctic, 50 kyrs after present – Arctic. The solid border lines of the coloured areas indicate the dry variant of the climate case and dashed ones the humid variant of the same case. For details on the calculations of ground surface temperatures, see /Hartikainen et al. 2010/.

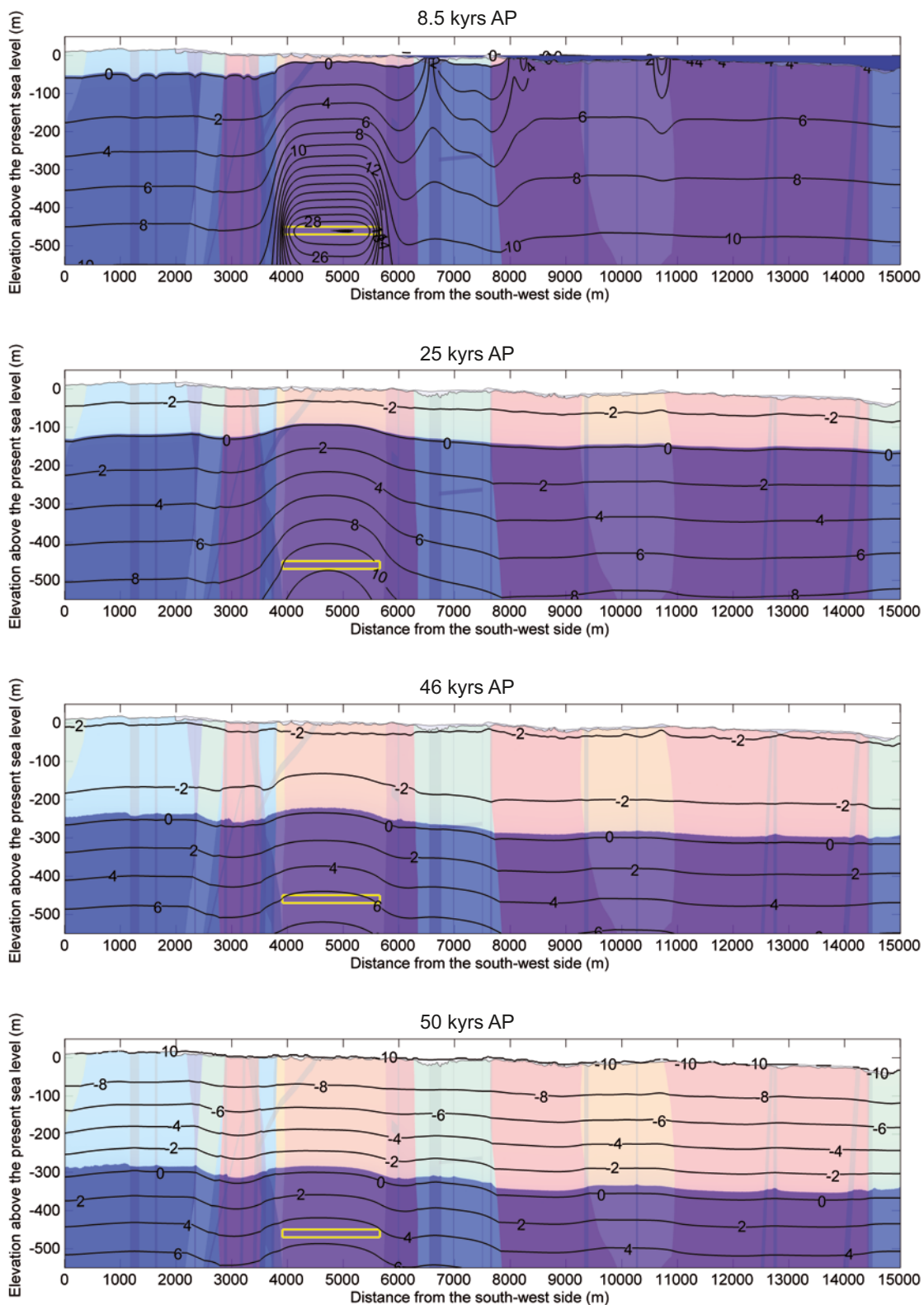


Figure 5-22. Exemplified temperature contours in (°C) and the extent of perennially frozen ground (light colour) within permafrost (0°C isotherm) at times 8.5, 25, 46, 50 kyr after present for the humid variant of the severe permafrost case. Blue colour blue on the top of the profile at 8.5 kyr after present shows the Baltic Sea. The yellow rectangle indicates the location of the repository.

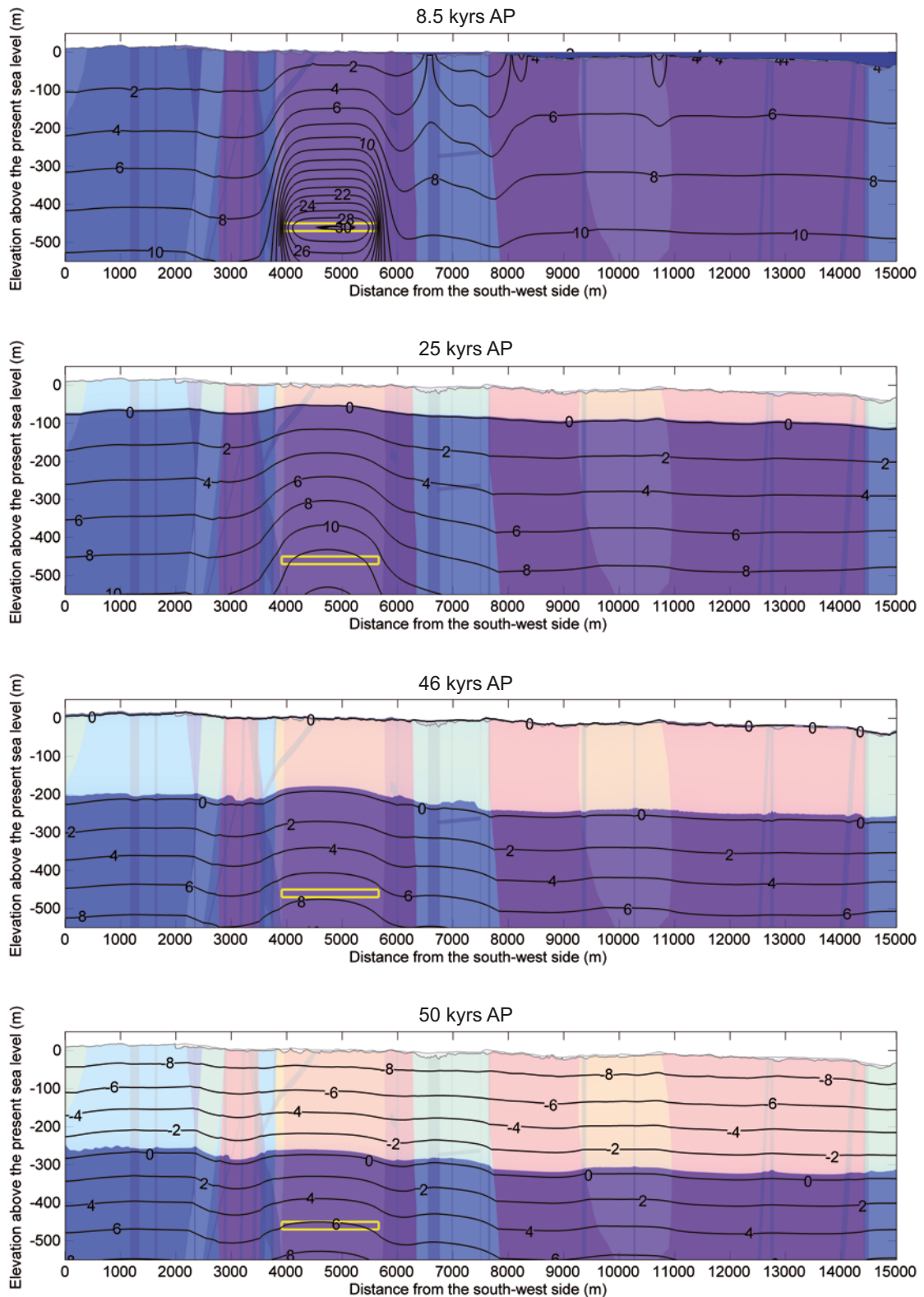


Figure 5-23. Exemplified temperature contours in (°C) and the extent of perennally frozen ground (light colour) within permafrost (0°C isotherm) at times 8.5, 25, 46, 50 kyrs after present for the dry variant of the severe permafrost case. Blue colour blue on the top of the profile at 8.5 kyrs after present shows the Baltic Sea. The yellow rectangle indicates the location of the repository.

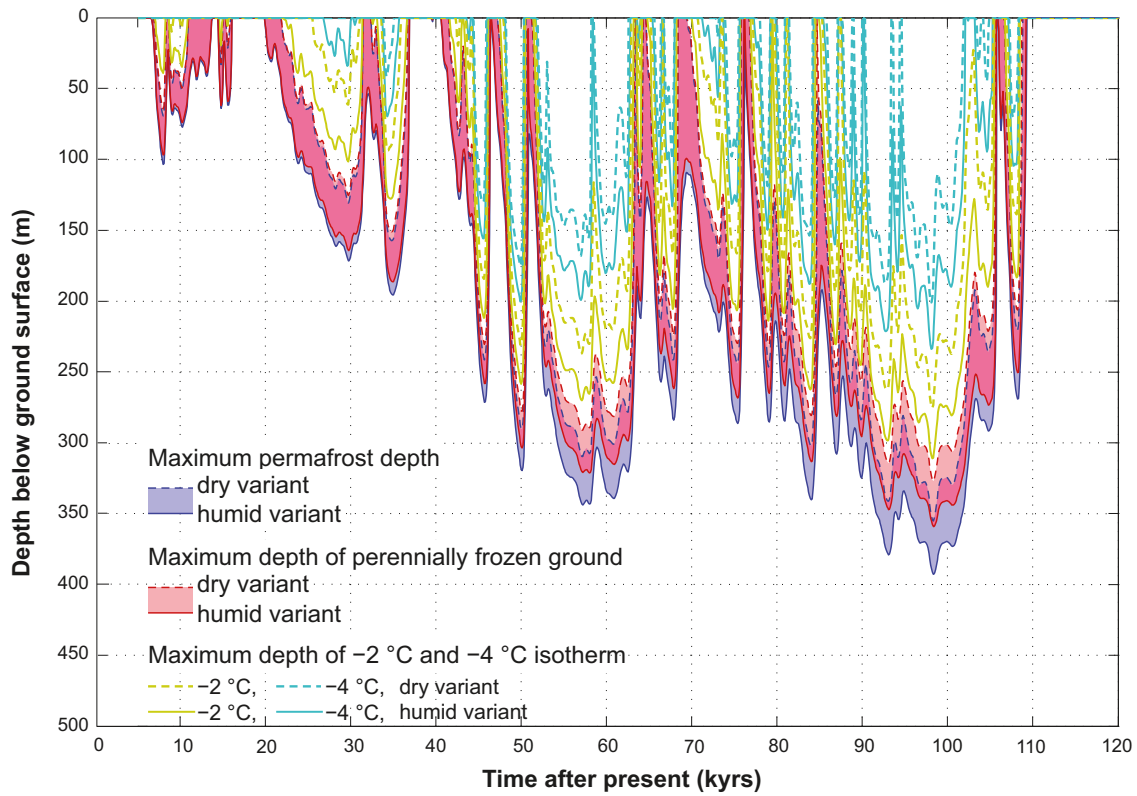


Figure 5-24. Evolution of maximum permafrost depth, maximum depth of perennially frozen ground and maximum depth of -2 °C and -4 °C isotherms over the repository for the severe permafrost case. The upper permafrost surface, for periods of permafrost degradation from above, is not shown. The shaded area in blue and red represents the range when considering the dry and humid climate variants of the severe permafrost case. The darker lilac colour indicates that the results for permafrost and perennially frozen ground overlap.

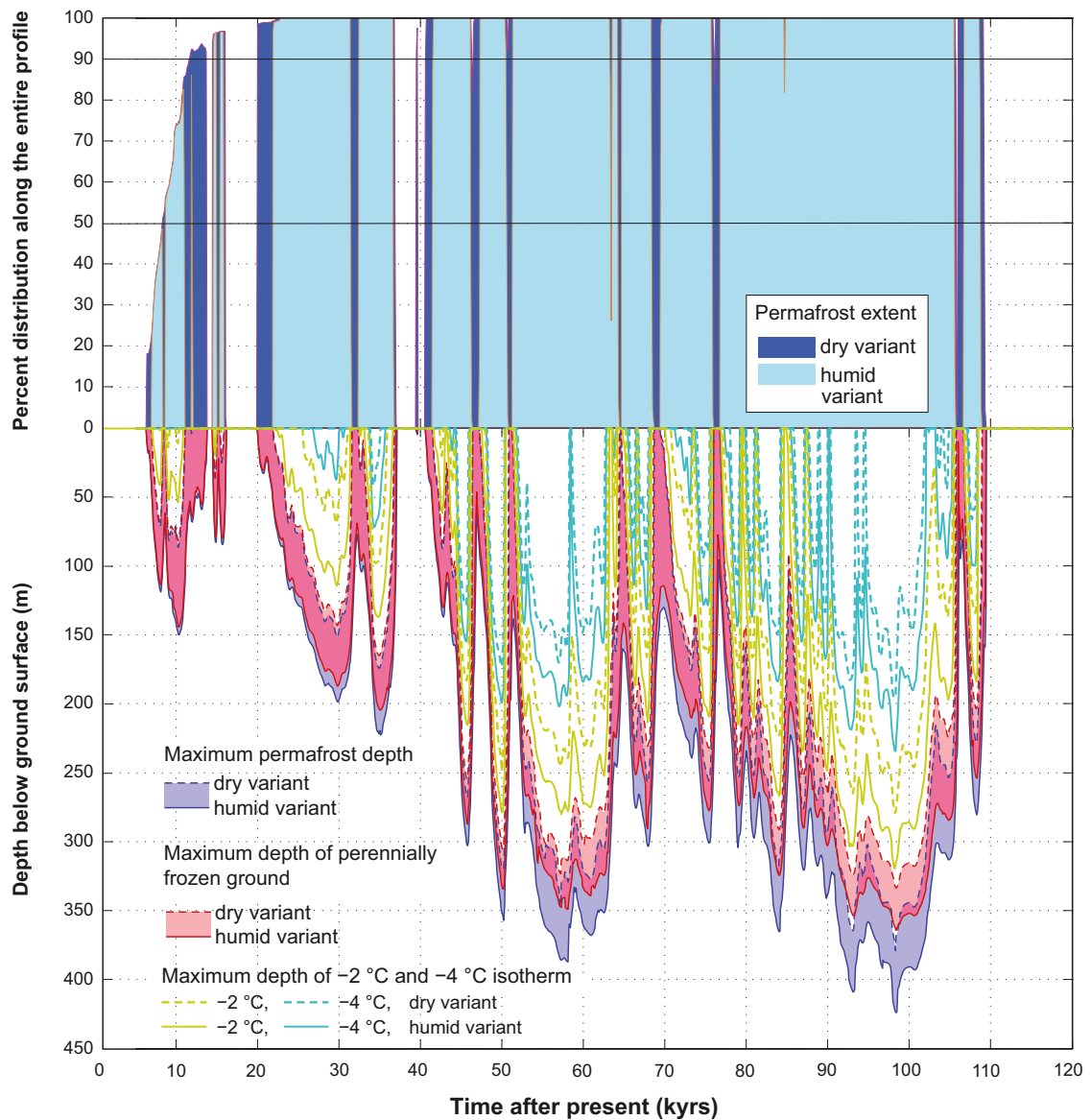


Figure 5-25. Evolution of maximum permafrost depth, maximum depth of perennially frozen ground and maximum depth of -2 and -4 °C isotherms over the whole profile for the severe permafrost case. The figure also shows the percent permafrost distribution along the profile. The transition from sporadic to discontinuous permafrost occurs at 50-% coverage and from discontinuous to continuous permafrost at 90-% coverage, indicated by two horizontal lines. The upper permafrost surface, for periods of degradation from above, is not shown. The shaded area in blue and red represents the range when considering the dry and humid climate variants. The darker lilac colour indicates that the results for permafrost and perennially frozen ground overlap.

The maximum permafrost depths, maximum depths of perennially frozen ground, and the extent of permafrost distribution have been summarised in Tables 5-8 and 5-9. In addition, Table 5-10 describes the evolution of permafrost depth and depth of perennially frozen ground at the repository site. For a corresponding table for the entire profile, see /Hartikainen et al. 2010/.

The results show that development of continuous permafrost is characteristic for both the dry and humid variants of the *severe permafrost case* (Figure 5-25). As expected this is a difference compared with the *reference glacial cycle* where longer periods of discontinuous permafrost prevailed both in the dry and humid climate variants (Figure 4-29).

Table 5-8. Times of permafrost occurrence and associated maximum permafrost depth and maximum depth of perennially frozen ground over the whole profile and over the repository location for the future humid variant of the severe permafrost case. The table also gives the time and horizontal location of maximum permafrost depth and the percent extent of permafrost distribution.

Time periods of permafrost occurrence (kyrs after present, AP)	Over the whole profile					Over the repository			
	Maximum permafrost depth (m)	Time of occurrence of maximum permafrost depth (ka AP)	Distance from the south-west side (m)	Maximum depth of perennially frozen ground (m)	Percent extent of permafrost distribution (%)	Maximum permafrost depth (m)	Time of occurrence of maximum permafrost depth (ka AP)	Distance from the south-west side (m)	Maximum depth of perennially frozen ground (m)
6.4 – 13.7	150	10.3	100	144	75	104	8	3,950	97
14.5 – 16.1	85	15.7	12,280	80	97	64	14.8	5,650	62
19.9 – 37	223	35.1	14,910	205	100	196	34.9	5,650	186
39.5 – 39.6	5	39.6	14,870	3	95	3	39.6	5,610	1
40.6 – 109.4	424	98.4	12,240	364	100	393	98.4	5,650	359

Table 5-9. Times of permafrost occurrence and associated maximum permafrost depth and maximum depth of perennially frozen ground over the whole profile and over the repository location for the future dry variant of the severe permafrost case. The table also gives the time and horizontal location of maximum permafrost depth and the percent extent of permafrost distribution.

Time periods of permafrost occurrence (kyrs after present, AP)	Over the whole profile					Over the repository			
	Maximum permafrost depth (m)	Time of occurrence of maximum permafrost depth (ka AP)	Distance from the south-west side (m)	Maximum depth of perennially frozen ground (m)	Percent extent of permafrost distribution (%)	Maximum permafrost depth (m)	Time of occurrence of maximum permafrost depth (ka AP)	Distance from the south-west side (m)	Maximum depth of perennially frozen ground (m)
7 – 8.3	72	8	3,020	68	44	69	8	3,950	64
8.7 – 11	87	10.3	7,990	81	74	52	10.2	5,650	50
11.8 – 12	4	11.9	12,360	1	79	2	11.9	5,620	0
14.6 – 15	36	14.8	14,280	35	96	33	14.8	5,650	32
15.4 – 15.8	25	15.6	14,280	22	97	21	15.6	5,650	20
21.9 – 31.5	152	29.8	14,840	143	100	131	29.7	5,650	125
32.4 – 36.7	174	34.9	14,880	165	100	157	34.8	5,650	151
41.5 – 46.3	268	45.7	13,890	255	100	242	45.7	5,650	231
47.2 – 50.8	320	50.1	13,790	306	100	290	50	5,650	277
51.3 – 64.4	326	58	14,890	314	100	310	57.2	5,650	291
64.7 – 68.6	257	67.9	14,980	231	100	241	67.8	5,650	224
69.5 – 75.9	256	75.4	14,980	232	100	244	75.4	5,650	230
76.8 – 105.7	379	98.3	13,940	333	100	355	98.3	5,650	327
106.7 – 108.9	229	108.2	14,980	204	100	221	108.2	5,650	206

Table 5-10. Evolution of maximum permafrost depth and maximum depth of perennially frozen ground at the repository site for the severe permafrost case. For comparison the table also include the results from the reference glacial cycle. The table also shows the prevailing mean annual air temperatures. For a table describing model results for the full glacial cycle of the severe permafrost case, see /Hartikainen et al. 2010 Appendix K/.

Time (kyrs after present)	Mean annual air temperature (°C)	Maximum permafrost depth (m)				Maximum depth of perennially frozen ground (m)			
		Humid variant of the reference glacial cycle case	Dry variant of the reference glacial cycle case	Humid variant of the severe permafrost case	Dry variant of the severe permafrost case	Humid variant of the reference glacial cycle case	Dry variant of the reference glacial cycle case	Humid variant of the severe permafrost case	Dry variant of the severe permafrost case
8	-3.4	31	84	104	69	29	79	97	64
8.5	-0.6	0	3	30	0	0	1	27	0
10	-3.5	15	47	71	46	15	46	68	44
12	-1.5	0	22	44	0	0	21	42	0
14	2.5	0	0	0	0	0	0	0	0
16	-0.6	0	6	33	0	0	5	30	0
18	1.6	0	0	0	0	0	0	0	0
20	-0.3	0	0	7	0	0	0	5	0
22	-1.9	2	30	55	9	0	28	52	8
24	-2.9	18	62	102	56	16	60	97	53
25	-3.2	23	69	110	64	20	66	105	61
26	-3.9	35	84	127	86	33	81	122	82
28	-4.8	49	108	158	117	47	103	151	113
30	-4.1	45	112	168	123	43	107	161	118
32	-0.9	0	15	54	0	0	13	49	0
34	-6.4	73	116	155	120	71	113	149	115
36	-3.1	31	108	164	105	29	104	156	98
38	2.1	0	0	0	0	0	0	0	0
40	0.4	0	0	0	0	0	0	0	0
42	-2.5	12	52	88	37	10	50	84	35
44	-4.2	45	101	147	102	43	97	140	98
45	-10.4	135	186	232	204	131	179	219	194
46	-1.3	85	180	256	211	77	168	241	198
48	-3.6	33	86	130	78	31	82	124	74
50	-10	181	259	319	290	175	246	303	277

For the *severe permafrost case*, i.e. when considering no ice sheet, sea, vegetation or snow cover over the Forsmark site throughout the glacial cycle, permafrost (0 °C isotherm) can reach a depth between ~360 m and ~390 m over the repository and between ~380 m and ~420 m outside the repository, in a time frame of 100,000 years. Meanwhile, the maximum depth of perennially frozen ground may vary between ~330 m and ~360 m over both the repository and the rest of the profile, see Figure 5-24 and 5-25.

Examples of vertical profiles of bedrock temperature at one selected location (in the middle of the repository location, at 4,783 m along the profile) corresponding the fresh-moist surface cover types are presented in Figures 5-26 (humid climate variant) and 5-27 (dry climate variant). The white colour envelope represents the range of bedrock temperature fluctuation simulated over the glacial cycle. Other examples of vertical bedrock temperature profiles, with other surface cover types (wet, dry, peatland) are found in /Hartikainen et al. 2010/.

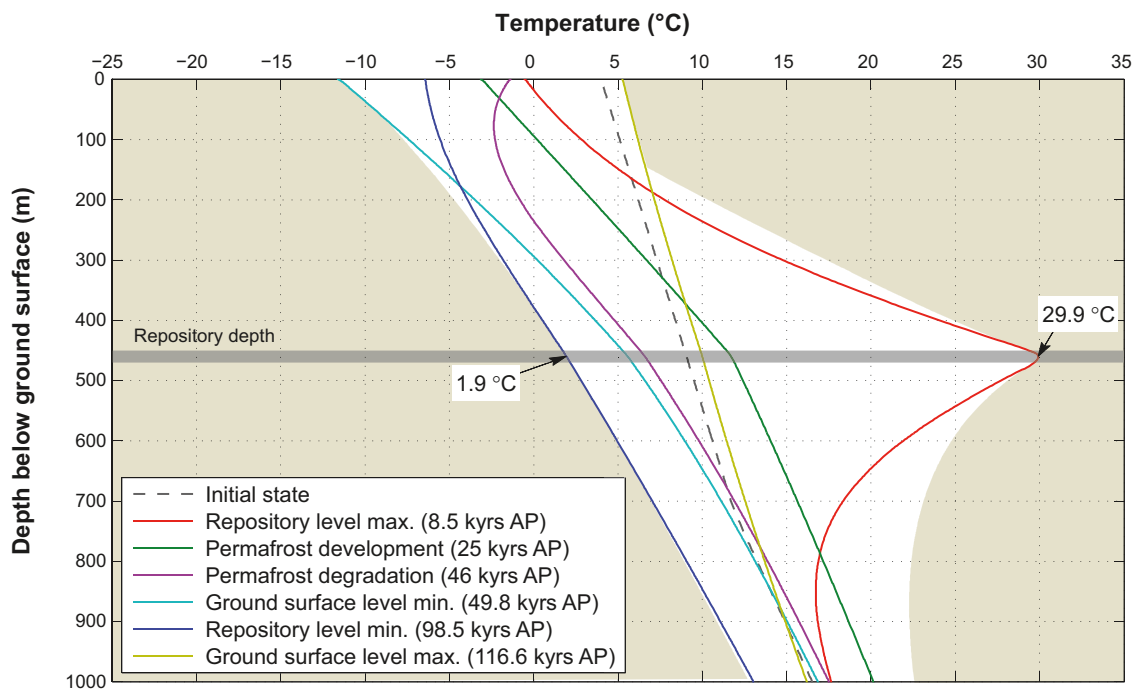


Figure 5-26. Ground temperature along a vertical profile located in the middle of the repository for the humid variant of the severe permafrost case and dry surface condition type. The white colour envelope represents the range of bedrock temperature fluctuation simulated over the glacial cycle.

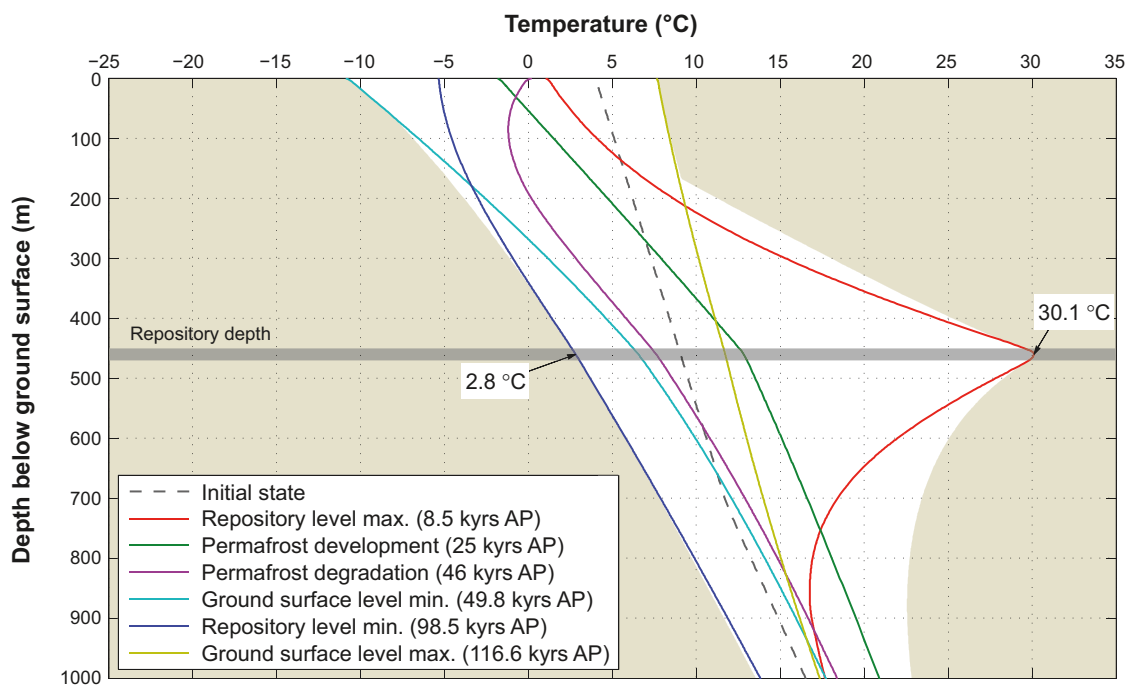


Figure 5-27. Ground temperature along a vertical profile located in the middle of the repository for the dry variant of the severe permafrost case and dry surface condition type. The white colour envelope represents the range of bedrock temperature fluctuation simulated over the glacial cycle.

Given the permafrost and freezing results presented above for the *severe permafrost case*, the associated results on salinity concentration are illustrated in Figures 5-28 and 5-29. In this study, the effect of freezing-out of salt is small. Due to low salinity concentrations at shallow depths, the impacts of freezing on salinity exclusion and redistribution are difficult to see from the results. However, under more extreme conditions than simulated in the *severe permafrost case*, if the air temperature curve reconstructed for the last glacial cycle is lowered by 8°C, the freezing occurs more intensively and an increase in salinity concentration due to salt exclusion can be seen (Figure 5-30).

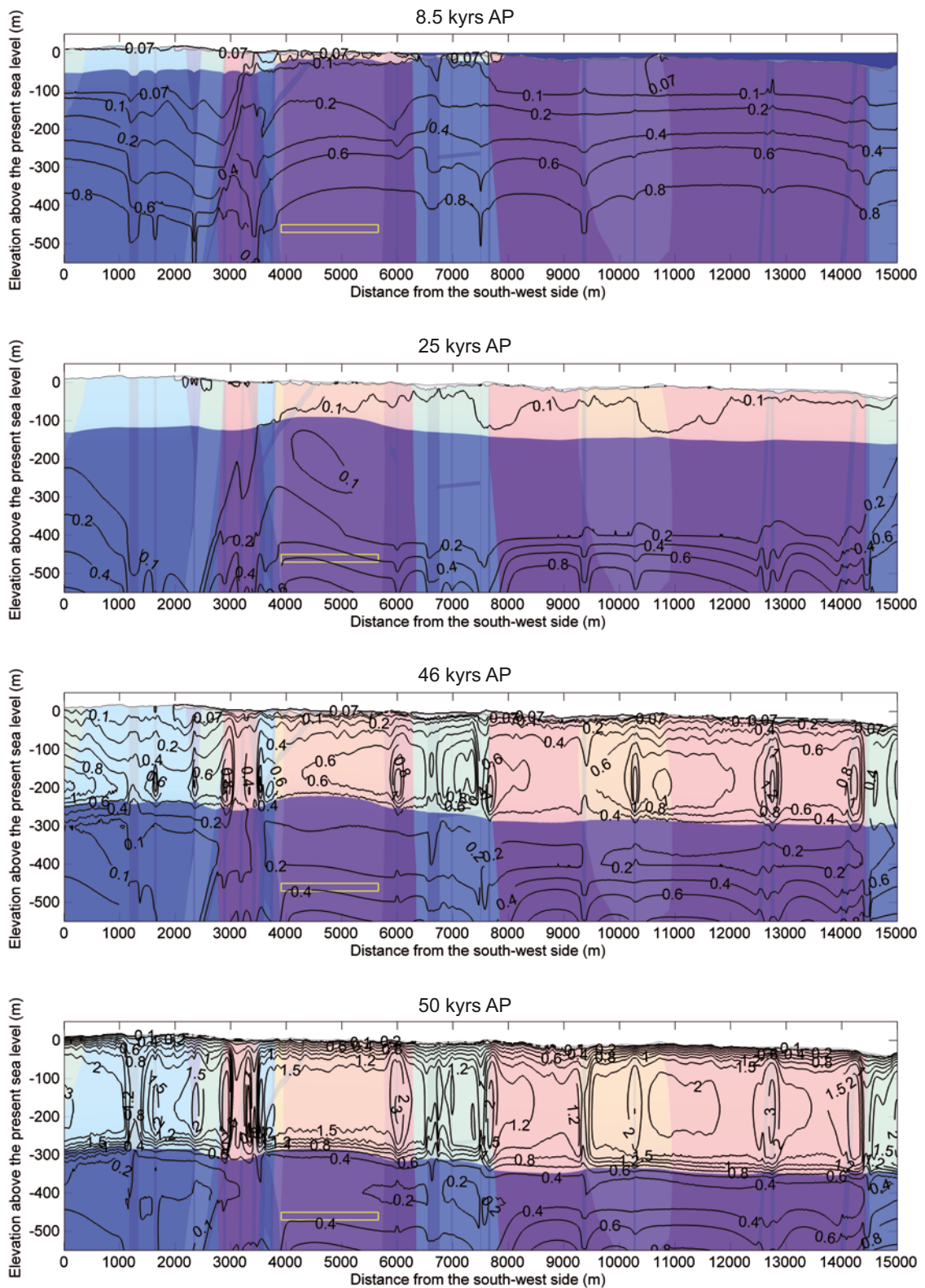


Figure 5-28. Salinity concentration isolines at times 8.5, 25, 46, 50 kyrs after present for the humid variant of the severe permafrost case. The isolines show salinity concentrations of 0.07, 0.1, 0.2, 0.4, 0.6, 0.8, 1, 1.2, 1.5, 2, 3, 4, 5 mass-%. Blue colour blue on the top of the profile at 8.5 kyrs after present shows the Baltic Sea and the light colour the extent of perennially frozen ground.

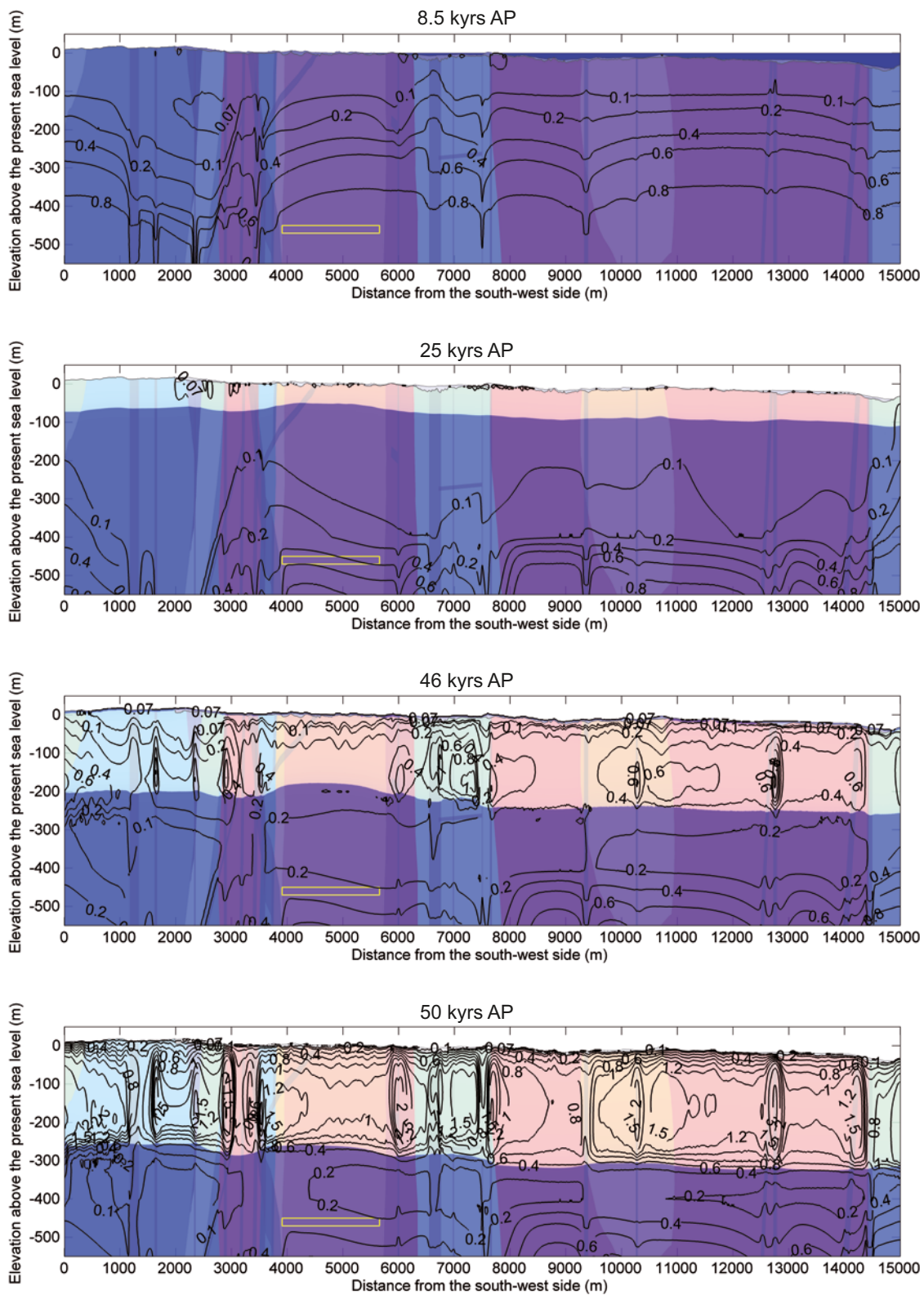


Figure 5-29. Salinity concentration isolines for the dry variant of the severe permafrost case at times 8.5, 25, 46, 50 kyr after present. The isolines show salinity concentrations of 0.07, 0.1, 0.2, 0.4, 0.6, 0.8, 1, 1.2, 1.5, 2, 3, 4, 5 mass-%. Blue colour on the top of the profile at 8.5 kyr after present shows the Baltic Sea and the light colour the extent of perennially frozen ground.

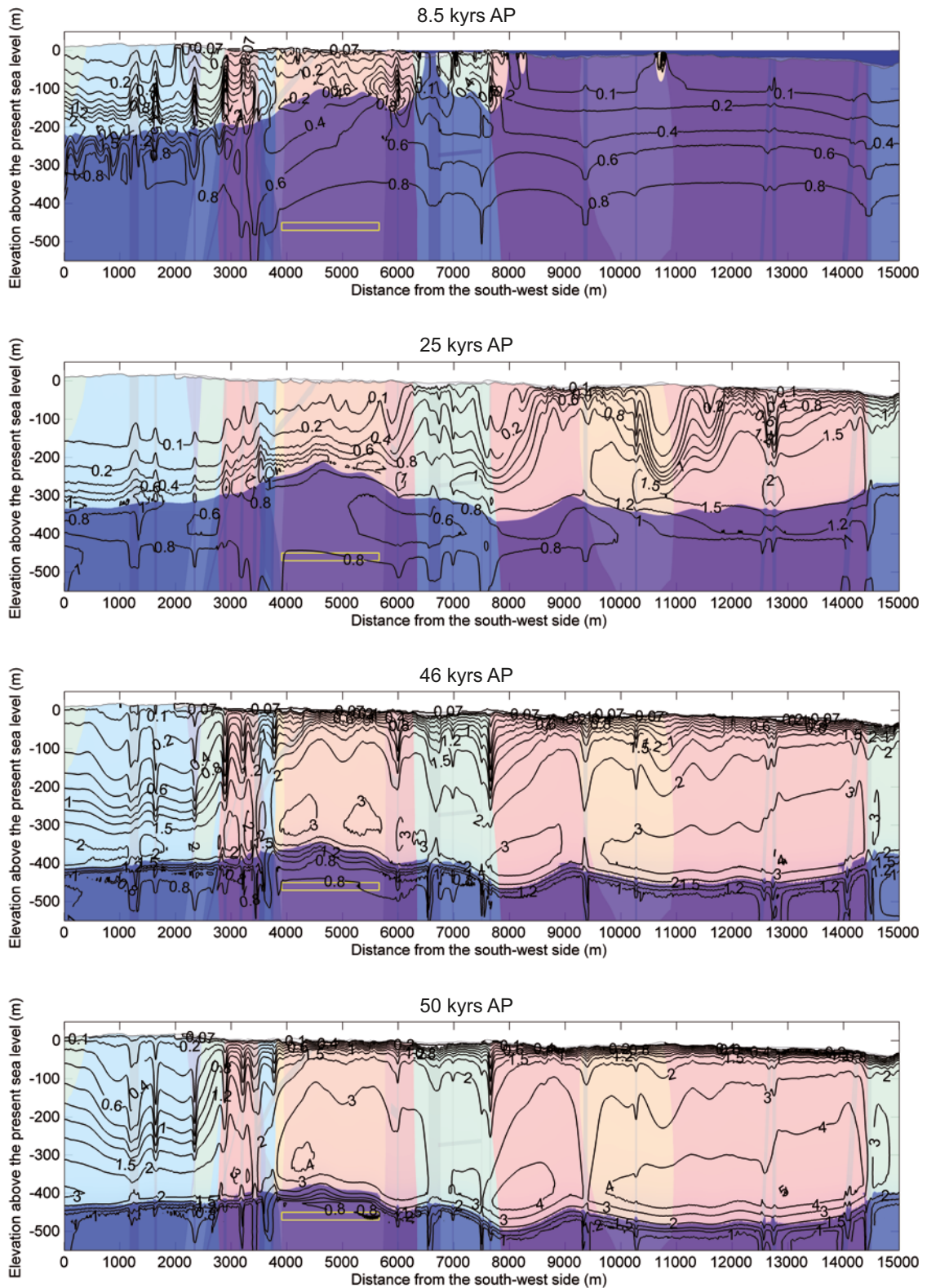


Figure 5-30. Salinity concentration isolines at times 8.5, 25, 46, 50 kyr after present for the humid variant of the severe permafrost case and air temperature decreased by 8°C. The isolines show the salinity concentrations 0.07, 0.1, 0.2, 0.4, 0.6, 0.8, 1, 1.2, 1.5, 2, 3, 4, 5 mass-%. Blue colour blue on the top of the profile at 8.5 kyr after present shows the Baltic Sea and the light colour the extent of perennially frozen ground.

Sensitivity experiments

In addition to the *severe permafrost case* simulations described above, a sensitivity experiment was made to study the effects of uncertainties in bedrock thermal properties together with uncertainties in surface conditions (excluding air temperature) for this case, i.e. the same experiment as sensitivity experiment number 6 conducted for the *reference glacial cycle*. To this end, the uncertainty interval is obtained by combining the dry climate variant with the thermal properties enhancing permafrost development, and the humid climate variant with thermal properties diminishing permafrost development, see Section 3.4.4. The resulting evolution of maximum permafrost depth and maximum depth of perennially frozen ground over the repository are shown in Figure 5-31.

Sensitivity studies have also been made to investigate the climate conditions required to develop permafrost and perennially frozen ground to repository depth /Hartikainen et al. 2010/. Based on the results of a similar study performed in SR-Can /SKB 2006a/, this was made by lowering the entire temperature curve reconstructed for the last glacial cycle by 4, 6, 8, 10, 12, 14 and 16°C, see Figure 3-63. A temperature of 0°C corresponds to the freezing point of fresh water at normal pressure. A temperature of -2°C corresponds to the freezing point of the backfill material in the deposition tunnels, whereas a temperature of -4°C constitutes the temperature criterion used in the safety assessment for freezing of the buffer clay /SKB 2011/.

The results show that if the reconstructed temperature curve for the last glacial cycle is lowered by 8°C, the 0°C isotherm (permafrost) reach repository depth (450 m) (Figure 5-32). The temperature curve needs to be lowered by more than 10°C in order to make the -2°C isotherm reach repository depth (Figure 5-33), and it needs to be lowered by as much as 14°C in order make the -4°C isotherm reach repository depth (Figure 5-34).

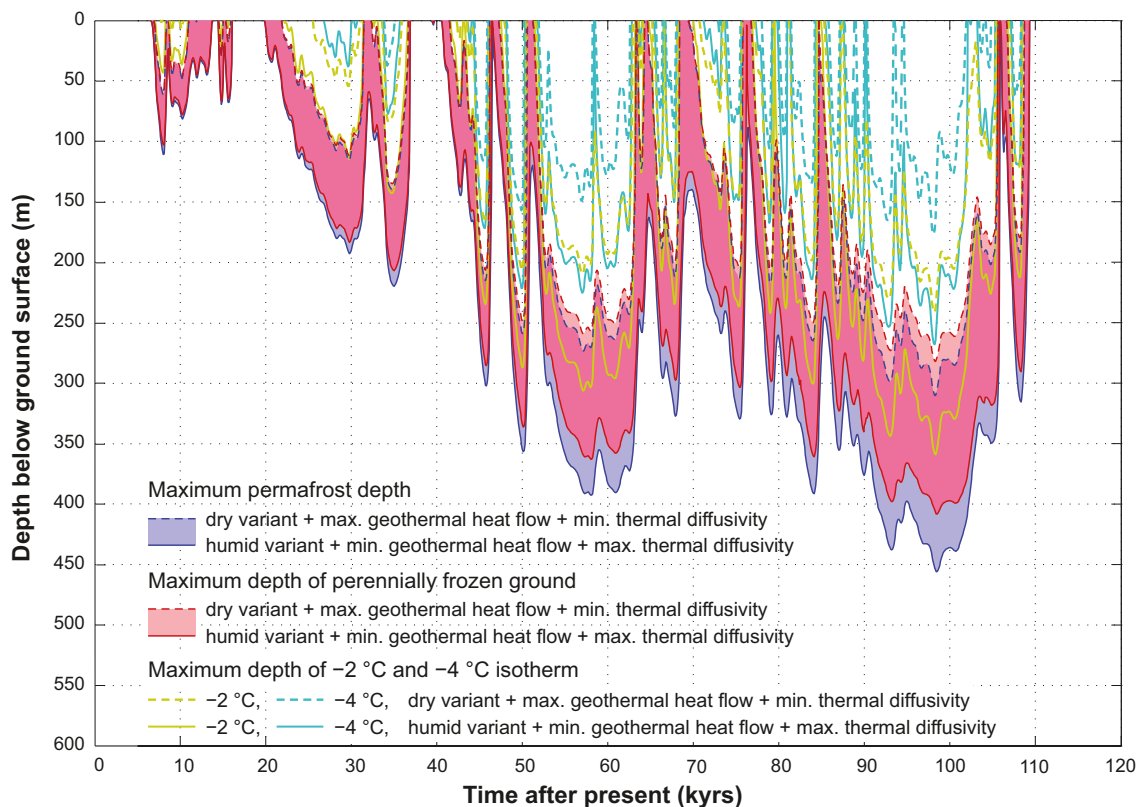


Figure 5-31. Evolution of maximum permafrost depth, maximum depth of perennially frozen ground and maximum depth of -2 and -4 °C isotherms over the repository for the severe permafrost case when considering combined uncertainties in surface conditions and thermal properties favourable for permafrost growth. The shaded area in blue and red represents the range when considering the dry and humid climate variants. The darker lilac colour indicates that the results for permafrost and perennially frozen ground overlap.

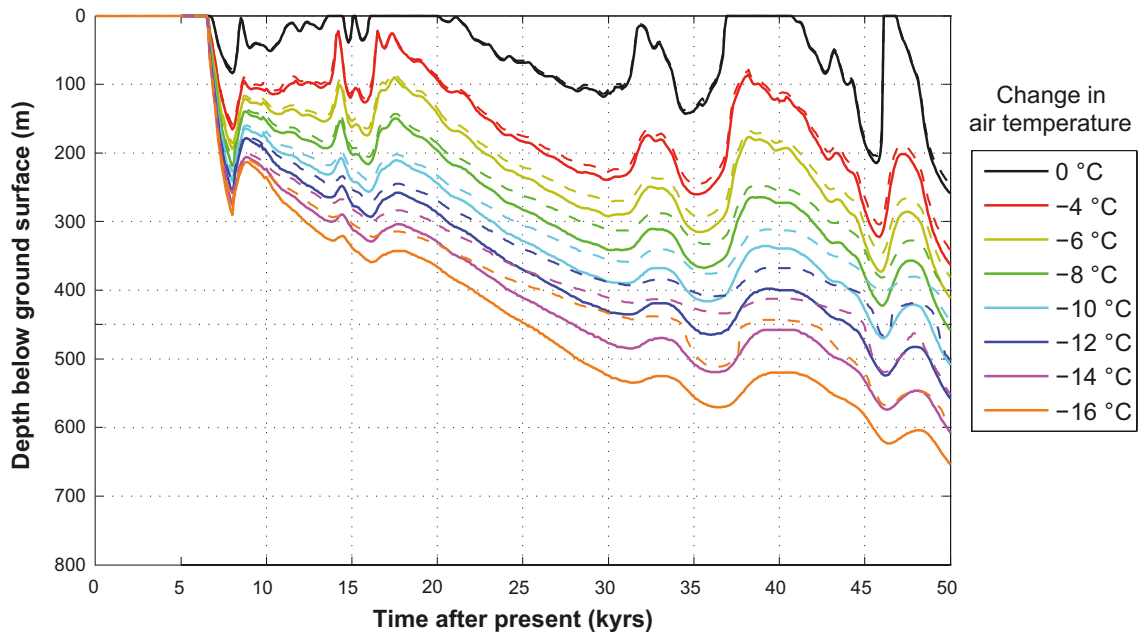


Figure 5-32. Evolution of 0°C isotherm (permafrost) depth (black solid line) and depth of perennially frozen ground (black dashed line) at the repository location for the reference glacial cycle (dry climate variant, see Section 3.4.4). The figure also show corresponding results for simulations where the temperature curve reconstructed for the last glacial cycle has been lowered by -4, -6, -8, -10, -12, -14 and -16°C compared to the reference glacial cycle.

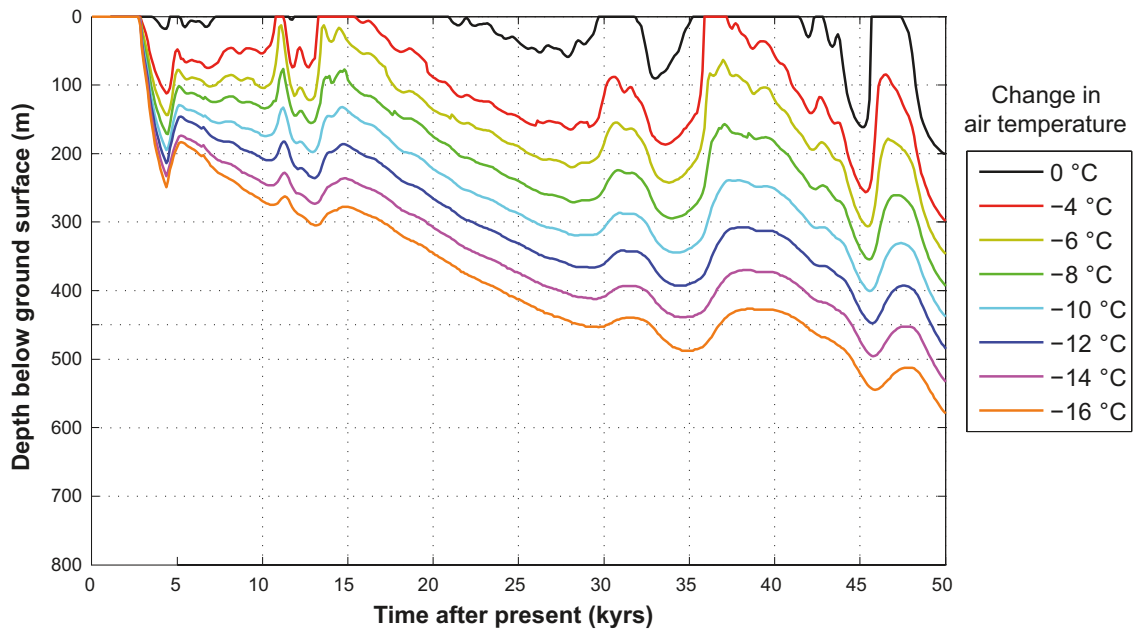


Figure 5-33. Evolution of -2°C isotherm depth at the repository location for the reference glacial cycle (dry climate variant, see Section 3.4.4) (black line). The figure also shows corresponding results for simulations where the temperature curve reconstructed for the last glacial cycle has been lowered by -4, -6, -8, -10, -12, -14 and -16°C compared to the reference glacial cycle (coloured lines).

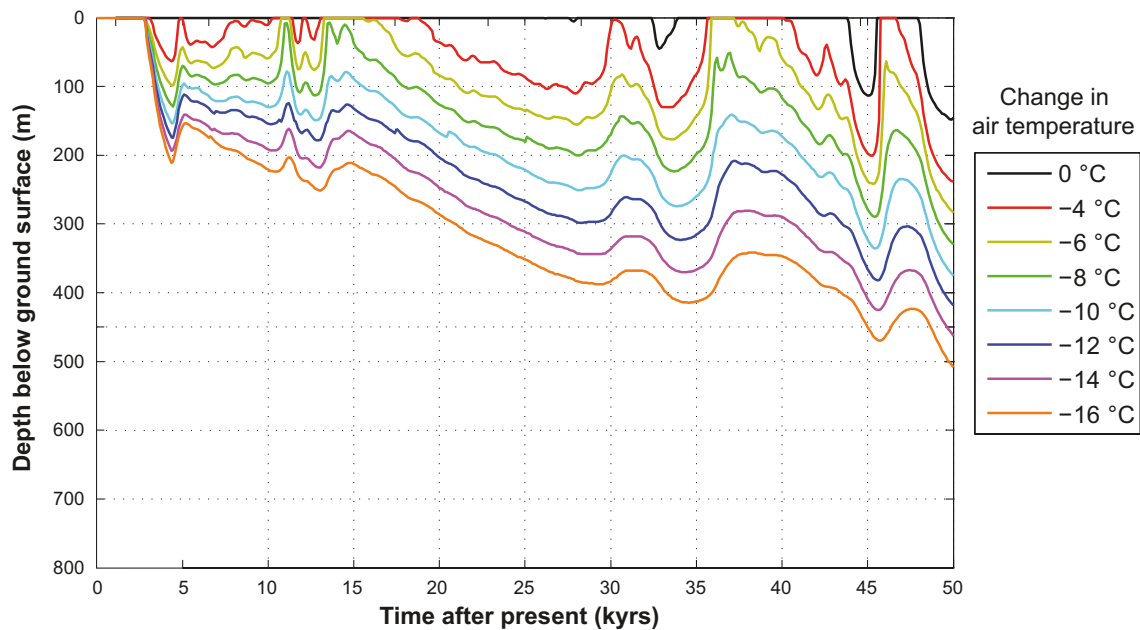


Figure 5-34. Evolution of -4°C -isotherm depth at the repository location for the reference glacial cycle ((dry climate variant, see Section 3.4.4) (black line). The figure also shows corresponding results for simulations where the temperature curve reconstructed for the last glacial cycle has been lowered by -4 , -6 , -8 , -10 , -12 , -14 and -16°C compared to the reference glacial cycle (coloured lines).

The evolution of subsurface temperatures and residual pore water pressures at a depth of 400 m at Forsmark for a case similar to the *severe permafrost case* described above is found in /SKB 2006a, Figure 3-64/.

Summary of the severe permafrost case and sensitivity studies

In the following, the main conclusions from the *severe permafrost case* and the sensitivity studies are summarized. When assuming a glacial cycle without any cover of ice sheet, sea, vegetation or snow, the range for the maximum permafrost depth (the 0°C isotherm) over the repository is 360–390 m depending on the surface conditions. The corresponding range for the entire investigated profile is 380–420 m. Likewise, for the same assumptions, the maximum depth of perennially frozen ground over the repository and the entire profile ranges between 330 and 360 m depending on the surface conditions. Very low surface temperatures are required in order to give an increase in salinity concentration due to salt exclusion. Making the unrealistic combination of the *severe permafrost case* (which assumes no ice sheet, winter snow, vegetation or sea coverage during the entire glacial cycle), with maximum thermal conductivity and minimum heat capacity for the subsurface, as well as using the minimum geothermal heat flow value, the simulated maximum permafrost depth over the repository may extend to 450 m depth in 95,000 years. However, it should be noted that this combination of assumptions is unrealistic. Assuming a similar climate variability as during the last glacial cycle, the temperature curve reconstructed for the last glacial cycle needs to be lowered by 8°C order in order to make the 0°C isotherm (permafrost) reach repository depth, while the temperature curve needs to be lowered by as much as 14°C in order make the -4°C isotherm reach repository depth. Also when considering the significant estimated maximum uncertainty in the reconstructed air temperature curve ($\pm 6^{\circ}\text{C}$, Appendix 1), this corresponds to an unrealistically large change in glacial climate conditions.

It should here be remembered that the *severe permafrost case* was designed to take care of remaining uncertainties (mainly related to ice sheet coverage) that was not covered in the extensive investigation of uncertainties reported in the *reference glacial cycle* (Section 4.5 and 3.4.4). Therefore, the resulting maximum uncertainty interval for e.g. permafrost and frozen depths (Table 5-11), may reach deeper in the *reference glacial cycle* than in the *severe permafrost case* (whereas calculated depths without the uncertainty interval are deeper for the *severe permafrost case*).

Table 5-11. Maximum depths of permafrost (0°C isotherm), perennially frozen ground, -2°C isotherm and -4°C isotherm for the severe permafrost case and the reference glacial cycle. The uncertainty interval for the severe permafrost case includes all uncertainties (set to their most pessimistic values) except air temperature, since lower air temperatures are not compatible with the main assumption of having no ice sheet development over the site. The uncertainty interval for the reference glacial cycle includes the unlikely combination of having all uncertainties, including air temperature, set to their most pessimistic values favouring permafrost growth.

	Maximum permafrost depth (0°C isotherm) [max uncertainty interval]	Maximum depth perennially frozen ground [max uncertainty interval]	Maximum depth -2°C isotherm [max uncertainty interval]	Maximum depth -4°C isotherm [max uncertainty interval]
Severe permafrost case	393 [down to 456]	359 [down to 408]	311 [down to 359]	234 [down to 268]
Reference glacial cycle	259 m [down to 463 m]	246 m [down to 422 m]	200 m [down to 388 m]	148 m [down to 316 m]

The information on freezing depths from the *severe permafrost case* and the *reference glacial cycle* is used to assess the potential for freezing of groundwater, buffer clay and deposition tunnel backfill material in the safety assessment freezing scenario /SKB 2011/.

The development of climate domains for the *severe permafrost case* is shown in Figure 5-35. For this construction, the dry climate variant, with most permafrost, was chosen. Temperate climate conditions prevail for 24 kyrs or 20% of the time, whereas periglacial conditions prevail for 96 kyrs or 80% of the time. There are no periods of glacial conditions.

5.5.4 Surface denudation

In the *severe permafrost case*, the main assumption is that there is no ice sheet present at Forsmark during the glacial cycle, and consequently the denudation process that contributed to the largest amount of denudation in the *reference glacial cycle* (glacial erosion) does not take place. In line with this, it is assumed that the amount of surface denudation in the present climate case is smaller than in the *reference glacial cycle*, and definitely smaller than in the case of extended ice sheet duration. Therefore, surface denudation is not described and treated further in the *severe permafrost case*.

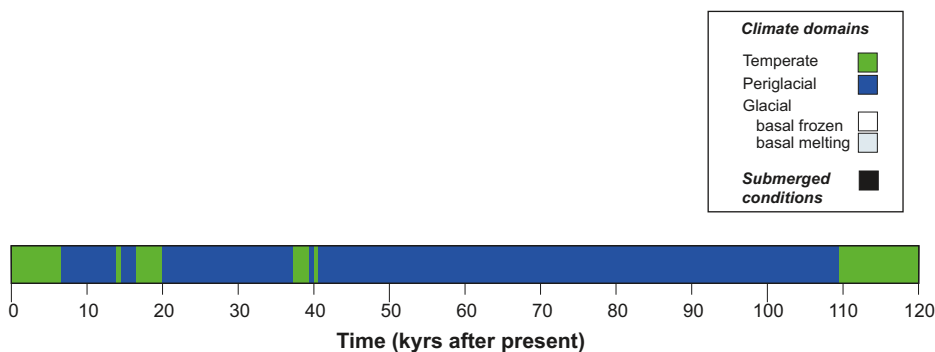


Figure 5-35. Evolution of climate conditions at the Forsmark repository location as a time series of climate domains for the severe permafrost case. Following from the assumptions used for this climate development, there are no periods of glacial or submerged conditions. The glacial cycle is dominated by periglacial conditions, with longer-lasting temperate climate conditions during periods that correspond to interglacial conditions.

5.6 Summary of climate cases for the SR-Site safety assessment

As stated in Section 1.2, a single most likely future climate evolution cannot be predicted with enough confidence and detail for the analyses of long-term safety of repositories for spent nuclear fuel. The longest safety assessment time scales range up to around 100,000 years and 1 million years /SKB 2011/. The 100,000 year time scale corresponds to the time scale of glacial cycles during the past 700,000 years. The selected approach in the SR-Site safety assessment, as well as in previous SKB safety assessments such as SR-Can, is therefore to use a reasonable future climate evolution, consisting of a repetition of conditions reconstructed for the last glacial cycle, as well as complementary climate evolutions with potentially larger impacts on repository safety (Section 1.2 and Figure 1-3). Given that the safety assessment needs to analyse repository safety on these very long time scales, the existing uncertainties in future climate development result in a wide range of possible climate developments that need to be addressed. Figure 5-36 and Table 5-12 summarise the climate developments included in the SR-Site safety assessment. These cases are based on the processes that have been identified as important for long-term KBS-3 repository safety and on the present scientific knowledge and uncertainties of future climate development with focus on these processes. The climate cases in Figure 5-36 are used as input to the description and analysis of various SR-Site safety assessment scenarios, see Figure 1-3 and /SKB 2011/.

The *reference glacial cycle* (Figure 5-36 and Section 4.5) contributes with a reasonable development of climate and climate-related conditions for the coming 120 kyrs, whereas the *global warming case* (Section 5.1) contributes with a variant of this development. The longest period of temperate climate conditions for the coming 120 kyrs, including an initial period with the warmest and wettest climate conditions, highest sea-level, as well as longest period of groundwater formation from precipitation, is found in the *extended global warming case* (Section 5.2). The most extended period of periglacial climate conditions, with longest periods of permafrost at Forsmark, is found in the *severe permafrost case* (Section 5.5). The deepest permafrost and frozen ground is also found in the *severe permafrost case*. The largest uncertainty for the development of permafrost and frozen ground, which is future air temperature, is however connected to the *reference glacial cycle*, resulting in the deepest uncertainty interval for freezing being documented in this climate case. The longest period of glacial conditions, and associated period of groundwater formation from glacial meltwater, is found in the *extended ice sheet duration case* (Section 5.3). The maximum future ice sheet thickness, and resulting largest increase in hydrostatic pressure at repository depth, is found in the *maximum ice sheet configuration case* (Section 5.4) (a case not depicted in Figure 5-36). The six climate cases together cover the expected maximum range within which climate and climate-related conditions of importance for long-term repository safety may vary within the time scales analysed in the SR-Site safety assessment.

In light of present-day knowledge on climate, some of the climate cases in Figure 5-36 might be regarded as more likely than others. However, the adopted approach in the SR-Site safety assessment is to handle *all* possible future climate developments relevant for repository safety. Therefore, there is in the safety assessment no need to quantify the probabilities of the identified individual climate developments. The *actual* development of climate and climate-related processes at the Forsmark site for the coming 120 kyrs are expected to lie within the range covered by the six climate cases presented in Figure 5-36.

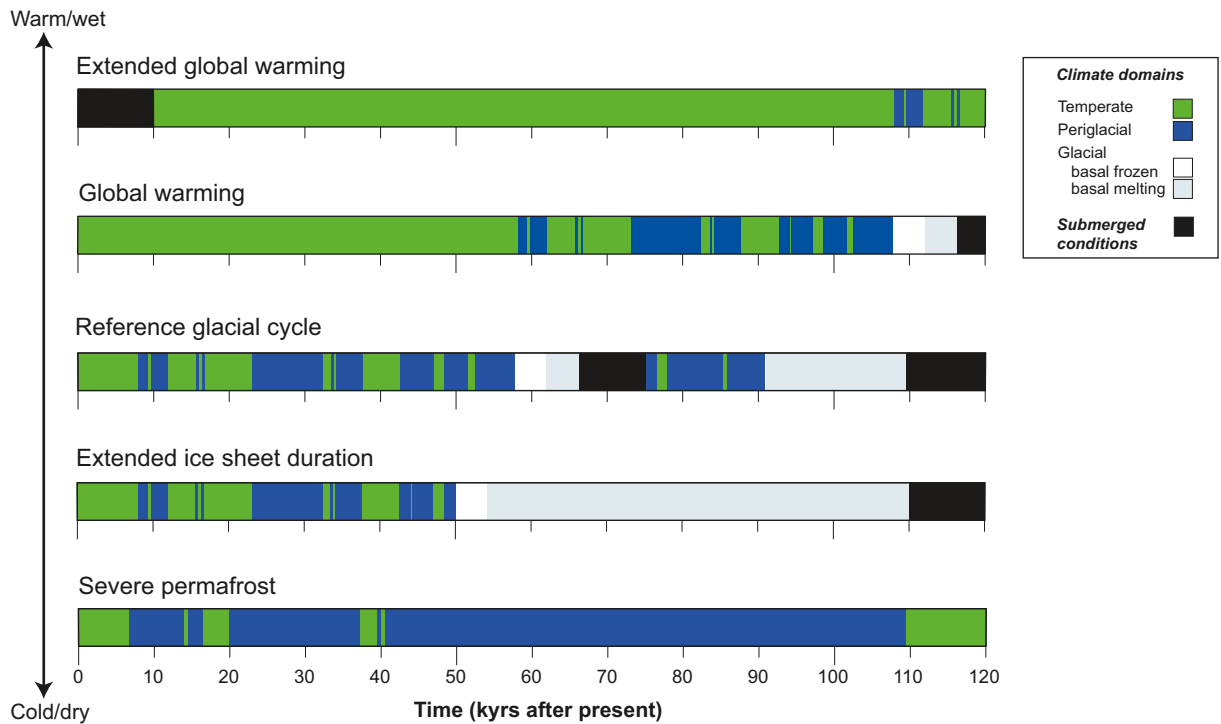


Figure 5-36. Summary of future climate cases analysed in the SR-Site safety assessment. The cases go from warmer/wetter climates at the top to colder/dryer climates at the bottom. The maximum ice sheet configuration case, with maximum ice thicknesses, is not shown. However, it could be contained within the temporal development of the extended ice sheet duration case.

Table 5-12. Summary of duration of climate domains for the six climate cases in SR-Site. For definitions of the climate domains, see Section 1.2.3.

Climate case	Temperate climate domain [kyrs] (percent of time of glacial cycle)	Periglacial climate domain [kyrs] (percent of time of glacial cycle)	Glacial climate domain [kyrs] (percent of time of glacial cycle)	Submerged conditions [kyrs] (percent of time of glacial cycle)
Extended global warming (Section 5.2)	106 kyrs (89%)	4 yrs (3%)	0 yrs (0%)	10 kyrs (8%)
Global warming (Section 5.1)	78 kyrs (65%)	28 kyrs (23%)	11 kyrs (9%)	3 kyrs (c. 3%)
Reference glacial cycle (Section 4.5)	31 kyrs (26%)	41 kyrs (34%)	28 kyrs (24%)	19 kyrs (16%)
Extended ice sheet duration (Section 5.3)	28 kyrs (23%)	22 kyrs (18%)	60 kyrs (50%)	10 kyrs (8%)
Severe permafrost (Section 5.5)	24 kyrs (20%)	96 kyrs (80%)	0 kyrs (0%)	0 kyrs (0%)

6 List of abbreviations

Except expressions in equations, chemical expressions and common units

1D	One dimensional
2D	Two dimensional
3D	Three dimensional
A1B	IPCC emission scenario
A1FI	IPCC emission scenario
A2	IPCC emission scenario
ACIA	Arctic Climate Impact Assessment
AD	Anno Domini
AMAP	Arctic Monitoring and Assessment Programme
AMS	Accelerator Mass Spectrometer
AMOC	Atlantic Meridional Overturning Circulation
AOGCM	Atmosphere-Ocean General Circulation Model
AP	After Present
AR4	Fourth Assessment Report of IPCC
B2	IPCC emission scenario
BACC	BALTEX Assessment of Climate Change for the Baltic Sea Basin
BC	Before Christ
BIFROST	Baseline Inferences for Fennoscandian Rebound, Sea-level, and Tectonics
BIOCLIM	Modelling sequential BIOSphere systems under CLIMate change for radioactive waste disposal
BP	Before Present
CCSM3	Community Climate System Model 3
CRU	Climate Research Unit (East Anglia)
CSM	Climate System Model
CMIP3	Climate Model Intercomparison Project, phase 3
DEM	Digital Elevation Model
Dfb	Köppen climate classification class (temperate, humid cold climate with year-round precipitation)
dGPS	Differential Global Positioning System
DJF	December, January, February (winter season)
DO event	Dansgaard-Oeschger event
DVM	Dynamic Vegetation Model
EAIS	East Antarctic Ice Sheet
EISMINT	European Ice Sheet Modeling Initiative
ELA	Equilibrium Line Altitude
EPICA	European Project for Ice Coring in Antarctica
FEP	Features, Events and Processes
GAP	Greenland Analogue Project
GCM	General Circulation Model, Global Circulation Model
GIA	Glacial Isostatic Adjustment
GIS	Geographical Information System
GISP2	Greenland Ice Sheet project 2
GPS	Global Positioning System
GRACE	Gravity Recovery and Climate Experiment

GRIP	European Greenland Ice Core Project
GS 12	Greenland Stadial number 12
HadCM3	Hadley Centre Coupled Climate Model, version 3
HFD	Heat Flow Density, <i>or</i> geothermal heat flow
ICE-3G	Global ice sheet reconstruction
ICE-5G	Global ice sheet reconstruction
InSAR	Interferometric Synthetic Aperture Radar
IPCC	Intergovernmental Panel on Climate Change
JJA	June, July, August (summer season)
KTH	Royal Institute of Technology (Stockholm)
LGM	Last Glacial Maximum
ka	kilo annum (thousands of years)
KBS-3	Kärnbränslesäkerhet 3 (method for final storage of spent nuclear fuel)
kyr	kilo year (thousand years)
kyrs	kilo years (thousands of years)
LPJ-GUESS	A dynamic vegetation model
Ma	Mega annum (millions of years)
MIS	Marine Isotope Stage
MX-80	Bentonite clay
Myr	million year (million years)
Myrs	Millions of years (millions of years)
NCAR	National Centre for Atmospheric Research
NEA	Nuclear Energy Agency
NGRIP	North Greenland Ice core Project
NorthGRIP	North Greenland Ice core Project
NSF	National Science Foundation
NWMO	Nuclear Waste Management Organization
OSL	Optically Stimulated Luminescence
PMIP1	Paleoclimate Modelling Intercomparison Project, phase 1
PMIP2	Paleoclimate Modelling Intercomparison Project, phase 2
PREM	Preliminary Reference Earth Model
QA	Quality assurance
RCA 3	Rosby Centre Regional Climate Model
RCM	Regional Circulation Model
RH70	Rikets höjdsystem 1970 (national elevation system in Sweden)
RT-90	Rikets Triangelnät 1990 (national coordinate system in Sweden)
ScanSAR	Scanning Synthetic Aperture Radar
SCAR	Scientific Committee on Antarctic Research
SGU	Geological Survey of Sweden
SKB	Swedish Nuclear Fuel and Waste Management Organisation
SMHI	Swedish Meteorological and Hydrological Institute
SSTs	Sea Surface temperatures
SWECLIM	Swedish Regional Climate Modelling Programme
THM	Thermo-Hydro-Mechanical
TWI	Topographic Wetness Index
UMISM	University of Maine Ice Sheet Model
UNFCCC	United Nation's Framework Convention on Climate Change
WAIS	West Antarctic Ice Sheet

7 References

SKB's (Svensk Kärnbränslehantering AB) publications can be found at www.skb.se/publications.

- ACIA, 2005.** Arctic Climate Impact Assessment. Cambridge: Cambridge University Press.
- Ahnert F, 1970.** Functional relationships between denudation, relief, and uplift in large, mid-latitude drainage basins. *American Journal of Science*, 268, pp 243–263.
- Ahonen L, 2001.** Permafrost: occurrence and physicochemical processes. Helsinki: Posiva.
- Ahrens C D, 1994.** Meteorology today: an introduction to weather, climate and the environment. 5th ed. Minneapolis/St. Paul: West Publishing Company.
- Allen D, Michel F, Judge A, 1988.** Paleoclimate and permafrost in the Mackenzie Delta. In: Proceedings of the fifth international conference on permafrost. Trondheim, 2–5 August 1988. Vol 1. Trondheim: Tapir.
- Alley R B, 1992.** Flow-law hypotheses for ice-sheet modeling. *Journal of Glaciology*, 38, pp 245–256.
- Alley R B, Clark P U, Huybrechts P, Joughin I, 2005a.** Ice-sheet and sea-level changes. *Science*, 310, pp 456–460.
- Alley R B, Dupont T K, Parizek B R, Anandakrishnan S, 2005b.** Access of surface meltwater to beds of sub-freezing glaciers: preliminary insights. *Annals of Glaciology*, 40, pp 8–14.
- Alley R B, Dupont T K, Parizek B R, Anandakrishnan S, Lawson D E, Larson G J, Evenson E B, 2006.** Outburst flooding and the initiation of ice-stream surges in response to climatic cooling. *Geomorphology*, 75, pp 76–89.
- Allison I, Bindoff N L, Bindshadler R A, Cox P M, de Noblet N, England M H, Francis J E, Gruber N, Haywood A M, Karoly D J, Kaser G, Le Quéré C, Lenton T M, Mann M E, McNeil B I, Pitman A J, Rahmstorf S, Rignot E, Schellnhuber H J, Schneider S H, Sherwood S C, Somerville R C J, Steffen K, Steig E J, Visbeck M, Weaver A J, 2009.** The Copenhagen diagnosis, 2009: updating the world on the latest climate science. Sydney: The University of New South Wales Climate Change Research Centre (CCRC).
- AMAP, 2009.** The Greenland ice sheet in a changing climate: snow, water, ice and permafrost in the Arctic (SWIPA) 2009. Oslo : Arctic Monitoring and Assessment Programme.
- Ampel L, Bigler C, Wohlfarth B, Risberg J, Lotter A F, Veres D, 2010.** Modest summer temperature variability during DO cycles in western Europe. *Quaternary Science Reviews*, 29, pp 1322–1327.
- Andersen B G, Mangerud J, 1989.** The last interglacial-glacial cycle in Fennoscandia. *Quaternary International*, 3-4, pp 21–29.
- Andersen K, Azuma N, Barnola J-M, Bigler M, Biscaye P, Caillon N, Chappellaz J, Clausen H B, Dahl-Jensen D, Fischer H, Flückiger J, Fritzsche D, Fujii Y, Goto-Azuma K, Grønvold K, Gundestrup N S, Hansson M, Huber C, Hvidberg C S, Johnsen S J, Jonsell U, Jouzel J, Kipfstuhl S, Landais A, Leuenberger M, Lorrain R, Masson-Delmotte V, Miller H, Motoyama H, Narita H, Popp T, Rasmussen S O, Raynaud D, Röthlisberger R, Ruth U, Samyn D, Schwander J, Shoji H, Siggaard-Andersen M-L, Steffensen J P, Stocker T, Sveinbjörnsdóttir A E, Svensson A, Takata M, Tison J-L, Thorsteinsson T, Watanabe O, Wilhelms F, White J W C, 2004.** High-resolution record of Northern Hemisphere climate extending into the last interglacial period. *Nature*, 431, pp 147–151.
- Andrews J T, Barber D C, 2002.** Dansgaard-Oeschger events: is there a signal off the Hudson Strait Ice Stream? *Quaternary Science Reviews*, 21, pp 443–454.
- Archer D, 2005.** Fate of fossil fuel CO₂ in geologic time. *Journal of Geophysical Research*, 110, C09S05, doi:10.1029/2004JC002625.
- Archer D, Brovkin V, 2008.** The millennial atmospheric lifetime of anthropogenic CO₂. *Climatic Change*, 90, pp 283–297.
- Archer D, Ganopolski A, 2005.** A movable trigger: Fossil fuel CO₂ and the onset of the next glaciation. *Geochemistry, Geophysics, Geosystems*, 6, Q05003, doi:10.1029/2004GC000891.

- Archibold O W, 1994.** Ecology of world vegetation. New York: Springer.
- Árnadóttir T, Lund B, Jiang W, Geirsson H, Björnsson H, Einarsson P, Sigurdsson T, 2009.** Glacial rebound and plate spreading: results from the first countrywide GPS observations in Iceland. *Geophysical Journal International*, 177, pp 691–716.
- Arndt D S, Baringer M O, Johnson M R (eds), 2010.** State of the climate in 2009. *Bulletin of the American Meteorological Society*, 91, pp 1–222.
- Arnold N, Sharp M, 2002.** Flow variability in the Scandinavian ice sheet: modelling the coupling between ice sheet flow and hydrology. *Quaternary Science Review*, 21, pp 485–502.
- Arnold N, Richards K, Willis I, Sharp M, 1998.** Initial results from a distributed, physically based model of glacier hydrology. *Hydrological Processes*, 12, pp 191–219.
- Artemieva I M, Mooney W D, 2001.** Thermal thickness and evolution of Precambrian lithosphere: a global study. *Journal of Geophysical Research*, 106, pp 16387–16414.
- BACC author team 2008.** Assessment of climate change for the Baltic Sea basin. Berlin, Heidelberg: Springer Verlag. (Regional climate studies)
- Balling N, 1984.** Gravity and isostasy in the Baltic Shield. In: Galson D A, Mueller S, Munch B (eds). *Proceedings of the first workshop on the European Geotraverse Project (EGT): The northern segment*. Strasbourg: European Science Foundation, pp 53–66.
- Bamber J L, Riva R E M, 2010.** The sea-level fingerprint of 21st century ice mass flux. *The Cryosphere Discussions*, 4, pp 1593–1606.
- Bamber J L, Layberry R L, Gogineni S P, 2001.** A new ice thickness and bed data set for the Greenland ice sheet. 1. Measurement, data reduction, and errors. *Journal of Geophysical Research*, 106, pp 33773–33780.
- Bamber J L, Alley R B, Joughin I, 2007.** Rapid response of modern day ice sheets to external forcing. *Earth and Planetary Science Letters*, 257, pp 1–13.
- Bamber J L, Riva R E M, Vermeersen B L A, LeBrocq A M, 2009.** Reassessment of the potential sea-level rise from a collapse of the West Antarctic ice sheet. *Science*, 324, pp 901–903.
- Barber D C, Dyke A, Hillaire-Marcel C, Jennings A E, Andrews J T, Kerwin M W, Bilodeau G, McNeely R, Southon J, Morehead M D, Gagnon J-M, 1999.** Forcing of the cold event of 8,200 years ago by catastrophic drainage of Laurentide lakes. *Nature*, 400, pp 344–348.
- Bard E, Hamelin B, Fairbanks R G, 1990.** U-Th ages obtained by mass spectrometry in corals from Barbados: sea-level during the past 130,000 years. *Nature*, 346, pp 456–458.
- Bard E, Hamelin B, Arnold M, Montaggioni L, Cabioch G, Faure G, Rougerie F, 1996.** Deglacial sea-level record from Tahiti corals and the timing of global meltwater discharge. *Nature*, 382, pp 241–244.
- Barron E, Pollard D, 2002.** High-resolution climate simulations of oxygen isotope stage 3 in Europe. *Quaternary Research*, 58, pp 296–309.
- Bassett S E, Milne G A, Mitrovica J X, Clark P U, 2005.** Ice sheet and solid Earth influences on far-field sea-level histories. *Science*, 309, pp 925–928.
- Bates B C, Kundzewicz Z W, Wu S, Palutikof J P (eds), 2008.** Climate change and water. Technical paper of the Intergovernmental Panel on Climate Change. Geneva: IPCC Secretariat.
- Bauder A, Mickelson D M, Marshall S J, 2003.** Modelling ice sheet permafrost interaction around the southern Laurentide ice sheet. EGS - AGU - EUG Joint Assembly. Abstracts from the meeting held in Nice, France, 6–11 April 2003, abstract 12348.
- Beardsmore G R, Cull J P, 2001.** *Crustal heat flow: a guide to measurement and modelling*. Cambridge: Cambridge University Press.
- Bell R E, 2008.** The role of subglacial water in ice-sheet mass balance. *Nature Geoscience*, 1, pp 297–304.
- Benn D I, Evans D J A, 1998.** *Glaciers & glaciation*. London: Arnold.

- Bennett M R, Waller R I, Midgley N G, Huddart D, Gonzalez S, Cook S J, Tomio A, 2003.** Subglacial deformation at sub-freezing temperatures? Evidence from Hagafellsjökull-Eystri, Iceland. *Quaternary Science Reviews*, 22, pp 915–923.
- Benson C S, 1961.** Stratigraphic studies in the snow and firn of the Greenland ice sheet. *Folia Geographica Danica*, 9, pp 13–37.
- Berger A, 1978.** Long-term variations of daily insolation and Quaternary climatic changes. *Journal of the Atmospheric Sciences*, 35, pp 2362–2367.
- Berger A, Loutre M F, 2002.** An exceptionally long interglacial ahead? *Science*, 297, pp 1287–1288.
- Bhattacharya I, Jezek K C, Wang L, Liu H, 2009.** Surface melt area variability of the Greenland ice sheet: 1979–2008. *Geophysical Research Letters*, 36, L20502, doi:10.1029/2009GL039798.
- Bills B G, James T S, 1996.** Late Quaternary variations in relative sea level due to glacial cycle polar wander. *Geophysical Research Letters*, 23, pp 3023–3026.
- Bintanja R, van de Wal R S W, 2008.** North American ice-sheet dynamics and the onset of 100,000-year glacial cycles. *Nature*, 454, pp 869–872.
- BIOCLIM, 2003.** Deliverable D7. Continuous climate evolution scenarios over western Europe (1000 km scale). Work package 2: Simulation of the future evolution of the biosphere system using the hierarchical strategy. Châtenay-Malabry: Agence Nationale pour la Gestion des Dechets Radioactifs (ANDRA).
- Birch F, Roy R F, Decker E R, 1968.** Heat flow and thermal history in New England and New York. In: Zen E-an (ed). *Studies of Appalachian geology: northern and maritime*. New York: Interscience, pp 437–451.
- Birgersson M, Karnland O, Nilsson U, 2008.** Freezing in saturated bentonite – a thermodynamic approach. *Physics and Chemistry of the Earth, Parts A/B/C*, 33, S527–S530.
- Birgersson M, Karnland O, Nilsson U, 2010.** Freezing of bentonite. Experimental studies and theoretical considerations. SKB TR-10-40, Svensk Kärnbränslehantering AB.
- Björck S, 1995.** A review of the history of the Baltic Sea, 13.0–8.0 ka BP. *Quaternary International*, 27, pp 19–40.
- Björck S, Noe-Nygaard N, Wolin J, Houmark-Nielsen M, Hansen H J, Snowball I, 2000.** Eemian lake development, hydrology and climate: a multi-stratigraphic study of the Hollerup site in Denmark. *Quaternary Science Reviews*, 19, pp 509–536.
- Bogren J, Gustavsson T, Loman G, 1998.** Klimatförändringar: naturliga och antropogena orsaker. Lund: Studentlitteratur (in Swedish).
- Bonelli S, Charbit S, Kageyama M, Woillez M-N, Ramstein G, Dumas C, Quiquet A, 2009.** Investigating the evolution of major Northern Hemisphere ice sheets during the last glacial-interglacial cycle. *Climate of the Past Discussions*, 5, pp 1013–1053.
- Bos J A A, Bohncke S J P, Engels E, Helmens K F, Coope G R, 2007.** Abrupt climatic events during MIS3 recorded in terrestrial sediments in NW Europe: multi-proxy approach. XVII INQUA congress. Cairns, Australia, 28 July–3 August 2007.
- Bos J A A, Helmens K F, Bohncke S J P, Seppä H, Birks H J B, 2009.** Flora, vegetation and climate at Sokli, northeastern Fennoscandia, during the Weichselian Middle Pleniglacial. *Boreas*, 38, pp 335–348.
- Bosson E, Sassner M, Sabel U, Gustafsson L-G, 2010.** Modelling of present and future hydrology and transport - SR Site Biosphere. SKB R-10-02, Svensk Kärnbränslehantering AB.
- Bougamont M, Bamber J L, Greuell W, 2005.** A surface mass balance model for the Greenland Ice Sheet. *Journal of Geophysical Research*, 110, F04018, doi:10.1029/2005JF000348.
- Boulton G S, Clark C D, 1990.** The Laurentide Ice Sheet through the last glacial cycle: the topography of drift lineations as a key to the dynamic behaviour of former ice sheets. *Transactions of the Royal Society of Edinburgh: Earth Sciences*, 81, pp 327–347.
- Boulton G S, Payne A, 1992.** Simulation of the European ice sheet through the last glacial cycle and prediction of future glaciation. SKB TR 93-14, Svensk Kärnbränslehantering AB.
- Boulton G S, Kautsky U, Morén L, Wallroth T, 2001a.** Impact of long-term climate change on a deep geological repository for spent nuclear fuel. SKB TR-99-05, Svensk Kärnbränslehantering AB.

- Boulton G S, Zatsepin S, Maillot B, 2001b.** Analysis of groundwater flow beneath ice sheets. SKB TR-01-06, Svensk Kärnbränslehantering AB.
- Brandefelt J, Strandberg G, 2007.** Simulating extreme climate conditions in Sweden in a 100,000 year perspective, abstract ICESM2007-A-00035 for the Second International Conference on Earth System Modelling (ICESM).
- Brandefelt J, Otto-Bliesner B L, 2009.** Equilibrium and variability in a Last Glacial Maximum climate simulation with CCSM3. *Geophysical Research Letters* 36, L19712, doi:10.1029/2009GL040364.
- Brandefelt J, Kjellström E, Näslund J-O, Smith B, Strandberg G, Voelker A H L, Wohlfarth B, 2011.** A coupled climate model simulation of Marine Isotope Stage 3 stadial climate. *Climate of the Past Discussions*, 7, pp 79–118. Manuscript under review for *Climate of the Past*.
- Brandefelt J, Kjellström E, Näslund J-O, Strandberg G, Voelker A, Wohlfarth B, 2010.** The importance of equilibration in glacial climate simulations. EGU2010-12736, EGU General Assembly 2010. *Geophysical Research Abstracts*, 12.
- Breckle S-W, 2002.** *Walter's vegetation of the earth: the ecological systems of the geo-biosphere.* 4th ed. Berlin: Springer.
- Bremer C W, Clark P U, Haggerty R, 2002.** Modeling the subglacial hydrology of the late Pleistocene lake Michigan Lobe, Laurentide Ice Sheet. *Geological Society of America Bulletin*, 114, pp 665–674.
- Broecker, 1991.** In: Watson R T, Zinyowera M C, Moss R H (eds). *Climate change 1995. Impacts, adaptations and mitigation of climate change: scientific-technical analyses.* Contribution of working group 2 to the second assessment report of the intergovernmental panel on climate change. Cambridge: Cambridge University Press.
- Brydsten L, Engqvist A, Näslund J-O, Lindborg T, 2009.** Expected extreme sea levels at Forsmark and Laxemar-Simpevarp up until year 2100. SKB TR-09-21, Svensk Kärnbränslehantering AB.
- Burroughs W J, 2001.** *Climate change: a multidisciplinary approach.* Cambridge: Cambridge University Press.
- Burn C R, 2002.** Tundra lakes and permafrost, Richards Island, western Arctic coast, Canada. *Canadian Journal of Earth Sciences*, 39, pp 1281–1298.
- Burt T P, Williams P J, 1976.** Hydraulic conductivity in frozen soils. *Earth Surface Processes*, 1, pp 349–360.
- Bøggild C E, Mayer C, Podlech S, Taurisano A, Nielsen S, 2004.** Towards an assessment of the balance state of the Greenland Ice Sheet. *Geological Survey of Denmark and Greenland Bulletin*, 4, pp 81–84.
- Calcagnile G, 1982.** The lithosphere asthenosphere system in Fennoscandia. *Tectonophysics*, 90, pp 19–35.
- Catania G A, Neumann T A, 2009.** Persistent englacial drainage features in the Greenland Ice Sheet. *Geophysical Research Letters*, 37, L02501, doi:10.1029/2009GL041108.
- Catania G A, Neumann T A, Price S F, 2008.** Characterizing englacial drainage in the ablation zone of the Greenland ice sheet. *Journal of Glaciology*, 54, pp 567–578.
- Cazenave A, Dominh K, Guinehut S, Berthier E, Llovel W, Ramillien G, Ablain M, Larnicol G, 2009.** Sea-level budget over 2003–2008: a reevaluation from GRACE space gravimetry, satellite altimetry and Argo. *Global and Planetary Change*, 65, pp 83–88.
- Čermák V, Balling N, Kukkonen I, Zui V I, 1993.** Heat flow in the Baltic Shield – results of the lithospheric geothermal modelling. *Precambrian Research*, 64, pp 53–65.
- Chappell J, Polach H, 1991.** Post-glacial sea-level rise from a coral record at Huon Peninsula, Papua New Guinea. *Nature*, 349, pp 147–149.
- Chappell J, Omura A, Esat T, McCulloch M, Pandolfi J, Ota Y, Pillans B, 1996.** Reconciliation of late Quaternary sea levels derived from coral terraces at Huon Peninsula with deep sea oxygen isotope records. *Earth and Planetary Science Letters*, 141, pp 227–236.
- Charbit S, Ritz C, Phillippon G, Peyaud V, Kageyama M, 2007.** Numerical reconstructions of the Northern Hemisphere ice sheets through the last glacial-interglacial cycle. *Climate of the Past*, 3, pp 15–37.

- Chen J L, Wilson C R, Tapley B D, 2006.** Satellite gravity measurements confirm accelerated melting of Greenland ice sheet. *Science*, 313, pp 1958–1960.
- Cheng H, Edwards L, Broecker W S, Denton G H, Kong X, Wang Y, Zhang R, Wang X, 2009.** Ice age terminations. *Science*, 326, pp 248–252.
- Christoffersen P, Tulaczyk S, Wattrus N J, Peterson J, Quintana-Krupinski N, Clark C D, Sjunneskog C, 2008.** Large subglacial lake beneath the Laurentide ice sheet inferred from sedimentary sequences. *Geology*, 36, pp 563–566.
- Church J A, 35 others, 2001.** Greenland and Antarctic Ice Sheets. In: Houghton J T (ed). *Climate Change 2001: the scientific basis*. New York: Cambridge University Press, ch 11.2.3.
- Clark J A, Farrell W E, Peltier W R, 1978.** Global changes in postglacial sea level: a numerical calculation. *Quaternary Research*, 9, pp 265–287.
- Clark P U, Mix A C, 2002.** Ice sheets and sea level of the Last Glacial Maximum. *Quaternary Science Reviews* 21, pp 1–7.
- Clark P U, Walder J S, 1994.** Subglacial drainage, eskers, and deforming beds beneath the Laurentide and Eurasian ice sheets. *Geological Society of America Bulletin*, 106, pp 304–314.
- Clark P U, Alley R B, Keigwin L D, Licciardi J M, Johnsen S J, Wang H X, 1996.** Origin of the first global meltwater pulse following the Last Glacial Maximum. *Paleoceanography*, 11, pp 563–577.
- Clark P, Archer D, Pollard D, Blum J, Rial J, Brovkin V, Mix A C, Pisias N, Roy M, 2006.** The middle Pleistocene transition: characteristics, mechanisms, and implications for long-term changes in atmospheric pCO₂. *Quaternary Science Reviews*, 25, pp 3150–3184.
- Clark P U, Dyke A S, Shakun J D, Carlson A E, Clark J, Wohlfarth B, Mitrovica J X, Hostetler S W, McCabe A M, 2009.** The Last Glacial Maximum. *Science*, 325, pp 710–714.
- Clarke G, Leverington D, Teller J, Dyke A, 2003.** Superlakes, megafloods, and abrupt climate change. *Science*, 301, pp 922–923.
- Clauser C, Huenges E, 1995.** Thermal conductivity of rocks and minerals. In: Ahrens T J (ed). *Rock physics and phase relations: handbook of physical constants*. Washington, D.C.: American Geophysical Union, pp 105–126.
- Colleoni F, Krinner G, Jakobsson M, Peyaud V, Ritz C, 2009.** Influence of regional parameters on the surface mass balance of the Eurasian ice sheet during the peak Saalian (140 kya). *Global and Planetary Change*, 68, pp 132–148.
- Collinson J, 2005a.** Erosional sedimentary structures. In: Selley R C, Cocks L R M, Plimer I R (eds). *Encyclopedia of geology*. Amsterdam: Elsevier Academic Press.
- Collinson J, 2005b.** Depositional sedimentary structures. In: Selley R C, Cocks L R M, Plimer I R (eds). *Encyclopedia of geology*. Amsterdam: Elsevier Academic Press.
- Cuffey K M, Alley R B, Grootes P M, Bolzan J M, Anandakrishnan S, 1994.** Calibration of the $\delta^{18}\text{O}$ isotopic paleothermometer for central Greenland, using borehole temperatures. *Journal of Glaciology*, 40, pp 341–349.
- Cuffey K M, Conway H, Gades A M, Hallet B, Lorrain R, Severinghaus J P, Steig E J, Vaughn B, White J W C, 2000.** Entrainment at cold glacier beds. *Geology*, 28, pp 351–354.
- Dahl-Jensen D, Gundestrup N, Gogineni S P, Miller H, 2003.** Basal melt at NorthGRIP modeled from borehole, ice-core and radio-echo sounder observations. *Annals of Glaciology*, 37, pp 207–212.
- Danielson E W, Levin J, Abrams E, 2003.** *Meteorology*. 2nd ed. New York: McGraw-Hill.
- Dansgaard W, Johnsen S J, Clausen H B, Dahl-Jensen D, Gundestrup N S, Hammer C U, Hvidberg C S, Steffensen J P, Sveinbjörnsdóttir A E, Jouzel J, Bond G, 1993.** Evidence for general instability of past climate from a 250-kyr ice-core record. *Nature*, 364, pp 218–220.
- Das S B, Joughin I, Behn M D, Howat I M, King M A, Lizarralde D, Bhatia M P, 2008.** Fracture propagation to the base of the Greenland ice sheet during supraglacial lake drainage. *Science*, 320, pp 778–781.
- Davis J L, Mitrovica J X, 1996.** Glacial isostatic adjustment and the anomalous tide gauge record of eastern North America. *Nature*, 379, pp 331–333.

- Davis J L, Mitrovica J X, Scherneck H G, Fan H, 1999.** Investigations of Fennoscandian glacial isostatic adjustment using modern sea level records. *Journal of Geophysical Research*, 104, pp 2733–2747.
- Delisle G, 1998.** Numerical simulation of permafrost growth and decay. *Journal of Quaternary Science* Vol. 13, pp 325–333.
- Denton G H, Hughes T J (eds), 1981.** The last great ice sheets. New York: John Wiley.
- Denton G E, Sugden D E, 2005.** Meltwater features that suggest Miocene ice-sheet overriding the Transantarctic Mountains in Victoria Land, Antarctica. *Geografiska Annaler*, 87A, pp 67–85.
- Drewry D, 1986.** Glacial geologic processes. London: Arnold.
- Drijfhout S, Hazeleger W, Selten F, Haarsma R, 2008.** Future changes in internal variability of the Atlantic Meridional Overturning Circulation. *Climate Dynamics*, 30, pp 407–419.
- Duval P, Ashby M F, Anderman I, 1983.** Rate-controlling processes in the creep of polycrystalline ice. *Journal of Physical Chemistry*, 87, pp 4066–4074.
- Dziewonski A M, Anderson D L, 1981.** Preliminary reference earth model. *Physics of the Earth and Planetary Interiors*, 25, pp 297–356.
- Ebert K, 2009.** Cenozoic landscape evolution in northern Sweden: geomorphological interpretation within a GIS-framework. Ph.D. thesis. Department of Physical Geography and Quaternary Geology, Stockholm University. (Dissertations from the Department of Physical Geography and Quaternary Geology 19)
- Ehlers J, Gibbard P L (eds), 2004.** Quaternary glaciations: extent and chronology. Part I: Europe. Amsterdam: Elsevier. (Developments in quaternary science 2)
- Ekman M, 1991.** A concise history of postglacial land uplift research (from its beginning to 1950). *Terra Nova*, 3, pp 358–365.
- Engelhardt H, Kamb B, 1998.** Basal sliding of Ice Stream B, West Antarctica. *Journal of Glaciology*, 44, pp 223–230.
- Engelhardt H, Humphrey N, Kamb B, Fahnestock M, 1990.** Physical conditions at the base of a fast moving Antarctic ice stream. *Science*, 248, pp 57–59.
- Engels S, Bohncke S J P, Boss J A A, Helmens K F, Heiri O, 2006.** A chironomid-based Middle Weichselian climate reconstruction from an unusual location: Finnish Lapland. *Nederlands Aardwetenschappelijk Congres 8*. Veldhoven, 24–25 April 2006.
- Engels S, Bohncke S J P, Bos J A A, Brooks S J, Heiri O, Helmens K F, 2008a.** Chironomid-based palaeotemperature estimates for northeast Finland during Oxygen Isotope Stage 3. *Journal of Palaeolimnology*, 40, pp 49–61.
- Engels S, Bohncke S J P, Bos J A A, Helmens K F, Heiri O, 2008b.** Chironomid-based inferences of local and regional environmental change during the early Middle Weichselian in Northeast Finland. In: *Proceedings of the 16th International Chironomid Symposium*, Funchal, Madeira, Portugal, 25–28 July 2006. *Boletim do Museu municipal do Funchal, Suppl.* 13, pp 191–196.
- Engels S, Helmens K F, Bohncke S J P, Bos J A A, Brooks S J, Heiri O, Väiliranta M, 2008c.** A multi-proxy record of environmental and climate changes during Oxygen Isotope Stages -3 and -5C from an unusual location: Finnish Lapland. *Geophysical Research Abstracts*, 10, EGU2008-A-08467.
- Engels S, Bohncke S J P, Heiri O, Vandenberghe J, 2008d.** Exploring Middle Weichselian climate variability in NW Europe by applying chironomids as a proxy. *Geophysical Research Abstracts*, 10, EGU2008-A-08604.
- Engels S, Helmens K F, Väiliranta M, Brooks S J, Birks H J B, 2010.** Early Weichselian (MIS 5d and 5c) temperatures and environmental changes in northern Fennoscandia as recorded by chironomids and macroremains at Sokli, northeast Finland. *Boreas*, 39, pp 689–704.
- EPICA community members, 2004.** Eight glacial cycles from an Antarctic ice core. *Nature*, 429, pp 623–628.
- Eronen M, Gluckert G, Hatakka L, van de Plassche O, van der Plicht J, Rantala P, 2001.** Rates of Holocene isostatic uplift and relative sea-level lowering of the Baltic in SW Finland based on studies of isolation contacts. *Boreas*, 30, pp 17–30.

- Eugster W, Rouse W R, Pielke R A, Mcfadden J P, Baldocchi D D, Kittel T G F, Chapin F, Stuart F, Liston G E, Vidale P L, Vaganov E, Chambers S, 2000.** Land-atmosphere energy exchange in Arctic tundra and boreal forest: available data and feedbacks to climate. *Global Change Biology*, 6 (Suppl. 1), pp 84–115.
- Evatt G W, Fowler A C, Clark C D, Hulton N R J, 2006.** Subglacial floods beneath ice sheets. *Philosophical Transactions of the Royal Society A*, 364, pp 1769–1794.
- Fahnestock M, Abdalati W, Joughin I, Brozena J, Gogineni P, 2001.** High geothermal heat flow, basal melt, and the origin of rapid ice flow in central Greenland. *Science*, 294, pp 2338–2342.
- Fairbanks R G, 1989.** A 17,000-year glacio-eustatic sea level record: influence of glacial melting rates on the Younger Dryas event and deep-ocean circulation. *Nature*, 342, pp 637–642.
- Farrell W E, Clark J A, 1976.** On postglacial sea level. *Geophysical Journal of the Royal Astronomical Society*, 46, pp 647–667.
- Fastook J L, 1990.** A map-plane finite-element program for ice sheet reconstruction: a steady-state calibration with Antarctica and a reconstruction of the Laurentide ice sheet for 18,000 BP. In: Brown H U (ed). *Computer assisted analysis and modelling on the IBM 3090*. White Plains, N.Y.: IBM Scientific and Technical Computing Department.
- Fastook J L, 1994.** Modeling the Ice Age: the finite-element method in glaciology. *Computing Science and Engineering*, 1, pp 55–67.
- Fastook J L, Chapman J E, 1989.** A map plane finite-element model: three modeling experiments. *Journal of Glaciology*, 35, pp 48–52.
- Fastook J L, Holmlund P, 1994.** A glaciological model of the Younger Dryas event in Scandinavia. *Journal of Glaciology*, 40, pp 125–131.
- Fastook J L, Prentice M, 1994.** A finite-element model of Antarctica: sensitivity test for meteorological mass-balance relationship. *Journal of Glaciology*, 40, pp 167–175.
- Fetterer F, Knowles K, Meier W, Savoie M, 2002, updated until 2010.** Sea ice index. Boulder, Colorado: National Snow and Ice Data Center. Digital media.
- Fisher U H, 2009.** Glacial erosion: a review of its modelling. *Nagra Arbeitsbericht NAB 09-23*, National Cooperative for the Disposal of Radioactive Waste, Switzerland.
- Fischer H, Goto-Azuma K, Hansson M E, Ruth U, 2006.** A new Greenland ice core chronology for the last glacial termination. *Journal of Geophysical Research*, 111, D06102, doi:10.1029/2005JD006079.
- Fjeldskaar W, 1994.** The amplitude and decay of the glacial forebulge in Fennoscandia. *Norsk Geologisk Tidsskrift*, 74, pp 2–8.
- Fleming K, Johnston P, Zwartz D, Yokoyama Y, Lambeck K, Chappell J, 1998.** Refining the eustatic sea-level curve since the Last Glacial Maximum using far- and intermediate-field sites. *Earth and Planetary Science Letters*, 163, pp 327–342.
- Flowers G E, Clarke G K C, 2002a.** A multicomponent coupled model of glacier hydrology. 1. Theory and synthetic examples. *Journal of Geophysical Research*, 107, 2287, doi:10.1029/2001JB001122.
- Flowers G E, Clarke G K C, 2002b.** A multicomponent coupled model of glacier hydrology. 2. Application to Trapridge Glacier, Yukon, Canada. *Journal of Geophysical Research*, 2288, doi:10.1029/2001JB001124.
- Forsström P-L, Sallasmaa O, Greve R, Zwinger T, 2003.** Simulation of fast-flow features of the Fennoscandian ice sheet during the Last Glacial Maximum. *Annals of Glaciology*, 37, pp 383–389.
- Forsström P-L, 2005.** Through a glacial cycle: simulation of the Eurasian ice sheet dynamics during the last glaciation. Ph. D. thesis. University of Helsinki, Faculty of Science, Department of Geology, Geology and Palaeontology and Center for Scientific Computing.
- Fotiev S M, 1997.** Permafrost groundwater Russian Literature Review. In: Haldorsen S, Liebman M, Nelson G, van Everdingen R O, Boike J, 1997: *State-of-the-art report on saturated water movement in permafrost areas*. Report No 4/97 (Inr 54). Ås: Norges landbrukshøgskole.
- Fountain A G, Walder J S, 1998.** Water flow through temperate glaciers. *Reviews of Geophysics*, 36, pp 299–328.

- Fountain A G, Jacobel R W, Schlichting R, Jansson P, 2005a.** Fractures as the main pathways of water flow in temperate glaciers. *Nature*, 433, pp 618–621.
- Fountain A G, Schlichting R, Jansson P, Jacobel R W, 2005b.** Observations of englacial flow passages: a fracture dominated system. *Annals of Glaciology*, 40, pp 25–30.
- Fredén C (ed), 2002.** Sveriges nationalatlas. Berg och Jord. Stockholm: SNA publishing (in Swedish).
- French H M, 2007.** The periglacial environment. 3rd ed. Chichester: John Wiley and Sons.
- Fronval T, Jansen E, 1996.** Late Neogene paleoclimates and paleoceanography in the Iceland-Norwegian Sea: evidence from the Iceland and Vøring plateaus. In: Thiede J, Myhre A M, Firth J V, Johnson G L, Ruddiman W F (eds). *Proceedings of the Ocean Drilling Program, Scientific results*, 151, pp 455–468.
- Funder S, Demidov I, Yelovicheva Y, 2002.** Hydrography and mollusc faunas of the Baltic and the White Sea-North Sea seaway in the Eemian. *Palaeogeography, Palaeoclimatology, Palaeoecology* 184, pp 275–304.
- Furlong K P, Chapman D S, 1987.** Crustal heterogeneities and the thermal structure of the continental crust. *Geophysical Research Letters*, 14, pp 314–317.
- GAP team members, 2009.** The Greenland Analogue Project (GAP) Annual report 2009. SKB R-10-59, Svensk Kärnbränslehantering AB.
- Garisto F, Avis J, Chshyolkova T, Gierszewski P, Gobien M, Kitson C, Melnyk T, Miller J, Walsh R, Wojciechowski L, 2010.** Glaciation scenario: safety assessment for a deep geological repository for used fuel. NWMO TR-2010-10, Nuclear Waste Management Organization, Canada.
- Gascoyne M, 2000.** A review of published literature on the effects of permafrost on the hydrogeochemistry of bedrock. SKB R-01-56, Svensk Kärnbränslehantering AB.
- Giovinetto M B, Zwally H J, 2000.** Spatial distribution of net surface accumulation on the Antarctic ice sheet. *Annals of Glaciology*, 31, pp 171–178.
- Glen J W, 1955.** The creep of polycrystalline ice. *Proceedings of the Royal Society of London, Series A*, 228, pp 519–538.
- Global Warming Art, 2007.** Five Myr climate change. Figure prepared by Robert A. Rohde / Global Warming Art. [Online]. Available at: http://www.globalwarmingart.com/wiki/File:Five_Myr_Climate_Change_Rev_png. [26 November 2010].
- Goodess C M, Palutikof, J P, Davies T D, 1992.** The Nature and causes of climate change: assessing the long-term future. London: Belhaven.
- Gregory J M, Huybrechts P, 2006.** Ice-sheet contributions to future sea-level change. *Philosophical Transactions of the Royal Society A*, 364, pp 1709–1731.
- Gregory J M, Huybrechts P, Raper S C B, 2004.** Threatened loss of the Greenland ice sheet. *Nature*, 428, p 616.
- Greve R, Hutter K, 1995.** Polythermal three-dimensional modelling of the Greenland ice sheet with varied geothermal heat flux. *Annals of Glaciology*, 21, pp 8–12.
- Grinsted A, Moore J C, Jevrejeva S, 2009.** Reconstruction of sea-level from paleo and projected temperatures 2000 to 2100 AD. *Climate Dynamics*, 34, pp 461–472.
- Hagdorn M K M, 2003.** Reconstruction of the Past and Forecast of the Future European and British Ice Sheets and Associated Sea-Level Change. Academic Dissertation, 2003, University of Edinburgh, School of GeoScience. 175 p.
- Hagdorn M, Hulton N, Payne A J, Rutt I, Boulton G, 2005.** Introducing GLIMMER – a 3D thermo-mechanical ice sheet model. Poster presented at European Geosciences Union General Assembly 2005, Vienna, Austria, April 24–29 2005.
- Hall D K, Williams R S, Luthcke S B, Digirolamo N E, 2008.** Greenland ice sheet surface temperature, melt and mass loss: 2000–06. *Journal of Glaciology*, 54, pp 81–93.
- Hallet B, Hunter L, Bogen J, 1996.** Rates of erosion and sediment evacuation by glaciers: a review of field data and their implications. *Global and Planetary Change*, 12, pp 213–235.

- Hambrey M J, Barrett P J, Ehrmann W U, Larsen B, 1992.** Cainozoic sedimentary processes on the Antarctic continental margin and the record from deep drilling. *Zeitschrift für Geomorphologie, Suppl.* 86, pp 77–103.
- Han D, Wahr J, 1989.** Post-glacial rebound analysis for a rotating Earth. In: Cohen S, Vanicek P (eds). *Slow deformations and transmission of stress in the Earth*. Washington D.C.: American Geophysical Union. (AGU Monograph Series 49), pp 1–6.
- Hanebuth T, Statterger K, Grootes P M, 2000.** Rapid flooding of the Sunda Shelf: a late-glacial sea-level record. *Science*, 288, pp 1033–1035.
- Hanna E, Huybrechts P, Steffen K, Cappelen J, Huff R, Shuman C, Irvine-Fynn T, Wise S, Griffiths M, 2008.** Increased runoff from melt from the Greenland ice sheet: a response to global warming. *Journal of Climate*, 21, pp 331–341.
- Hanna E, Cappelen J, Fettweis X, Huybrechts P, Luckman A, Ribergaard M H, 2009.** Hydrologic response of the Greenland ice sheet: the role of oceanographic warming. *Hydrological Processes*, 23, pp 7–30.
- Haq B U, Hardenbol J, Vail P R, 1987.** Chronology of fluctuating sea levels since the Triassic. *Science*, 235, pp 1156–1165.
- Harrison S P, Braconnot P, Joussaume S, Hewitt C, Stouffer R J, 2002.** Comparison of palaeoclimate simulations enhances confidence in models. *EOS*, 83, p 447.
- Hartikainen J, 2004.** Permafrost modeling in DECOVALEX III for BMT3. In: Eloranta E (ed). *DECOVALEX III, 1999–2003. An international project for the modelling of coupled thermo-hydro-mechanical processes for spent fuel disposal*. Finnish national contributions. STUK-YTO-TR 209, Finnish Centre for Radiation and Nuclear Safety (STUK), Helsinki.
- Hartikainen J, Mikkola M, 2006.** Thermomechanical modelling for freezing of solute saturated soil. In: Gladwell G M L, Huyghe J M, Raats P A C, Cowin S C (eds). *IUTAM Symposium on the mechanics of physicochemical and electromechanical interactions in porous media*, pp 335–341.
- Hartikainen J, Kouhia R, Wallroth T, 2010.** Permafrost simulations at Forsmark using a numerical 2D thermo-hydro-chemical model. SKB TR-09-17, Svensk Kärnbränslehantering AB.
- Hays J D, Imbrie J, Shackleton N, 1976.** Variations in the Earth's orbit: pacemaker of the ice ages, *Science*, 194, pp 1121–1132.
- Heginbottom J A, Dubreuil M A, Harker P A, 1995.** Canada – Permafrost. In: *National Atlas of Canada*, 5th ed. Ottawa: National Atlas Information Service, Natural Resources Canada.
- Heinrich H, 1988.** Origin and consequences of cyclic ice rafting in the northeast Atlantic Ocean during the past 130,000 years. *Quaternary Research*, 29, pp 142–152.
- Helmens K F, 2009a.** Climate, vegetation and lake development at Sokli (northern Finland) during early MIS 3 at ~50 kyr: Revising earlier concepts on climate, glacial and vegetation dynamics in Fennoscandia during the Weichselian. SKB TR-09-16, Svensk Kärnbränslehantering AB.
- Helmens K F, 2009b.** Late Quaternary climate variability in high latitude northern Europe: data-model comparison. 4th BBCC (Bert Bolin Climate Centre, Stockholm University) annual meeting, Stockholm, Sweden, 14–15 September 2009.
- Helmens K F, Engels S, 2010.** Ice-free conditions in eastern Fennoscandia during early Marine Isotope Stage 3: lacustrine records. *Boreas*, 39, pp 399–409.
- Helmens K F, Bos J A A, Engels S, Van Meerbeeck C J, Bohncke S J P, Renssen H, Heiri O, Brooks S J, Seppä H, Birks H J B, Wohlfarth B, 2007a.** Present-day temperatures in northern Scandinavia during the last glaciation. *Geology*, 35, pp 987–990.
- Helmens K F, Bos J A A, Engels E, Seppä H, Bohncke S J P, Van Meerbeeck C J, Renssen H, Risberg J, Wohlfarth B, 2007b.** Ice free and warm conditions in the central area of the Scandinavian glaciations during MIS 3. XVII INQUA congress. Cairns, Australia, 28 July–3 August 2007.
- Helmens K F, Bos J A A, Engels S, Van Meerbeeck C J, Seppä H, Birks H J B, Brooks S J, Risberg J, Wohlfarth B, 2007c.** Present-day temperatures at Sokli (northern Finland) during MIS 3 recorded by high-resolution multi-proxy analysis and climate modeling. 1st NEPAL (Nordic Network on Palaeoclimatology) workshop. Palmse, Estonia, 10–12 May 2007.

- Helmens K F, Seppä H, Bos J A A, Engels S, Väliranta M, Birks H J B, 2008.** Weichselian vegetation dynamics in the central area of the Scandinavian glaciations recorded in a long sediment sequence from Sokli (N-Finland). 33rd IGC congress. Oslo, 6–14 August 2008.
- Helmens K F, Engels S, Väliranta M, Bergman J, 2009a.** Environmental and climate conditions at Sokli (N Finland) during MIS 5d-c: first integration of multi-proxy evidence. 3rd NEPAL (Nordic Network of Palaeoclimatology) workshop. Bergen, Norway, 3–5 June 2009.
- Helmens K F, Risberg J, Jansson K N, Weckström J, Berntsson A, Kaislahti Tillman P, Johansson P W, Wastegård S, 2009b.** Early MIS 3 glacial lake evolution, ice-marginal retreat pattern and climate at Sokli (northeastern Fennoscandia). *Quaternary Science Reviews*, 28, pp 1880–1894.
- Helmens K F, Väliranta M, Engels S, Luoto T P, Self A, submitted.** Dramatic shifts in Early Glacial climate regimes recorded by multi-proxy data from the high latitude site Sokli (N Finland). XVIII INQUA congress. Bern, Switzerland, 20–27 July 2011.
- Hemming S R, 2004.** Heinrich events: massive late Pleistocene detritus layers of the North Atlantic and their global climate imprint. *Reviews of Geophysics*, 42, RG1005, doi:10.1029/2003RG000128.
- Henton J A, Craymer M R, Ferland R, Dragert H, Mazotti S, Forbes D L, 2006.** Crustal motion and deformation monitoring of the Canadian landmass. *Geomatica*, 60, pp 173–191.
- Hindmarsh R C A, Boulton G S, Hutter K, 1989.** Modes of operation of thermo-mechanically coupled ice sheets. *Annals of Glaciology*, 12, pp 57–69.
- Hock R, 1998.** Modelling of glacier melt and discharge. Zürich: Geographisches Institut ETH. (Zürcher Geographische Schriften 70)
- Hock R, 2005.** Glacier melt: a review of processes and their modelling. *Progress in Physical Geography*, 29, pp 362–391.
- Hock R, Jansson P, 2005.** Modelling glacier hydrology. In: Anderson M G, McDonnell J (eds). *Encyclopedia of hydrological sciences*. Chichester: John Wiley and Sons, vol 4, pp 2647–2655.
- Hock R, Jansson P, Braun L, 2005.** Modelling the response of mountain glacier discharge to climate warming. In: Huber U M, Bugmann H K M, Reasoner M A (eds). *Global change and mountain regions: an overview of current knowledge*. Dordrecht: Springer, pp 243–252.
- Hohl V, 2005.** Northern European long term climate archives. SKB TR-05-01, Svensk Kärnbränslehantering AB.
- Hohmann M, 1997.** Soil freezing – the concept of soil water potential. State of the art. *Cold Regions Science and Technology*, 25, pp 101–110.
- Holland D M, Thomas R H, de Young B, Ribergaard M H, Lyberth B, 2008.** Acceleration of Jakobshavn Isbræ triggered by warm subsurface ocean waters. *Nature Geoscience*, 1, pp 659–664.
- Holmlund P, Fastook J, 1995.** A time dependent glaciological model of the Weichselian ice sheet. *Quaternary International*, 27, pp 53–58.
- Holmlund P, Jansson P, 2003.** *Glaciologi* (in Swedish). Stockholm: Stockholm University and the Swedish Research Council.
- Hooke R LeB, 1977.** Basal temperatures in polar ice sheets: a qualitative review: *Quaternary Research*, 7, pp 1–13.
- Hooke R LeB, 1984.** On the role of mechanical energy in maintaining subglacial water conduits at atmospheric pressure. *Journal of Glaciology*, 30, pp 180–187.
- Hooke R LeB, 1989.** Englacial and subglacial hydrology: a qualitative review. *Arctic and Alpine Research*, 21, pp 221–233.
- Hooke R LeB, 1991.** Positive feedbacks associated with erosion of glacial cirques and overdeepenings. *Geological Society of America Bulletin*, 103, pp 1104–1108.
- Hooke R LeB, 2004.** *Principles of glacier mechanics*. Second edition. Cambridge: Cambridge University Press.

- Hooke R LeB, Lauman T, Kohler J, 1990.** Subglacial water pressures and the shape of subglacial conduits. *Journal of Glaciology*, 36, pp 67–71.
- Houmark-Nielsen M, 2009.** MIS 3 interstadial climate and rapid ice advances in the south-western Baltic. SKB P-09-10, Svensk Kärnbränslehantering AB.
- Houmark-Nielsen M, Kjær K H, 2003.** Southwest Scandinavia, 40–15 kyr BP: palaeogeography and environmental change. *Journal of Quaternary Science*, 18, pp 769–786.
- Howat I M, Joughin I, Tulaczyk S, Gogineni S, 2005.** Rapid retreat and acceleration of Helheim Glacier, east Greenland. *Geophysical Research Letters*, 32, L22502, doi:10.1029/2005GL024737.
- Howat I M, Joughin I, Scambos T A, 2007.** Rapid changes in ice discharge from Greenland outlet glaciers. *Science*, 315, pp 1559–1561.
- Howat I M, Joughin I, Fahnestock M, Smith B E, Scambos T A, 2008.** Synchronous retreat and acceleration of southeast Greenland outlet glaciers 2000-06: ice dynamics and coupling to climate. *Journal of Glaciology*, 54, pp 646–660.
- Hubbard B, Nienow P, 1997.** Alpine subglacial hydrology. *Quaternary Science Reviews*, 16, pp 939–955.
- Huber C, Leuenberger M, Spahni R, Flückiger J, Schwander J, Stocker T F, Johnsen S, Landais A, Jouzel J, 2006.** Isotope calibrated Greenland temperature record over Marine Isotope Stage 3 and its relation to CH₄. *Earth and Planetary Science Letters*, 243, pp 504–519.
- Humlum O, Houmark-Nielsen M, 1994.** High deglaciation rates in Denmark during the late Weichselian – implications for the palaeoenvironment. *Geografisk Tidsskrift*, 94, pp 26–37.
- Huybrechts P, 1986.** A three dimensional time-dependent numerical model for polar ice sheets: some basic testing with a stable and efficient finite difference scheme. Report 86-1, Geografisch Instituut, Vrije Universiteit Brussel, Belgium.
- Huybrechts P, 1990.** A 3D model for the Antarctic ice sheet: a sensitivity study on the glacial-interglacial contrast. *Climate Dynamics*, 5, pp 79–92.
- Huybrechts P, 2006.** Numerical modeling of ice sheets through time. In: Knight P G (ed). *Glacier science and environmental change*. Malden: Blackwell Publishing, pp 406–412.
- Huybrechts P, de Wolde J, 1999.** The dynamic response of the Greenland and Antarctic ice sheets to multiple-century climate warming. *Journal of Climate*, 12, pp 2169–2188.
- Huybrechts P, T'siobbel S, 1995.** Thermomechanical modelling of northern hemisphere ice sheets with a two-level mass-balance parameterization. *Annals of Glaciology*, 21, pp 111–116.
- Huybrechts P, Payne A J, EISMINT Intercomparison Group, 1996.** The EISMINT benchmarks for testing ice-sheet models. *Annals of Glaciology*, 23, pp 1–12.
- Huybrechts P, Gregory J, Janssens I, Wild M, 2004.** Modelling Antarctic and Greenland volume changes during the 20th and 21st centuries forced by GCM time slice integrations, *Global and Planetary Change*, 42, pp 83–105.
- Hökmark H, Lönnqvist M, Fälth B, 2010.** T-H-M issues in repository rock. Thermal, mechanical, thermo-mechanical and hydro-mechanical evolution of the rock at the Forsmark and Laxemar sites. SKB TR-10-23, Svensk Kärnbränslehantering AB.
- Hönisch B, Hemming N G, Archer D, Siddall D, Mcmanus J F, 2009.** Atmospheric carbon dioxide concentrations across the mid-Pleistocene transition. *Science*, 324, pp 1551–1554.
- Imbrie J, Boyle E A, Clemens S C, Duffy A, Howard W R, Kukla G, Kutzbach J, Martinson D G, McIntyre A, Mix A C, Molfino B, Morley J J, Peterson L C, Pisias N G, Imbrie J, Hays J D, Martinson D G, McIntyre A, Mix A C, Morley J J, Pisias N G, W L Prell, Shackleton N J, 1984.** The orbital theory of Pleistocene climate: support from a revised chronology of the marine $\delta^{18}\text{O}$ record. In: Berger A L, Imbrie J, Hays J D, Kukla G, Saltzman B (eds). *Milankovitch and climate: understanding the response to astronomical forcing*. Dordrecht: Reidel, pp 269–305.
- Imbrie J, Boyle E A, Clemens S C, Duffy A, Howard W R, Kukla G, Kutzbach J, Martinson D G, McIntyre A, Mix A C, Molfino B, Morley J J, Peterson L C, Pisias N G, Prell W L, Raymo M E, Shackleton N J, Toggweiler J R, 1992.** On the structure and origin of major glaciation cycles. 1. Linear responses to Milankovitch forcing. *Paleoceanography*, 7, pp 701–738.

- IPCC, 2001.** Climate change 2001: the scientific basis. Contribution of Working Group I to the third assessment report of the Intergovernmental Panel on Climate Change. New York: Cambridge University Press.
- IPCC, 2007.** Climate change 2007: the physical science basis. Contribution of Working Group I to the fourth assessment report of the Intergovernmental Panel on Climate Change. Cambridge: Cambridge University Press.
- Isaksen K, Holmlund P, Sollid J L, Harris C, 2001.** Three deep alpine-permafrost boreholes in Svalbard and Scandinavia. *Permafrost and Periglacial Processes*, 12, pp 13–26.
- Iverson N R, 1991.** Potential effects of of subglacial water-pressure fluctuations on quarrying. *Journal of Glaciology*, 37, pp 27–36.
- Iverson N R, 1993.** Regelation of ice through debris at glacier beds: implications for sediment transport. *Geology*, 21, pp 559–562.
- Iverson N R, 2000.** Sediment entrainment by a soft-bedded glacier: a model based on regelation into the bed. *Earth Surface Processes and Landforms*, 25, pp 881–893.
- Iverson N R, Hanson B, Hooke R LeB, Jansson P, 1995.** Flow mechanism of glaciers on soft beds. *Science*, 267, pp 80–81.
- Ivins E R, 2009.** Ice sheet stability and sea-level. *Science*, 324, pp 888–889.
- Jansen E, Sjøholm J, 1991.** Reconstruction of glaciation over the past 6 Myr from ice-borne deposits in the Norwegian Sea. *Nature*, 349, pp 600–603.
- Jansson P, 2010.** Ice sheet hydrology from observations. SKB TR-10-68, Svensk Kärnbränslehantering AB.
- Jansson P, Näslund J-O, 2009.** Spatial and temporal variations in glacier hydrology on Stor-glaciären, Sweden. SKB TR-09-13, Svensk Kärnbränslehantering AB.
- Jansson P, Hock R, Schneider T, 2003.** The concept of glacier storage: a review. *Journal of Hydrology*, 282, pp 116–129.
- Jansson P, Näslund J-O, Rodhe L, 2007.** Ice sheet hydrology – a review. TR-06-34, Svensk Kärnbränslehantering AB.
- Jaquet O, Siegel P, 2006.** Regional groundwater flow model for a glaciation scenario. Simpevarp subarea – version 1.2. SKB R-06-100, Svensk Kärnbränslehantering AB.
- Jaquet O, Namar R, Jansson P, 2010.** Groundwater flow modelling under ice sheet conditions: scoping calculations. SKB TR-10-46, Svensk Kärnbränslehantering AB.
- Johansson J M, Davis J L, Scherneck H-G, Milne G A, Vermeer M, Mitrovica J X, Bennett R A, Jonsson B, Elgered G, Elósegui P, Koivula H, Poutanen M, Rönnäng B O, Shapiro I I, 2002.** Continuous GPS measurements of postglacial adjustment in Fennoscandia. 1. Geodetic results. *Journal of Geophysical Research* 107, pp 400–428.
- Johansson P-O, 2008.** Description of surface hydrology and near-surface hydrogeology at Forsmark. Site descriptive modelling, SDM-Site Forsmark. SKB R-08-08, Svensk Kärnbränslehantering AB.
- Johnsen S J, Dahl-Jensen D, Dansgaard W, Gundestrup N, 1995.** Greenland palaeotemperatures derived from GRIP bore hole temperature and ice core isotope profiles. *Tellus*, 47B, pp 624–629.
- Johnsen S J, Dahl-Jensen D, Gundestrup N, Steffensen J P, Clausen H B, Miller H, Masson-Delmotte V, Sveinbjörnsdóttir A E, White J, 2001.** Oxygen isotope and palaeotemperature records from six Greenland ice-core stations: Camp Century, Dye-3, GRIP, GISP2, Renland and NorthGRIP. *Journal of Quaternary Science*, 16, pp 299–307.
- Johnson J, 1994.** A basal water model for ice sheets. Ph. D. thesis. University of Minnesota.
- Johnson J, 2004.** Estimating basal melt rate in Antarctica. International Symposium on Ice and Water Interactions: processes across the phase boundary. Portland, Oregon, 26–30 July 2004.
- Johnston, P, 1993.** The effect of spatially non-uniform water loads on predictions of sea-level change. *Geophysical Journal International*, 114, pp 615–634.
- Jol A, Šťastný P, Raes F, Lavallo C, Menne B, Wolf T, 2008.** Impacts of Europe’s changing climate: 2008 indicator-based assessment. EEA report 4/2008. Copenhagen: European Environment Agency.

- Joughin I, Tulaczyk S, 2002.** Positive mass balance for the Ross Ice Streams, West Antarctica. *Science*, 295, pp 476–480.
- Joughin I, Tulaczyk S, Fahnestock M, Kwok R, 1996.** A mini-surge on the Ryder Glacier, Greenland, observed by satellite radar interferometry. *Science*, 274, pp 228–230.
- Joughin I, Abdalati W, Fahnestock M, 2004.** Large fluctuations in speed on Greenland's Jakobshavn Isbræ glacier. *Nature*, 432, pp 608–610.
- Joughin I, Das S B, King M A, Smith B E, Howat I M, Moon T, 2008.** Seasonal speedup along the western flank of the Greenland Ice Sheet. *Science*, 320, pp 781–783.
- Joussaume S, Taylor K E, 2000.** The paleoclimate modeling intercomparison project. In: Braconnot P (ed). *Proceedings of the third Paleoclimate Modelling Intercomparison Project (PMIP) workshop*. La Huardière, Canada, 4–8 October 1999. (WCRP-111, WMO/TD-1007)
- Jouzel J, Stievenard M, Johnsen S J, Landais A, Masson-Delmotte V, Sveinbjornsdottir A, Vimeux F, von Grafenstein U, White J W C, 2007.** The GRIP deuterium-excess record. *Quaternary Science Reviews*, 26, pp 1–17.
- Joyce S, Simpson T, Hartley L, Applegate D, Hoek J, Swan D, Marsic N, Follin S, 2010.** Ground-water flow modelling of periods with temperate climate conditions – SR-Site Forsmark. SKB R-09-20, Svensk Kärnbränslehantering AB.
- Kageyama M, Laîné A, Abe-Ouchi A, Braconnot P, Cortijo E, Crucifix M, de Vernal A, Guiot J, Hewitt C D, Kitoh A, Kucera M, Marti O, Ohgaito R, Otto-Bliesner B, Peltier W R, Rosell-Melé A, Vettoretti G, Weber S L, Yu Y, MARGO project members, 2006.** Last Glacial Maximum temperatures over the North Atlantic, Europe and western Siberia: a comparison between PMIP models, MARGO sea-surface temperatures and pollen-based reconstructions. *Quaternary Science Reviews*, 25, pp 2082–2102.
- Kahr G, Kraehenbuehl F, Stoeckli H F, Müller-Vonmoos M, 1990.** Study of the water-bentonite system by vapour adsorption, immersion calorimetry and X-ray techniques: II. Heats of immersion, swelling pressures and thermodynamic properties. *Clay Minerals*, 25, pp 499–506.
- Kaislahti-Tillman P, Berntsson A, Risberg J, Helmens K F, Jansson K, 2007.** Diatom stratigraphy of the MIS 3 deposit at Sokli, Northern Finland. *Nordic Diatomists Meeting*. Lillehammer, Norway, 11–14 May 2007.
- Kamb B, 1987.** Glacier surge mechanism based on linked cavity configuration of the basal water conduit system. *Journal of Geophysical Research*, 92, pp 9083–9100.
- Kamb B, 2001.** Basal zone of the West-Antarctic ice streams and its role in their rapid motion. In: Alley R B, Bindschadler R A (eds). *The West Antarctic ice sheet: behavior and environment*. Washington D.C.: American Geophysical Union, pp 157–200.
- Kamb B, Echelmeyer K A, 1986.** Stress-gradient coupling in glacier flow: IV. Effects of the “T” term. *Journal of Glaciology*, 32, pp 342–349.
- Kapitsa A P, Ridley J K, Robin G de Q, Siegert M J, Zotikov I A, 1996.** A large deep freshwater lake beneath the ice of central East Antarctica. *Nature*, 381, pp 684–686.
- Karnland O, Olsson S, Nilsson U, 2006.** Mineralogy and sealing properties of various bentonites and smectite-rich clay materials. SKB TR-06-30, Svensk Kärnbränslehantering AB.
- Karnland O, Olsson S, Dueck A, Birgersson M, Nilsson U, Hernan-Håkansson T, Pedersen K, Nilsson S, Eriksen T E, Rosborg B, 2009.** Long term test of buffer material at the Äspö Hard Rock Laboratory, LOT Project. Final report on the A2 test parcel. SKB TR-09-29, Svensk Kärnbränslehantering AB.
- Karunaratne K C, Burn C R, 2004.** Relations between air and surface temperature in discontinuous permafrost terrain near Mayo, Yukon Territory. *Canadian Journal of Earth Sciences*, 41, pp 1437–1451.
- Kaufmann G, Lambeck K, 2002.** Glacial isostatic adjustment and the radial viscosity profile from inverse modeling. *Journal of Geophysical Research*, 107, 2280, doi:10.1029/2001JB000941.
- Kaufmann G, Wu P, 1998.** Lateral asthenospheric viscosity variations and postglacial rebound: a case study for the Barents Sea. *Geophysical Research Letters*, 25, pp 1963–1966.

- Kaufmann G, Wu P, 2002.** Glacial isostatic adjustment in Fennoscandia with a three-dimensional viscosity structure as an inverse problem. *Earth and Planetary Science Letters*, 197, pp 1–10.
- Kaufmann G, Wu P, Li G Y, 2000.** Glacial isostatic adjustment in Fennoscandia for a laterally heterogeneous earth. *Geophysical Journal International*, 143, pp 262–273.
- Kendall R A, Mitrovica J X, Milne G A, 2005.** On post-glacial sea level – II. Numerical formulation and comparative results on spherically symmetric models. *Geophysical Journal International*, 161, pp 679–706.
- Kim S-J, Crowley T J, Erickson D J, Govindasamy B, Duffy P B, Lee B Y, 2008.** High-resolution climate simulation of the last glacial maximum. *Climate Dynamics*, 31, pp 1–16.
- King L, 1984.** Permafrost in Skandinavien: Untersuchungsergebnisse aus Lappland, Jotunheimen und Dovre/Rondane. Heidelberg: Geographisches Institut der Univ. (Heidelberger geographische Arbeiten 76)
- King-Clayton L (ed), Chapman N, Ericsson L O, Kautsky F, 1997.** Glaciation and hydrogeology, Proceedings of the workshop on the impact of climatic change and glaciations on rock stresses, groundwater flow and hydrochemistry: past, present and future. Hässelby, Sweden, 17–19 April 1996. SKI Report 97:13, Statens kärnkraftinspektion (Swedish Nuclear Power Inspectorate).
- Kjellström E, Brandefelt J, Strandberg G, Smith B, Wohlfarth B, Näslund J-O, 2008.** Global and regional climate model simulations of extreme climate conditions in Sweden in a 100,000 year perspective. EGU2008-A-02249. Abstracts of the contributions of the EGU General Assembly 2008. *Geophysical Research Abstracts*, 10.
- Kjellström E, Brandefelt J, Strandberg G, Smith B, Wohlfarth B, Näslund J-O, 2009a.** Global and regional climate model simulations of extreme climate conditions in Sweden in a 100,000 year perspective. UN Climate Change Conference March 2009, Copenhagen. Theme 1: Exploring the risks: understanding climate change. Session: Informing the future by understanding the past.
- Kjellström E, Strandberg G, Brandefelt J, Näslund J-O, Smith B, Wohlfarth B, 2009b.** Climate conditions in Sweden in a 100,000-year time perspective. SKB TR-09-04, Svensk Kärnbränslehantering AB.
- Kjellström E, Brandefelt J, Näslund J-O, Smith B, Strandberg G, Voelker A H L, Wohlfarth B, 2010a.** Simulated climate conditions in Europe during a Marine Isotope Stage 3 stadial. *Boreas*, 39, pp 436–456.
- Kjellström E, Nikulin G, Hansson U, Strandberg G, Ullerstig A, 2010b.** 21st century changes in the European climate: uncertainties derived from an ensemble of regional climate model simulations. *Tellus A*, doi: 10.1111/j.1600-0870.2010.00475.x.
- Kleman J, 1994.** Preservation of landforms under ice sheets and ice caps. *Geomorphology*, 9, pp 19–32.
- Kleman J, Glasser N F, 2007.** The subglacial thermal organisation (STO) of ice sheets. *Quaternary Science Reviews*, 26, pp 585–597.
- Kleman J, Hättstrand C, 1999.** Frozen-based Fennoscandian and Laurentide ice sheets during the last glacial maximum. *Nature*, 402, pp 63–66.
- Kleman J, Stroeven A P, 1997.** Preglacial surface remnants and Quaternary glacial regimes in north-western Sweden. *Geomorphology*, 19, pp 35–54.
- Kleman J, Hättstrand C, Borgström I, Stroeven A, 1997.** Fennoscandian palaeoglaciology reconstructed using a glacial geological inversion model. *Journal of Glaciology*, 43, pp 283–299.
- Kleman J, Stroeven A, Lundqvist J, 2008.** Patterns of Quaternary ice sheet erosion and deposition in Fennoscandia and a theoretical framework for explanation. *Geomorphology*, 97, pp 73–90.
- Klene A E, Nelson F E, Shiklomanov N I, Hinkel K M, 2001.** The N-factor in natural landscapes: Variability of air and soil-surface temperatures, Kuparuk River Basin, Alaska. *Arctic, Antarctic, and Alpine Research*, 33, pp 140–148.
- Kohler J, 1995.** Determining the extent of pressurized flow beneath Storglaciären, Sweden, using results of tracer experiments and measurements of input and output discharge. *Journal of Glaciology*, 41, pp 217–231.

- Koppes M N, Montgomery D R, 2009.** The relative efficacy of fluvial and glacial erosion over modern to orogenic timescales. *Nature Geoscience*, 2, pp 644–647.
- Krabill W, Abdalati W, Frederick E, Manizade S, Martin C, Sonntag J, Swift R, Thomas R, Wright W, Yungel J, 2000.** Greenland ice sheet: high elevation balance and peripheral thinning. *Science*, 289, pp 428–430.
- Krawczynski M J, Behn M D, Das S B, Joughin I, 2009.** Constraints on the lake volume required for hydro-fracture through ice sheets. *Geophysical Research Letters*, 36, L10501, doi:10.1029/2008GL036765.
- Krinner G, Genthon C, Jouzel J, 1997.** GCM analysis of local influence on ice core δ signals. *Geophysical Research Letters*, 24, pp 2825–2828.
- Krogh Andersen K, Svensson A, Rasmussen S O, Steffensen J P, Johnsen S, Bigler M, Röthlisberger R, Ruth U, Siggaard-Andersen M-L, Dahl-Jensen D, Vinther B M, Clausen H B, 2006.** The Greenland ice core chronology 2005, 15–42 kyr. Part 1: constructing the time scale. *Quaternary Science Reviews*, 25, pp 3246–3257.
- Kukkonen, I, 1989.** Terrestrial heat flow and radiogenic heat production in Finland, the central Baltic Shield. *Tectonophysics*, 164, pp 219–230.
- Kukkonen I T, Šafanda J, 2001.** Numerical modelling of permafrost in bedrock in northern Fennoscandia during the Holocene. *Global and Planetary Change*, 29, pp 259–274.
- Lachenbruch A H, 1968.** Preliminary geothermal model of the Sierra Nevada. *Journal of Geophysical Research*, 73, pp 6977–6989.
- Lagerbäck R, 1988a.** The Veiki moraines in northern Sweden – widespread evidence of an Early Weichselian deglaciation. *Boreas*, 17, pp 469–486.
- Lagerbäck R, 1988b.** Periglacial phenomena in the wooded areas of northern Sweden – relicts from the Tarendö Interstadial. *Boreas*, 17, pp 487–499.
- Lagerbäck R, Robertsson A-M, 1988.** Kettle holes – stratigraphical archives for Weichselian geology and palaeoenvironment in northernmost Sweden. *Boreas*, 17, pp 439–468.
- Lagerlund E, Persson K M, Krzyszkowski D, Johansson P, Dobracka E, Dobracki R, Panzig W-A, 1995.** Unexpected ice flow directions during the Late Weichselian deglaciation of the South Baltic area indicated by a new lithostratigraphy in NW Poland and NE Germany. *Quaternary International*, 28, pp 127–144.
- Lambeck K, 1995.** Late Devensian and Holocene shorelines of the British Isles and North Sea from models of glacio-hydroisostatic rebound. *Journal of the Geological Society*, 152, pp 437–448.
- Lambeck K, 1999.** Shoreline displacements in southern-central Sweden and the evolution of the Baltic Sea since the last maximum glaciation. *Journal of the Geological Society*, 156, pp 465–486.
- Lambeck K, Chappell J, 2001.** Sea level change through the last glacial cycle. *Science*, 292, pp 679–686.
- Lambeck K, Nakada M, 1990.** Late Pleistocene and Holocene sea-level change along the Australian coast. *Palaeogeography, Palaeoclimatology, Palaeoecology*, 89, pp 143–176.
- Lambeck K, Smither C, Johnston P, 1998.** Sea-level change, glacial rebound and mantle viscosity for northern Europe. *Geophysical Journal International*, 134, pp 102–144.
- Lambeck K, Yokoyama Y, Purcell T, 2002.** Into and out of the Last Glacial Maximum: sea-level change during Oxygen Isotope Stages 3 and 2. *Quaternary Science Reviews*, 21, pp 343–360.
- Lambeck K, Purcell A, Funder S, Kjær K H, Larsen E, Möller P, 2006.** Constraints on the Late Saalian to early Middle Weichselian ice sheet of Eurasia from field data and rebound modelling. *Boreas*, 35, pp 539–575.
- Lambeck K, Purcell A, Zhao J, Svensson N-O, 2010.** The Scandinavian Ice Sheet: from MIS 4 to the end of the Last Glacial Maximum. *Boreas*, 39, pp 410–435.
- Lambert A, Courtier N, Sasagawa G S, Klopping F, Winester D, James T S, Liard J O, 2001.** New constraints on Laurentide postglacial rebound from absolute gravity measurements. *Geophysical Research Letters*, 28, pp 2109–2112.

- Landström O, Larsson, S Å, Lind G, Malmqvist D, 1979.** Geothermal investigations in the Bohus granite area in southwestern Sweden. *Tectonophysics*, 64, pp 131–162.
- Lang H, 1987.** Forecasting meltwater runoff from snow-covered areas and from glacier basins. In: Kraijenhoff D A, Moll J R (eds). *River flow modelling and forecasting*. Dordrecht: D. Reidel, pp 99–127.
- Lang C, Leuenberger M, Schwander J, Johnsen S, 1999.** 16°C rapid temperature variation in central Greenland 70,000 years ago. *Science*, 286, pp 934–937.
- Latychev K, Mitrovica J X, Tamisiea M E, Tromp J, Moucha R, 2005a.** Influence of lithospheric thickness variations on 3D crustal velocities due to glacial isostatic adjustment. *Geophysical Research Letters*, 32, L01304, doi:10.1029/2004GL021454.
- Latychev K, Mitrovica J X, Tromp J, Tamisiea M E, Komatitsch D, Christara C C, 2005b.** Glacial isostatic adjustment on 3D Earth models: a finite-volume formulation. *Geophysical Journal International*, 161, pp 421–444.
- Lemieux J-M, Sudicky E A, Peltier W R, Tarasov L, 2008a.** Dynamics and groundwater recharge and seepage over the Canadian landscape during the Wisconsinian glaciation. *Journal of Geophysical Research*, 113, F01011, doi:10.1029/2007JF000838.
- Lemieux J-M, Sudicky E A, Peltier W R, Tarasov L, 2008b.** Simulating the impact of glaciations on continental groundwater flow systems: 1. Relevant processes and model formulation. *Journal of Geophysical Research*, 113, F03017, doi:10.1029/2007JF000928.
- Lemieux J-M, Sudicky E A, Peltier W R, Tarasov L, 2008c.** Simulating the impact of glaciations on continental groundwater flow systems: 2. Model application to the Wisconsinian glaciation over the Canadian landscape. *Journal of Geophysical Research* 113, F03018, doi:10.1029/2007JF000929.
- Lenton T M, Britton C, 2006.** Enhanced carbonate and silicate weathering accelerates recovery from fossil fuel CO₂ perturbations. *Global Biogeochemical Cycles*, 20, GB3009, doi:10.1029/2005GB002678.
- Lenton T M, Williamson M S, Edwards N R, Marsh R, Price A R, Ridgwell A J, Shepherd J G, Cox S J, The GENIE team, 2006.** Millennial timescale carbon cycle and climate change in an efficient Earth system model. *Climate Dynamics*, 26, pp 687–711.
- Lewis A R, Marchant D R, Kowalewski D E, Baldwin S L, Webb L E, 2006.** The age and origin of the labyrinth, western Dry Valleys, Antarctica: evidence for extensive middle Miocene subglacial floods and freshwater discharge to the Southern Ocean. *Geology*, 34, pp 513–516.
- Lidberg M, 2007.** Geodetic reference frames in presence of crustal deformations. Ph.D. thesis. Department of Radio and Space Science, Chalmers University of Technology.
- Lide D R (ed), 1999.** CRC handbook of chemistry and physics: a ready-reference book of chemical and physical data. 80th ed. Cleveland, Ohio: CRC Press.
- Lidmar-Bergström K, 1995.** Relief and saprolites through time on the Baltic shield. *Geomorphology*, 12, pp 45–61.
- Lidmar-Bergström K, 1997.** A long-term perspective on glacial erosion. *Earth Surface Processes and Landforms*, 22, pp 297–306.
- Lidmar-Bergström K, Näslund J-O, 2002.** Landforms and uplift in Scandinavia. In: Doré A G, Cartwright J A, Stoker M S, Turner J P, White N (eds). *Exhumation of the North Atlantic margin: timing, mechanisms, and implications for petroleum exploration*. London: Geological Society. (Special publication 196), pp 103–116.
- Lidmar-Bergström K, Näslund J-O, 2005.** Major landforms and bedrock. In: Seppälä M (ed). *The physical geography of Fennoscandia*, Oxford: Oxford University Press.
- Lidmar-Bergström K, Olsson S, Olvmo M, 1997.** Palaeosurfaces and associated saprolites in southern Sweden. In: Widdowson M (ed). *Palaeosurfaces: recognition, reconstruction and palaeoenvironmental interpretation*. London: Geological Society. (Special publication 120), pp 95–124.
- Lind P, Kjellström E, 2008.** Temperature and precipitation changes in Sweden: a wide range of model-based projections for the 21st century. Norrköping: Sveriges meteorologiska och hydrologiska institut (Swedish Meteorological and Hydrological Institute). (SMHI reports. Meteorology and Climatology 113)

- Lisiecki L E, Raymo M E, 2005.** A Pliocene-Pleistocene stack of 57 globally distributed benthic $\delta^{18}\text{O}$ records. *Paleoceanography*, 20, pp 1–17.
- Lockwood J G, 1979.** Causes of climate. Edward Arnold, London.
- Lohmann U, Sausen R, Bengtsson L, Cubasch U, Perlwitz J, Roeckner E, 1993.** The Köppen climate classification as a diagnostic tool for general circulation models. *Climate Research*, 3, pp 177–193.
- Lokrantz H, Sohlenius G, 2006.** Ice-marginal fluctuations during the Weichselian glaciation in Fennoscandia, a literature review. SKB TR-06-36, Svensk Kärnbränslehantering AB.
- Loutre M F, Berger A, 2000.** Future climatic changes: are we entering an exceptionally long interglacial? *Climatic Change*, 46, pp 61–90.
- Luckman A, Murray T, de Lange R, Hanna E, 2006.** Rapid and synchronous ice-dynamic changes in East Greenland. *Geophysical Research Letters*, 33, L03503, doi:10.1029/2005GL025428.
- Lunardini V J, 1978.** Theory of n-factors and correlation of data. In: Proceedings of the 3rd International Conference on Permafrost. Edmonton, Alta, 10–13 July 1978. Ottawa: National Research Council of Canada, vol 1, pp 40–46.
- Lunardini V J, 1981.** Heat transfer in cold climates. New York: Van Nostrand Reinhold.
- Lunardini V J, 1995.** Permafrost formation time. CRREL Report 95-8, U.S. Army Cold Regions Research and Engineering Laboratory.
- Lund B, Näslund J-O, 2009.** Glacial isostatic adjustment: implications for glacially induced faulting and nuclear waste repositories. In: Connor C B, Chapman N A, Connor L J (eds). Volcanic and tectonic hazard assessment for nuclear facilities. Cambridge: Cambridge University Press, pp 142–155.
- Lund B, Schmidt P, Hieronymus C, 2009.** Stress evolution and fault stability during the Weichselian glacial cycle. SKB TR-09-15, Svensk Kärnbränslehantering AB.
- Lundqvist J, 1992.** Glacial stratigraphy in Sweden. Geological Survey of Finland Special Paper, 5, pp 43–59.
- Lundqvist J, 2007.** Surging ice and break-down of an ice dome – a deglaciation model for the Gulf of Bothnia. *Geologiska Föreningens i Stockholm Förhandlingar*, 129, pp 329–336.
- Lundqvist J, Wohlfarth B, 2000.** Timing and east-west correlation of south Swedish ice-marginal lines during the Late Weichselian. *Quaternary Science Reviews*, 20, pp 1127–1148.
- Lunkka J P, Johansson P, Saarnisto M, Sallasmaa O, 2004.** Glaciation of Finland. In: Ehlers J, Gibbard P L (eds). Quaternary glaciations: extent and chronology. Part I: Europe. Amsterdam: Elsevier. (Developments in Quaternary Science 2), pp 93–100.
- Lunt D J, Foster G L, Haywood A M, Stone E J, 2008.** Late Pliocene Greenland glaciation controlled by a decline in atmospheric CO_2 levels. *Nature*, 454, pp 1102–1105.
- Lunt D J, Haywood A M, Foster G L, Stone E J, 2009.** The Arctic cryosphere in the Mid-Pliocene and the future. *Philosophical Transactions of the Royal Society A: Mathematical, Physical and Engineering Sciences*, 367, pp 49–67.
- Luthcke S B, Zwally H J, Abdalati W, Rowlands D D, Ray R D, Nerem R S, Lemoine F G, McCarthy J J, Chinn D S, 2006.** Recent Greenland ice mass loss by drainage system from satellite gravity observations. *Science*, 314, pp 1286–1289.
- Lythe M B, Vaughan D G, the BEDMAP Consortium, 2001.** BEDMAP: a new ice thickness and subglacial topographic model of Antarctica. *Journal of Geophysical Research*, 106, pp 11335–11351.
- Löfgren A (ed), 2010.** The terrestrial ecosystems at Forsmark and Laxemar-Simpevarp. SKB TR-10-01, Svensk Kärnbränslehantering AB.
- Lönnqvist M, Hökmark H, 2010.** Assessment of potential for glacially induced hydraulic jacking at different depths. SKB R-09-35, Svensk Kärnbränslehantering AB.
- Mackay J R, 1997.** A full-scale field experiment (1978–1995) on the growth of permafrost by means of lake drainage, western Arctic coast: a discussion of the method and some results. *Canadian Journal of Earth Sciences*, 34, pp 17–33.

- Mai H, Thomsen T, 1993.** Permafrost studies in Greenland. In: Proceedings of the sixth international conference on permafrost. Beijing, 5–9 July 1993. Guangzhou: South China University of Technology, vol 2.
- Malmqvist D, Larson S Å, Landström O, Lind G, 1983.** Heat flow and heat production from the Malingsbo granite, central Sweden. *Bulletin of the Geological Institutions of the University of Uppsala*, 9, pp 137–152.
- Mangerud J, Gyllencreutz R, Øystein L, Svendsen J I, 2011.** Glacial history of Norway. In: Ehlers J, Gibbard P L (eds). *Quaternary glaciations: extent and chronology. Part IV: a closer look.* Amsterdam: Elsevier.
- Marchant D R, Denton G H, Sugden D E, Swisher C C, 1993.** Miocene glacial stratigraphy and landscape evolution of the western Asgard Range, Antarctica. *Geografiska Annaler*, 75A, pp 303–330.
- Marshall S J, Clarke G K C, 1997.** A continuum mixture model of ice stream thermodynamics in the Laurentide Ice Sheet. 1. Theory. *Journal of Geophysical Research*, 102, pp 20599–20614.
- Marks L, 2002.** Last Glacial Maximum in Poland. *Quaternary Science Reviews*, 21, pp 103–110.
- Masson-Delmotte M, Jouzel J, Landais A, Stievenard M, Johnsen S J, White J W C, Werner M, Sveinbjörnsdóttir A, Fuhrer K, 2005.** GRIP deuterium excess reveals rapid and orbital-scale changes in Greenland moisture origin. *Science*, 309, pp 118–121.
- McConnell R K, 1968.** Viscosity of the mantle from relaxation time spectra of isostatic adjustment. *Journal of Geophysical Research*, 73, pp 7089–7105.
- McIntyre K, Delaney M L, Ravelo A C, 2001.** Millennial-scale climate change and oceanic processes in the late Pliocene and early Pleistocene. *Paleoceanography*, 16, pp 535–543.
- Meehl G A, Stocker T F, Collins W D, Friedlingstein P, Gaye A T, Gregory J M, Kitoh A, Knutti R, Murphy J M, Noda A, Raper S C B, Watterson I G, Weaver A J, Zhao Z-C, 2007.** Global climate projections. In: IPCC, 2007. *Climate change 2007: the physical science basis. Contribution of Working Group I to the fourth assessment report of the Intergovernmental Panel on Climate Change.* Cambridge: Cambridge University Press.
- Meese D A, Gow A J, Alley R B, Zielinski G A, Grootes P M, Ram M, Taylor K C, Mayewski P A, Bolzan J F, 1997.** The Greenland Ice Sheet Project 2 depth-age scale: methods and results. *Journal of Geophysical Research*, 102, pp 26411–26423.
- Meier M F, Dyurgerov M B, Rick U K, O’Neel S, Pfeffer W T, Anderson R S, Anderson S P, Glazovsky A F, 2007.** Glaciers dominate eustatic sea-level rise in the 21st century. *Science*, 317, pp 1064–1067.
- Mernild S H, Liston G E, Hiemstra C A, Steffen C, Hanna E, Christensen J H, 2009.** Greenland ice sheet surface mass-balance modelling and freshwater flux for 2007, and in a 1995–2007 perspective. *Hydrological Processes*, 23, pp 2470–2484.
- Miljövärdberedningen, 2007.** Vetenskapligt underlag för klimatpolitiken: rapport från vetenskapliga rådet för klimatfrågor (in Swedish). Stockholm: Miljövärdberedningen. (Miljövärdberedningens rapport 2007:03).
- Milne G A, 1998.** Refining models of the glacial isostatic adjustment process. Ph. D. thesis. University of Toronto.
- Milne G A, Mitrovica J X, 1998.** Postglacial sea-level change on a rotating Earth. *Geophysical Journal International*, 133, pp 1–19.
- Milne G A, Mitrovica J X, Davis J L, 1999.** Near-field hydro-isostasy: the implementation of a revised sea-level equation. *Geophysical Journal International*, 139, pp 464–482.
- Milne G A, Davis J L, Mitrovica J X, Scherneck H-G, Johansson J M, Vermeer M, Koivula H, 2001.** Space-geodetic constraints on glacial isostatic adjustment in Fennoscandia. *Science*, 291, pp 2381–2385.
- Milne G A, Mitrovica J X, Schrag D P, 2002.** Estimating past continental ice volume from sea-level data. *Quaternary Science Reviews*, 21, pp 361–376.

- Milne G A, Mitrovica J X, Scherneck H G, Davis J L, Johansson J M, Koivula H, Vermeer M, 2004.** Continuous GPS measurements of postglacial adjustment in Fennoscandia: 2. Modeling results. *Journal of Geophysical Research*, 109, B02412, doi:10.1029/2003JB002619.
- Milne, G A, Gehrels W R, Hughes C W, Tamisiea M E, 2009.** Identifying the causes of sea-level change. *Nature Geoscience*, 2, pp 471–478.
- Ministry of the Environment, 2001.** Sweden's third national communication on Climate Change: under the United Nations Framework Convention on Climate Change. Stockholm: Ministry of the Environment. (Ds 2001:71)
- Mitrovica J X, 2003.** Recent controversies in predicting post-glacial sea-level change. *Quaternary Science Reviews*, 22, pp 127–133.
- Mitrovica J X, Forte A M, 1997.** Radial profile of mantle viscosity: results from the joint inversion of convection and postglacial rebound observables. *Journal of Geophysical Research*, 102, pp 2751–2769.
- Mitrovica J X, Forte A M, 2004.** A new inference of mantle viscosity based upon joint inversion of convection and glacial isostatic adjustment data. *Earth and Planetary Science Letters*, 225, pp 177–189.
- Mitrovica J X, Milne G A, 2002.** On the origin of late Holocene sea-level highstands within equatorial ocean basins. *Quaternary Science Reviews*, 21, pp 2179–2190.
- Mitrovica J X, Milne G A, 2003.** On post-glacial sea level: I. General theory. *Geophysical Journal International*, 154, pp 253–267.
- Mitrovica J X, Peltier W R, 1991.** On post-glacial geoid subsidence over the equatorial oceans. *Journal of Geophysical Research*, 96, pp 20053–20071.
- Mitrovica J X, Davis J L, Shapiro I I, 1994.** A spectral formalism for computing three-dimensional deformations due to surface loads. 2. Present-day glacial isostatic-adjustment. *Journal of Geophysical Research*, 99, pp 7075–7101.
- Mitrovica J X, Milne G A, Davis J L, 2001a.** Glacial isostatic adjustment on a rotating earth. *Geophysical Journal International*, 147, pp 562–579.
- Mitrovica J X, Tamisiea M E, Davis J L, Milne G A, 2001b.** Recent mass balance of polar ice sheets inferred from patterns of global sea-level change. *Nature* 409, pp 1026–1029.
- Mitrovica J X, Wahr J, Matsuyama I, Paulson A, 2005.** The rotational stability of an ice-age Earth. *Geophysical Journal International*, 161, pp 491–506.
- Mitrovica J X, Gomez N, Clark P U, 2009.** The sea-level fingerprint of West Antarctic Collapse. *Science*, 323, p 753.
- Moberg A, Sonechkin D M, Holmgren K, Datsenko N M, Karlén W, 2005.** Highly variable Northern Hemisphere temperatures reconstructed from low- and high-resolution proxy data. *Nature*, 433, pp 613–617.
- Moberg A, Gouirand I, Wohlfarth B, Schoning K, Kjellström E, Rummukainen M, de Jong R, Linderholm H, Zorita E, 2006.** Climate in Sweden during the past millennium – Evidence from proxy data, instrumental data and model simulations. SKB TR-06-35, Svensk Kärnbränslehantering AB.
- Montagnat M, Duval P, 2000.** Rate controlling processes in the creep of polar ice, influence of grain boundary migration associated with recrystallization. *Earth and Planetary Science Letters*, 183, pp 179–186.
- Montenegro A, Brovkin V, Eby M, Archer D, Weaver A J, 2007.** Long term fate of anthropogenic carbon. *Geophysical Research Letters*, 34, L19707, doi:10.1029/2007GL030905.
- Moon T, Joughin I, 2007.** Changes in ice front position on Greenland's outlet glaciers from 1992 to 2007. *Journal of Geophysical Research*, 113, F02022, doi:10.1029/2007JF000927.
- Munro-Stasiuk M J, 2003.** Subglacial Lake McGregor, south-central Alberta, Canada. *Sedimentary Geology*, 160, pp 325–350.
- Müller F, 1962.** Zonation in the accumulation area of the glaciers of Axel Heiberg Island, N.W.T, Canada. *Journal of Glaciology*, 4, pp 302–313.
- Müller U C, Pross J, 2007.** Lesson from the past: present insolation minimum holds potential for glacial inception. *Quaternary Science Reviews*, 26, pp 3025–3029.

- Mäkinen J, Engfeldt A, Harsson B G, Routsalainen H, Strykowski G, Oja T, Wolf D, 2005.** The Fennoscandian land uplift gravity lines 1966–2003. In: Jekeli C, Bastos L, Fernandes J (eds). Gravity, geoid and space missions. Berlin: Springer. (International Association of Geodesy symposia 129), pp 328–332.
- Mörner N-A, 1977.** Past and present uplift in Sweden: glacial isostasy, tectonism and bedrock influence. *Geologiska föreningen i Stockholms förhandlingar*, 99, pp 48–54.
- Mörner N-A, 1979.** The Fennoscandian uplift and Late Cenozoic geodynamics: geological evidence. *GeoJournal*, 3, pp 287–318.
- Naish T, Powell R, Levy R, Wilson G, Scherer R, Talarico F, Krissek L, Niessen F, Pompilio M, Wilson T, Carter L, DeConto R, Huybers P, McKay R, Pollard D, Ross J, Winter D, Barrett P, Browne G, Cody R, Cowan E, Crampton J, Dunbar G, Dunbar N, Florindo F, Gebhardt C, Graham I, Hannah M, Hansaraj D, Harwood D, Helling D, Henrys S, Hinnov L, Kuhn G, Kyle P, Läufer A, Maffioli P, Magens D, Mandernack K, McIntosh W, Millan C, Morin R, Ohneiser C, Paulsen T, Persico D, Raine I, Reed J, Riesselman C, Sagnotti L, Schmitt D, Sjunneskog C, Strong P, Taviani M, Vogel S, Wilch T, Williams T, 2009.** Obliquity-paced Pliocene West Antarctic ice sheet oscillations. *Nature*, 458, pp 322–328.
- Nakada M, Lambeck K, 1989.** Late Pleistocene and Holocene sea-level change in the Australian region and mantle rheology. *Geophysical Journal International*, 96, pp 497–517.
- Nakićenović N, Swart R (eds), 2000.** Special report on emissions scenarios. A Special Report of Working Group III of the Intergovernmental Panel on Climate Change. Cambridge: Cambridge University Press.
- Nerheim S, 2008.** Extrema vattenstånd för ett högt klimatscenario perioden 2071–2100 för Forsmark och Oskarshamn. SMHI rapport 2008–80. 5 sid.
- Nienow P, Sharp M, Willis I, 1998.** Seasonal changes in the morphology of the subglacial drainage system, Haut Glacier d’Arolla, Switzerland. *Earth Surface Processes and Landforms*, 23, pp 825–843.
- NorthGRIP community members, 2004.** High-resolution record of the Northern Hemisphere climate extending into the last interglacial period. *Nature*, 431, pp 147–151.
- NSF, 2000.** GEO 2000 Full Report. NSF 00-27, National Science Foundation.
- Nye J F, 1976.** Water flow in glaciers: jökulhlaups, tunnels and veins. *Journal of Glaciology*, 17, pp 181–207.
- Näslund J-O, 1997.** Subglacial preservation of valley morphology at Amundsenisen, western Dronning Maud Land, Antarctica. *Earth Surface Processes and Landforms*, 22, pp 441–455.
- Näslund J-O, 1998.** Ice sheet, climate, and landscape interactions in Dronning Maud Land, Antarctica. Ph. D. thesis. Department of Physical Geography, Stockholm University. (Dissertation series 11)
- Näslund J-O, 2001.** Landscape development in western and central Dronning Maud Land, East Antarctica. *Antarctic Science*, 13, pp 302–311.
- Näslund J-O, Fastook J L, Holmlund P, 2000.** Numerical modelling of the ice sheet in western Dronning Maud Land, East Antarctica: impact of present, past, and future climates. *Journal of Glaciology*, 46, pp 54–66.
- Näslund J-O, Rodhe L, Fastook J L, Holmlund P, 2003.** New ways of studying ice sheet flow directions and glacial erosion by computer modelling – examples from Fennoscandia. *Quaternary Science Reviews*, 22, pp 245–258.
- Näslund J-O, Jansson P, Fastook J L, Johnson J, Andersson L, 2005.** Detailed spatially distributed geothermal heat-flow data for modeling of basal temperatures and meltwater production beneath the Fennoscandian ice sheet. *Annals of Glaciology*, 40, pp 95–101.
- Näslund J-O (ed), Wohlfarth B (ed), Alexanderson H, Helmens K, Hättstrand M, Jansson P, Kleman J, Lundqvist J, Brandefelt J, Houmark-Nielsen M, Kjellström E, Strandberg G, Knudsen K L, Krogh Larsen N, Ukkonen P, Mangerud J, 2008.** Fennoscandian paleo-environment and ice sheet dynamics during Marine Isotope Stage (MIS) 3. Report of a workshop held September 20–21, 2007 in Stockholm, Sweden. SKB R-08-79, Svensk Kärnbränslehantering AB.
- Näslund J-O, Fastook J, Jansson P, 2010.** A numerical model reconstruction of the Weichselian ice sheet. SKB TR-09-19. Svensk Kärnbränslehantering AB.

- Olvmo M, 2010.** Review of denudation processes and quantification of weathering and erosion rates at a 0.1 to 1 Ma time scale. SKB TR-09-18, Svensk Kärnbränslehantering AB.
- Olvmo M, Johansson M, 2002.** The significance of rock structure, lithology, and pre-glacial deep weathering for the shape of intermediate-scale glacial erosional landforms. *Earth Surface Processes and Landforms*, 27, pp 251–268.
- Olvmo M, Lidmar-Bergström K, Ericson K, Bonow J M, 2005.** Saprolite remnant as indicators of pre-glacial landform genesis in southeast Sweden. *Geografiska annaler*, 87A, pp 447–460.
- O’Neill K, Miller R D, 1985.** Exploration of rigid ice model of frost heave. *Water Resources Research*, 21, pp 281–296.
- Oswald G K A, Gogineni S P, 2008.** Recovery of subglacial water extent from Greenland radar survey data. *Journal of Glaciology*, 54, pp 94–106.
- Otto-Bliesner B L, Brady E C, Clauzet G, Thomas R, Levis S, Kothavala Z, 2006.** Last glacial maximum and Holocene climate in CCSM3. *Journal of Climate*, 19, pp 2526–2544.
- Otto-Bliesner B L, Hewitt C D, Marchitto T M, Brady E, Abe-Ouchi A, Crucifix M, Murakami S, Weber S L, 2007.** Last Glacial Maximum ocean thermohaline circulation: PMIP2 model intercomparisons and data constraints. *Geophysical Research Letters*, 34, L12706, doi:10.1029/2007GL029475.
- Overpeck J, Weiss J, 2009.** Projections of future sea level becoming more dire. *Proceedings of the National Academy of Sciences of the United States of America*, 106, pp 21461–21462.
- Paananen M, Ruskeenieni T, 2003.** Permafrost at Lupin: Interpretation of SAMPO electromagnetic soundings at Lupin. Report YST-117, Geological Survey of Finland.
- Padilla F, Villeneuve J-P, 1992.** Modelling and experimental studies of frost heave including solute effects. *Cold Regions Science and Technology*, 20, pp 183–194.
- Paillard D, 2001.** Glacial cycles: toward a new paradigm. *Reviews of Geophysics*, 39, pp 325–346.
- Paterson W S B, 1994.** The physics of glaciers. 3rd ed. Oxford: Pergamon.
- Pattyn F, 2003.** A new three-dimensional higher-order thermomechanical ice sheet model: basic sensitivity, ice-stream development, and ice flow across subglacial lakes. *Journal of Geophysical Research*, 108, 2382, doi:10.1029/2002JB002329.
- Pattyn F, Huybrechts P, Declair H, 1989.** Modelling glacier fluctuations in the Sør Rondane, Dronning Maud Land, Antarctica. *Zeitschrift für Gletscherkunde und Glazialgeologie*, 25, pp 33–47.
- Pattyn F, de Smedt, B, Souchez R, 2004.** Influence of subglacial Vostok lake on the regional ice dynamics of the Antarctic ice sheet: a model study. *Journal of Glaciology*, 50, pp 583–589.
- Paulson A, Zhong S, Wahr J, 2005.** Modelling post-glacial rebound with lateral viscosity variations. *Geophysical Journal International*, 163, pp 357–371.
- Payne A J, 1995.** Limit cycles in the basal thermal regime of ice sheets. *Journal of Geophysical Research*, 100, pp 4249–4263.
- Payne A J, Baldwin D J, 1999.** Thermomechanical modelling of the Scandinavian ice sheet: implications for ice-stream formation. *Annals of Glaciology*, 28, pp 83–89.
- Payne A J, Dongelmans P W, 1997.** Self-organization in the thermomechanical flow of ice sheets. *Journal of Geophysical Research*, 102, pp 12219–12234.
- Payne A J, Huybrechts P, Abe-Ouchi A, Calov R, Fastook J L, Greve R, Marshall S J, Marsiat I, Ritz C, Tarasov L, Thomassen M P A, 2000.** Results from the EISMINT model intercomparison: the effects of thermomechanical coupling. *Journal of Glaciology*, 46, pp 227–238.
- Peltier W R, 1994.** Ice age palaeotopography. *Science*, 265, pp 195–201.
- Peltier W R, 1998.** Postglacial variations in the level of the sea: implications for climate dynamics and solid-earth geophysics. *Reviews of Geophysics*, 36, pp 603–689.
- Peltier W R, 2002.** On eustatic sea level history: Last Glacial Maximum to Holocene. *Quaternary Science Reviews*, 21, pp 377–396.
- Peltier W R, 2004.** Global glacial isostasy and the surface of the ice-age Earth: the ICE-5G (VM2) model and GRACE. *Annual Review of Earth and Planetary Science*, 32, pp 111–149.

- Peltier W R, 2005.** On the hemispheric origins of meltwater pulse 1a. *Quaternary Science Reviews*, 24, pp 1655–1671.
- Peltier W R, Drummond R, 2002.** A “broad-shelf effect” upon postglacial relative sea level history. *Geophysical Research Letters* 29, 1169, doi:10.1029/2001GL014273.
- Peltier W R, Farrell W E, Clark J A, 1978.** Glacial isostasy and relative sea level: a global finite element model. *Tectonophysics*, 50, pp 81–110.
- Pérez-Gussinyé M, Lowry A R, Watts A B, Velicogna I, 2004.** On the recovery of effective elastic thickness using spectral methods: examples from synthetic data and from the Fennoscandian Shield. *Journal of Geophysical Research*, 109, B10409, doi:10.1029/2003JB002788.
- Person M, McIntosh J, Bense V, Remenda V H, 2007.** Pleistocene hydrology of North America: the role of ice sheets in reorganizing groundwater flow systems. *Reviews of Geophysics*, 45, RG3007, doi:10.1029/2006RG000206.
- Persson G, Barring L, Kjellström E, Strandberg G, Rummukainen M, 2007.** Climate indices for vulnerability assessments. Norrköping: Sveriges meteorologiska och hydrologiska institut (Swedish Meteorological and Hydrological Institute). (SMHI reports. Meteorology and Climatology 111)
- Peyaud V, Ritz C, Krinner G, 2007.** Modelling the early Weichselian Eurasian ice sheets: role of ice shelves and influence of ice-dammed lakes. *Climate of the Past Discussions*, 3, pp 221–247.
- Pfeffer W T, Harper J T, O’Neel S, 2008.** Kinematic constraints on glacier contributions to 21st-century sea-level rise. *Science*, 321, pp 1340–1343.
- Placidi L, Greve R, Seddik H, Faria S H, 2010.** Continuum-mechanical, Anisotropic Flow model for polar ice masses, based on an anisotropic Flow Enhancement factor. *Continuum Mechanics and Thermodynamics*, 22, pp 221–237.
- Pollack H N, Hurter S J, Johnson, J R, 1991.** A new global heat flow compilation. [Online]. Available at: http://www.wdcb.ru/sep/data/hdata/hf_global.dat.
- Pollack H N, Hurter S J, Johnson J R, 1993.** Heat flow from the Earth’s interior: analysis of the global data set. *Reviews of Geophysics*, 31, pp 267–280.
- Porter S C, 1989.** Some geological implications of average Quaternary glacial conditions. *Quaternary Research*, 32, pp 245–261.
- Poudjom Djomani Y H, Fairhead J D, Griffin W L, 1999.** The flexural rigidity of Fennoscandia: reflection of the tectonothermal age of the lithospheric mantle. *Earth and Planetary Science Letters*, 174, pp 139–154.
- Price S F, Payne A J, Catania G A, Neumann T A, 2008.** Seasonal acceleration of inland ice via longitudinal coupling to marginal ice. *Journal of Glaciology*, 54, pp 213–219.
- Påsse T, 2001.** An empirical model of glacio-isostatic movements and shore-level displacement in Fennoscandia. SKB R-01-41, Svensk Kärnbränslehantering AB.
- Påsse T, 2004.** The amount of glacial erosion of the bedrock. SKB TR-04-25, Svensk Kärnbränslehantering AB.
- Raab B, Vedin H, 1995.** National Atlas of Sweden. Climate, Lakes and Rivers. Stockholm: SNA publishing.
- Radtke U, Grün R, Schwarcz H P, 1988.** Electron spin resonance dating of the Pleistocene coral reef tracts of Barbados. *Quaternary Research*, 29, pp 197–215.
- Rahmstorf S, Ganopolski A, 1999.** Long-Term Global Warming Scenarios Computed with an Efficient Coupled Climate Model. *Climatic Change*, 43 (2), pp 353–367. DOI: 10.1023/A:1005474526406
- Rahmstorf S, 2007.** A semi-empirical approach to projecting future sea-level rise. *Science*, 315, pp 368–370.
- Ramillien G, Lombard A, Cazenave A, Ivins E R, Llubes M, Remy F, Biancale R, 2006.** Interannual variations of the mass balance of the Antarctica and Greenland ice sheets from GRACE. *Global and Planetary Change*, 33, pp 198–208.

- Ramstein G, Kageyama M, Guiot J, Wu H, Hély C, Krinner G, Brewer S, 2007.** How cold was Europe at the Last Glacial Maximum? A synthesis of the progress achieved since the first PMIP model-data comparison. *Climate of the Past*, 3, pp 331–339.
- Rasmussen S O, Andersen K K, Svensson A M, Steffensen J P, Vinther B, Clausen H B, Siggaard-Andersen M-L, Johnsen S J, Larsen L B, Dahl-Jensen D, Bigler M, Röthlisberger R, Fisher H, Goto-Azuma K, Hansson M E, Ruth U, 2006.** A new Greenland ice core chronology for the last glacial termination. *Journal of Geophysical Research*, 111, D06102, doi:10.1029/2005JD006079.
- Rasmussen S O, Seierstad I K, Andersen K K, Bigler M, Dahl-Jensen D, Johnsen S J, 2008.** Synchronization of the NGRIP, GRIP, and GISP2 ice cores across MIS 2 and palaeoclimatic implications. *Quaternary Science Reviews*, 27, pp 18–28.
- Raymo M E, Nisancioglu K, 2003.** The 41 kyr world: Milankovitch's other unsolved mystery. *Paleoceanography*, 18, 1011, doi:10.1029/2002PA000791.
- Raymo M E, Ganley K, Carter S, Oppo D W, McManus J, 1998.** Millennial-scale climate instability during the early Pleistocene epoch. *Nature*, 392, pp 699–702.
- Raymond C F, Harrison W D, 1975.** Some observations on the behaviour of the liquid and gas phases in temperate glacier ice. *Journal of Glaciology*, 14, pp 213–234.
- Reiche P, 1950.** Survey of weathering processes and products. (University of New Mexico publications in geology 3)
- Remy F, Minster J F, 1993.** Precise altimetric topography in ice-sheet flow studies. *Annals of Glaciology*, 17, pp 195–200.
- Rial J A, 2004.** Abrupt climate change: chaos and order at orbital and millennial time scales. *Global and Planetary Change*, 41, pp 95–109.
- Richardson C, 2004.** Spatial characteristics of snow accumulation in Dronning Maud Land, Antarctica. *Global and Planetary Change*, 42, pp 31–43.
- Richardson K, Steffen W, Schellnhuber H J, Alcamo J, Barker T, Kammen D M, Leemans R, Liverman D, Munasinghe M, Osman-Elasha B, Stern N, Wæver O, 2009.** Synthesis report from CLIMATE CHANGE - Global risks, challenges and decisions. Copenhagen, 10–12 March 2009. Copenhagen: University of Copenhagen.
- Riddihough R P, 1972.** Regional magnetic anomalies and geology in Fennoscandia: a discussion. *Canadian Journal of Earth Sciences*, 9, pp 219–232.
- Ridley J K, Huybrechts P, Gregory J M, Lowe J A, 2005.** Elimination of the Greenland ice sheet in a high CO₂ climate. *Journal of Climate*, 18, pp 3409–3427.
- Rignot E, Kanagaratnam P, 2006.** Changes in the velocity structure of the Greenland ice sheet. *Science*, 311, pp 986–990.
- Rignot E J, Gogineni S P, Krabill W B, Ekholm S, 1997.** North and Northeast Greenland ice discharge from satellite radar interferometry. *Science*, 276, pp 934–937.
- Rignot E, Bamber J L, van den Broeke M R, Davis C, Li Y, van de Berg W J, van Meijgaard E, 2008.** Recent Antarctic ice mass loss from radar interferometry and regional climate modelling. *Nature Geoscience*, 1, pp 106–110.
- Rignot E, Koppes M, Velicogna I, 2010.** Rapid submarine melting of the calving faces of West Greenland glaciers. *Nature Geoscience*, 3, pp 187–191.
- Riis F, 1996.** Quantification of Cenozoic vertical movements of Scandinavia by correlation of morphological surfaces with offshore data. *Global and Planetary Change*, 12, pp 331–357.
- Riseborough D W, Shiklomanov N, Etzelmüller B, Gruber S, Marchenko S, 2008.** Recent advances in permafrost modelling. *Permafrost and Periglacial Processes*, 19, pp 137–156.
- Ritz C, Fabre A, Letreguilly A, 1996.** Sensitivity of a Greenland ice sheet model to ice flow and ablation parameters: Consequences for evolution through the last climatic cycle. *Climate Dynamics*, 13, pp 11–24.
- Roberts M J, 2005.** Jökulhlaups: a reassessment of floodwater flow through glaciers. *Reviews of Geophysics*, 43, RG1002, doi:10.1029/2003RG000147.

- Roberts M J, Russell A J, Tweed F S, Knudsen Ó, 2000.** Ice fracturing during jökulhlaups: implications for englacial floodwater routing and outlet development. *Earth Surface Processes and Landforms*, 25, pp 1429–1446.
- Robinson A, Calov R, Ganopolski A, 2010.** An efficient regional energy-moisture balance model for simulation of the Greenland Ice Sheet response to climate change. *The Cryosphere*, 4, pp 129–144.
- Rohling E J, Grant K, Bolshaw M, Roberts A P, Siddall M, Hemleben C, Kucera M, 2009.** Antarctic temperature and global sea level closely coupled over the past five glacial cycles. *Nature Geoscience*, doi:10.1038/ngeo557.
- Rudberg S, 1954.** Västerbottens berggrundsmorfologi: ett försök till rekonstruktion av preglaciala erosionsgenerationer i Sverige. Ph. D. thesis. Uppsala University. (*Geographica* 25)
- Ruddiman W F, 2001.** *Earth's climate: past and future*. New York: Freeman.
- Ruddiman W F, 2003.** The anthropogenic greenhouse era began thousands of years ago. *Climate Change*, 61, pp 261–293.
- Rummukainen M, 2003.** The Swedish regional climate modeling program, SWECLIM, 1996–2003. Final report. Norrköping: Sveriges meteorologiska och hydrologiska institut (Swedish Meteorological and Hydrological Institute). (SMHI Meteorologi 104)
- Rummukainen M, Källén E, 2009.** Ny klimatvetenskap 2006–2009. Kommissionen för hållbar utveckling, Regeringskansliet (in Swedish).
- Ruskeeniemä T, Paananen M, Ahonen L, Kaija J, Kuivamäki A, Frape S, Moren L, Degnan P, 2002.** Permafrost at Lupin: report of Phase I. Report YST-112, Geological Survey of Finland.
- Ruskeeniemä T, Ahonen L, Paananen M, Frape S, Stotler R, Hobbs M, Kaija J, Degnan P, Blomqvist R, Jensen M, Lehto K, Moren L, Puigdomenech I, Snellman M, 2004.** Permafrost at Lupin: report of Phase II. Report YST-119, Geological Survey of Finland.
- Röthlisberger H, 1972.** Water pressure in intra- and subglacial channels. *Journal of Glaciology*, 11, pp 177–203.
- Röthlisberger H, Lang H, 1987.** Glacial hydrology. In: Gurnell A M, Clark M J (eds). *Glacio-fluvial sediment transfer: an alpine perspective*. Chichester: Wiley.
- Salas J, Gimeno M J, Molinero J, Auqué L F, Gómez J, Juárez I, 2010.** SR-Site. Hydrogeochemical evolution of the Forsmark site. SKB TR-10-58, Svensk Kärnbränslehantering AB.
- Sawagaki T, Hirakawa K, 1997.** Erosion of bedrock by subglacial meltwater, Soya Coast, East Antarctica. *Geografiska Annaler*, 79A, pp 223–238.
- SCAR, 2007.** A need for more realistic ice-sheet models. SCAR report 30, Scientific Committee on Antarctic Research.
- Scherneck H-G, Johansson J M, Vermeer M, Davis J L, Milne G A, Mitrovica J X, 2001.** BIFROST project: 3D crustal deformation rates derived from GPS confirm postglacial rebound in Fennoscandia. *Earth Planets Space*, 53, pp 703–708.
- Schneider T, 2000.** Hydrological processes in the wet-snow zone of glaciers: a review. *Zeitschrift für Gletscherkunde und Glazialgeologie*, 36, pp 89–105.
- Seipold U, 1995.** The variation of thermal transport properties in Earth's crust. *Journal of Geodynamics*, 20, pp 145–154.
- Selby M J, 1993.** *Hillslope materials and processes*. 2nd ed. Oxford: Oxford University Press.
- Shackleton N J, Kennett J P, 1975.** Paleotemperature history of the Cenozoic and the initiation of Antarctic glaciation: oxygen and carbon isotopic analyses in DSDP sites 277, 279, and 281. In: Kennett J P, Houtz R (eds). *Initial reports of the Deep Sea Drilling Project*, 29, pp 743–755.
- Shaffer G, Olsen S M, Pedersen J O P, 2009.** Long-term ocean oxygen depletion in response to carbon dioxide emissions from fossil fuels. *Nature Geoscience*, 2, pp 105–109.

- Shala S, Helmens K F, Risberg J, Löwemark L, Jansson K, Kuhry P, submitted.** Early Holocene glacial-lake evolution in northern Finland – a multi-proxy approach. XVIII INQUA congress. Bern, Switzerland, 20–27 July 2011.
- Sharp R P, 1960.** *Glaciers*. Eugene: University of Oregon Press. (Condon lectures 1960).
- Shepherd A, Wingham D, 2007.** Recent sea-level contribution of the Antarctic and Greenland ice sheets. *Science*, 315, pp 1529–1532.
- Shepherd A, Hubbard A, Nienow P, King M, McMillan M, Joughin I, 2009.** Greenland ice sheet motion coupled with daily melting in late summer. *Geophysical Research Letters*, 36, L01501, doi:10.1029/2008GL035758.
- Shin S-I, Liu Z, Otto-Bliesner B, Brady E C, Kutzbach J E, Harrison S P, 2003.** A simulation of the Last Glacial Maximum climate using the NCAR-CSM. *Climate Dynamics*, 20, pp 127–151.
- Shreve R, 1972.** Movement of water in glaciers. *Journal of Glaciology*, 11, pp 205–214.
- Shur Y L, Slavin-Borovskiy V B, 1993.** N-factor maps of Russian permafrost region. Proceedings of the sixth international conference on permafrost. Beijing, 5–9 July 1993. Guangzhou: South China University of Technology, pp 564–568.
- Siddall M, Rohling E J, Almogi-Labin A, Hemleben C, Meischner D, Schmelzer I, Smeed D A, 2003.** Sea-level fluctuations during the last glacial cycle. *Nature*, 423, pp 853–858.
- Siddall M, Stocker T F, Clark P U, 2009.** Constraints on future sea-level rise from past sea-level change. *Nature Geoscience*, 2, pp 571–575.
- Siegert M J, 2005.** Lakes beneath the ice sheet: the occurrence, analysis and future exploration of Lake Vostok and other Antarctic subglacial lakes. *Annual Review of Earth and Planetary Sciences*, 33, pp 215–245.
- Siegert M J, Dowdeswell J A, 1996.** Spatial variations in heat at the base of the Antarctic ice sheet from analysis of the thermal regime above subglacial lakes. *Journal of Glaciology*, 42, pp 501–509.
- Siegert M J, Dowdeswell J A, Gorman M R, McIntyre N F, 1996.** An inventory of Antarctic sub-glacial lakes. *Antarctic Science*, 8, pp 281–286.
- Siegert M J, Carter S, Tabacco I, Popov S, Blankenship D D, 2005.** A revised inventory of Antarctic subglacial lakes. *Antarctic Science*, 17, pp 453–460.
- Simons M, Hager B H, 1997.** Localization of the gravity field and the signature of glacial rebound. *Nature*, 390, pp 500–504.
- Six D, Letréguilly A, Reynaud L, 2001.** Greenland ice-sheet mass-balance distribution: a variance analysis of existing field data. *Journal of Glaciology*, 47, pp 441–451.
- SKB, 2005a.** Preliminary site description. Forsmark area – version 1.2. SKB R-05-18, Svensk Kärnbränslehantering AB.
- SKB, 2006a.** Climate and climate-related issues for the safety assessment SR-Can. SKB TR-06-23, Svensk Kärnbränslehantering AB.
- SKB, 2006b.** Geosphere process report for the safety assessment SR-Can. SKB TR-09-19, Svensk Kärnbränslehantering AB.
- SKB, 2010a.** Data report for the safety assessment SR-Site. SKB TR-10-52, Svensk Kärnbränslehantering AB.
- SKB, 2010b.** FEP-report for the safety assessment SR-Site. SKB TR-10-45, Svensk Kärnbränslehantering AB.
- SKB, 2010c.** Geosphere process report for the safety assessment SR-Site. SKB TR-10-48, Svensk Kärnbränslehantering AB.
- SKB, 2010d.** Landscape Forsmark, SR-Site Biosphere. SKB TR-10-05, Svensk Kärnbränslehantering AB.
- SKB, 2010e.** Biosphere assessment of SR-Site Forsmark – synthesis and summary of results. SKB TR-10-09, Svensk Kärnbränslehantering AB.

- SKB, 2010f.** Comparative analysis of safety related site characteristics. SKB TR-10-54, Svensk Kärnbränslehantering AB.
- SKB 2010g.** Model summary report for the safety assessment SR-Site. TR-10-51, Svensk Kärnbränslehantering AB.
- SKB, 2011.** Long-term safety for the final repository for spent nuclear fuel at Forsmark. Main report of the SR-Site project. SKB TR-11-01, Svensk Kärnbränslehantering AB.
- Skinner L C, 2008.** Revisiting the absolute calibration of the Greenland ice-core age-scales. *Climate of the Past*, 4, pp 295–302.
- SMHI, 2001.** Temperaturen och nederbörden i Sverige 1961–1990: referensnormaler. 2. utg. Norrköping: Sveriges meteorologiska och hydrologiska institut (Swedish Meteorological and Hydrological Institute). (SMHI Meteorologi 99)
- Smith M W, Riseborough D W, 1996.** Permafrost monitoring and detection of climate change, *Permafrost and Periglacial Processes*, 7, pp 301–309.
- Sohlenius G, Hedenström A, Rudmark L, 2004.** Forsmark site investigation. Mapping of unconsolidated Quaternary deposits 2002–2003. Map description. SKB R-04-39, Svensk Kärnbränslehantering AB.
- SOU 2007.** Klimat- och sårbarhetsutredningen. Sverige inför klimatförändringarna: hot och möjligheter (in Swedish). Stockholm: Fritzes. (Statens offentliga utredningar 2007:60)
- Spada G, Antonioli A, Cianetti S, Giunchi C, 2006.** Glacial isostatic adjustment and relative sea-level changes: the role of lithospheric and upper mantle heterogeneities in a 3D spherical Earth. *Geophysical Journal International*, 165, pp 692–702.
- Spring U, Hutter K, 1981.** Numerical studies of jökulhlaups. *Cold Regions Science and Technology*, 4, pp 227–244.
- Staiger J K W, Gosse J C, Johnson J V, Fastook J, Gray J T, Stockli D F, Stockli L, Finkel R, 2005.** Quaternary relief generation by polythermal glacier ice. *Earth Surface Processes and Landforms*, 30, pp 1145–1159.
- Steffen K, Nghiem S V, Huff R, Neumann G, 2004.** The melt anomaly of 2002 on the Greenland Ice Sheet from active and passive microwave satellite observations. *Geophysical Research Letters*, 31, L20402, doi:10.1029/2004GL020444.
- Stone E J, Lunt D J, Rutt I C, Hanna E, 2010a.** The effect of more realistic forcings and boundary conditions on the modelled geometry and sensitivity of the Greenland ice-sheet. *The Cryosphere Discussion*, 4, pp 233–285.
- Stone E J, Lunt D J, Rutt I C, Hanna E, 2010b.** Investigating the sensitivity of numerical model simulations of the modern state of the Greenland ice sheet and its future response to climate change. *The Cryosphere*, 4, pp 379–417.
- Strandberg G, Brandefelt J, Kjellström E, 2008.** Modelling last glacial maximum climate variability with a high resolution regional climate model. EGU2008-A-03244. Abstracts of the contributions of the EGU General Assembly 2008. *Geophysical Research Abstracts*, 10.
- Strandberg G, Brandefelt J, Kjellström E, 2009a.** High-resolution regional climate model simulations for a 50-year period under Last Glacial Maximum conditions. Abstracts of the contributions of the EGU General Assembly 2009. *Geophysical Research Abstracts*, 11.
- Strandberg G, Brandefelt J, Kjellström E, Smith B, 2009b.** Simulating cold palaeo climate conditions in Europe with a regional climate model. In: Rockel B, Bärring L, Reckermann M (eds). *Proceedings from WCRP workshop on regional climate modelling*. Lund, 4–8 May 2009. (International BALTEX Secretariat publication 41), pp 280–281.
- Strandberg G, Brandefelt J, Kjellström E, Smith B, 2010.** High resolution simulation of Last Glacial Maximum climate and vegetation in Europe. *Tellus*, doi: 10.1111/j.1600-0870.2010.00485.x.
- Straneo F, Hamilton G S, Sutherland D A, Stearns L A, Davidson F, Hammill M O, Stenson G B, Rosing-Asvid A, 2010.** Rapid circulation of warm subtropical waters in a major glacial fjord in East Greenland. *Nature Geoscience*, 3, pp 182–186.

- Stroeven A P, Fabel D, Hättestrand C, Harbor J, 2002a.** A relict landscape in the centre of Fennoscandian glaciation: cosmogenic radionuclide evidence of tors preserved through multiple glacial cycles. *Geomorphology*, 44, pp 145–154.
- Stroeven A P, Fabel D, Hättestrand C, Kleman J, 2002b.** Quantifying the erosional impact of the Scandinavian ice sheet in the Torneträsk-Narvik corridor, northern Sweden, based on cosmogenic radionuclide data. *Geografiska Annaler*, 84A, pp 275–287.
- Sugden D E, 1977.** Reconstruction of the morphology, dynamics and thermal characteristics of the Laurentide ice sheet at its maximum. *Arctic and Alpine Research*, 9, pp 27–47.
- Sugden D E, 1978.** Glacial erosion by the Laurentide ice sheet. *Journal of Glaciology*, 20, pp 367–391.
- Sugden D E, John B S, 1976.** *Glaciers and landscape: a geomorphological approach*. London: Arnold.
- Sundberg J, 1988.** Thermal properties of soils and rocks. Ph. D. thesis. Chalmers tekniska högskola. (Geologiska institutionen publ. A 57)
- Sundberg J, Back P-E, Ländell M, Sundberg A, 2009.** Modelling of temperature in deep boreholes and evaluation of geothermal heat flow at Forsmark and Laxemar. SKB TR-09-14, Svensk Kärnbränslehantering AB.
- Sundh M, Sohlenius G, Hedenström A, 2004.** Forsmark site investigation. Stratigraphical investigation of till in machine cut trenches. SKB P-04-34, Svensk Kärnbränslehantering AB.
- Svendsen J I, Mangerud J, 1987.** Late Weichselian and Holocene sea-level history for a cross-section of western Norway. *Journal of Quaternary Science*, 2, pp 113–132.
- Svendsen J I, Astakhov V I, Bolshiyakov D Y, Demidov I, Dowdeswell J A, Gataullin V, Hjort C, Hubberten H W, Larsen E, Mangerud J, Melles M, Möller P, Saarnisto M, Siegert M J, 1999.** Maximum extent of the Eurasian ice sheets in the Barents and Kara Sea region during the Weichselian. *Boreas*, 28, pp 234–242.
- Svendsen J I, Alexanderson H, Astakhov V I, Demidov I, Dowdeswell J A, Funder S, Gataullin V, Henriksen M, Hjort C, Houmark-Nielsen M, Hubberten H W, Ingólfsson O, Jakobsson M, Kjær K H, Larsen E, Lokrantz H, Lunkka J P, Lyså A, Mangerud J, Matiouchkov A, Murray A, Moller P, Niessen F, Nikolskaya O, Polyak L, Saarnisto M, Siegert C, Siegert M J, Spielhagen R F, Stein R, 2004.** Late Quaternary ice sheet history of northern Eurasia. *Quaternary Science Reviews*, 23, pp 1229–1271.
- Svensson A, Andersen K K, Bigler M, Clausen H B, Dahl-Jensen D, Davies S M, Johnsen S J, Muscheler R, Parrenin F, Rasmussen S O, Röthlisberger R, Seierstad I, Steffensen J P, Vinther B M, 2008.** A 60 000 year Greenland stratigraphic ice core chronology. *Climate of the Past*, 4, pp 47–57.
- Svensson P D, Hansen S, 2010.** Freezing and thawing of montmorillonite – a time resolved X-ray diffraction study. *Applied Clay Science*, 49, pp 127–134.
- Swantesson J O H, 1992.** Recent micro-weathering phenomena in southern and central Sweden. *Permafrost and Periglacial Processes*, 3, pp 275–292.
- Söderbäck B, 2008.** Geological evolution, palaeoclimate and historical development of the Forsmark and Laxemar-Simpevarp areas. Site descriptive modelling. SDM-Site. SKB R-08-19, Svensk Kärnbränslehantering AB.
- Tamisiea M E, Mitrovica J X, Milne G A, Davis J L, 2001.** Global geoid and sea level changes due to present-day ice mass fluctuations. *Journal of Geophysical Research*, 106, pp 30849–30863.
- Tamisiea M E, Mitrovica J X, Davis J L, Milne G A, 2003.** Long wavelength sea level and solid surface perturbations driven by polar ice mass variations: fingerprinting Greenland and Antarctic ice sheet flux. *Space Science Reviews*, 108, pp 81–93.
- Tarasov L, Peltier W R, 2004.** A geophysically constrained large ensemble analysis of the deglacial history of the North American ice-sheet complex. *Quaternary Science Reviews*, 23, pp 359–388.
- Tarback E J, Lutgens F K, 1999.** *Earth: an introduction to physical geology*. 6th ed. Upper Saddle River, N.J.: Prentice Hall.

- Taylor A E, 1995.** Field measurements of n-factors for natural forest areas, Mackenzie Valley, Northwest Territories. Geological Survey of Canada, Current Research, 1995-B, pp 89–98.
- Taylor A E, 2001.** Relationship of ground temperatures to air temperatures in forests. Geological Survey of Canada, Bulletin, 547, pp 111–117.
- Thomas M F, 1994.** Geomorphology in the tropics: a study of weathering and denudation in low latitudes. Chichester: Wiley.
- Thomas R, Frederick, E, Krabill W, Manizade S, Martin C, 2009.** Recent changes on Greenland outlet glaciers. *Journal of Glaciology*, 55, pp 147–162.
- Thomsen H H, Thorning L, Olesen O B, 1989.** Applied glacier research for planning hydro-electric power, Ilulissat/Jakobshavn, West Greenland. *Annals of Glaciology*, 13, pp 257–261.
- Tjernström M, Rummukainen M, Bergström S, Rodhe J, Persson G, 2003.** Klimatmodellering och klimatscenarier ur SWECLIMS perspektiv (in Swedish). Norrköping: Sveriges meteorologiska och hydrologiska institut (Swedish Meteorological and Hydrological Institute). (SMHI reports. Meteorology and Climatology 102)
- Toniazzo T, Gregory J M, Huybrechts P, 2004.** Climatic impact of a Greenland deglaciation and its possible irreversibility. *Journal of Climate*, 17, pp 21–33.
- Turcotte D L, 1980.** On the thermal evolution of the Earth. *Earth and Planetary Science Letters*, 48, pp 53–58.
- Turkington A V, Phillips J D, Campbell S W, 2005.** Weathering and landscape evolution. *Geomorphology*, 67, pp 1–6.
- Tushingham A M, Peltier W R, 1991.** ICE-3G: a new global model of Late Pleistocene deglaciation based upon geophysical predictions of post-glacial relative sealevel change. *Journal of Geophysical Research*, 96, pp 4497–4523.
- Tyrell T, Sheperd J G, Castle S, 2007.** The long-term legacy of fossil fuels. *Tellus B*, 59, pp 664–672.
- Tzedakis P C, Raynaud D, McManus J F, Berger A, Brovkin V, Kiefer T, 2009.** Interglacial diversity. *Nature Geoscience*, 2, pp 751–755.
- Tziperman E, Gildor H, 2003.** On the mid-Pliocene transition to 100-kyr glacial cycles and the asymmetry between glaciation and deglaciation times. *Paleoceanography* 18, 1001, doi:10.1029/2001pa000627.
- UNEP/GRID-Arendal, 2005.** Permafrost distribution in the Arctic. UNEP/GRID-Arendal Maps and Graphics Library. [Online]. Available at: <http://maps.grida.no/go/graphic/permafrost-distribution-in-the-arctic>. [26 November 2010].
- van de Wal R S W, 1996.** Mass-balance modelling of the Greenland ice sheet: a comparison of an energy-balance model and a degree-day model. *Annals of Glaciology*, 23, pp 36–45.
- van de Wal R S W, Boot W, van den Broeke M R, Smeets C J P P, Reijmer C H, Donker J J A, Oerlemans J, 2008.** Large and rapid melt-induced velocity changes in the ablation zone of the Greenland Ice Sheet. *Science*, 321, pp 111–113.
- van den Broeke M, Bamber J, Ettema J, Rignot E, Schrama E, van de Berg W J, van Meijgaard E, Velicogna I, Wouters B, 2009.** Partitioning recent Greenland mass loss. *Science*, 326, pp 984–986.
- van der Veen C J, 1998a.** Fracture mechanics approach to penetration of surface crevasses on glaciers. *Cold Regions Science and Technology*, 27, pp 31–47.
- van der Veen C J, 1998b.** Fracture mechanics approach to penetration of bottom crevasses on glaciers. *Cold Regions Science and Technology*, 27, pp 213–223.
- van der Veen C J, 2007.** Fracture propagation as means of rapidly transferring surface meltwater to the base of glaciers. *Geophysical Research Letters*, 34, L01501, doi:10.1029/2006GL028385.
- van Huissteden K, Pollard D, 2003.** Oxygen isotope stage 3 fluvial and eolian successions in Europe compared with climate model results. *Quaternary Research*, 59, pp 223–233.
- van Huissteden K, Vandenberghe J, Pollard D, 2003.** Palaeotemperature reconstructions of the European permafrost zone during oxygen isotope Stage 3 compared with climate model results. *Journal of Quaternary Science*, 18, pp 453–464.

- Van Meerbeeck C J, Renssen H, Roche D M, Wohlfarth B, Bohncke S J P, Bos J A A, Engels S, Helmens K F, Sánchez-Goñi M F, Svensson A, Vandenberghe J, submitted.** The nature of MIS 3 stadial-interstadial transitions in Europe: new insights from model-data comparisons. Submitted to *Quaternary Science Reviews*.
- Van Tatenhove F G M, Huybrechts P, 1996.** Modelling of the thermal conditions at the Greenland ice sheet margin during Holocene deglaciation: boundary conditions from moraine formation. *Geografiska Annaler*, 78A, pp 83–99.
- Velicogna I, 2009.** Increasing rates of ice mass loss from the Greenland and Antarctic ice-sheets revealed by GRACE. *Geophysical Research Letters*, 36, L19503, doi:10.1029/2009GL040222.
- Velicogna I, Wahr J, 2006.** Acceleration of Greenland ice mass loss in spring 2004. *Nature*, 443, pp 329–331.
- Vidstrand P, 2003.** Surface and subsurface conditions in permafrost areas – a literature review. SKB TR-03-06, Svensk Kärnbränslehantering AB.
- Vidstrand P, Follin S, Zugec N, 2010.** Groundwater flow modelling of periods with periglacial and glacial conditions – SR-Site Forsmark. SKB R-09-21, Svensk Kärnbränslehantering AB.
- Vinther B M, Buchardt S L, Clausen H B, Dahl-Jensen D, Johnsen S J, Fisher D A, Koerner R M, Raynaud D, Lipenkov V, Andersen K K, Blunier T, Rasmussen S O, Steffensen J P, Svensson A M, 2009.** Holocene thinning of the Greenland ice sheet. *Nature*, 461, pp 385–388.
- Väliranta M, Helmens K F, 2007.** Palaeobotanical and lithological review of a 7-m-thick sediment sequence, dated to MIS 5d-c, from Sokli, Finnish Lapland: preliminary results and interpretation. 1st NEPAL (Nordic Network on Palaeoclimatology) workshop. Palmse, Estonia, 10–12 May 2007.
- Väliranta M, Birks H H, Engels S, Helmens K F, 2008.** Early Weichselian botanical features in Finnish Lapland. 33rd IGC congress. Oslo, 6–14 August 2008.
- Väliranta M, Birks H H, Helmens K F, Engels S, Piirainen M, 2009.** Early-Weichselian interstadial (MIS 5c) summer temperatures were higher than today in northern Fennoscandia. *Quaternary Science Reviews (rapid communications)*, 28, pp 777–782.
- Waddington E D, 1987.** Geothermal heat flux beneath ice sheets. In: Waddington E D, Walder J S (eds). *The physical basis of ice sheet modelling*. Wallingford, Oxfordshire: International Association of Hydrological Sciences. (IAHS Publication 170), pp 217–226.
- Wadham J L, Lis G P, Bartholomew I, Sole, A, Nienow P, Mair D, Hubbard A, Watson A, Das S, Stibal M, Lawson E, Dubnick A, Criscitiello A, Barnett M, submitted.** Observed rapid meltwater drainage via channels beneath the GIS. Submitted to *Science*.
- Waelbroeck C, Labeyrie L, Michel E, Duplessy J C, McManus J F, Lambeck K, Balbon E, Labracherie M, 2002.** Sea-level and deep water temperature changes derived from benthic foraminifera isotopic records. *Quaternary Science Reviews*, 21, pp 295–305.
- Wake L M, Huybrechts P, Box J E, Hanna E, Janssens I, Milne G A, 2009.** Surface mass-balance changes of the Greenland ice sheet since 1866. *Annals of Glaciology*, 50, pp 178–184.
- Walder J S, Fowler A, 1994.** Channelized subglacial drainage over a deformable bed. *Journal of Glaciology*, 40, pp 3–15.
- Waller R I, 2001.** The influence of basal processes on the dynamic behaviour of cold-based glaciers. *Quaternary International*, 86, pp 117–128.
- Washburn A L, 1979.** *Geocryology: a survey of periglacial processes and environments*. 2nd ed. London: Arnold.
- Watts A B, 2001.** *Isostasy and flexure of the lithosphere*. Cambridge: Cambridge University Press.
- Weart S R, 2003.** *The discovery of global warming*. Cambridge: Harvard University Press.
- Weertman J, 1972.** General theory of water flow at the base of a glacier or ice sheet. *Reviews of Geophysics and Space Physics*, 10, pp 287–303.
- Weertman J, 1973.** Can a water-filled crevasse reach the bottom surface of a glacier? In: *Symposium on the Hydrology of Glaciers*, Cambridge, 7–13 September 1969. Wallingford, Oxfordshire: International Association of Hydrological Sciences. (IAHS Publication 95), pp 139–145.

- Werner M, Heimann M, Hoffman G, 2001.** Isotopic composition and origin of polar precipitation in present and glacial climate simulations. *Tellus*, 53B, pp 53–71.
- Whalley W B, Warke P A, 2005.** Weathering. In: Selley R C, Cocks L R M, Plimer I R (eds.) *Encyclopedia of geology*. Amsterdam: Elsevier.
- Whitehouse P, 2009.** Glacial isostatic adjustment and sea-level change. State of the art report. SKB TR-09-11. Svensk Kärnbränslehantering AB.
- Whitehouse P, Latychev K, Milne G A, Mitrovica J X, Kendall K, 2006.** Impact of 3D Earth structure on Fennoscandian glacial isostatic adjustment: Implications for space-geodetic estimates of present-day crustal deformations. *Geophysical Research Letters* 33, L13502, doi:10.1029/2006GL026568.
- Williams P J, Smith M W, 1989.** *The frozen earth: fundamentals of geocryology*. Cambridge: Cambridge University Press.
- Wingham D J, Wallis D W, Shepherd A, 2009.** Spatial and temporal evolution of Pine Island Glacier thinning, 1995–2006. *Geophysical Research Letters*, 36, L17501, doi:10.1029/2009GL039126.
- Witt A, Schumann A Y, 2005.** Holocene climate variability on millennial scales recorded in Greenland ice cores. *Nonlinear Processes in Geophysics*, 12, pp 345–352.
- Wohlfarth B, 2009.** Ice-free conditions in Fennoscandia during Marine Oxygen Isotope Stage 3? SKB TR-09-12, Svensk Kärnbränslehantering AB.
- Wohlfarth B, 2010.** Ice free conditions in Sweden during Marine Oxygen Isotope Stage 3? *Boreas*, 39, pp 377–398.
- Wohlfarth B, Näslund J-O (eds), 2010.** Fennoscandian ice sheet in MIS 3. *Boreas*, 39, pp 325–456.
- Woth K, Weisse R, von Storch H, 2006.** Climate change and North Sea storm surge extremes: an ensemble study of storm surge extremes expected in a changed climate projected by four different regional climate models. *Ocean Dynamics*, 56, pp 3–15.
- Wouters B, Chambers D, Schrama E J G, 2008.** GRACE observe small-scale mass loss in Greenland. *Geophysical Research Letters*, 35, L20501, doi:10.1029/2008GL034816.
- Wu P, Peltier W R, 1983.** Glacial isostatic adjustment and the free air gravity anomaly as a constraint on deep mantle viscosity. *Geophysical Journal of the Royal Astronomical Society*, 74, pp 377–449.
- Wu P, Wood R, Stott P, 2004.** Does the recent freshening trend in the North Atlantic indicate a weakening thermohaline circulation? *Geophysical Research Letters*, 31, L02301, doi:10.1029/2003GL018584.
- Wu P, Wang H, Schotman H, 2005.** Postglacial induced surface motions, sea-levels and geoid rates on a spherical, self-gravitating laterally heterogeneous earth. *Journal of Geodynamics*, 39, pp 127–142.
- Wu H, Guiot J, Brewer S, Guo Z, 2007.** Climatic changes in Eurasia and Africa at the last glacial maximum and mid-Holocene: reconstruction from pollen data using inverse vegetation modelling. *Climate Dynamics*, 29, pp 211–229.
- Yershov E D, 1998.** *General Geocryology*. Cambridge: Cambridge University Press.
- Yin Q Z, Berger A, 2010.** Insolation and CO₂ contribution to the interglacial climate before and after the Mid-Brunhes Event. *Nature Geoscience*, 3, pp 243–246.
- Yokoyama Y, Lambeck K, De Deckker P, Johnston P, Fifield L K, 2000.** Timing of the last glacial maximum from observed sea level minima. *Nature*, 406, pp 713–716.
- Zickfeld K, Levermann A, Morgan M G, Kuhlbrodt T, Rahmstorf S, Keith D W, 2007.** Expert judgement on the response of the Atlantic meridional overturning circulation to climate change. *Climate Change*, 82, pp 235–265.
- Zwally H J, Abdalati W, Herring T, Larson K, Saba J, Steffen K, 2002.** Surface melt-induced acceleration of Greenland ice-sheet flow. *Science*, 297, pp 218–222.
- Zweck C, Huybrechts P, 2003.** Modeling the marine extent of northern hemisphere ice sheets during the last glacial cycle. *Annals of Glaciology*, 37, pp 173–180.

Air temperature data

A1.1 Introduction

With the approach used to handle climate issues in the safety assessment, Section 1.2, estimates of past and possible future temperature variations are necessary for various studies within the safety assessment, such as simulations of ice sheet and permafrost development. The approach taken in SR-Site is to reconstruct temperatures for the last glacial cycle and use them to construct a *reference glacial cycle* for the coming 100 kyrs, Section 1.2. This *reference glacial cycle* is not a forecast of the future climate that will occur at Forsmark, but instead i) one relevant example of a possible future climate, and ii) a starting point for the construction of complementary, and more pessimistic, climate cases also to be analysed in the safety assessment.

In the following text the term *air temperature* is used as representing annual mean air temperatures, while *ground surface temperature* describes the annual mean temperature on the ground surface below vegetation including the humus layer. The ground can be mineral or organic soil or rock. *Subglacial temperature* describes the temperature at the interface between the basal part of an ice sheet and its bed, while *submerged temperature* describes an assumed water temperature at the sea bed during periods when the site is submerged by the Baltic Sea.

A1.2 Greenland proxy data on last glacial cycle temperatures used for ice sheet modelling

In the absence of a complete last glacial cycle palaeotemperature curve from Fennoscandia, proxy data on palaeotemperatures from the GRIP ice core /Dansgaard et al. 1993, Johnsen et al. 1995/ are typically used in model simulations of the Weichselian ice sheet e.g. /Fastook and Holmlund 1994, Holmlund and Fastook 1995, Hagdorn 2003, Hagdorn et al. 2005, Forsström 2005/. The ice sheet modelling performed for SR-Site also uses palaeotemperature information from the GRIP core (Section 3.1.4). Figure A1-1 (red line) shows the GRIP temperature curve (50 year average values plotted on the on the ss09 time scale, see below) used as input to the SR-Site ice sheet modelling performed with the University of Maine Ice Sheet Model (UMISM).

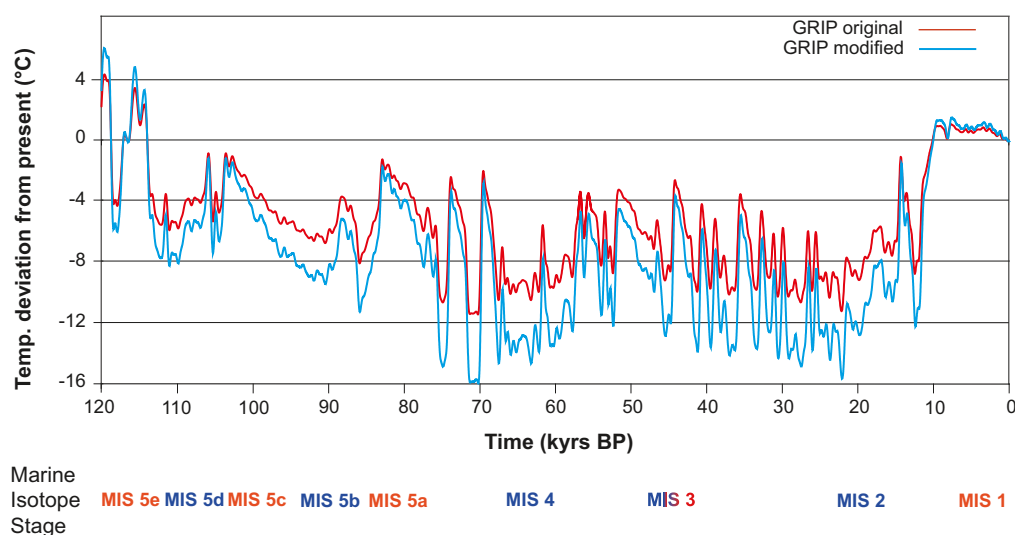


Figure A1-1. Palaeotemperature curve from the GRIP ice core /Johnsen et al. 1995/ (red) and modified temperature curve resulting from the ice sheet model calibration (blue). Cold stadials and warm interstadials are shown in blue and red text respectively, denoted by their Marine Isotope Stage (MIS) numbers. The uncertainty of the temperature curves is discussed in Section A1.5.

Although $\delta^{18}\text{O}$ values from ice cores are useful temperature proxies, transferring $\delta^{18}\text{O}$ values to air temperatures and using them as proxy data for palaeotemperatures is not straightforward e.g. /Cuffey et al. 1994, Huber et al. 2006/. In part, this is because of changes in the source of precipitation over time and changes in the distribution of snow on the ice sheet. Also seasonal variations in temperature and precipitation affect the isotopic composition of the ice core /Krinner et al. 1997/. Studies of $\delta^{15}\text{N}$ isotopes from the NorthGRIP (NGRIP) ice core /NorthGRIP community members 2004/ has shown that the $\delta^{18}\text{O}$ – Temperature relationship changes over time, for instance between glacial and interglacial periods and between stadials and interstadials /Huber et al. 2006/. The results by /Huber et al. 2006/ may be used as input in an estimation of the errors present in the GRIP temperature curve. This is discussed in Section A1.5 together with the errors associated with using the GRIP temperature curve for reconstructing Fennoscandian temperatures. Despite the uncertainties, the temperature reconstructions from the Greenland ice cores are one of the best continuous archives of palaeoclimate information available in the vicinity of Fennoscandia.

In the simulation of the Weichselian ice sheet, the modelled ice sheet configurations were calibrated against known dated ice-marginal positions (Section 3.1.4). The calibration was done by making systematic changes of the entire input GRIP temperature curve. The resulting modified temperature curve after calibration is shown in Figure A1-1. Keeping all other input data constant in the calibration process, the modified temperature curve after model calibration results in Late and Middle Weichselian ice sheet configurations in good agreement with dated stadial ice-marginal positions from glacial geology and Early Weichselian configurations in reasonably good agreement with geological interpretations. The main difference between the original GRIP curve and the temperature curve after calibration is that the latter shows generally colder conditions during stadials (Figure A1-1). The temperatures during interstadials are similar.

A1.3 Reconstructed last glacial cycle temperatures in the Forsmark region

A1.3.1 Air temperatures with and without a Weichselian ice sheet

From the calibrated ice sheet model, a regional temperature curve was extracted for the terrestrial grid cell closest to the Forsmark site (Figure A1-2, blue line). This local temperature curve thus originates from the modified GRIP curve of Figure A1-1. For periods without an ice sheet cover over the Forsmark region, the extracted temperature curve shows air temperature in the Forsmark region as represented in the ice sheet model simulation. For periods with ice sheet cover over Forsmark, the curve shows the simulated basal ice temperatures from the ice sheet model.

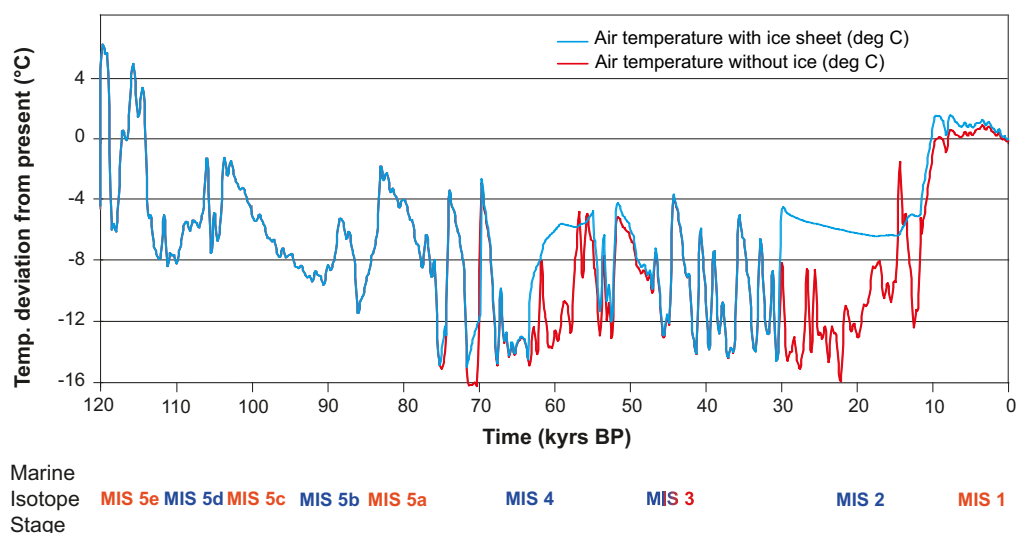


Figure A1-2. Extracted air temperature curve for the Forsmark region for the past 120 kyrs, obtained from the calibrated ice sheet model (Section 3.1.4). The blue line shows the temperatures as obtained from the ice sheet model, comprising ground-level temperatures for ice free periods and basal ice temperatures for glaciated periods. A temperature curve constructed to show conditions without the presence of the ice sheet is shown by the red line. The uncertainty of the temperature curves is discussed in Section A1.5.

In addition to the temperature curve containing ice covered periods, a temperature curve was calculated to show glacial cycle temperatures *without* the presence of an ice sheet. First, a calculation of the annual air temperature that would prevail at the ground-level if the ice sheet was not present was made for the glaciated periods. This was done by applying an atmospheric lapse rate temperature dependence to the ice sheet surface temperatures and ice surface elevation variations. The resulting ground-level air temperatures were subsequently combined with the ground-level air temperatures for ice-free periods resulting in a temperature evolution without ice sheet temperatures (Figure A1-2).

A1.3.2 Adjustment of Forsmark air temperature curves to include estimated Eemian, Mid-Weichselian and Holocene conditions

Eemian conditions

In the temperature reconstruction for the past 120 kyrs (Figure A1-2), the likely environmental conditions in the Forsmark region during interglacials and interstadials also need to be considered. Following the deglaciation of the large Saalian ice sheet (with a maximum ice configuration at around 140 kyrs BP), it is very likely that the Forsmark site was submerged by the Baltic Sea during a large part of the Eemian interglacial, much in the same way as following the Weichselian glaciation. The reconstructed temperature curve (Figure A1-2) was adjusted to reflect these submerged conditions. According to /Björck et al. 2000/, the Eemian interglacial period started at 127 kyrs BP and ended at 116 kyrs BP, resulting in an 11 kyrs long Eemian period. Other studies define the start of the Eemian at 133 and 130 kyrs BP. The length of the Eemian in the GRIP ice core is more than 15 kyrs, although with poor dating /Dansgaard et al. 1993/. It can be concluded that the length and timing, especially the starting time, of the Eemian period from geological data is uncertain. However, in order to make a locally defined Eemian period for the Forsmark site, the ending of the Eemian is selected to occur at the time of the first permafrost development in the SR-Site permafrost simulations, at 114 kyrs BP.

Based on the Saalian glaciation having been more severe than the Weichselian, and with a thicker ice sheet over e.g. Fennoscandia (Section 5.4), it was assumed that the Forsmark site was submerged for several thousands of years longer during the Eemian than in the Holocene. The uncertainty of how much longer the site may have been submerged is of course large. In accordance with this reasoning, the air temperature curve (Figure A1-2) was adjusted to show a mean water temperature of +4°C during the period –120 to –115,000 kyrs at Forsmark (Figure A1-3). The Eemian temperatures for the period following submerged conditions were kept the same as in Figure A1-2.

One result of including, the very likely, submerged conditions in the Forsmark region for the main part of the Eemian interglacial is that not much of the warm Eemian temperatures are seen in the resulting ground temperature curve (Figure A1-3). After 115 kyrs BP, there is a 1,000 year long period of warm Eemian terrestrial conditions before temperatures start to drop. It should be emphasized that this is a coarse reconstruction of Eemian conditions, both in terms of timing, length and prevailing conditions. Nevertheless it is very likely that this reconstruction provides a better estimate of Eemian conditions for the Forsmark region than simply applying the air temperature curve without submerged conditions (Figure A1-2). In addition, the assumption of a submerged temperature of +4°C for the major part of the Eemian constitutes a pessimistic assumption of thermal conditions for the permafrost simulations, see Section 3.4.4 and /Hartikainen et al. 2010/. Keeping a long period of very warm terrestrial conditions would have heated the bedrock prior to cooling and resulted in less permafrost than with the approach taken here.

In the 1D permafrost reconstructions of Weichselian permafrost conditions, see Section 3.4.4 and /SKB 2006a/, the correction for submerged conditions at Forsmark during the Eemian was not made, whereas the temperature curve adjusted for submerged Eemian conditions was used for the 2D permafrost reconstructions (/Hartikainen et al. 2010/ and Section 3.4.4).

Mid-Weichselian conditions

In the reference glacial cycle, ice sheet modelling (Section 3.1.4) resulted in ice-free conditions at Forsmark during Marine Isotope Stage 3, between c. 55 and 30 kyrs BP (Section 4.4). According to the results of the Glacial Isostatic Adjustment (GIA) model simulations (Section 3.3.4), the Forsmark region remained submerged beneath the Baltic Sea for the initial ~8 kyrs of this interstadial period (Section 4.4). Therefore, a submerged temperature of +4°C was set for the first part of this ice-free period of MIS 3 (Figure A1-3, blue curve).

Holocene conditions

The starting time for the Holocene period is here locally defined as the time of the Weichselian deglaciation of Forsmark, occurring at c. 8,800 BC (10,800 years ago) /Söderbäck 2008/. In line with the method above, the temperature curve has been adjusted to show a submerged temperature of +4°C from that time up to near-present conditions (Figure A1-3).

At present, the Forsmark site is located at the Baltic Sea shore. The past and future isostatic land uplift affects the site gradually, discussed in e.g. the section on transition between climate domains (Section 4.5.4). Detailed studies of how the land uplift is affecting the Forsmark site are presented in /SKB 2010d/. However, for the present temperature reconstruction it is sufficient to use the estimate that the repository site in Forsmark emerged from the sea ~1,000 years ago, and adjust the temperature curves accordingly (Figure A1-3).

A1.3.3 Ground surface temperatures

As mentioned in e.g. Section 3.4 and in Figure 4-10, the annual mean ground surface temperature is typically a few degrees warmer than the annual mean air temperature. Therefore, the air temperature curve in Figure A1-3 was used to calculate ground surface temperatures using the 1D permafrost model /SKB 2006a/ (Figure A1-4). This ground surface temperature has been used in the SR-Site studies of /Sundberg et al. 2009/ and /Vidstrand et al. 2010/. For details on how the ground surface temperature was derived, see /SKB 2006a/.

In the 2D permafrost simulations made for SR-Site (see /Hartikainen et al. 2010/ and Sections 3.4.4 and 5.5.3), ground surface temperatures were constructed from the same air temperature curve but in a more detailed way accounting for e.g. dry/wet climate conditions and various surface cover types, see /Hartikainen et al. 2010/. An example of the resulting ground surface temperatures is seen in Figure A1-5. These ground surface temperatures were used to simulate the 2D permafrost development described in Section 3.4.4 and 5.5.

The more simplified ground surface temperature reconstruction (Figure A1-4) typically lies within the range of ground surface temperatures reconstructed in a more detailed way (Figure A1-5).

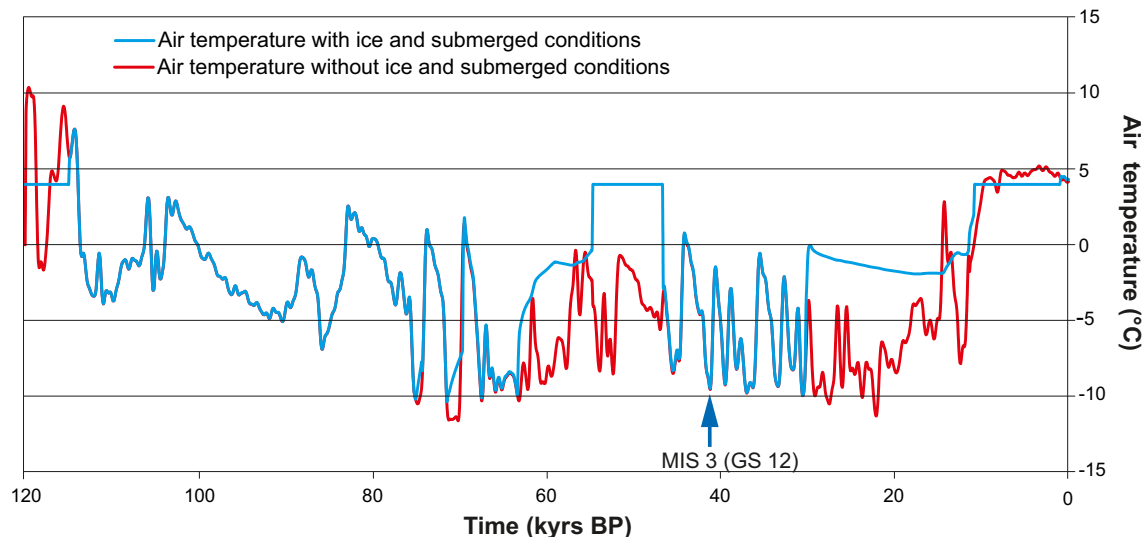


Figure A1-3. Reconstructed air temperature curve for the Forsmark region for the past 120 kyrs, including estimated submerged periods of the Eemian, Mid-Weichselian and Holocene (blue line). The red line shows last glacial cycle air temperatures without the presence of an ice sheet and submerged periods. The temperature scale shows absolute temperatures. The curves have been used as input to e.g. the 1D and 2D permafrost simulations /SKB 2006a, Hartikainen et al. 2010/, see Section 3.4.4 and 5.5. The uncertainties of the temperature curves are discussed in the present appendix, Section A1.5, and the implications for modelled permafrost depths in Section 3.4.4 (sensitivity studies made with the 2D model).

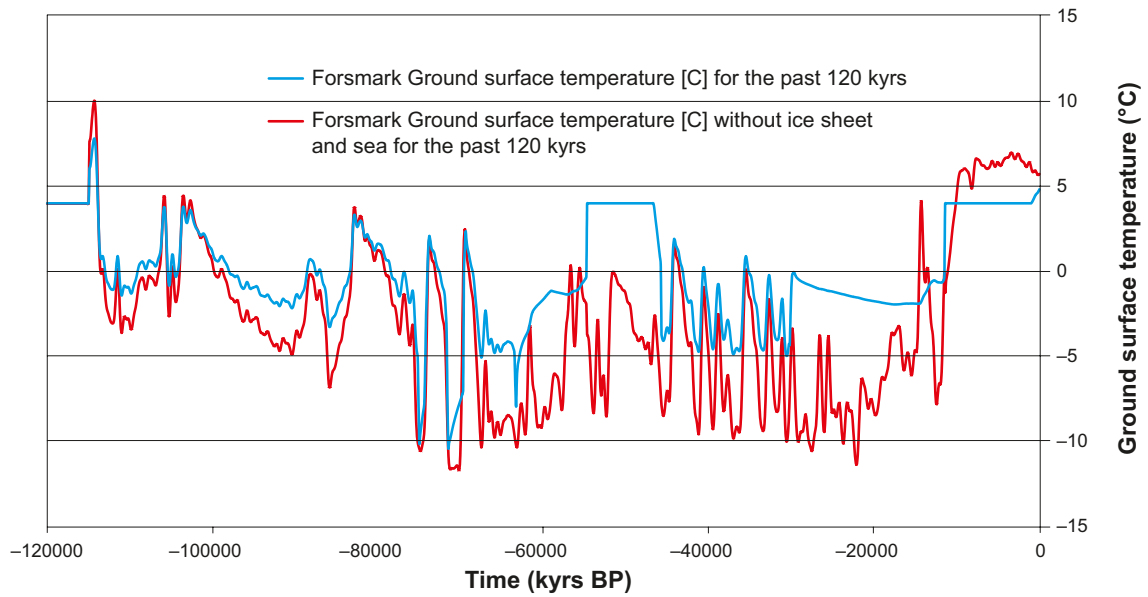


Figure A1-4. Ground surface temperature for Forsmark for the past 120 kyrs with ice sheet (blue) and without ice sheet and sea (red) reconstructed with the 1D permafrost model /SKB 2006a/. The ground surface temperature data has been used as input to /Sundberg et al. 2009/ and /Vidstrand et al. 2010/. The temperature scale shows absolute temperatures. The uncertainty of the temperature curves is discussed in Section A1.5.

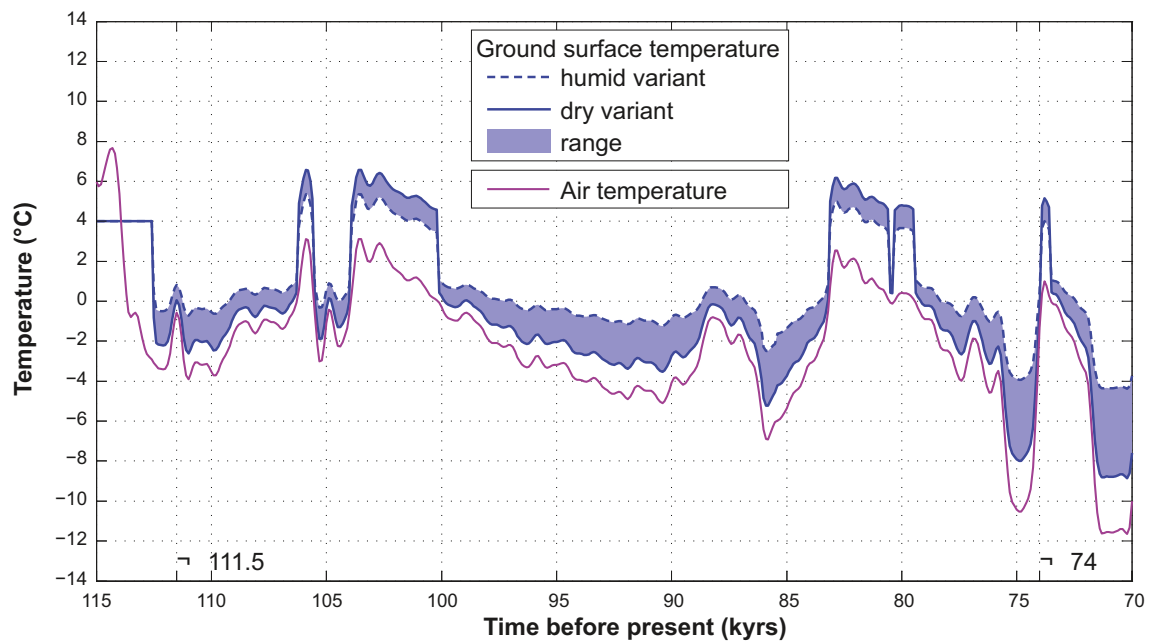


Figure A1-5. Examples of reconstructed ground surface temperatures for Forsmark for the first part of the last glacial cycle (see Section 3.4.4 and /Hartikainen et al. 2010/). The ground surface temperatures cover a range of dry/humid climate conditions, see /Hartikainen et al. 2010/. The example is for one part of the 15 km long investigated profile, with fresh-moist surface conditions just above the repository location (~4,800 m from the south-west side of the profile in Figure 3-58).

A1.4 Temperature conditions during the Holocene and reference glacial cycle

A1.4.1 The ending and duration of the Holocene interglacial in the reference glacial cycle

In the *reference glacial cycle* (Section 4.5), reconstructed last glacial cycle conditions (Section 4.4) are assumed to be repeated during the coming 120 kyrs. To this end, the present day is selected to correspond to 120 kyrs BP in the reconstructed last glacial cycle. This, together with the local definition of the ending of the Holocene (defined as the time of the first occurrence of permafrost at the Forsmark repository location, see Section 4.5.4), results in a total duration of the Holocene period of ~18 kyrs (Table 4-5). This duration is in line with the longer of the two types of interglacials, with durations roughly of either ~20 kyrs or ~10 kyrs, that have occurred during the past eight glacial cycles /Tzedakis et al. 2009/.

This way of defining the ending and duration of the Holocene interglacial is a simple way of treating a complicated subject. For instance, the *reference glacial cycle* described here should be seen as a climate development dominated by natural climate change, i.e. without anthropogenic warming. As mentioned in Section 4.5.4, the uncertainties in the *actual* length of the present interglacial period are naturally very large. Given this uncertainty, it is again emphasized that the evolution of climate domains as described in the *reference glacial cycle* (Figures 4-33, 4-34, 4-35) is not an *expected* future climate evolution. It is one relevant example of an evolution covering the climate-related conditions that can be met in a 100 kyr time perspective. Other possibilities for the length of the present interglacial period are handled in the additional climate cases, such as the *global warming case* (Section 5.1) and *extended global warming case* (Section 5.2).

Looking at Fennoscandia as a whole, glacial and permafrost conditions at other places would come and go at other times, which would result in shorter or longer locally defined interglacial periods if the same approach were to be applied. This way of using locally defined times for start and end of the interglacial results in that the Holocene in northern Sweden being many thousand years shorter in duration than in southern Sweden. From the safety assessment point of view, this is a proper approach to defining interglacial periods, since it is specifically the local conditions, such as the disappearance of an ice sheet or development of permafrost, that are of importance for other relevant processes such as e.g. groundwater flow and chemistry, biosphere conditions, and thermo- mechanical conditions in the bedrock.

As mentioned above, the *reference glacial cycle* assumes that the reconstructed development of ice sheets, permafrost and shore-level are repeated during the coming 120 kyrs. Given this and the treatment of the onset of the last glacial cycle conditions described above, there is no need to explicitly repeat also the temperature curves reconstructed for the last glacial cycle into the future. This is also motivated by the fact that the temperatures at the ground surface, as such, are not of importance for repository safety. The temperature curves reconstructed for the last glacial cycle formed the basis for the reconstruction of last glacial cycle ice sheet and permafrost development, and therefore also the basis for the corresponding development during the future *reference glacial cycle*. Therefore, the temperature curves of Figure A1-3 and A1-4 do not need to be repeated for the future *reference glacial cycle*.

In this context it is important to notice that the uncertainties estimated for the temperature curve reconstructed for the last glacial cycle (Figure A1-3), discussed in Section A1.5, are dealt with: i) in dedicated sensitivity tests in the permafrost simulations (Section 3.4.4), and ii) in an indirect way by e.g. the complementary climate case dealing with larger future ice sheets than those reconstructed for the last glacial cycle.

A1.4.2 Holocene temperatures

From extrapolations of measured temperature bore hole loggings in Forsmark, the present-day ground surface temperature is estimated as +6.5°C /Sundberg et al. 2009/. This value lies between the present ground surface temperatures suggested by the 2D permafrost modelling, which yields a value of +6.1°C for the evolution with dry climate, and +7.4°C for the evolution humid climate variant /Hartikainen et al. 2010/. A future Holocene ground surface temperature of around +6.5°C could therefore be envisaged for the remaining part of the Holocene. This estimate of *reference glacial cycle* conditions (which is completely dominated by natural climate change, see Section 1.2.3 and 4.5) thus excludes the anthropogenic contribution to the ~0.7 degrees of climate warming that has taken place during the last 100 years /IPCC 2007/. For the climate cases with global warming, air- and ground surface temperatures are considerably higher than in the *reference glacial cycle*, see Sections 5.1 and 5.2.

As mentioned above, in the adopted approach to repeating last glacial cycle reconstructions of ice sheet, permafrost and shore-level development for the coming 120 kyrs, there is no need to explicitly repeat also the air temperature curve used for these reconstructions. If such a projection were to be made, it would be very similar to the curve seen in Figure A1-3 (blue line), with the exception that initial temperatures would not reflect submerged conditions (as the initial conditions in the last glacial cycle reconstruction). Submerged temperature conditions would however prevail later on in the development (as in Figure A1-3 blue line).

A1.5 Estimates of uncertainties in the reconstructed temperature curve

There are a number of different uncertainties and assumptions that contribute to the overall uncertainty in the air temperature curve reconstructed for the Forsmark region for the last glacial cycle (Figure A1-3): i) uncertainties in the calculations of air temperatures from $\delta^{18}\text{O}$ values in the GRIP ice core, ii) temporal uncertainties in the time scales used for the ice core data, iii) the representativity of GRIP ice core data for Fennoscandian conditions.

A1.5.1 Uncertainties in the GRIP temperature curve

Uncertainties in calculated Greenland temperatures

The isotopic record used for the calculation of GRIP temperatures (Figure A1-1, red line) is the one used in /Johnsen et al. 1995/. For the transformation of $\delta^{18}\text{O}$ values to air temperatures, /Johnsen et al. 1995/ used the relationship:

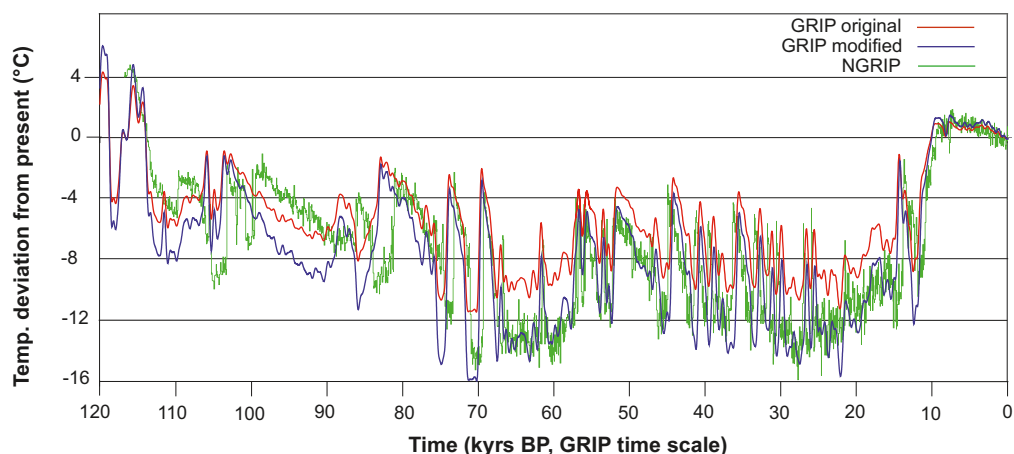
$$T = 1.5 (\delta^{18}\text{O} + 35.27) \quad \text{Equation A1-1}$$

where T is the temperature deviation from year 1989, and $\delta^{18}\text{O}$ is the oxygen isotope value recorded in the ice core. Equation A1-1 represents a *present day* $\delta^{18}\text{O}$ -T relationship averaged for the last 50 years up to 1989, and assuming that the temperature over these 50 years is the same as in 1989 /Johnsen et al. 1995/. As previously mentioned, it has been shown that the present day $\delta^{18}\text{O}$ – T relationship is less suitable for glacial conditions, and that this relationship also changes between stadials and interstadials /Huber et al. 2006/. Changes in the $\delta^{18}\text{O}$ – T relationship over time are caused by several factors such as changes in the source of precipitation /Masson-Delmotte et al. 2005/, changes in the distribution of precipitation on the ice sheet /Werner et al. 2001/, and by seasonal variations in temperature and precipitation /Krinner et al. 1997/. This introduces errors in the temperature curve when produced according to /Johnsen et al. 1995/.

Results of /Huber et al. 2006/ show that the $\delta^{18}\text{O}$ – T relationships during last glacial cycle interstadials are closer to the present-day relationship, used by /Johnsen et al. 1995/, than is the $\delta^{18}\text{O}$ – T relationship during last glacial cycle stadials. It is therefore expected that stadial temperatures in the /Johnsen et al. 1995/ temperature curve (Figure A1-1, red line) contain a larger error than the warmer interstadial temperatures. The uncertainty in the temperature estimates for Marine Isotope Stage 3 (MIS 3) by /Huber et al. 2006/ is minimum c. 3 degrees and maximum c. 6 degrees. From $\delta^{15}\text{N}$ measurements a symmetric uncertainty of $\pm 3^\circ\text{C}$ would be applicable for these periods /Huber et al. 2006/.

For a comparison with the temperatures reconstructed for the NGRIP ice core /Huber et al. 2006/, $\delta^{18}\text{O}$ values from the NGRIP ice core /NorthGRIP community members 2004/ were transformed to tentative temperatures using the same transfer function (Equation A1-1) as used in the production of the GRIP temperature curve. The resulting curve is seen in Figure A1-6 (green line), together with the original GRIP curve and the temperature curve modified in the ice sheet model calibration process (Section A1.2 and Figure A1-1). It is important to note that the temperatures calculated from the NorthGRIP data within the present study are not to be taken as solid scientific results. They are included only to make the first-order analysis of the errors introduced by using the present day $\delta^{18}\text{O}$ – temperature relationship for the GRIP data.

Table A1-1 summarizes the temperature amplitudes of individual Dansgaard-Oeschger (DO) events during MIS 3 from /Huber et al. 2006/ together with corresponding temperature amplitudes from using the present day $\delta^{18}\text{O}$ – T relationship of /Johnsen et al. 1995/ on the NGRIP $\delta^{18}\text{O}$ data (Figure A1-6, green line). The results show that, during the MIS 3 DO events studied by /Huber et al. 2006/, the temperature lowering is underestimated by between c. 20 and 40% or c. 2–4°C (Table A1-1) when using the present-day $\delta^{18}\text{O}$ – T relationship in the reconstruction of GRIP ice core Greenland temperatures (Figure A1-1, red line).



Marine Isotope Stage MIS 5e MIS 5d MIS 5c MIS 5b MIS 5a MIS 4 MIS 3 MIS 2 MIS 1

Figure A1-6. Palaeotemperature curve from the GRIP ice core /Johnsen et al. 1995/ (red) and modified GRIP temperature curve resulting from the ice sheet model calibration (blue). For comparison, a tentative temperature record from the NGRIP ice core /NorthGRIP community members 2004/ is shown in green, see the text. The NGRIP temperature curve was constructed within the present study. Note that the time scale only applies for the GRIP data. The NGRIP data is not plotted on the same time scale, which contributes to a temporal mismatch between GRIP and NGRIP results in the plot. However, the tentative NGRIP curve is here included only for general comparison of temperature amplitudes between the two ice cores.

This means that the temperature curve used for the ice sheet model calibration (Figure A1-1, red line) probably underestimates Greenland air temperatures during cold stadial periods by c. 2–4°C due to the use of the present day $\delta^{18}\text{O} - T$ relationship. This uncertainty needs to be considered in the overall estimate of uncertainty in the temperature curve reconstructed for Forsmark for the last glacial cycle (Figure A1-3), see below. Given the result by /Huber et al. 2006/, using the present day $\delta^{18}\text{O} - T$ relationship for warmer interstadial periods most probably introduces a considerably smaller error.

An additional error is introduced by the treatment of the air temperatures from the GRIP ice core as annual mean air temperatures when they in fact are affected by a seasonality signal /Krinner et al. 1997/.

Table A1-1. Difference in temperature amplitude for Dansgaard-Oeschger (DO) events during MIS 3 between the NGRIP curve as described by /Huber et al. 2006/ and if applying the simple present-day $\delta^{18}\text{O}$ -Temperature relationship used for the GRIP data. The results indicate that the GRIP data (Figure A1-1 and A1-6) may underestimate the temperature amplitude associated with DO-events by up to 3–4 degrees. However, this also assumes that the climate signal in the NGRIP and GRIP temperature curves are the same.

Dansgaard-Oeschger event	Mean ΔT (°C) from NGRIP data /Huber et al. 2006/	ΔT if applying simple GRIP $\delta^{18}\text{O}$ -T relationship on NGRIP $\delta^{18}\text{O}$ data	Difference (°C and percent)
9	9	7	2 (-22%)
10	11.5	8	3.5 (-30%)
12	12.5	9.5	3 (-24%)
14	12.5	8	4 (-32%)
15	10	6	4 (-40%)
16	9	5	4 (-44%)
17	12	8	4 (-33%)

It is also worth noting that the modified GRIP temperature curve (from the ice sheet model calibration process) (Figure A1-6, blue line) specifically has resulted in that temperatures during stadial are colder than in the original GRIP curve, whereas warm interstadial temperatures are similar. This shows that the ice sheet model calibration process has reduced the error introduced from using the present day $\delta^{18}\text{O} - T$ relationship for the original GRIP temperature curve.

Temporal uncertainties in the ice core data

In the Greenland ice cores, such as GRIP, NGRIP, GISP2 etc, temporal uncertainties exist in the timing of individual climatic events. From the beginning, different ice cores were dated by different methods, which yielded inherited differences in the resulting time-scales. The actual climate information also differs between the cores, which contributes to the difficulties in matching them against each other.

The most commonly used ice core time scales are the Meese-Sowers GISP2 stratigraphic time scale /Meese et al. 1997/ and the modelled “ss09sea” time scale that was applied to the GRIP and NGRIP ice cores /Johnsen et al. 2001/. The glacial section of the GRIP core (Figure A1-1) was dated by employing an ice flow model with an empirical $\delta^{18}\text{O}$ -accumulation relationship and two dated fix-points /Dansgaard et al. 1993, Johnsen et al. 1995/. This resulted in the improved ss09sea time scale /Johnsen et al. 2001/. According to /Svensson et al. 2008/, these time scales agree within 750 years back to 40 kyrs, but further back in time the disagreement becomes several thousands of years. Further adjustments of the time scales used for ice core data are also made, e.g. /Skinner 2008, Svensson et al. 2008/.

There are still significant temporal uncertainties related to the Greenland ice cores, e.g. /Rasmussen et al. 2006 and 2008, Skinner 2008, Svensson et al. 2008/. For example, /Skinner 2008/ showed that the NGRIP age scale probably is missing up to 1,200 years for the last glaciation period. Any reconstruction of last glacial cycle conditions that are based on these ice core data also includes these uncertainties. However, in the safety assessment work, the *exact* temporal development of temperature during the last glacial cycle, and more specifically the exact temporal development of other processes that are dependent on the temperature such as ice sheets and permafrost, is of minor importance for repository safety (Section 1.2.3). Furthermore, the reconstructed last glacial cycle conditions (including their temporal uncertainties) are used to construct a future *reference glacial cycle*, which in turn is complemented by other possible future climate developments in which e.g. permafrost and ice sheets may develop at other times than in the *reference glacial cycle*.

A1.5.2 Uncertainties in the reconstructed Forsmark region temperature curve – comparison with other data on Fennoscandian palaeotemperatures

As previously mentioned, the modified GRIP temperature curve (Figure A1-1, blue line) was subsequently used to extract a temperature curve for the Forsmark region (Figure A1-2 and A1-3). Other independent proxy data and model data on Fennoscandian temperatures during the last glacial cycle may be used for a first-order check of the validity of this reconstructed Forsmark region temperature curve (Figure A1-3). In such comparisons, it is important to remember that both climate proxy data and modelled climate data may contain significant uncertainties, e.g. /Kjellström et al. 2010b/. The temperature curve reconstructed for Forsmark is compared with other palaeoclimate data for the MIS 5d stadial, the MIS 5c interstadial, the early MIS 3 interstadial, and the middle MIS 3 stadial, see Section 4.2 and 4.3.

The palaeoclimate data from the Sokli site in northern Fennoscandia e.g. /Helmens 2009a, Väiliranta et al. 2009, Engels et al. 2010/, used in the comparisons, consists of reconstructed summer (July) air temperatures, whereas the temperature curve reconstructed for the Forsmark region (Figure A1-3) reflects annual mean air temperatures. Therefore, the comparison between the two regions does not make use of absolute temperatures, but instead the *temperature difference* to present climate conditions in each region for each period. With this approach, potential differences between the sites in terms of the amount of change in seasonal temperature cycle between present conditions and the past is neglected. However, it is considered that this is of minor importance and that the comparisons still contribute with important information.

Early Weichselian (MIS 5d stadial)

During ice-free stadial conditions of MIS 5d (the Hering stadial 117–105 kyrs BP), July summer temperatures of +7°C were reconstructed for the Sokli site in northern Finland, see Section 4.3.1 and /Engels et al. 2010/. This is c. 6°C colder than the present summer mean temperature of +13°C.

The reconstructed air temperature curve for the Forsmark region indicate MIS 5d annual mean air temperatures from c. –1°C down to c. –4°C (Figure A1-3), i.e. around 6 down to 9°C colder than at present.

Early Weichselian (MIS 5c interstadial)

During MIS 5c (the Brørup interstadial, 105–93 kyrs BP), summer temperatures inferred from plant macrofossil remnants indicate warm conditions in northern Fennoscandia. Reconstructed July temperatures for this period are as high as +16°C, which is 3°C warmer than at present /Väliranta et al. 2009, Engels et al. 2010/. Other (lower-resolution) MIS 5c reconstructions from northern Fennoscandia indicate summer temperatures 6–7°C lower than present, see /Engels et al. 2010/. However, several central European sites indicate that there was a phase during the MIS 5d interstadial that was characterized by high summer temperatures, see /Engels et al. 2010/.

The reconstructed annual air temperature for the Forsmark region during the MIS 5c interstadial (105–93 kyrs BP) is from c. +2°C down to c. –4°C (Figure A1-3), i.e. between 3 and 9°C lower than at present.

Middle Weichselian (early MIS 3 interstadial)

Mean July air temperatures for early MIS 3 (at ~50 kyrs BP) in northern Fennoscandia, inferred from fossil chironomides, are 12–13 ± 1.15°C /Helmens 2009a/. This corresponds to the present-day summer temperature (13°C) in the region. Mean July air temperatures inferred from terrestrial pollen data from the same site lie within the range of 11–12 ± 1.5°C /Helmens 2009a/. The reconstructed high summer temperatures are in part ascribed to enhanced July insolation compared with present at the high latitude site of the site. Warm early MIS 3 temperatures are in line with the ice-free conditions in northern Fennoscandia and elsewhere (Section 4.2 and 4.3.2).

In the reconstructed annual air temperature curve (Figure A1-3), the Forsmark region is submerged under the Baltic Sea during early MIS 3 (at ~50 kyrs BP). However, the values for non-submerged conditions amount to around –1 to –4°C, which is between c. 6 and 9°C lower than at present.

Middle Weichselian (middle MIS 3 stadial)

Simulated temperatures for the MIS 3 (Greenland Stadial 12) period (44 kyrs BP), see Section 4.3.2 and /Kjellström et al. 2009b/, suggest that the annual mean air temperature in the Forsmark region was –7.6°C during this cold stadial. This is c. 12.5°C colder than the present annual mean air temperature.

The reconstructed last glacial cycle air temperature curve for Forsmark suggests that the annual air temperature during the same stadial was c. –9°C (Figure A1-3, blue arrow), or c. 14°C colder than at present.

Discussion

In this comparison, it should be emphasized that all data on palaeotemperatures, from proxy data and from climate modelling, including the temperature curve reconstructed for the Forsmark region, contain uncertainties. Nevertheless, a comparison between the temperature reconstructions contributes with an overall picture of how the reconstructed curve for the Forsmark region (Figure A1-3) relates to other independent estimates of palaeotemperatures.

Table A1-2 summarizes the estimated approximate temperature difference between present day conditions and the conditions during the four last glacial cycle stadials and interstadials as described above.

Table A1-2. Estimated approximate temperature difference between present day conditions and conditions during four last glacial cycle stadials and interstadials as reflected in the reconstructed temperature curve for the Forsmark region (Figure A1-3) and in other palaeoclimate proxy- and model data (see the text). It should be noted that many of the reconstructed palaeotemperatures should be regarded with caution, such as the MIS 5d value for Northern Fennoscandia /Engels et al. 2010/.

	Approximate ΔT MIS 5d stadial – present	Approximate ΔT MIS 5c interstadial – present	Approximate ΔT Early MIS 3 inter- stadial – present	Approximate ΔT Middle MIS 3 stadial – present
Northern Fennoscandia (Sokli region)	6°C colder	3°C warmer	0–2°C colder	–
Other Fennoscandian MIS 5c sites	–	6–7°C colder	–	–
South-central Sweden from modelling (Forsmark region)	–	–	–	12.5°C colder
South-central Sweden from temp curve (Forsmark region)	6–9°C colder	3–9°C colder	6–9°C colder	c. 14°C colder

The only comparison above which uses the same geographical region, as well as estimates of absolute numbers on annual mean air temperature in both reconstructions, is the one for the middle MIS 3 stadial, where climate model results from the Forsmark region are compared with the reconstructed Forsmark region air temperature curve (Figure A1-3). This comparison shows that, for this cold stadial period 44 kyrs ago, the reconstructed temperature curve gives a $\sim 1.5^\circ\text{C}$ lower temperature than the climate model simulation (Table A1-2), and thus that these two independent temperature estimates of temperature in the Forsmark region are well in line with each other. This suggests that, although the temperature curve for Forsmark was constructed in a crude way, the resulting Middle Weichselian stadial temperatures in the Forsmark region curve may well be realistic.

For the Early Weichselian MIS 5d stadial and MIS 5c interstadial, values from the reconstructed Forsmark temperature curve indicates a similar, or some degrees larger, lowering of temperature than the other proxy data (Table A1-2).

For the early MIS 3 interstadial (at ~ 50 kyrs BP), proxy data e.g. /Helmens 2009a/ suggests present-day summer temperature conditions in northern Fennoscandia. When such warm interstadial conditions prevail in northern Fennoscandia, similar near-present temperature conditions would be expected also in south-central Sweden, given that the region is free of ice such as in the *reference glacial cycle*. However, for early MIS 3, the temperature in the reconstructed curve (Figure A1-3) is c. 6–9°C colder than at present, i.e. far from present-day temperatures. This might be due to several reasons, i) similar near-present temperatures did occur also in south-central Sweden (including the Forsmark region), but the warm conditions over Fennoscandia did not have a corresponding rise in temperature over Greenland, and are thus not found in the ice core record, ii) the climate in south-central Sweden was significantly colder than in northern Fennoscandia during this period, iii) one (or both) of the reconstructions may have a large error in reconstructed temperatures for this period (the temperature estimate by /Helmens 2009a/ has an uncertainty of only $\pm 1.5^\circ\text{C}$, which in this case would indicate that the temperature reconstruction for the Forsmark region has temperatures that are much too low for this period), or iv) a combination of the above reasons.

The resulting overall picture from the comparisons is that the reconstructed temperature curve (Figure A1-3) is in agreement with or gives somewhat lower temperatures (by some degrees) than the other reconstructions. The comparison thus suggests that the reconstructed temperature curve for Forsmark probably does not overestimate the temperatures during the investigated last glacial cycle stadials and interstadials.

A1.5.3 Estimated temperature uncertainty and treatment of this uncertainty in SR-Site

The modified GRIP temperature curve (after ice sheet model calibration) (Figure A1-1) has reduced uncertainties present in the original GRIP curve, but there still remains a significant uncertainty of several degrees in this curve (Table A1-1). When this curve was used to construct the temperature

curve for the Forsmark region (Figure A1-3), it is, as expected, obvious that also the reconstructed Forsmark temperature curve has significant uncertainties. The comparison with proxy data seems, however, to indicate that the reconstructed Forsmark temperature curve is in broad agreement with the (few available) proxy data and furthermore that it does not overestimate temperatures for the compared last glacial cycle stadials and interstadials. The general picture from the comparison with Fennoscandian proxy data is that the reconstructed temperature curve gives roughly correct or slightly too low temperatures by a few degrees.

Based on how the air temperature curve has been constructed, on the comparison against Fennoscandian last glacial cycle stadial and interstadial proxy data, and on remaining uncertainties associated with the temperature curve that have not been quantified above, it is here pessimistically estimated that the uncertainty in the reconstructed Forsmark region temperature curve (Figure A1-3) is not larger than 6°C for the periods with largest uncertainties. Furthermore, an uncertainty of up to c. 4–5°C is estimated for the major part of the curve, and for some parts of the curve, such as for the Holocene and the Eemian, smaller than 4°C.

In SR-Site, the uncertainties in the reconstructed temperature curve for the Forsmark region mainly affect the permafrost modelling, see /Hartikainen et al. 2010/ and Section 3.4.4 and 5.5.3 and /Vidstrand et al. 2010/. In the permafrost simulations performed for Forsmark, see /Hartikainen et al. 2010/, Section 3.4.4 and 5.5.3, the uncertainties in the air temperature curve are covered by a range of sensitivity tests specifically on the air temperature curve and on surface conditions (for the calculation of ground surface temperatures). In some of the sensitivity tests, the entire air temperature curve reconstructed for the last glacial cycle (Figure A1-3) was lowered (and raised) by 6°C, in accordance with the estimated maximum uncertainty. This was also done in combination with uncertainties in other parameters of importance for the development of permafrost, see /Hartikainen et al. 2010/ and Section 3.4.4. Other sensitivity tests on the air temperature curve for permafrost simulations covered a temperature range significantly wider than the estimated uncertainty described in this section, up to a 16°C lowering of the air temperature curve in Figure A1-3, see /Hartikainen et al. 2010/ and Section 3.4.4.

Uncertainties in the original GRIP temperature curve have a direct effect only on the ice sheet modelling (Section 3.1.4), but the uncertainty is here to a large extent taken care of by the ice sheet modelling process (in which the ice sheet configurations during stadials periods, when the error is largest, were calibrated against known ice-marginal positions).

The *temporal* uncertainty in the reconstructed temperature curve, discussed above, is covered by the additional climate cases (Chapter 5), where e.g. permafrost might develop earlier than in the *reference glacial cycle* (based on the Weichselian reconstruction that includes the reconstructed temperature curve).

Ice sheet profiles

A2.1 Background

In various SR-Site studies, e.g. on groundwater flow and THM processes, ice sheet profiles are useful as input for investigating how these processes are affected by glacial conditions. This section gives background and data for selection of two ice surface profiles to be used in the SR-Site safety assessment. Two different types of ice sheet profiles are discussed; ice profiles derived mainly from theoretical considerations, and ice profiles derived from more complex numerical ice sheet modelling.

The steepness of an ice sheet surface is determined by the combination and interplay of several factors such as basal shear stresses, englacial ice temperatures, temperatures at the ice sheet bed, the basal hydrological conditions and the presence or absence of deformable sediments at the bed. As a general rule of thumb, a retreating ice sheet has a less steep profile than an advancing ice sheet, and so does an ice sheet ending in the sea compared with a terrestrial ice sheet. Warm basal conditions, with presence of basal water, and presence of deformable bed sediments also results in less steep ice than cold-based conditions. The steepness of the ice sheet surface is important for the ice flow and for the water routing and water flow at the base of the ice. In addition, it is also of high importance for e.g. the flow of groundwater in the bedrock and for the stress situation in the Earth's crust.

A2.2 Theoretical ice sheet profiles

The easiest way of describing an ice sheet profile is by assuming that ice is a perfectly-plastic material. One can further assume that this ice sheet is circular and situated on a flat and horizontal bed, and that the ice sheet is in steady-state, i.e. that no change in ice configuration occurs over time. In this case the ice sheet surface profile constitutes a simple parabola e.g. /Paterson 1994/, and is calculated by:

$$h^2 = \frac{2\tau_0}{\rho g}(L-x) \quad \text{Equation A2-1}$$

where h is the ice thickness at distance x from the centre, L is the radius of the ice sheet, τ_0 is the basal shear stress, ρ is the ice density and g is the acceleration of gravity. With $L = 400$ km, $\rho = 0.9$ kg/dm³, $g = 9.81$ m/s² and τ_0 set to 50 and 100 kPa, the resulting parabolas are seen in Figure A2-1. A basal shear stress of 100 kPa is more valid for small valley glaciers while 50 kPa (with large variation) is more representative for ice sheet conditions.

In order to have a more realistic description, Equation A2-2 introduces a flow of the ice /Paterson 1994/. The same assumptions are made as above, except for a removal of the perfect-plasticity assumption, and the introduction of an assumption of basal frozen conditions.

$$(h/H)^{2+2/n} + (x/L)^{1+1/n} = 1 \quad \text{Equation A2-2}$$

Here H is the ice thickness at the centre of the ice sheet and n is a flow parameter (the strain-rate exponent) in Glen's flow law of ice, often set to 3, e.g. /Paterson 1994/. The resulting profile when L is set to 400 km and 900 km, $H = 3,000$ m and $n=3$ is seen also in Figure A2-1.

Equation A2-2 results in a steeper profile (for the corresponding profile length) than the parabolas described by Equation A2-1, and presumably it is more in line with real ice sheet profiles /Paterson 1994/. For the further use of theoretical ice profiles, the steeper theoretical profiles of Equation A2-2 are chosen. Furthermore, steeper profiles also give larger impacts in studies of groundwater flow and crustal stresses under glacial conditions, and thus is a more pessimistic choice from the safety assessment point of view.

The theoretical profiles (Equation A2-1 and A2-2) are compared with an ice sheet profile from the western part of the Greenland ice sheet in Figure A2-2, see also /Jaquet et al. 2010/. Note that in this figure the ice sheet surface topography for the theoretical profiles is reflecting the full relief of the bed topography, which is not the case in the real world. The less steep theoretical profile is similar to the Greenland profile, whereas the steeper theoretical profile is steeper than the Greenland ice sheet profile.

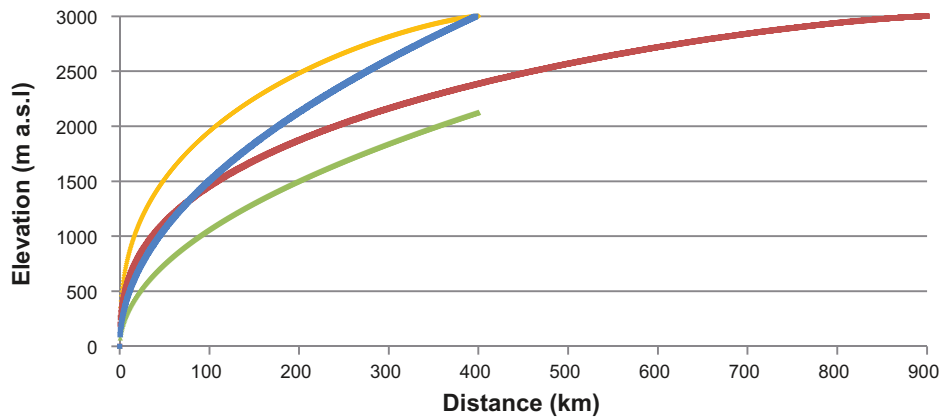


Figure A2-1. Theoretical steady-state ice sheet profiles according to /Paterson 1994/. Parabolas produced by Equation A2-1 are shown in green (400 km long profile with a basal shear stress of 50 kPa) and blue (400 km long profile with a basal shear stress of 100 kPa). The steeper profiles produced by Equation A2-2 are shown in yellow (400 km long profile) and red (900 km long profile). The latter two profiles are considered to be more realistic representations of steady-state ice sheet profiles /Paterson 1994/.

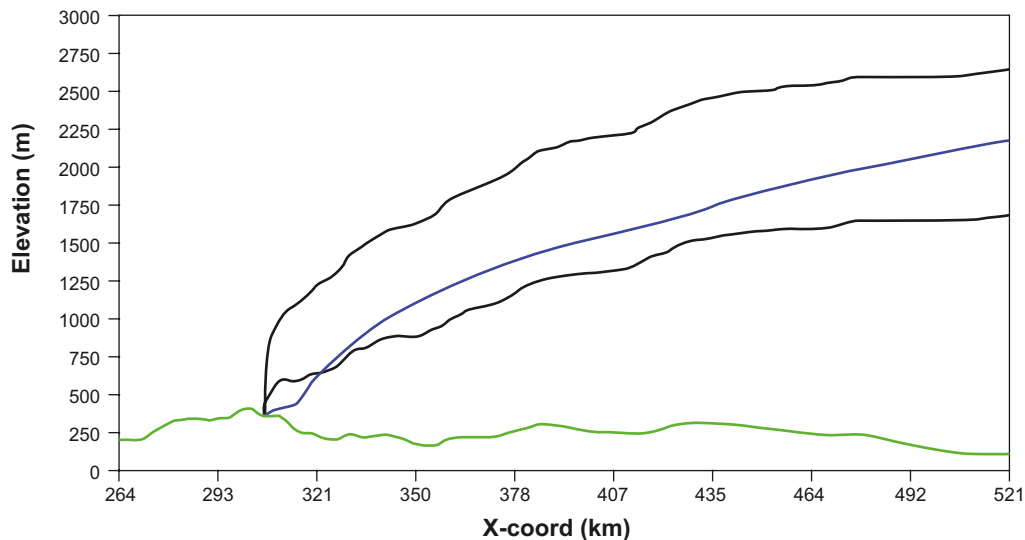


Figure A2-2. Comparison between the theoretical ice profiles (Equation A2-1 with τ_0 set to 50 kPa upper black line and Equation A2-2 lower black line) with an ice sheet profile from the Greenland ice sheet (blue). The bed is shown in green. The theoretical profiles are, unrealistically, displayed as reflecting the full relief of the bed topography, which has resulted in too much relief in the ice surface. From /Jaquet et al. 2010/.

A2.3 Ice profiles from numerical ice sheet simulations

For SR-Site, ice profiles were extracted from the time-transient reconstruction of the Weichselian ice sheet simulated by the University of Maine Ice Sheet Model (UMISM), see Section 3.1.4. In the following text, this model simulation is denoted the *reference glacial cycle ice sheet simulation*. The location of the transect from which the profiles were extracted is seen in Figure A2-3. Several ice sheet profiles from the last stadial of the reconstructed Weichselian ice sheet (e.g. from MIS 2 that included the Last Glacial Maximum (see Section 4.2), are seen in Figure A2-4. Figure A2-4a shows profiles from the advancing phase and Figure A2-4b from the retreating phase of the simulated MIS 2 ice sheet.

In the Weichselian ice sheet simulation, the ice sheet advances over the Forsmark region from NW-NNW while during the deglaciation it generally retreats in a more northerly direction. All profiles in Figure A2-4 were extracted along transect 1 (Figure A2-3). The orientation of transect 1 was selected in order to capture the steepest surface gradients during ice advance (i.e. generally oriented

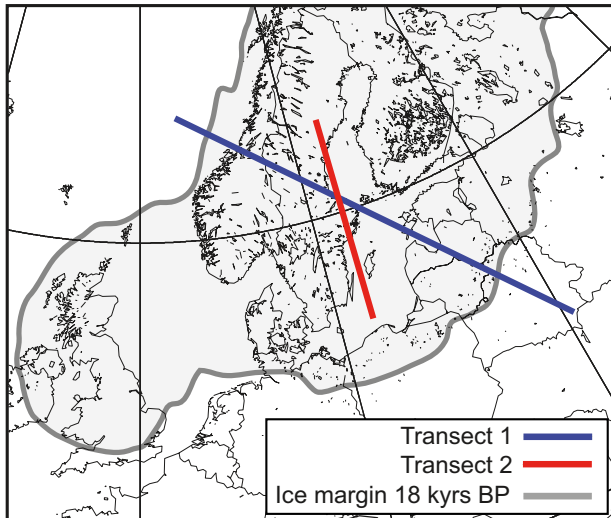


Figure A2-3. Locations of ice sheet profiles. Transect 1: transect for all profiles seen in Figure A2-4 a and b. Transect 2: location of retreat profile extracted for 14.3 kyrs BP seen in Figure A2-7.

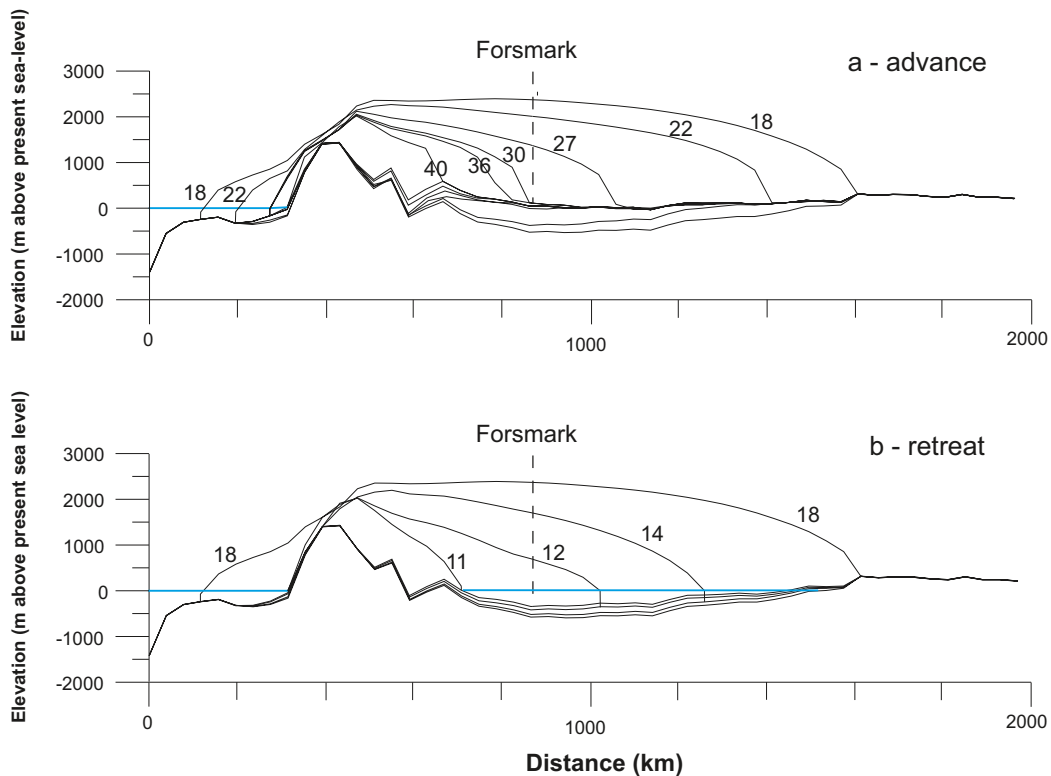


Figure A2-4. Examples of ice sheet profiles from the Weichselian ice sheet simulation during the MIS 2 advance and retreat. Profiles are extracted from transect 1 (Figure A2-3). Numbers indicate time (kyrs BP). It should be noted that the y-scale has a vertical exaggeration of 100x and that sea-level change associated with ice sheet growth is not shown. In the frontal-most part of the profile, the 10 km spatial resolution of the ice sheet model can be seen as a sharp knick in the ice surface. Present-day sea-level is shown in blue. The LGM sheet configuration, along this specific profile, occurs at around 18 kyrs BP.

along the flow lines of the advancing ice, perpendicular to the advancing ice margin). Consequently, profiles extracted along the same transect but for the retreat phase, which occurred in a somewhat other direction, are somewhat underestimating the steepness of the ice sheet surface.

In addition to the profiles selected along transect 1 (Figure A2-3), a c. 900 km long retreat profile was selected along transect 2. This profile was extracted for the time 14,300 kyrs BP. All profiles selected from the ice sheet advance phase are discussed in Section A2.4.1, while all profiles from the retreat phase are discussed in Section A2.4.3.

Ice surface gradients

Figure A2-5 shows the ice surface gradients that occur above the Forsmark site in the *reference glacial cycle* ice sheet model run. There are two phases of ice sheet coverage in this model simulation, during MIS 4 and MIS 2, and hence two periods with gradients in Figure A2-5. Steep gradients occur during the short periods when the ice front passes that area, while low gradients prevail during the long periods of time when the ice front is located far from the repository. For the second and main ice covered period, the mean value of low gradients is around 0.06 degrees (or 0.98 m/km), corresponding to about one third of the present-day regional topographic gradient at Forsmark (3 m/km) /Vidstrand et al. 2010/. The resulting steepest hydraulic gradient in the *reference glacial cycle* is about 0.8 degrees (0.014 m/m) over the first 10 km of the modelled ice sheet profile.

A2.4 Comparison of ice profiles from numerical simulations with the theoretical profile

In all comparisons below, it should be remembered that at a given time, the ice configuration of a realistically modelled ice sheet, such as the one used here, is quite complex; the ice surface is irregular on both small and large spatial scales, and thus far from being a circular and regularly shaped dome as in the theoretical examples. This is due to variations in the dynamics and flux of the ice as a response to e.g. varying mass balance at the surface and variations in bed topography. Such complex ice configurations are seen also on the present day Greenland and Antarctic ice sheets. Consequently, at a given time, ice surface profiles derived from one part of the simulated ice sheet may differ from profiles extracted from another part. When selecting profiles from the Weichselian ice sheet simulation, the aim has been to select profiles both relevant for a broad understanding of how the ice sheet looks and behaves and profiles specifically relevant for the Forsmark site.

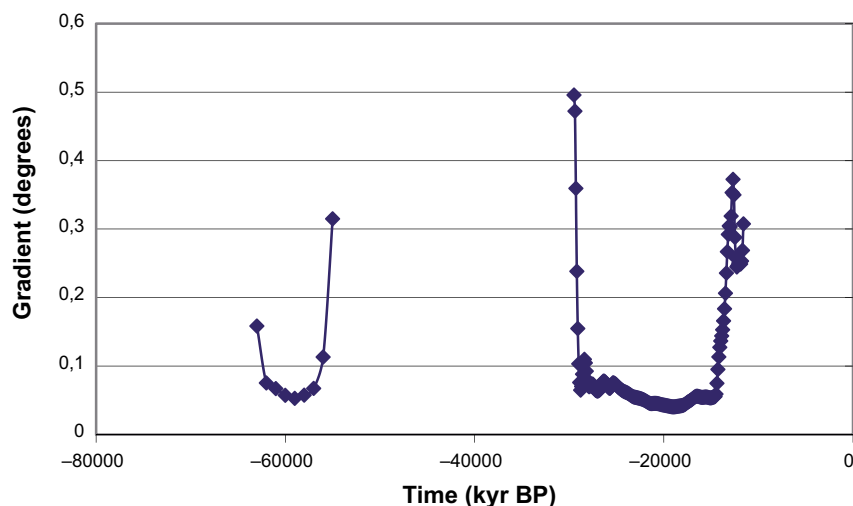


Figure A2-5. Modelled ice surface gradients above the Forsmark site for the reference glacial cycle. Note that the steepest part of the ice sheet is not included in the figure and is estimated to have an inclination of 0.8° (0.014 m/m). Steep gradients occur when the ice front passes the site, whereas low gradients prevail when the ice margin is situated far from the site.

A2.4.1 Simulated advancing profiles compared with the theoretical steady-state profile

In the Weichselian ice sheet simulation, the main phase of ice sheet coverage at Forsmark takes place during the MIS 2 stadial (Section 4.4), with the ice sheet margin reaching Forsmark at around 30 kyrs BP (Section 4.5.1 and Figure A2-4a).

In Figure A2-6, all extracted profiles from the ice sheet *advance* phase (Figure A2-4a) are stacked and compared with the theoretical profiles of Equation A2-2 (Figure A2-1). It is seen that none of the simulated advancing profiles are steeper than the two theoretical steady-state profiles.

It is also seen that the steepest advancing profile, at 30 kyrs BP, is close to being as steep as one of the theoretical profiles described by Equation A2-2. The simulated 30 kyr BP profile is the ice sheet profile when the ice margin is located in the Forsmark area (Figure A2-6).

Having the seemingly contradiction that the steady-state profiles are not steeper than the advancing profiles, is in this case not surprising. Such differences are expected since the profiles are produced in completely different ways. All profiles derived from the numerical ice sheet model incorporate a number of parameters with considerably more realistic representations than how they are treated in the theoretical profile calculation. The ice sheet model includes for instance realistic bed topography instead of a flat horizontal bed, a description of ice sheet thermodynamics, where ice flow and ice temperatures are allowed to interact, and also a better representation of basal conditions (Section 3.1.4). Even if the ice sheet model is far from being a full and complete representation of the natural system, it is significantly better than the theoretical equations. Consequently, the simulated less steep profiles are here considered more realistic for the advancing phases than the steeper theoretical profiles.

There are no large variations in the steepness of the advancing profiles extracted from the ice sheet simulation (Figure A2-6). The steepest simulated advancing profile (from 30 kyrs BP) is close to being as steep as the least steep theoretical profile. Although the simulated profiles are here considered more realistic than the theoretical profiles, the above results show that if one uses the theoretical profiles of Equation A2-2, the ice sheet steepness is not underestimated if compared with the simulated advancing profiles. Therefore, the theoretical profiles of Equation A2-2 may be used as a good and pessimistic (from a safety assessment point of view) mathematical representation of an *advancing* ice sheet over Forsmark (Figure A2-6).

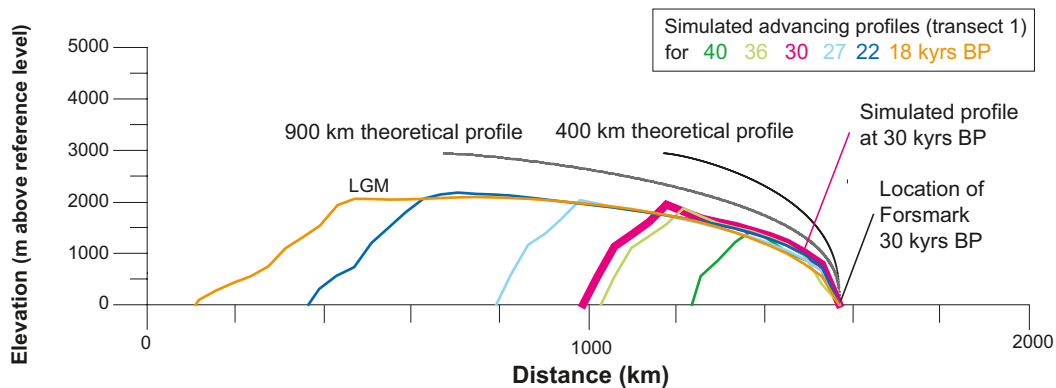


Figure A2-6. Comparison of ice surface topography from simulated advancing Weichselian ice profiles (from Figure A2-4a) and two theoretical steady-state profiles of Equation A2-2 (from Figure A2-1) /Paterson 1994/. In order to make the comparison meaningful, the fronts of all simulated profiles have been normalized to start at the same position and elevation (0 m) as the theoretical profile. Note that the simulated profiles would be somewhat “steeper” if they were to show ice thickness instead of surface topography (since the bedrock in the ice sheet simulation gets depressed, Figure A2-4), i.e. if they were normalized also to have a flat bed, such as the theoretical profiles. However, for e.g. groundwater flow simulations, it is the gradient of the upper ice surface that is of interest for the water flux, and accordingly that is what is shown also for the simulated profiles. However, this results in differences between the theoretical and simulated profiles appearing larger. The frontal parts of all simulated advancing profiles are less steep than the theoretical steady-state profiles.

In line with this, the theoretical profiles of Equation A2-2 are used in several other, but not all, safety assessment studies where the effect of a simple mathematical ice profile advancing over Forsmark is studied, for instance in groundwater flow studies /Vidstrand et al. 2010/ and THM studies of hydraulic jacking /Lönnqvist and Hökmark 2010/.

A2.4.2 Simulated LGM profile compared with the steady-state profile

The LGM profile at 18 kyrs BP represents the profile closest to steady-state in the Weichselian ice sheet simulation. In Figure A2-6 it is seen that both theoretical steady-state profiles are steeper than the simulated LGM profile. Given the expected differences due to the different approaches taken to produce the profiles, see above, there is also one additional reason why the simulated LGM profile is less steep than the theoretical steady-state profile. It is likely that the modelled Weichselian ice sheet never reached steady-state conditions during the LGM. This was most probably the case also for the real Weichselian ice sheet. In nature, ice sheets are constantly trying to adapt to the ever changing climate conditions, and the ice sheet probably did not have time to build a maximum-thick, steep ice at LGM.

A2.4.3 Simulated retreating profiles compared with theoretical steady-state profile

In Figure A2-7, the extracted profiles from the *retreat* phase of ice sheet model simulation (from Figure A2-4b), together with the retreat profile extracted from year 14.3 kyrs BP (Figure A2-3), are stacked and compared with the theoretical profiles of Equation A2-2.

The profile extracted along transect 2 for 14.3 kyrs BP has an ice margin that ends in the Baltic Sea, and so do the 14 and 12 kyr BP profiles along transect 1. When comparing the profiles in Figure A2-7, only the grounded parts of all profiles are seen and compared, i.e. the parts of the profiles that are located upstream the grounding-line.

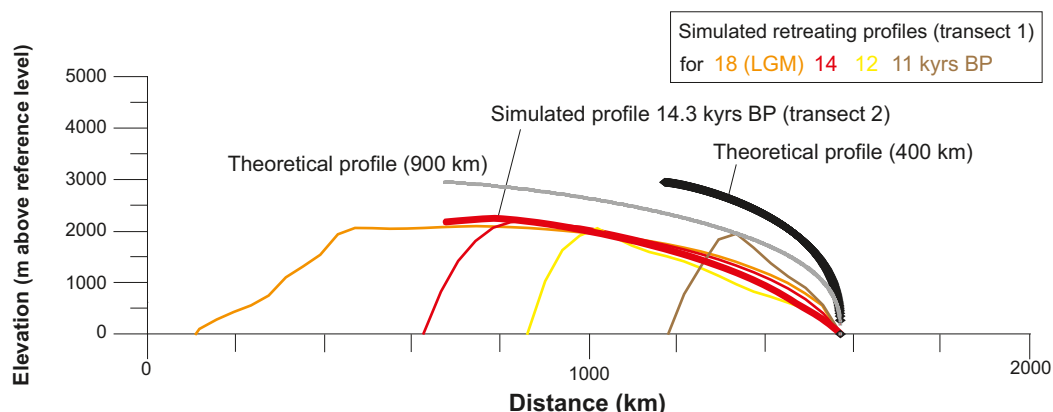


Figure A2-7. Comparison of ice surface topography between simulated retreating reference glacial cycle ice profiles (from Figure A2-4b and the profile extracted from transect 2 for 14.3 kyrs BP) and the theoretical steady-state profiles of Equation A2-2 (from Figure A1-1). In order to make the comparison meaningful, the fronts of all simulated profiles have been normalized to start at the same position and elevation (0 m) as the theoretical profiles. Note that the simulated profiles would be somewhat “steeper” if they were to show ice thickness instead of surface topography (since the bedrock in the ice sheet simulation gets depressed, Figure A2-4), i.e. if they were normalized also to have a flat bed, such as the theoretical profiles. However, for e.g. groundwater flow simulations, it is the gradient of the upper ice surface that is of interest for the water flux, and accordingly that is what is shown also for the simulated profiles. However, this results in the differences between the theoretical and simulated profiles appearing larger. The frontal parts of all retreating profiles are considerably less steep than the theoretical steady-state profiles. Profiles selected for other SR-Site studies are shown as bold lines.

In line with theory, it can be seen when comparing Figures A2-6 and A2-7 that the simulated profiles generally are steeper during the ice sheet advance than for the retreat. In Figure A2-7 it is also seen that the retreating profiles are, as expected, considerably less steep than the theoretical steady-state profiles. The steepest of the retreat profiles is from 11 kyrs BP. At this time the ice has a relatively steep profile caused by the steep bed topography in the mountainous region from where the profile is located (see Figure A2-4b). These topographic conditions of the ice sheet bed are not at all representative for the Forsmark area, and this profile is therefore not discussed further.

Comparing the steepness of the frontal parts of the profiles along transect 1, it can be seen that the steepest profile is the 18 kyrs BP (LGM) profile, followed by the 14, and 12 kyrs BP profiles (Figure A2-7), i.e. the ice sheet is getting less and less steep during the deglaciation over the lowland. It can also be noted that the 14.3 kyr BP profile from transect 2 has a steepness that is very similar to profile 14 kyrs of transect 1 (Figure A2-7), even though the profiles have different orientations. It is clearly seen that, for the Weichselian ice sheet simulation, profiles describing the retreat phase should be considerably less steep than the theoretical profiles.

Average hydraulic gradients from the selected theoretical ice sheet profile for various distances from the ice sheet margin are found in Table A2-1. The maximum hydraulic gradient associated with the steep frontal part of the theoretical profile is up to c. 1.5 m/m.

A2.4.4 Selection of profiles to use in SR-Site

Since the theoretical profiles of Equation A2-2 are considered to be more realistic than profiles from Equation A2-1, and because it is steeper than the steepest of the simulated advancing ice profiles (Figure A2-6), the steepest theoretical profile is selected to represent an advancing ice sheet over Forsmark for the SR-Site *reference glacial cycle*.

The frontal near parts of the profile extracted for 14.3 kyrs BP (transect 2) is the least steep retreat profile from the Weichselian ice sheet simulation (Figure A2-7). This profile is selected to represent a retreating ice sheet over Forsmark for the SR-Site *reference glacial cycle*.

The two selected profiles are shown by the bold lines in Figure A2-7. These two profiles constitute, in their frontal parts, the steepest and the least steep profiles of all profiles analyzed, and they are considered to cover a broad enough span of possible profiles to be employed in other SR-Site studies, such as modelling of groundwater flow under glacial conditions /Vidstrand et al. 2010/ and THM studies /Lönnqvist and Hökmark 2010/.

A2.5 Conclusions

1. The steepest theoretical profile (Equation A2- 2, Figure A2-7) /Paterson 1994/ is selected to represent an advancing ice sheet over Forsmark in the SR-Site *reference glacial cycle*. This profile is denoted “*the theoretical reference glacial cycle profile*”.
2. The least steep simulated profile from 14.3 kyrs BP (Figure A2-7) is selected to represent a retreating ice sheet over Forsmark in the SR-Site *reference glacial cycle*. This profile is denoted “*the simulated reference glacial cycle profile*”.

The profiles can of course be used in other ways than suggested above, e.g. for sensitivity studies on ice sheet steepness.

Table A2-1. Hydraulic gradients (m/m) from the selected theoretical ice sheet profile (Equation A2-2) averaged over various distances from the ice sheet margin.

Distance from ice margin (m)	Hydraulic gradient (m/m)	Hydraulic gradient (degrees)
100	1.49	56
200	0.96	44
400	0.62	32
1,000	0.35	19
2,000	0.23	13
4,000	0.15	8.5

Combination of buffer erosion and freezing

A3.1 Background

Based on the results on freezing depths analysed in the *reference glacial cycle* (Section 4.5.3) and the *severe permafrost case* (Section 5.5.3), freezing of water were excluded at repository depth for the first future glacial cycle in the buffer freezing scenario /SKB 2011/. For subsequent glacial cycles in the 1 Myr long safety assessment period, repository heat has declined. If making the most pessimistic combination of uncertainties in the input data to the permafrost simulations, there is a small risk of freezing of water at repository depth for these glacial cycles, while there is still ample margin to freezing of the bentonite buffer and deposition tunnel back-fill material, see the scenario on buffer freezing in /SKB 2011/. Because of this risk of freezing of water at repository depth, even if the risk is extraordinarily small, and for illustrative purposes, a combined case of buffer erosion and freezing at repository depth is here presented. If groundwater were to freeze in cavities formed by buffer erosion, the associated volume expansion would induce an additional pressure that possibly could affect the copper canister.

Two studies were made in order to illustrate the pressure effects of this hypothetical combined buffer erosion and freezing case. The first study (study A) investigated resulting freezing-point temperatures and freezing-induced pressures in buffer erosion cavities by considering various assumptions on compressibilities of remaining buffer, erosion cavity geometry, and surrounding ambient pressure (in this case surrounding groundwater pressure plus clay swelling pressure). It was also assumed that the cavity was filled with ordinary compressible water, free from solutes and impurities. The second study (study B) considered the chemical potential of water in bentonite in order to investigate equilibrium pressures in systems with various proportions of ice and bentonite and the resulting freezing temperatures and pressures. Effects of erosion cavity geometries were not included.

A3.2 Study A

A simple model was used to estimate the freezing point and pressure increase in a ring-shaped erosion cavity surrounding the canister (Figure A3-1). The full study was reported in /SKB 2006a, Section 4.4.1/. The compressibility of remaining clay was estimated from the swelling pressure of bentonite. It was also assumed that the erosion cavity was completely filled with ordinary compressible water, free from solutes and impurities. The effect of including these compressibilities is that they allow the freezing-induced expansion to occur at considerably higher temperatures than if the surroundings were incompressible. The compressibility of ice was also included, whereas the canister and the rock were assumed to be incompressible. Moreover, mean freezing temperatures for the erosion cavity as well as mean pressures for the erosion cavity and bentonite were assumed. For further details, see /SKB 2006a, Section 4.4.1/.

The surrounding groundwater pressure may vary between the ambient hydrostatic pressure, for completely unfrozen conditions, to a value up to the maximum freezing pressure for partially or fully frozen groundwater conditions. However, for a certain freezing temperature and for ambient pressures lower than the maximum freezing pressure, the pressure increase from freezing is affected by the ambient pressure, including the swelling pressure, in such a way that the resulting total pressure is constant, see below.

Calculations of freezing temperatures and associated pressure increases were made for ambient pressures between 4 and 100 MPa /SKB 2006a, Section 4.4.1/. As an example, the results of the calculations for an ambient pressure of 10 MPa are shown in Figure A3-2. Examples of pressure increase and total pressure after freezing for various ambient pressures are presented in Table A3-1. For further results see /SKB 2006a, Section 4.4.1/.

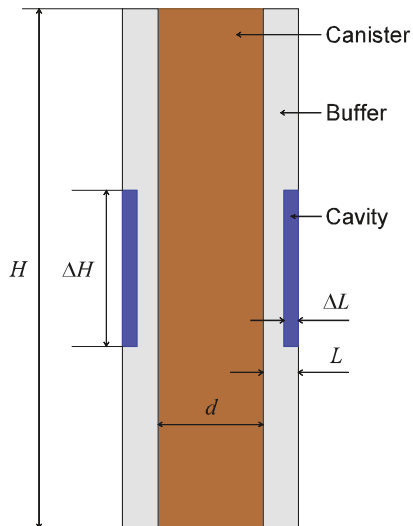


Figure A3-1. Geometry for calculations of freezing temperatures and freezing-induced pressures in buffer erosion cavities.

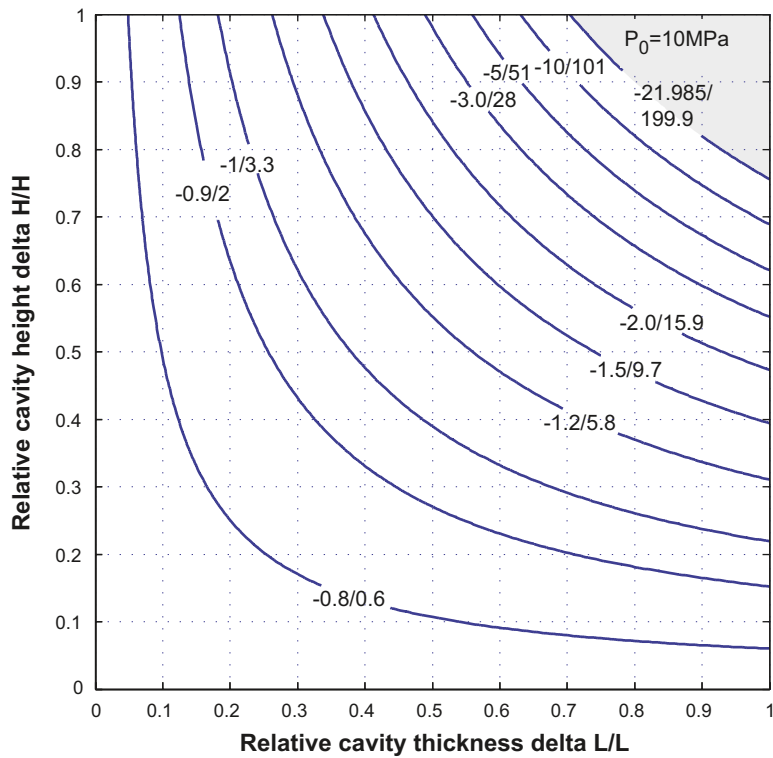


Figure A3-2. Freezing point temperature ($^{\circ}\text{C}$) and associated maximum pressure increase (MPa) in the erosion cavity, as a function of relative cavity thickness and height, at an ambient pressure of 10 MPa. In the figure, the first number is the freezing temperature and the second number is resulting pressure (i.e. temp/pressure). The shaded area represents a region with very low temperatures, below approximately -22°C .

Table A3-1. Examples of pressure increase and total pressure after freezing in an erosion cavity for various ambient pressures at a freezing temperature of -2°C . Note that the total pressure after freezing is independent of erosion cavity geometry and size.

Ambient pressure (sum of groundwater pressure and clay swelling pressure) (MPa)	Pressure increase from freezing in erosion cavity (MPa)	Total pressure (maximum freezing pressure) (MPa)
4	22	26
5	21	26
10	16	26
20	6	26
26	0	26
50	0 (no freezing occurs)	50

The results can be summarised as follows:

1. Freezing of water in an erosion cavity at a given freezing temperature can increase the pressure from the ambient pressure to the maximum freezing pressure, i.e. the maximum pressure at which freezing can occur at that temperature. For a freezing temperature of -2°C for instance, the *maximum* freezing pressure is ~ 26 MPa. For a freezing temperature of -2°C , the total pressure after freezing in the erosion cavity thus is between the ambient pressure and 26 MPa, depending on the size of the erosion cavity.
2. The *maximum* freezing pressure for a certain freezing temperature is independent of the geometry and size of the erosion cavity.
3. The pressure increase from freezing depends on the freezing temperature, the ambient pressure and the size or geometry of the erosion cavity. For certain combinations of freezing temperature and ambient pressure, complete freezing takes place and the resulting pressure increase grows with the size of the cavity. This occurs up to a certain point, at which the sum of the ambient pressure and the pressure increase equals the maximum freezing pressure. After that point, the freezing pressure is at its maximum and complete freezing can no longer take place.
4. If the ambient pressure exceeds the maximum freezing pressure of 26 MPa, no freezing can occur at a temperature of -2°C , see also Table A3-1.

A3.3 Study B

In order to assess the possible maximum pressure if an eroded KBS-3 buffer were to freeze, the equilibrium pressure between ice and bentonite was first considered. By considering this equilibrium pressure, and the expected deformation when ice is formed in a restricted volume, the maximum freezing pressure was estimated.

A3.3.1 Pressure of ice and bentonite in equilibrium

The chemical potential of water in bentonite is generally lower than in liquid bulk water at the same pressure and temperature. In order to reach equilibrium in a system with a confined clay sample contacted with an external reservoir of liquid water, a pressure difference between the clay and the external reservoir is therefore sustained. This pressure difference is usually referred to as the swelling pressure.

It is important to note that the occurrence of swelling pressure requires the external water reservoir to be mechanically separated from the clay, as is the case in a KBS-3 deposition hole where water is supplied by fractures in the surrounding rock or through the rock matrix itself. Liquid bulk water and bentonite at the same pressure cannot exist simultaneously in equilibrium (unless the clay density is very low).

The chemical potential of ice, on the other hand, can be lower, higher, or equal to that of bentonite water at the same pressure and temperature depending on the specific values of these variables as well as on the amount of water in the clay. In particular, this means that ice and bentonite can co-exist in equilibrium at the same pressure. The equilibrium pressure in a system containing both bentonite and ice can be derived by considering the following expression for the chemical potential of water in the bentonite /Birgersson et al. 2008/

$$\mu_{clay} = \mu_0 - s_{liq} \cdot T + v_{liq} \cdot P - v_{liq} \cdot P_s^0(w_u) \quad \text{Equation A3-1}$$

where μ_0 is the potential of a non-pressurized bulk water reference state at 0°C, T denotes temperature in °C, P denotes pressure, $P_s^0(w_u)$ is the measured swelling pressure at water to solid mass ratio w_u at 0°C, and s_{liq} and v_{liq} are the partial molar entropy and volume of liquid bulk water, respectively. Note that all chemical potentials used here refer to water in different phases. The partial molar quantities of the water in the clay is here approximated by the corresponding liquid bulk water properties and are further assumed independent of temperature and pressure. Note that $P_s^0(w_u)$ is not a physical pressure in the current state of the clay (the physical pressure is P), but rather a quantity describing the water retention properties of the specific clay under consideration. This function resembles an exponential expression at low enough water to solid mass ratios for typical bentonite materials, see e.g. /Kahr et al. 1990/.

$$P_s^0(w_u) \approx Ae^{-B \cdot w_u} \quad \text{Equation A3-2}$$

Using the data in /Karnland et al. 2006/ and /Karnland et al. 2009/, the least square fitted parameters for MX-80 bentonite in the range 0.5–12 MPa are $A \approx 382$ MPa and $B \approx 13.9$. The chemical potential in the ice can be expressed in a similar way as for the bentonite water

$$\mu_{ice} = \mu_0 - s_{ice} \cdot T + v_{ice} \cdot P \quad \text{Equation A3-3}$$

Note that this expression lacks the water retention term and that the partial molar properties are associated with ice (naturally). The equilibrium pressure is deduced by putting the two above expressions for the chemical potential of water equal,

$$P = \frac{\Delta s \cdot T + v_{liq} \cdot P_s^0(w_u)}{\Delta v} \quad \text{Equation A3-4}$$

where $\Delta s = s_{liq} - s_{ice}$ and $\Delta v = v_{liq} - v_{ice}$.

Notice that Δv is a negative quantity since ice has a lower density than liquid bulk water. Note further that the equilibrium pressure becomes negative for a given value of w_u if the temperature is high enough (although negative), indicating that ice and bentonite do not co-exist in equilibrium under such conditions. Consequently, the temperature where the equilibrium pressure is zero also defines the freezing point of the bentonite under consideration

$$T_c(w_u) = -\frac{v_{liq} \cdot P_s^0(w_u)}{\Delta s} \quad \text{Equation A3-5}$$

This expression for the freezing point is in agreement with earlier derivations /Birgersson et al. 2010/. Equation 5-4 can be re-expressed using $T_c(w_u)$ as

$$P = \frac{\Delta s \cdot (T - T_c(w_u))}{\Delta v} \quad \text{Equation A3-6}$$

which can be viewed as a generalized Clausius–Clapeyron relation where the presence of clay influences the phase boundary between ice and liquid water by a shift of the temperature scale.

A3.3.2 Pressure increase due to ice formation in a restricted volume

When a confined and water-saturated bentonite sample freezes (e.g. a KBS-3 buffer), some of the water will leave the bentonite (the montmorillonite interlayers) to form a separate ice phase (small ice crystals) /Svensson and Hansen 2010/. Because ice has lower density than liquid (clay) water, a pressure increase is expected under such a transformation. The pressure increase can be quantified by first considering the volume change when a certain amount of water, Δm , is transferred from clay to ice under non-pressurized conditions in an initially ice-free bentonite sample of water to solid mass ratio w_{tot}

$$\Delta V = \left(\frac{1}{\rho_{ice}} - \frac{1}{\rho_w} \right) \cdot \Delta m = \left(\frac{\rho_w}{\rho_{ice}} - 1 \right) \cdot \frac{\Delta m}{\rho_w} = \xi \cdot \frac{m_s}{\rho_w} (w_{tot} - w_u) \quad \text{Equation A3-7}$$

Here ρ_{ice} and ρ_w denotes the density of ice and liquid bulk water, respectively, $\xi \equiv \rho_w / \rho_{ice} - 1$, m_s is the mass of dry clay and w_u denotes the amount of water in the bentonite after the transition (i.e. the amount of unfrozen water). If the total system (bentonite + ice) is to be kept a constant volume, a pressure causing the deformation $-\Delta V$ must be applied. Assuming isotropic stress state (hydrostatic pressure), bulk modulus β , and using Equation A3-7, the pressure after the transition is given by

$$P = -\beta \frac{-\Delta V}{V_w} = \beta \xi \frac{m_s}{V_w \cdot \rho_w} (w_{tot} - w_u) = \beta \xi \left(1 - \frac{w_u}{w_{tot}} \right) \quad \text{Equation A3-8}$$

where the first equality utilizes the definition of bulk modulus and V_w denotes the total water volume (liquid + ice). The presence of the total water volume rather than total volume in Equation A3-8 is equivalent to assuming that the dry clay particles are incompressible.

A3.3.3 Estimated pressure of confined bentonite below 0°C

It can be shown /Birgersson et al. 2010/ that the swelling pressure decreases approximately linearly with temperature in the range between the freezing point of the external water reservoir (here assumed to be 0°C) and the freezing point of the bentonite. Furthermore, at the freezing point of the bentonite, the swelling pressure is zero. If the temperature of a confined bentonite sample is lowered below the freezing point, the pressure will start to increase due to the volume expansion of the water transformed from liquid state to ice. The equilibrium pressure at a given temperature below T_c can be deduced by first calculating the amount of unfrozen water by combining Equations A3-2, A3-4 and A3-8 (assuming that the system has the total water to solid mass ratio w_{tot})

$$\frac{\Delta s \cdot T - v_{liq} \cdot A \cdot e^{-B \cdot w_u}}{\Delta v} = \beta \xi \left(1 - \frac{w_u}{w_{tot}} \right) \quad \text{Equation A3-9}$$

Once the unfrozen amount of water is calculated, the equilibrium pressure is given by either of Equations A3-4 or A3-8. All parameters in Equation A3-9 except for the bulk modulus β are firmly determined by either fundamental properties of bulk water or by accurate swelling pressure measurements. The parameter set when applied to MX-80 bentonite is listed in Table A3-2.

The specific value to be used of the bulk modulus, on the other hand, is not as clear. The compressibility of the full system will depend on the separate bulk moduli of clay, water and ice as well as the relative fraction of these phases. Hence, it is to be expected that β is a function of both w_u and w_{tot} . A way to treat this complication is to solve Equation A3-9 for two limiting values of β in order to achieve a pressure interval for the actual equilibrium pressure. Here the limiting values of β is chosen as that of pure ice (8,800 MPa) and that of liquid bulk water (2,200 MPa), and are assumed independent of temperature and pressure.

A solution to Equation A3-9 for MX-80 bentonite (Table A3-3) is illustrated in Figure A3-3. This example assumes $w_{tot} = 0.366$, which corresponds to a swelling pressure at 0°C of ca 2.5 MPa, and a freezing point of -2°C. In the diagram the ice/clay equilibrium line at -3°C (Equation A3-4) is displayed. When lowering the temperature from -2 to -3°C, water is expelled from the clay and pressure increases according to the compression curves (Equation A3-8, with two different values of the bulk modulus). The actual pressure of the system is given by the intersection between the compression and the ice/clay equilibrium curve. Hence, in the case of a bulk modulus of ice, the unfrozen water content is ca 0.360 and pressure is ca 13 MPa. If the bulk modulus instead is that of liquid bulk water, the unfrozen water content is ca 0.351 and the pressure is ca 8 MPa. Hence when lowering the temperature from -2°C to -3°C, this particular sample increases its pressure from 0 to 8–13 MPa.

Table A3-2. Values of parameters used in Equation A3-9. The partial molar entropies and volumes are approximated by bulk values (ice and liquid water) at 0°C. The swelling pressure parameters (Equation A3-2) are fitted to data for MX-80 bentonite /Karnland et al. 2006, Karnland et al. 2009/.

Δs (J/mol/°C)	v_{ice} (cm ³ /mol)	v_{liq} (cm ³ /mol)	A (MPa)	B (-)	$\Delta v = v_{liq} - v_{ice}$ (cm ³ /mol)	$\xi = v_{ice} / v_{liq} - 1$ (-)
22.0	19.65	18.03	382.1	13.86	1.62	0.09

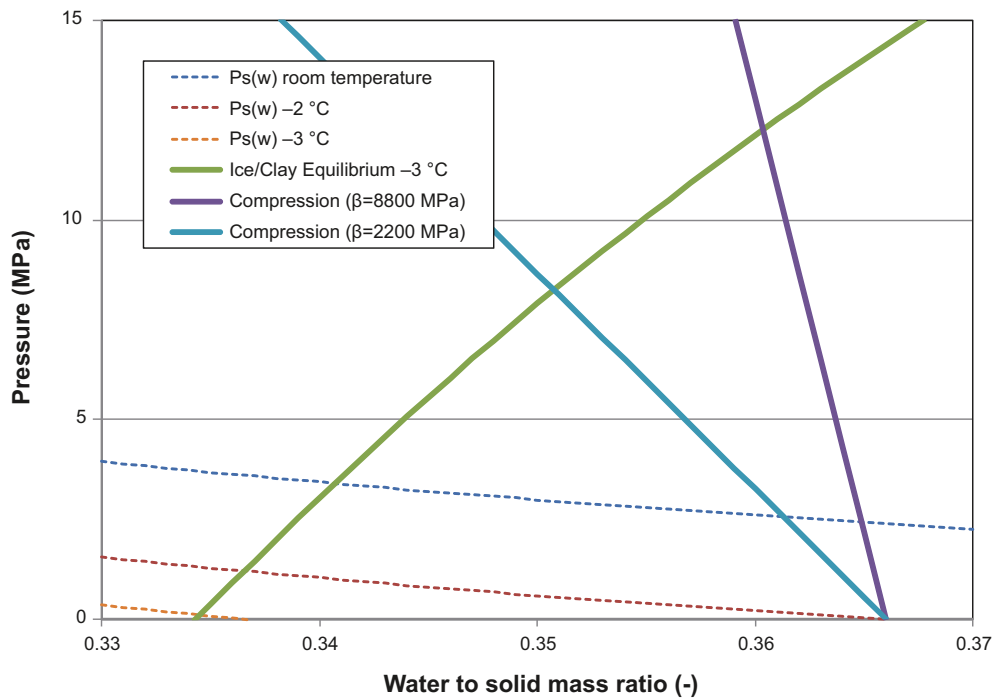


Figure A3-3. Illustration of the obtained equilibrium pressure when ice forms in a confined MX-80 sample. Equilibrium pressure is reached where the compression line intersects the Ice/clay equilibrium line. Included in the figure is also the swelling pressure curve for different temperatures /Birgersson et al. 2010/.

A3.3.4 The combination of erosion and freezing in a KBS-3 buffer

The nominal buffer density is 2.0 g/cm^3 , corresponding to a water to solid mass ratio of ~ 0.27 . The freezing point of the undisturbed buffer thus equals -7°C according to Equation A3-5. It is however evident from Equation A3-2 that swelling pressure, and thereby the freezing point, is a strong function of water content in this density region. This means that the buffer freezing point is expected to increase substantially if bentonite is lost from the deposition hole due to erosion. A freezing point of -2°C , for example, corresponds to a water to solid mass ratio of 0.366, or a density of 1.87 g/cm^3 . This, in turn, corresponds to a mass loss of ca 13% or ca $2.7 \cdot 10^3 \text{ kg}$ if the buffer density can be assumed homogeneous (initial mass: $2.0 \cdot 10^4 \text{ kg}$).

Table A3-3 shows the expected pressure intervals and unfrozen water contents at different temperatures for different values of buffer freezing points (i.e. different densities). Included in Table A3-3 is also the case where all clay has eroded. The equilibrium pressures for this case are given by the ordinary Clausius-Claperyon equation for phase equilibrium between liquid water and ice (Equation A3-6 with $T_c = 0$) and are independent of the value of the bulk modulus.

Table A3-3. The limiting pressures and unfrozen water contents at different temperatures for MX-80 bentonite of different freezing points (i.e. different densities). The listed eroded mass assumes a homogeneously distributed buffer with initial mass $2.0 \cdot 10^4 \text{ kg}$.

T_c °C	w_{tot} -	ρ_b g/cm ³	Eroded mass kg	at -1°C		at -2°C		at -3°C		at -4°C		at -5°C	
				P MPa	w_u -	P MPa	w_u -	P MPa	w_u -	P MPa	w_u -	P MPa	w_u -
0	-	1.00	$2.0 \cdot 10^4$	14	-	27	-	41	-	54	-	68	-
-1	0.416	1.82	$3.8 \cdot 10^3$	0	0.416	10-13	0.396-0.409	18-25	0.377-0.403	26-38	0.361-0.396	33-49	0.346-0.390
-2	0.366	1.87	$2.7 \cdot 10^3$	Unfrozen	0.366	0	0.366	8-13	0.351-0.360	15-24	0.338-0.355	22-35	0.326-0.350
-3	0.337	1.91	$1.9 \cdot 10^3$	Unfrozen	0.337	Unfrozen	0.337	0	0.337	7-12	0.324-0.332	14-23	0.314-0.327
-4	0.316	1.94	$1.4 \cdot 10^3$	Unfrozen	0.316	Unfrozen	0.316	Unfrozen	0.316	0	0.316	7-12	0.305-0.311

Table A3-3 lists the expected pressures in a frozen deposition hole whose buffer is eroded in such a way that the remaining clay is homogeneously distributed, which is the equilibrium state. However, since erosion occurs at the rock-buffer interface, substantial internal redistribution of the buffer mass is required to reach this state. Therefore, it cannot be excluded that the buffer density to a certain degree is inhomogeneous when it freezes, e.g. because of long equilibration times, or because of internal “friction”. This means that freezing could occur above the freezing points listed in Table A3-3, as these correspond to buffer mean density. Consider for instance a homogeneous buffer of (mean) density 1.87 g/cm^3 . This system would not experience any pressure increase at -2°C (which is the freezing point for this particular density). If instead the mass was distributed so that a certain fraction of the buffer had a density of 1.82 g/cm^3 (and a density higher than 1.87 g/cm^3 in the rest), a pressure increase would be experienced at -2° because the freezing point of the low density part is -1°C . The pressure increase, however, is smaller than for the case of a homogeneous buffer at density 1.82 g/cm^3 because the entire buffer is involved in the deformation. Hence, the values in Table A3-3 also put an upper limit for the pressure increase in inhomogeneous buffers if the density instead refers to minimum density.

It should be noted that the more heterogeneous the density distribution is the more unlikely the state, because larger and larger forces will act to redistribute the mass (Equation A3-2). But even for the highly unrealistic density distribution of a bulk water cavity ($\rho_b = 1.0 \text{ g/cm}^3$) in conjunction with unaffected clay ($\rho_b = 2.0 \text{ g/cm}^3$), the pressure increase will never exceed that for the case of a completely eroded deposition hole. Note further that the pressure increases experienced in heterogeneously distributed buffers are transient states; when freezing occur (in the part of the buffer with lowest density), the stress state changes radically and mass redistribution is expected, leading to a more homogeneous state of the clay and lower pressures.

The above considerations have not taken into account the additional hydrostatic pressure present under unfrozen conditions in a KBS-3 repository. However, the effect of any additional load (affecting both clay and reservoir) would, on one hand, lower the freezing point according to the conventional Clausius-Clapeyron relation (ca 0.074°C/MPa), but on the other hand the pressure would be non-zero at the freezing point (equal to the additional load). Similarly, if the groundwater (and thus the clay) contains a certain amount of salt, the freezing point of the external reservoir would lower accordingly and also the ice/clay equilibrium would adjust in such a way that the clay would contain more water for a given temperature and pressure. Consequently, neither the effect of a hydraulic head, nor the effect of salt in the water, will contribute to increase the values listed in Table A3-3.

A3.4 Discussion and conclusions

The lowest temperature at repository depth when considering the results of maximum freezing depths in the *reference glacial cycle* and the *severe permafrost case* (Table 5-11), and including the most pessimistic combination of all uncertainties relevant for the respective case, is approximately -0.5°C . In line with this the -2°C isotherm does not reach repository depth in the reference evolution, nor in the *severe permafrost case*. Nevertheless, as a pessimistic basis for a discussion on the theoretical consequences of the combined buffer erosion and freezing case, a lowest temperature of -2°C is assumed at repository depth. This corresponds to a lowering of the entire temperature curve reconstructed for the last glacial cycle of more than 10°C (Figure 5-33) which is considered unrealistic also when including the significant uncertainties associated with the temperature curve (Appendix 1).

The results from study A show that for a temperature of -2°C , the pressure increase from freezing of pure groundwater in buffer erosion cavities results in a maximum cavity pressure of 26 MPa (Table A3-1). Freezing at higher temperatures would yield lower freezing-induced pressures (Figure A3-2), while other ambient pressures would not result in a total pressure higher than 26 MPa. This pressure is in line with the maximum pressure obtained from study B for an ambient temperature of -2°C . Here the pressure in the cavity is 27 MPa for a case with a completely eroded buffer (Table A3-3), corresponding to a buffer loss of 20,000 kg. Cases with a less eroded buffer (i.e. a partially eroded buffer with a higher buffer density and lower freezing point, Table A3-3), yields lower erosion cavity pressures. For example, a buffer loss of 1,400 kg, which is close to the value of 1,200 kg of buffer loss that is used for the assumption of getting advective conditions in the buffer /SKB 2011/, results in unfrozen conditions if the temperature is -2°C (Table A3-3). For this case, the temperature needs to be as low as -5°C in order to freeze the buffer cavity, with a resulting maximum cavity pressure of 12 MPa.

A maximum pressure of 26–27 MPa in the erosion cavity is considerably lower than the maximum total pressure deduced for the SR-Site scenario on isostatic load where the maximum thick ice sheet from Section 5.4 is combined with clay swelling pressure and hydrostatic pressure due to the repository depth, resulting in a total pressure of around 50 MPa /SKB 2011/. Since this isostatic load scenario does not result in canister failure /SKB 2011/, the same is here concluded for the hypothetical case combining buffer erosion and freezing.

If the pressure from a maximum large ice sheet (30 MPa) (Section 5.4) were to be directly and unrealistically combined with the maximum pressure resulting from freezing in buffer erosion cavities (27 MPa), the resulting pressure would be 57 MPa. However, this case is not relevant since for ambient pressures greater than 26 MPa, a repository depth bedrock temperature of -2°C would not be low enough to freeze water in erosion cavities. In addition, during phases of ice sheet overriding, pre-existing permafrost degrades due to the insulation effect of the ice sheet, e.g. (Section 4.5.3), which means that deep permafrost is not compatible with large ice sheet thicknesses.

All in all, the following conclusions can be made:

- Based on the results on maximum permafrost and freezing depths in the *reference glacial cycle* (Section 4.5.3) and in the *severe permafrost case* (Section 5.5.3), freezing of water at repository depth was excluded for the first future glacial cycle in the buffer freezing scenario /SKB 2011/.
- Calculations made show that the maximum freezing-induced pressure in buffer erosion cavities would be 26–27 MPa for a pessimistically chosen ambient temperature of -2°C . This case corresponds to a total loss of buffer in the deposition hole. This pressure is considerably lower than the critical pressure for canister collapse as discussed in the scenario treating canister collapse due to isostatic load /SKB 2011/.
- The amount of buffer loss affects the freezing point of the remaining buffer and the resulting cavity pressures. A case with buffer loss approximately corresponding to the buffer loss assumed for getting advective conditions in the buffer does not result in frozen conditions in the erosion cavity if the ambient temperature is -2°C . In this case, the temperature needs to be -5°C in order to get freezing, with a resulting cavity pressure of up to 12 MPa as result.

A freezing-induced pressure in buffer erosion cavities and large pressures from ice sheet load do not occur simultaneously